QUANTIFICATION OF QUALITY OF FOAMED WARM MIX ASPHALT BINDERS AND MIXTURES

By

Hande Isik Ozturk

A DISSERTATION

Submitted to
Michigan State University
in partial fulfilment of the requirements
for the degree of

Civil Engineering- Doctor of Philosophy

2013

ABSTRACT

QUANTIFICATION OF QUALITY OF FOAMED WARM MIX ASPHALT BINDERS AND MIXTURES

By

Hande Isik Ozturk

Warm Mix Asphalt (WMA), which is the general term used for the asphalt pavements produced and placed at lower temperatures, is introduced to the pavement industry to overcome the environmental and economic challenges of Hot Mix Asphalt (HMA). WMA technologies reduce the overall mixture viscosity at lower temperatures to increase the workability of the loose mixtures, provide improved (better) compaction and facilitate aggregate coating at low temperatures. However, there are still many unknowns related to their long term performance.

Foam-based WMA's are the most commonly used techniques; however there is no specification or method to evaluate the quality of foam generated by different techniques. Although producing foamed binder is relatively simple process, where hot binder is mixed with a limited amount of water (typically 2-3% by weight of the binder), the rheology of the foamed binder is not very simple. The quality of the foamed binder depends on various factors such as the binder type, grade and modification, the foaming technology used, amount of water, and temperature. Moreover, the quality of the binder plays a crucial role during the mixing, laying and compaction stages of WMA pavement production. Asphalt foams used in base stabilization applications were typically characterized using following three parameters: Expansion Ratio (ER), Half-life (HL) and Foam Index (FI). However, there is no available method to measure these parameters precisely. Therefore, an accurate and repeatable procedure is needed for the

measurement of initial expansion and reduction in height of foamed asphalt in order to calculate the foam binder quality parameters.

Asphalt Foam Collapse Test (AFCT), an automated test to measure the reduction in the height of the foam binder over time via image analysis, is developed during this study and validated with nondestructive 3D imaging methods (i.e., x-ray microtomography). The height reduction data obtained from AFCT is used to accurately calculate the commonly used foam quality parameters. In addition, two new parameters, Bubble Size Distribution (BSD) and Surface Area Index (SAI), are introduced as quality parameters in this study. It is found that these parameters are strong candidates for evaluating the workability and coating, as well as the performance of the pavements.

A nozzle-based laboratory foamer was utilized in this study to determine the effect of water content and air pressure on the foam quality individually and in combination. Results revealed that the water content and air pressure have significant influence on ER, HL, FI, BSD, and SAI. It was observed that the low water content and low pressure produced foams with relatively small bubbles as compared to foams made with high water content and pressure. The current WMA pavement design procedures are based on limited empirical data and recommendations of the WMA technology suppliers. WMA design procedures do not consider the foam quality since its importance has not been fully understood. Therefore, the long term performance of the WMA mixtures prepared with foamed binders prepared with various injected water content and air pressures was evaluated via laboratory performance tests and compared with the foamed binder quality parameters. It was concluded that a WMA mix design should consider the foam quality, which is currently ignored.

TO MY PARENTS & MY GRANDMOTHER'S SOUL

ACKNOWLEDGEMENTS

I would like to express my gratitude to Dr. M. Emin Kutay for his guidance and support throughout my study at Michigan State University. I would have never completed this work without his encouragement and his look for the positive.

I would like to extend my appreciation to Dr. Lalita Udpa for her valuable course. I also would like to thank Dr. Karim Chatti and Dr. Neeraj Buch for reading my thesis and their valuable comments.

I would like to acknowledge Craig Burck for his technical assistance and Gerrit Littrup for his support throughout the laboratory work.

I would also like to thank the graduate and undergraduate students in Advanced Asphalt Characterization Laboratory (AACL) at Michigan State University.

I would like to express my gratitude towards Dr. Denis Keane, the DND-CAT Director, for his help while scanning the images at the Advanced Photon Source (APS) of the Argonne National Laboratory (ANL). Use of the APS, an Office of Science User Facility operated for the U.S. Department of Energy (DOE) Office of Science by ANL, was supported by the U.S. DOE under Contract No. DE-AC02-06CH11357.

I deeply thank my parents for their love, support and understanding throughout my life. I would like to acknowledge my grandmother, who encoraged me to go to the graduate school.

TABLE OF CONTENTS

LIST OF TABLES

LIST OF FIGURES

CHAPTER 1

INTRODUCTION

Global warming and increase in fuel prices have made researchers to consider alternative construction techniques to conventional Hot Mix Asphalt (HMA). According to Environmental Protection Agency (EPA), more than 500 million tons of HMA were produced at the 3,600 (estimated) active asphalt plants in United States in 1996 to construct and maintain thousands of miles of roads (EPA-454/R-00-019, 2000). It is reported that average asphalt plants emits approximately 2500 tons of CO_2. Overall, it makes emission of 8.75 megaton of CO_2 only in the USA, which is equivalent to approximately 0.5% of total gas emissions (Bahia and Miller, 2009). It is more than to be neglected for the sustainability of the asphalt pavements. Meanwhile, approximately 1 billion gallons of fuel is used annually for HMA production, material extraction and usage. About 90% of total life cycle energy is solely spent in production (Bahia and Miller, 2009).

Recent developments in asphalt production technologies lead to decrease in the production costs and greenhouse emissions. One way of classifying the technologies is by the degree of temperature reduction. Figure 1 shows a classification of various application temperatures for asphaltic concrete. Cold Mix asphalt has been used as an alternative to HMA, reducing mixing and compaction temperatures by emulsifying the asphalt in water prior to mixing with the aggregate. The asphalt emulsion is less viscous and the mixture is easy to work

with and compact at relatively low temperatures. However, insufficient aggregate coating, higher air void contents, limited workability duration and reduction of strength for long term performance has made it unsuitable for all conditions. It is commonly used as a patching material and on low volume traffic service roads (Blades and Kearney, 2004). To overcome the limitations of cold mix asphalt, Warm Mix Asphalt (WMA) has been introduced, which is produced between cold and hot mix asphalt temperatures (Prowell, 2008).

WMA is the general term used for the asphalt pavements produced and placed at lower temperatures as compared to conventional Hot Mix Asphalt (HMA) (D'Angelo et al., 2008; Hurley, 2006; Diefenderfer et al., 2007; Prowell, 2008). Lower production temperatures are achieved by means of various WMA technologies including foaming, wax-based additives, emulsion-based products and surfactants.

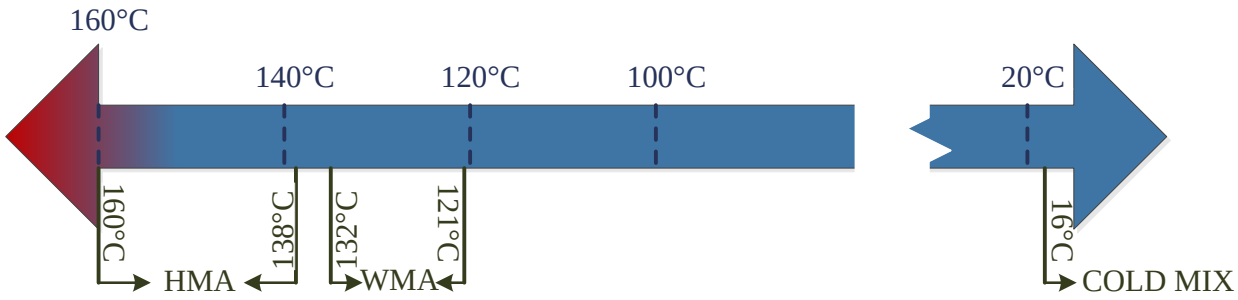

Figure 1: Typical mixing temperatures for asphalt pavements (For interpretation of the references to color in this and all other figures, the reader is referred to the electronic version of this dissertation.)

WMA mixing temperatures are about 20 to 30°C lower than conventional HMA and slightly above 100°C as shown in Figure 1 (Prowell, 2007). This amounts to about 20-30% reduction in paving temperatures, which leads to numerous benefits including: (i) economical

aspects (reduced fuel usage, increased paving season), (ii) environmental aspects (reduced green house emissions), (iii) engineering aspects (improved (better) field compaction, less aging (i.e., oxidation) of the mixture, less permanent deformation etc.) and (iv) worker exposure (decrease in exposure to fumes for the paving crew) (De Groot et al., 2001; Larsen et al., 2004; Cervarich, 2003; Prowell et al.; 2007). The fuel saving due to usage of WMA instead of HMA is approximately 30 to 35% (Prowell, 2008). WMA also improves the compaction in cold weather, extends the allowable compaction period, increases the haul distance and potentially more suitable for using high percentage of reclaimed asphalt pavement (RAP) (Kristjánsdóttir et al., 2007). Aged RAP binder compensates for the softness of virgin binder in WMA and helps towards rutting susceptibility. WMA's advantages (e.g., reduced fuel cost and greenhouse emissions) over traditional HMA have made it very appealing to state and local roadway agencies as well as the industry (Hassan, 2009; Mallick et al., 2009). In 2010, just six years after the first trial in the U.S., 13% of the pavements were constructed with WMA (Prowell et al., 2012). This corresponds to ~47 million of tons of WMA, which amounts to approximately 30 million gallons of fuel savings that is worth $80 million (Nadeau, 2012). The WMA lessens the carbon dioxide release around 800,000 tons. To date, all 50 states in US constructed WMA trial sections (Prowell et al., 2012).

MOTIVATION

Most of the current design methodology of WMA foamed asphalt pavements are based on the WMA plant manufacturers' recommendations and past experience of the contractors. Such design approach has lead to premature WMA pavement failures (Kim et al., 2011). Recently, an NCHRP project produced recommended WMA mixture design specifications

(Bonaquist, 2011), which is primarily based on limited empirical data. Most of the current knowledge on WMA is based on empirical data and there is a significant lack of understanding of the fundamental behavior of the foamed binder used in WMA pavement. Understanding the WMA foamed binder characteristics that affect the mechanical behavior of pavements is crucial to accurately predict and improve its long term performance.

OBJECTIVE AND SCOPE OF THE RESEARCH

The main objectives of this study are listed as follows:

(1) To develop new parameters to assess the quality of the foamed binder (i.e., bubble size distribution, surface area, etc.)

(2) To develop an accurate and repeatable laboratory/ field equipment and protocol to measure the reduction in the height of the foam binder over time.

(3) To develop links between the foam binder quality parameters (i.e., expansion ratio, half-life, foam index etc.) and asphalt pavement performance (i.e., rutting, fatigue cracking, moisture susceptibility etc.).

(4) To investigate the characteristics of foamed binders using different types of binders (Performance Grade (PG), Crumb Rubber (CR), etc.)

OUTLINE OF THE DISSERTATION

The thesis divided into seven chapters including CHAPTER 1, which is the introduction. In CHAPTER 2, the literature and background on WMA pavements and foamed based binders is presented. In CHAPTER 3, foamed binder quality indicators (i.e., Expansion Ratio, Foam Index, Half-Life) are discussed and new parameters (i.e., Bubble Size Distribution and Surface Area Index) are introduced to assess the quality of the foamed binder. In CHAPTER 4, a novel testing

methodology called as Asphalt Foam Collapse Test (AFCT) is introduced to measure the height reduction of the foamed binder as it collapses in order to precisely calculate the foamed binder quality indicators. In CHAPTER 5, the long term performance of the WMA mixtures prepared with different foamed binders in the laboratory is evaluated via performance tests and compared with the foamed binder quality parameters presented in CHAPTER 3. In CHAPTER 6, X-ray Microtomography (XRM) imaging technique is used to analyze the binder type and foaming technology on the generation and evolution of the foam. The findings and the impact of research are summarized in CHAPTER 7.

CHAPTER 2

LITERATURE REVIEW AND BACKGROUND

HISTORY OF WMA PAVEMENTS

WMA technologies are developed to significantly reduce the mixture viscosity at lower temperatures to facilitate better coating of the aggregates, increase the workability of the loose mixtures and provide improved (better) compaction. These technologies have been extensively used in Europe since the first laboratory experiments starting with Aspha-min zeolite by Mitteldeutsche Hartstein-Industrie AG in 1995 and WAM foam by Shell Bitumen and Kolo Veidekke in Norway in 1996. In 1997, the first WMS pavement section was constructed with Sasobit in Hamburg, Germany. The earliest WAM foam and Aspha-min zeolite field trials were in Norway and Germany in 1999.

In 2002, National Asphalt Pavement Association (NAPA) organized a study tour to Denmark, Germany and Norway to investigate the following warm mix technologies: (i)Aspha-min, (ii)WAM foam, and (iii) Sasobit (Prowell, 2008). Brief descriptions of these technologies are given below:

(i) Aspha-min is a foaming additives that is a kind of synthetic zeolite, which is composed of aluminosilicates and alkalimetals that contain about 20% crystallized water. The water is released by increasing the temperature above the boiling point of water, creating a controlled foaming effect. This leads to an increase in binder volume

and reduction in binder viscosity, which provides 6-7 hours of workability period till the temperature drops below approximately 100°C (212°F).

(ii) WAM-Foam is a foaming process that includes two-stage mixing of soft and hard binders, in order to obtain the desired performance grade (PG) binder. The soft binder controls the coating of coarse aggregates while the stiffer binder increases the overall stiffness, reducing susceptibility to rutting. Water is added for foaming approximately 2-5% by weight of the hard binder (i.e. about 1.6 lb water per ton of mix assuming 5% total asphalt content, 80% of which is hard binder) at approximately 175 -180°C (347-356°F).

(iii) Sasobit is a synthetic paraffin wax, which combines hot coal and natural gas with steam with the aid of a catalyst. Sasobit has higher viscosity than binder below its melting point and lower viscosity than binder above its melting point. They harden in asphalt from 65 to 155°C into regularly distributed, microscopic stick-shaped particles.

The study tour by NAPA is followed by a research, which was initiated at National Center for Asphalt Technology (NCAT) and sponsored by NAPA, FHWA, Eurovia and Sasol in 2003 (Prowell, 2008). Interests in WMA technologies in the U.S. have significantly increased after the first field trials with Aspha-min in 2004 in Florida and North Carolina (D'Angelo et al., 2008) and continued with field trials in Florida, Indiana, Maryland, New Hampshire, Ohio and Texas in 2005. In 2007, AASHTO and FHWA organized a scan tour to Belgium, France, Germany and Norway. D'Angelo et al. (2008) reported that WMA performance in Europe is

same or better than HMA. In 2008, it was documented that 32 U.S. states has WMA trial sections. Moreover, Texas DOT introduced the first WMA specification, which allows WMA to be used statewide. The number of states having trial sections and specifications drastically increased by the end of 2011, where 45 U.S. states had trial sections and 30 U.S. states had specifications. It was reported that all 50 states in U.S. conducted trial WMA sections by the end of 2011 (recent record available). FHWA survey reported that WMA usage was 19.2 millions of tons in 2009 and 47.6 million tons in 2010, which was equivalent to 13% of overall asphalt production (Prowell, 2008).

There are currently over 30 different WMA technologies being used in U.S., more available worldwide. These technologies are based on various chemical additives/surfactants, foaming methods and non-foaming additives. The most well-known chemical additives/surfactants in U.S. markets are Cecabase, Evotherm, HyperTherm and Rediset. Common Non-foaming additives in U.S. can be listed as BituTech, Leadcap, Sasobit, SonneWarmix, and Thiopave (Prowell, 2008). However, the two thirds of the technologies are based on foaming methods, which are explained in detail at Section 0 (Prowell et al., 2012).

BENEFITS OF WMA

Engineering Aspects

There are several engineering benefits that could be gained from adopting WMA technologies in asphalt pavement construction, which are discussed below.

Aging of WMA binders

The WMA binders are not exposed to elevated temperatures during the production and construction. Therefore, the WMA mixtures are less susceptible to aging and cracking, which can lead to longer pavement service life (Hossain et al., 2009; Rubio et al., 2012).

Workability and Compactability of WMA pavements

WMA technologies reduce the overall binder viscosity, which improves the workability of asphalt mixtures at lower temperatures. Thus, the mixtures can be compacted with less number of roller passes to reach the targeted density (D'Angelo et al., 2008; Hossain et al., 2009). Stiff mixes (i.e., mixes with high percent of Reclaimed Asphalt Pavement (RAP) and Recycled Asphalt Shingles (RAS)) have compactability problems, which lead to lower in-place densities. In order to suppress the compaction densities to target levels, the compaction temperatures or efforts may be increased, which can result aggregate breakdowns and damage in the pavement, even during construction. Therefore, WMA technologies help in the compactabilty of the relatively stiff asphalt mixtures in conventional compaction temperatures (Prowell, 2008).

Usage of RAS in WMA pavements

Usage of Recycled Asphalt Shingles (RAS) in asphalt pavements has four major advantages: (i) high asphalt binder content, 20% to 30% by weight of the shingle, (ii) high grade frictional aggregate, (iii) fiberglass fibers that promote flexibility in the asphalt mixes and, (iv) lime dust that is a natural anti-strip for asphalt aggregates. RAS used in paving mixtures range from 3% to 5% by weight of HMA or WMA mixture. WMA enables the incorporation of both RAP and RAS in many mixtures not possible with HMA. In St. Louis, Missouri, an off-ramp at

the exit 249 interchange on Interstate 70 was constructed with RAP, RAS and WMA mix in 2010. The mixture was a 12.5mm Superpave surface mix containing limestone and traprock plus 17% RAP and 3% RAS. (Jackson, 2011). Jackson (2011) reported that the pavement has been performing well, although there were concerns when it was initially placed.

Usage of High Percentage RAP in WMA pavements

WMA technologies potentially allow use of less virgin materials, by utilizing high percentage of RAP in asphalt mixtures at lower temperatures. The decreased aging of the binder due to lower WMA production temperatures helps in rejuvenating the RAP binder, particularly in regard to low-temperature cracking (D'Angelo et al., 2008).

High RAP asphalt pavements are frequently constructed in Europe, though it is not common in U.S. In Germany, a trial base course section containing 45% RAP was successfully placed at a range of -1°C to 3°C ambient temperature as the mixture temperature during the placement varied from 102°C to 139°C (D'Angelo et al., 2008). It was reported that better compaction was achieved with WMA as compared to HMA with the same and fewer roller passes. Additionally, mixtures prepared with low energy asphalt (LEAB) WMA method are commonly used with 50% unfractionated RAP in Netherlands. Moreover, trial sections have been constructed with 90 to 100 % RAP using Aspha-min zeolite and Sasobit in Germany (D'Angelo et al., 2008).

In the U.S., majority of State DOT's are hesitant to use of high percent RAP in the surface layer of the asphalt pavements. It was reported in 2011 that 10% of the states (Alaska, Washington, North Dakota, Iowa and Connecticut) do not permit more than 25 % RAP in any of

HMA layers. Another 10% of states such as California, Nevada, Michigan, Louisiana and New York only permit more than 25 % RAP in the base layer. Using high RAP content in both base and intermediate layers is allowed by 32% of the states (e.g., Colorado, Arizona, New Mexico, Oklahoma, Texas). About 48% of the states (e.g. Illinois, Montana, North Carolina, and Alabama) allow high percent RAP in all layers. Meanwhile, about 55 % of the states are experimenting the use of high RAP in the surface layer (FHWA-HRT-11-021, 2011).

Mississippi DOT studied the use of high RAP (50 % to 100%) mixtures containing warm mix additives as a base layer on low and medium level traffic highways (FHWA/MS-DOT-RD-09-200, 2009). Compactability and indirect tensile (IDT) strength were evaluated on samples with varying RAP contents and sources, virgin asphalt content, Sasobit content and temperature. It was concluded that compactability of the WMA samples was not challenging if moderate amount of binder used. IDT strengths of samples with higher RAP content were much greater, which could indicate cracking potential (FHWA/MS-DOT-RD-09-200, 2009).

Mallick et al. (2008) studied mixtures with Sasobit at 75% RAP level at lower construction temperatures. In that study, HMA control mixes were prepared at 150°C with PG64-28 binder and at 135°C with PG52-28 binder. WMA mixtures were prepared at 125°C with both PG52-28 and PG42-42 binders. The performance tests conducted were rutting and indirect tensile strength. It was concluded that the air void of mixtures prepared with Sasobit had low variance. Similar air voids were achieved at lower temperatures. The mixtures with lower PG grade (42-42) had respectively better performance. However, long term durability and fatigue properties of these mixtures were not evaluated, which was the significant dilemma in this research.

NCAT placed two full-depth 50% RAP sections with HMA and foamed WMA, and one control HMA section with no RAP to NCAT Pavement Test Track in 2009. After the application of 10 million equivalent standard axle loads (ESAL), the high RAP WMA section performed as well as the control. No cracking, excellent rut resistance and lower texture changes were observed in the high RAP WMA section as compared to HMA control section. The performance of as the high RAP WMA was as good as high RAP HMA section (NCAT Asphalt Technology E-news, 2012).

Florida DOT placed foamed WMA section with 45 % RAP to State Route 11 in Deland, FL (Copeland et al., 2010). Additionally, a high RAP HMA mix was placed and its performance was evaluated to compare with the high RAP WMA. Performance tests included PG determination of binders, dynamic modulus and flow number. It was observed that high RAP WMA mix is softer than the control. Therefore, the high RAP WMA mix had a lower flow number than the high RAP HMA. In addition, dynamic modulus tests also confirmed that the high RAP WMA mix is slightly softer than the high RAP HMA control mix, especially at intermediate temperatures (Copeland et al., 2010).

Pennsylvania DOT initiated a study to evaluate the usage of high percent RAP in WMA pavements due to poor performance of a field section produced with 35% RAP content. The laboratory experiments were limited with one aggregate and RAP source, one virgin binder (PG64-22) with two RAP contents; 15% and 35%. In addition, the WMA technologies used in this study were limited to foaming, Sasobit and Evotherm. Although the rutting and moisture susceptibility of the mixtures were evaluated, fatigue performance and low-temperature cracking resistance were not evaluated as part of this research. It was concluded that use of anti-stripping

agent is mandatory with the foaming mixtures at 15 % and 35% RAP levels. Mixtures with Evotherm and Sasobit at 15% RAP level yielded a higher or similar TSR value compared to HMA. On the other hand, mixtures with both additives at 35% RAP level yielded lower TSR value, though they passed the minimum TSR criteria. Rutting resistance of foaming mixtures at 15% and 35% RAP levels is better than conventional HMA. On the contrary, mixtures with Evotherm and Sasobit at 15% and 35% RAP performed poor rutting resistance (Solaimanian et al., 2011).

Zhao et al. (2012) studied the performance of the WMA foamed mixtures with 30% RAP as compared to HMA with 0% and 30% RAP. It was concluded that WMA with high percentage of RAP exhibited higher rut resistance, better moisture damage resistance, and better fatigue performance.

Shu et al. (2012) studied the moisture susceptibility of plant produced WMA containing high percent RAP in Tennessee. The loose mixtures were compacted and subjected to one Freeze-Thaw cycle in AASHTO 283 and Moisture Induced Stress Tester (MIST). Their performance was evaluated through tensile strength ratio, indirect tension, dynamic modulus, and Asphalt Pavement Analyzer (APA) Hamburg wheel tracking tests. It was concluded that IDT and dynamic modulus tests are capable of accurately characterizing the moisture susceptibility. Foamed WMA with high RAP content performed as well as HMA in terms of moisture susceptibility.

Usage of Crumb Rubber in WMA pavements

Scrap tire rubber has been used in asphalt pavements since 1950s. There are numerous laboratory and field studies that showed superior performance of CR modified asphalt pavements over traditional HMA (Heitzman, 1992). However, CR modified pavements are mixed and compacted at higher temperatures as compared to conventional HMA due to their poor workability at conventional temperatures. Zhao and Amirkhanian (2009) proved that WMA technologies (Aspha-min and Sasobit) in conjunction with CR modified mixtures have the potential to decrease the construction temperature requirements while maintaining the high-performance characteristics of the pavement. In addition, Massachusetts DOT has been working on a specification to specify WMA for CR modified gap-graded asphalt mixtures (Prowell, 2009).

Cold Weather Paving

The paving season in colder regions can be extended by utilizing WMA technologies due to WMA's ability to maintain workability at lower temperatures. However, the production temperatures of WMA at cold weather applications depend on the WMA technology, ambient conditions and haul distance (D'Angelo et al., 2008).

Kristjansdottir (2006) studied the performance of WMA pavements produced with WAM Foam, Aspha-min zeolite and Sasobit wax under cold weather conditions. It was stated that dense graded mixtures are more stable and have low permeability, which is especially important when compacting in cold weather. In addition, the mixtures prepared with Sasobit and WAM Foam was found to be more resistant to rutting. Furthermore, it was shown that achieving

adequate moisture damage resistance may be a challenge when using warm mix methods and using anti-stripping agents are mostly desirable. Therefore, it is very crucial to determine the moisture susceptibility of WMA pavements in cold weather conditions. In Germany, paving was completed in various case studies using different WMA technologies when ambient temperatures were between -3°C and 4°C (D'Angelo et al., 2008).

Environmental Aspects

Environmental advantages of WMA technologies include reduced emissions and better working conditions (Anderson et al., 2008). Increased environmental awareness in Europe and the emission regulations in Kyoto protocol motivate the European researchers on developing and improving various WMA technologies. Therefore, HMA industry in Europe has been actively investigating the ways of reducing CO_2 emissions. Plant emission data from the WMA suppliers from Netherlands, Norway, Italy and France are given in Table 1 (D'Angelo et al., 2008). Futhermore, the worker exposure while placing WMA is lower than HMA, was also stated in the French, German, and Italian researches (D'Angelo et al., 2008).

Table 1: Reported reductions in plant emissions (percent) with WMA

Emission	Norway	Italy	Netherlands	France
CO_2	31.5	30-40	15-30	23
SO_2	NA	35	NA	18
VOC	NA	50	NA	19
CO	28.5	10-30	NA	NA
NO	61.5	60-70	NA	NA
NO_2	NA	NA	NA	18
Dust	54	25-55	NA	NA

In the U.S., the provision of Clean Air Act in 1990 manifested the emission regulations. Many states in the U.S. have been struggling to achieve national air-quality standards set by Environmental Project Agency (EPA). On the other hand, the gas emitted by asphalt plants is only equivalent to 0.5% of total gas emissions and EPA does not consider the asphalt plants as main concerns of the air pollution as the emission levels are lower than the regulations. Though, it is more than to be neglected by the environmentalists. In 2001, the National Institute for Occupational Safety and Health (NIOSH) in USA published a hazard review on Health Effects of Occupational Exposure to Asphalt. In this review, NIOSH evaluated the potential health effects of occupational exposure to asphalt. Lange and Stroup-Gardiner (2007) showed that the asphalt plant emission is dependent on the plant temperature. It is reported in the German Bitumen Forum that there is no emission measured below 80°C and emission is about 1 mg/h at approximately 150°C (Ruhl and Lindemeier, 2006). On the other hand, the emission drastically increases above 180°C (D'Angelo et al., 2008). Moreover, Hossain et al. (2009) stated that WMA plant emissions are about 30% to 98% of HMA plant emissions.

Economical Aspects

The economical advantages of using WMA technologies include the reduced fuel usage, long haul distance, rapid compaction and early traffic opening, which are summarized below.

Reduced Fuel Usage in WMA Pavements

The operation temperatures of WMA mixtures are generally lower that the HMA mixtures. For instance, a temperature reduction of 28°C in an average asphalt plant corresponds to about 11% fuel savings (Cervarich, 2007). As part of the NCHRP 9-47 project, it was

reported that the fuel savings in different WMA field trials varies from 15.4% increase to 77% reduction. Prowell (2009) reported the average fuel saving as 23% in WMA applications. In addition to the reduction in temperature, there are significant operational factors affecting the plant emissions such as plant design, aggregate moisture, RAP/RAS content in the mixtures and fuel type. D'Angelo et al. (2008) reported the burner fuel savings vary from 20% to 35%. In addition, Hossain et al. (2009) indicated that the overall energy consumption ranges from 20% to 75% between HMA and WMA based on the utilized technology.

Long Haul Distances and Fast Construction/Traffic Opening

The rate of cooling of WMA mixes is lower than that of the conventional HMA. Therefore, the haul distance of the mixes can be longer as the cooling rate is reduced. Thus, the proper use of WMA may result in reduced overall paving costs. In Norway, Kolo Veidekke reported that WAM foam mixture still had the ability to be placed after 48 hours. In another study, a mixture containing Sasobit was hauled up to 9 hours in Australia (D'Angelo et al., 2008).

The road constructed or maintained by WMA can be opened to traffic faster than conventional HMA. This is very promising for high maintenance roads and intersections and airports (Zaumanis, 2010). Hurley and Prowell (2006) studied the curing time of the laboratory mixtures prepared with Aspha-min, Evotherm and Sasobit. It was concluded that the WMA mixtures did not gain strength with time as compared to conventional HMA and WMA pavements do not require curing time before opening to traffic. A field section in Italy was opened to traffic five hours after paving began by Schumann Sasol (Hurley and Prowell, 2005).

Twenty four inches of WMA (Sasobit) were placed in 7.5 hours while repaving the Frankfurt airport. The runway was opened to jet aircrafts at a temperature of 85°C (Hurley and Prowell, 2005). Texas DOT opened Loop 368 at San Antonio to traffic in 2 hours after laying the WMA pavement with Evotherm (Rand, 2008).

COMMON FIELD AND LABARATORY WARM MIX ASPHALT (WMA) FOAMING TECHNOLOGIES

WMA foaming technologies in the common ground introduce small amounts of water to hot binder, either via a foaming nozzle or using a hydrophilic material such as zeolite, or through wet fine aggregates. The field and laboratory foaming technologies, that are commonly used in U.S. are listed in Table 2. Foaming is reported to be the most cost effective WMA technology as far as the long term production is concerned and also due to less material cost and ease of the production (Bennert, 2008; Middleton and Forfylow, 2009). Technologies involving water-based foaming techniques require additional equipment installed at the plant to measure and deliver the additives.

As shown in Table 2, the field foaming technologies can be divided into four major categories: (i) foaming nozzle-based methods, (ii) synthetic zeolite-based methods, (iii) indirect foaming via mixing hot aggregates with asphalt and wet fine aggregate, and (iv) shear-based mixing. All of these technologies utilize significantly different methods. Because of a wide variety of methods, WMA mixtures are produced at very different conditions (i.e., temperature, water content, asphalt absorption by aggregates, etc.). As a result, the degree of coating, amount of trapped moisture, asphalt binder absorption of aggregates may exhibit great variation. These parameters play a crucial role on the performance of the WMA pavements. However, there is no

clear understanding of the effects of different WMA technologies on the quality of the foam generated, which can significantly affect the overall global performance of the mixture. This is partly because there is no standard test method for measuring the characteristics (i.e., the quality) of foamed binders and evaluating the characteristics of the WMA mix designs.

Table 2: Common field and laboratory foaming tests

Type	Name (Manufacturer)	Warm Mix Additive / Process
(I)	Almix WMA System	Foaming Nozzle
	AquaFoam (Reliable Asphalt Products)	Foaming Nozzle
	Eco-Foam II	Foaming Nozzle
	Meeker Warm Mix	Foaming Nozzle
	Tri-Mix Warm Mix injection System	Foaming Nozzle
	WAM-Foam (Kolo Veidekke, Shell Bitumen)	Aggregate coated with soft binder then hard foamed binder is added.
	AQUABlack (Maxam Equipment Inc.)	Foaming unit installed in an existing A/C line
	Double Barrel Green (ASTEC)	Foaming Nozzle
	Terex Warm Mix Asphalt System (Terex Roadbuilding)	Foaming Nozzle
	Ulrafoam GX (Gencor)	Foaming Nozzle
(II)	Aspha-min (Eurovia)	Synthetic zeolite (~0.25% by weight of mixture)
	Advera (PQ Corporation)	Synthetic zeolite (~0.3% by weight of mixture)
(III)	Low Energy Asphalt (LEACO)	Hot coarse aggregate mixed with wet sand. Also coating & adhesion additive added (~0.5% by weight of binder)
	Low Emission Asphalt (McConnaughary Technologies)	Sequential coating using wet fine aggregate and unspecified additive
(IV)	Accu-Shear™ (Stansteel)	Mixing asphalt and water via shearing action.
(Lab)	The Foamer (Pavement Technology Inc.)	Laboratory foamer (Foaming Nozzle)
	WLB 10 Laboratory Foaming Device (Wirtgen America, Inc.)	Laboratory foamer (Foaming Nozzle)
	Accu-Foamer(D&H Equipment Ltd.)	Laboratory foamer (Foaming Nozzle)
	Asphalt Hydro-FoamerPP (D&H Equipment Ltd.)	Laboratory foamer (Foaming Nozzle)
	WAM Foam Laboratory Foaming Device (Kolo Veidekke)	Laboratory foamer (Foaming Nozzle)

Foaming Nozzle Based Methods

The working principle of the nozzle based foaming methods is to inject air and water into hot binder (>100°C) through a spraying nozzle. The water is turned into steam at atmospheric pressure, creating moisture bubbles in the binder, and significantly decreasing the overall viscosity. Yunus and Boles (1994) stated that the binder expands by a factor of 1.673. This aids in aggregate coating, mixture workability and compaction at lower temperatures. Currently, there are numerous different field and laboratory nozzle based foaming techniques. In order to illustrate the difference in working principles, a few of the methods are discussed in the following paragraphs.

AquaFoam is a nozzle based foaming method by AquaFoam, LCC (Prowell, 2008). The system consists of two fan nozzles mounted 180° apart, which are mounted perpendicular to the asphalt stream, just before it enters the drum. Addition of 1. % water by weight of the total mix is recommended by plant manufacturers.

Double Barrel Green by Astec Industries Inc. is a multi-nozzle system that microscopically foam the binder with water (Prowell, 2008). The air/water mixture (at different concentrations, typically 2% by weight of the binder) is sprayed into binder to create foam, and then the foam is forced through a narrow nozzle before mixing with aggregate. Approximately one pound of water is used per ton of mix and the mixture temperature is recommended to be from 121°C to 135°C.

In order to simulate the nozzle based foaming in the field, laboratory foaming devices are developed by several companies. As the nozzle design and foaming methods differ from technology to technology in the field, the same difference is evident in the laboratory foamers.

WLB 10 Laboratory Foaming Device by Wirtgen America Inc. is one of the devices where, air and water are individually sprayed to pressurized binder in the expansion chamber as illistrated in Figure 2b. On the other hand, "The Foamer" by Pavement Technology Inc. has a totally different nozzle system as sketched in Figure 2a. The binder flows down in a pipe (via gravity) around an air/water injection nozzle that creates conical water spray. The binder hits the injected air/water mixture, which creates the steam bubbles. In this dissertation, The Foamer is used with major modifications to increase the control on the water content and pressure as well as air pressure.

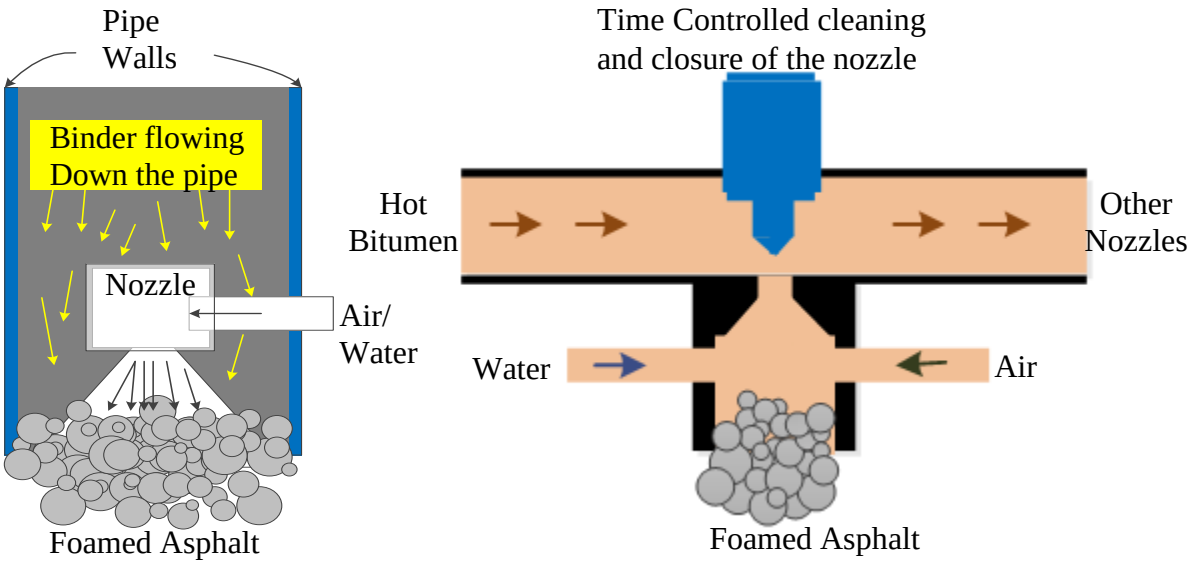

Figure 2: Working principle of a) The Foamer b) WLB 10 Laboratory Foaming Device

Synthetic Zeolite Based Methods

WMA foaming additives, Advera by PQ Corporation and Aspha-min by Aspha-min GmbH are the most common synthetic zeolites. They are composed of aluminosilicates and alkalimetals that hold about 20 % crystallized water. The water is released by increasing the temperature above the boiling point of water and creating a controlled foaming effect. It leads a

slight increase in binder volume and reduces the binder viscosity as well as providing 6-7 hours workability period till the temperature drops below approximately 100°C (212°F). It was documented that the mixing and compaction temperatures of the WMA are approximately 30^{o}C less than conventional HMA. However, foamed binder with these additives is prepared and added in different ways. Advera is added to the binder shortly prior to mixing with aggregates and generally added at 0.20% to 0.25% by weight of the total mix. Lower dosage of the additive is used as a compaction aid. On the contrary, higher dosage of the additive is used if the binder content of the mix exceeds 7% by weight of the total mix. However, Aspha-min is mixed with the aggregates and the binder at the same time and added about 0.30% by weight of the total mix.

Indirect Foaming Based Methods

The most well-known indirect foaming method through wet and hot aggregates are Low Emission Asphalt (LEA) by McConnaughay Technologies and Low Energy Asphalt (LEACO) by Lea-Co (Prowell, 2008). In LEA and LEACO technologies, coarse aggregates are initially heated to about 150°C, mixed with (unfoamed) binder along with a coating/adhesion additive. Then, cold wet fine aggregate containing approximately 3% to 4% water and recycled asphalt pavement (RAP) is added. While mixing, the moisture in the wet fine aggregate turns into steam and creates the foam.

Shear Based Mixing Methods

Accu-Shear is a shear based method by Stansteel Asphalt Plant Products that applies mechanical shear to mix the water and/or WMA additives by a colloidal mill (Prowell, 2008). The binder is foamed dynamically by adjusting the rate of shear, which is assumed to increase

the life of the foam. Typically, one gallon of water is used for one ton of mixture (personal communication with Oldcastle Materials, a nationwide paving contractor).

WMA MIX DESIGN AND SPECIFICATIONS

In Europe and U.S., WMA pavements are constructed with a range of layer thickness, in a wide variety of traffic levels, utilizing different aggregate skeletons such as dense graded, stone matrix, porous and mastic asphalt pavement. In Norway, WAM foam process is allowed by Norwegian Public Roads Administration. In Germany, a bulletin called as "Merkblatt" is released for the construction of WMA pavements utilizing five modifiers, i.e. Fischer-Tropsch wax, Montan wax, fatty acid amides, a blend of Montan wax and fatty acid amides, and zeolite (Prowell, 2008). In France, Service of Technical Studies of the Roads and Expressways (SETRA) certified Aspha-min zeolite in 2007 (Prowell, 2008).

Asphalt pavement mix design is typically different in Europe as compared to U.S. In addition, materials used in the asphalt pavements are also different. For instance, the water absorption of aggregates is less than 2% in most regions of the Europe, though it is much higher in the U.S. Although WMA technologies significantly drop the pavement production temperatures, the production temperatures are above the suggested temperatures in U.S. than Europe in order to ensure the coarse aggregate dryness.

NAPA and FHWA formed WMA Technical Working Group (WMA TWG) in 2005 (Prowell, 2008). The group had representatives from FHWA, NAPA, NCAT, NIOSH, State Asphalt Pavement Associations (SAPA), American Association of State Highway and Transportation Officials (AASHTO) and the Hot Mix Asphalt Industry. Their mission was to evaluate and validate WMA technologies and foster the environmental concerns. The WMA

TWG submitted three high priority research needs statements that were combined into two projects by the NCHRP: i) Project 09-43 "Mix Design Practices for Warm Mix Asphalt Technologies" for fiscal year 2007, ii) Project 09-47 "Engineering Properties, Emissions, and Field Performance of Warm Mix Asphalt Technologies" for fiscal year 2008.

The objective of NCHRP 09-43 was to develop a WMA mixture design and performance analysis procedure for a wide range of WMA technologies in the U.S. Therefore, a procedure similar to AASHTO R35 was developed for the design of dense graded WMA mixtures based on limited empirical data. The first phase of this project included analyzing: (i) the effect of sample reheating on the properties, (ii) the binder grade selection, (iii) the conditions for short term conditioning, (iv) the degree of mixing that occurs between the RAP and new binder, (v) the workability of mixtures, and (vi) the continuum damage fatigue analysis. The second phase of the project was to evaluate the first phase and included: 1) the mix design study, 2) the validation study to compare the laboratory and field produced WMA mixes, 3) the study to assess the fatigue properties of mixes produced at lower temperatures. NCHRP Report 691: Mix Design Practices for Warm Mix Asphalt was published as the final report of NCHRP 9-43 in 2011. The NCHRP Report 691 suggested that the compactability, moisture sensitivity and rutting resistance of WMA are significantly different than HMA and should be evaluated according to draft Appendix of AASHTO R35 for WMA. The findings of the project in binder selection can be listed as followings: The stiffness of the recovered binder from the mixtures can drastically decrease when the production temperatures are extremely low. However, low WMA production temperatures enable minor improvements in the low temperature grade of the binder. On the

contrary, if the production temperatures are extremely low, the high temperature grade of the binder needs to be increased in order to meet the flow number (rutting resistance) requirements.

The foamed WMA binder properties (such as viscosity) continuously change with time. Therefore, mixing and compaction temperatures cannot be determined from the binder viscosity. It was suggested in NCHRP 9-43 that the coating and compactability of the mixtures should be determined directly. In addition, WMA pavements can be more prone to moisture damage than HMA pavements. Therefore, the effect of anti-stripping agents was also studied during the NCHRP 9-43 project. It was stated that 67% of the mixes with the help of the agents had the same or improved TSR value than WMA mixtures prepared without agents.

The mixture tests indicated that short-term aging (2 hours) is adequate to condition WMA mixtures. It was observed that the virgin binder coats the virgin aggregates and RAP during the mixing period, and then the RAP and virgin binder continue to mix during the storage at elevated temperatures. Thus, the short term conditioned samples better represent the field performance of WMA pavements because of the less aging at lower mixing/compaction temperatures. The performance test sample preparation criteria for WMA mixtures are set as 2 hours of short-term conditioning at the compaction temperature since this duration is adequate the simulate the binder absorption and stiffening that occurs during the construction.

Recent national research projects on WMA are: NCHRP 9-47A: Properties and Performance of Warm Mix Asphalt Technologies, NCHRP 9-53: Properties of Foamed Asphalt for Warm Mix Asphalt Applications, and NCHRP 9-55: Recycled Asphalt Shingles in Asphalt Mixtures with Warm Mix Asphalt Technologies. In both Europe and U.S., there are still lots of

unknowns and concerns about the WMA technologies and their long term performance. In addition, there is no standard preparation, production, evaluation and lay down specifications on the WMA pavements.

FOAMED BASED WMA PAVEMENT APPLICATIONS

While there are numerous advantages of WMA over HMA, WMA is still a relatively new technology and several concerns about WMA technology such as long-term performance and moisture susceptibility still need to be addressed (D'Angelo et al., 2008). Foamed binder was first developed by Dr. Ladis Csanyi to improve the properties of poor quality Iowa aggregates in Bituminous Research Laboratory of the Engineering Experiment Station at Iowa State University about fifty years ago (Jenkins, 2000). The steam was injected to heated binder using a nozzle to produce controlled foam. Cold and wet aggregates or soils were easily coated with the foam binder due to its reduced viscosity and the increased surface energy (Lee, 1980). Mobil of Australia got the patent rights of Csanyi's foamed binder process in 1968. They developed and patented the expansion chamber and nozzle system, called as Foamix, to inject 1-2% cold water with steam in 1971.

Foamed binder in base/subbase applications

Foamed binder has long been used in the soil and base/subbase stabilizations. In these applications, typically wet unheated aggregates and asphalt cement are mixed while the asphalt is in foamed state to form fairly stiff (mortar like) material. In the 1970's, over 16 countries were using foamed binder for the base/subbase stabilization in Europe and South Africa. Although foamed binder was first developed in U.S., the first documented application was by the Georgia Department of Transportation, in Ware County in 1982 (Raffaelli, 2004).

Nataatmadja (2001) summarized the advantages of foamed binder stabilization as: (i) increase in strength over unbound materials, (ii) quick construction, (iii) lower cost than reconstruction, (iv) immediate traffic and (v) improved durability. In addition, past researches indicated that a wide range of aggregates from crushed stone to silty sands can be used with foamed-bitumen in the stabilization. However, the fine content of mixes is crucial and should preferably be above 5% by weight of the mix (Ruckel et al, 1983). Sakr and Manke (1985) and Bissada (1987) showed that the mixes with high percentage fines (around 10%) were more stable and had high tensile strength since the binder primarily concentrated in the finer fraction of the aggregates. However, there were many concerns in these applications since there are no complete specifications and standards. The most extensive design guides are: (i) South African Interim Technical Guideline: The Design and Use of Foamed Bitumen Treated (2002), (ii) Wirtgen Cold Recycling Manual (2004).

Moisture is crucial to soften and break the agglomerations between the aggregates and to diffuse the binder in the mixture during the mixing and compaction. However, one of the primary concerns in the stabilization is the trapped moisture in the pavement layers. It was indicated by Csanyi (1960) and Ruckel at al. (1983) that the quantity of the water is not critical. However, if inadequate amount of water is used, it prevents the dispersion of foam, workability and compaction of the mixture. On the contrary, if excessive water is used, it extends the curing time and reduces the density and strength of the mixture (Brennen et al., 1983). Bowering (1970) indicated that the mixture gains full strength only after certain period of time where curing (water evaporation/dissipation) takes place. Ruckel et al. (1983) stated that the failure (rutting and raveling) of foamed asphalt mixtures occurs usually weeks after the construction not years.

This is because of insufficient curing (water dissipation) of the foamed asphalt mixture. Clarke (1976) confirmed this when he found out that the engineering properties of the mixture improve with age and temperature. Because of these findings, Lee (1981) recommended that effects of curing on the strength development of specific mixtures should be evaluated locally and the specifications should be created accordingly. Engelbrecht et al. (1985) suggested using low stockpiles (i.e., store in relatively small quantities to increase exposed surface area) after mixing so that the moisture dissipates more rapidly and mixture gains full strength faster. However, care should be taken not to "over-cure" the mixtures in order not to hinder the workability during placement and compaction.

Initial foam binder base stabilization was performed using virgin materials (Acott, 1979; Bowering, 1970; Bowering, 1976; Lee, 1981; Ruckel et al., 1980). Due to the shortage of virgin materials, foamed asphalt begun to be implemented in the form of full depth reclamation (FDR) to efficiently utilize old asphalt pavement (Brennen et al., 1983; Engelbrecht et al., 1985; Van Wijk et al., 1983). In the 1980s, several foamed asphalt projects were placed in Colorado and Wyoming. In Maine, the first foamed asphalt full depth reclamation project was constructed in June 2001 (Marquis et al., 2003). In Louisiana, the foamed asphalt treated RAP was utilized for the first time as a base material in lieu of a crushed lime stone base underneath a concrete pavement layer in January 2002. This study consisted laboratory foamed asphalt treated RAP mix designs, field test sections and field evaluation of strength/stiffness of foamed asphalt base course. It was concluded that foam asphalt treated RAP mixtures had higher in-situ stiffness than the lime stone base. In addition, it was indicated that there was no significant stiffness

changed between the 100% RAP mix and thee mix with the combination of 75% RAP and 25% crushed stone (Mohammad et al., 2003).

The foamed asphalt improves the workability, stiffness, and strength, and reduces moisture sensitivity with the inclusion of active (portland cement, lime) and/or inert (fly ash, mineral fines) fillers. FDR is generally used to rehabilitate the crack pavements and to eliminate the effects of reflective cracks in California (Jones et al., 2008). Jones et al. (2008) studied the identification of the properties affecting the performance and distress mechanisms of materials recycled with foamed asphalt and the determination of the acceptable ranges of the properties of FDR foamed asphalt materials in California. It was concluded that foamed asphalt material with a cementitious filler can be used as a rehabilitation option on thick and crack asphalt pavements on highways, in which the traffic is less than 20,000 vehicles per day. This method is also applicable to pavements where multiple overlays have been placed on a weak base and where cracks reflect through overlay. In addition, the recycled layer can be used as a subbase underneath a new base layer. However, the performance of FDR should be assessed for each project, mix design and construction.

Cold in-place recycling (CIR) with foamed binders is another common way of rehabilitation of existing pavements (Kim and Lee, 2006; Kim et al., 2006). In 2002, two different stabilizing agents (asphalt emulsion and foamed binder) used at a section of Route 20 in Iowa. Foamed and emulsion based stabilization differs in many ways such as aggregate coating. As indicated before, the foam binder tends to initially coat the fine and small aggregates. The coarse aggregates adhered with the asphalt mastic. On the contrary, emulsions coat the coarse aggregates and they bind the uncoated fine aggregate. Moreover, foamed asphalts have shorter

curing time and results early opening to traffic due to the lower water contents in foamed asphalt stabilization compared to the water in emulsion treatments. It was concluded that indirect tensile strength (IDT) of foamed CIR is critical and should be evaluated. However, IDT is not adequate by itself and it was recommended that further tests such as dynamic modulus and dynamic creep tests should be conducted. Ramanujam and Jones (2007) also indicated that foamed asphalt stabilization performed better than emulsion-treated stabilization.

Foamed Binder in the Surface Layer Applications

WMA pavements in surface layer applications are relatively new and there are similar unknowns and questions to be answered as stabilization (Diefenderfer and Hearon, 2008). These questions are primarily related to their long-term performance. One of the primary concerns is their potential moisture susceptibility (Kvasnak et al., 2009). In most of the WMA products, water (steam) is introduced into the mixture to reduce the viscosity at low temperatures. It is still unclear if additional moisture added to the mix can cause long-term problems such as stripping. Incomplete drying of the aggregates at lower temperatures may further accelerate the moisture damage in WMA pavements (especially with absorptive limestones) (Diefenderfer and Hearon, 2008). Current knowledge on diffusion and evaporation of moisture in foamed WMA is limited. The foaming process decreases the over viscosity of the asphalt mixture so that it is workable during construction. However, after construction, viscosity increases rapidly as the foam disappears and temperature drops. During the process of dissipation of foam, if the temperature decreases rapidly, the moisture may not escape and may be trapped inside the mixture. This trapped moisture can cause detrimental failures by breaking the adhesive bonds between the aggregates and the asphalt binder (through diffusion and because of freeze/thaw cycles). It can

also destroy the cohesive bond within the binder over time and during application of the traffic load. Therefore, it is crucial to know how the moisture escapes from the asphalt mixture as the specimen cools down and foam disappears. However, the knowledge on evidence of moisture susceptibility is limited and mostly depends on the empirical studies.

Hurley and Prowell (2005) reported that WMA mixtures made of Aspha-min exhibited low Tensile Strength Ratio (TSR). A laboratory research performed by Bhusal (2008) indicated that TSR values for WMA mixtures made with Zeolite were lower than the TSR of control (HMA) mixtures. Hurley and Prowell (2005) showed that Hamburg wheel tracking tests showed evidence of moisture damage, with lower number of cycles to stripping inflection point. Field cores in that project also showed low TSR. On the other hand, Powers (2008) indicated that there is no visible difference in TSR tests between WMA and HMA samples on 7 different WMA projects in Ohio. In all of these projects, ASTEC Double Barrel Green (DBG) foaming technology was used. Kvasnak et al. (2009) analyzed the moisture susceptibility of two laboratory and plant prepared mixtures with Evotherm DAT in Birmingham, AL. The study indicated that laboratory prepared WMA mixtures had more tendency to moisture susceptibility than plant produces mixtures. Additionally, the control (HMA) mixtures performed better than WMA, though most of the WMA samples met the moisture criteria. Xiao et al. (2010) investigated the moisture damage in WMA mixtures containing moist aggregates. The conventional moisture susceptibility tests such as indirect tensile strength (ITS), TSR, toughness and percentage of toughness loss were run to laboratory prepared samples with Aspha-min and Sasobit. ITS values and deformation resistance decreased for mixtures containing moist aggregates. WMA modification method did not show significant effect on toughness values.

Kavussi and Hashemian (2011) investigated the WMA foam mixes based on their moisture susceptibility and rutting potential by utilizing ITS and wheel tracking tests. These studies indicate that there is no common ground regarding to the moisture susceptibility of different WMA technologies. Wielinski et al. (2009) assessed the field and laboratory performance of WMA utilizing ASTEC DBG and HMA sections composed of same aggregate skeleton. Production temperature was the only property changed in the design. Therefore, the initial stiffness of the WMA section was lower than HMA due to lower production temperatures. As expected, the performance tests indicated lower Hveem stability, Marshall Stability and flow, and higher Asphalt Pavement Analyzer (APA) rut tests.

Rutting is the other main concern in WMA mixture design (NCHRP Report 891 and 714). WMA pavements have early rutting failure potential, right after construction under traffic load. Rutting potential increases due to reduced aging of the binder (Su et al., 2009). Goh and You (2007) studied the performance of WMA prepared with Aspha-min in the laboratory. Lower rutting depth and a higher indirect tensile resilient modulus were observed at higher compaction temperatures. On the other hand, there was no significant difference on the resilient modulus of samples compacted at low (100°C) and relatively high temperatures (120°C). Dynamic modulus of samples compacted at high temperatures (120°C) was significantly higher than WMA compacted at 100°C. Hurley and Prowell (2008) analyzed WMA field sections in St. Louis, Missouri, and Milwaukee, Wisconsin by utilizing the following WMA technologies: Sasobit, Evotherm, and Aspha-min. The conclusions drawn were: WMA sections had better or equal in-place densities than control sections, 6 months after the construction. It was observed that WMA sections are slightly more susceptible to rutting based on the results of APA rutting test. West

(2009) indicated that lower compaction temperatures make the WMA mixtures more susceptible to moisture damage. Kanitpong (2007) showed that Sasobit improved the compactability of asphalt mixtures at significantly reduced temperatures and these mixtures performed better in rutting and fatigue resistance and achieved higher shear complex modulus. You et al. (2011) evaluated the mixtures prepared with Aspha-min. Dynamic modulus tests (|E*|) were performed and resulted that WMA with Aspha-min had no significant effect. It was also found that increasing amount of Aspha-min significantly improved the rutting resistance of the mixture. Xiao et al. (2012) studied the effect of compaction temperature on the moisture susceptibility and rutting of foamed WMA mixtures based on foamed aggregates. The experimental matrix consisted two aggregate moisture levels (0% and ~0.5% by weight of the dry mass of the aggregate), one lime content (1% lime by weight of dry aggregate), two foaming water contents (2% and 3%) with control, and two aggregate sources. Compactability, ITS, rut depth of both conditioned and unconditioned and flow number of each samples was assessed. It was concluded that the aggregate source drastically affects the ITS and rutting resistance regardless of the foaming water content, aggregate moisture content, and compaction temperature. The samples with moist aggregates were more compactable regardless of aggregate type, foaming technology and compaction temperature. In addition, the ITS values of foamed mixtures containing moist aggregate increased as the compaction temperature increased. Moreover, the rut depths of all the conditioned and unconditioned mixtures slightly increased when their compaction temperatures decreased, regardless of aggregate moisture content, foaming water content, and aggregate type. Ayman et al. (2012) studied the performance of laboratory foamed WMA and compared with the conventional HMA. The test matrix was composed of two aggregates (crushed limestone and

natural gravel) and two asphalt binders (neat PG64-22 and polymer modified PG70-22M) and following tests were utilized: ITS, |E*|, TSR and APA. Foamed WMA mixes had lower ITS values and more susceptible to moisture damage than HMA. Meanwhile, there was no significant difference in the dynamic modulus of WMA and HMA, though WMA mixes were more susceptible to rutting failure. It was proved that the aggregate and binder type had a significant effect on the performance WMA pavements.

Fatigue life of WMA pavements is another issue to be investigated. WMA pavements may have longer fatigue life and higher fatigue characteristics because of the reduced aging of the binder during mixing/compaction (NCHRP 374). However, Jones et al. (2009) stated that WMA technologies do not affect the fatigue performance. Additionally, mixture stiffness decrease due to the limited aging of the binder. Therefore, it provides WMA mixtures to incorporate more recycled asphalt pavement than HMA mixtures. It was observed that some of the WMA additives can increase the potential for low temperature cracking based on the binder tests (Jones et al., 2009). Xiao et al. (2009) investigated the fatigue performance of rubberized WMA pavements. The test beams (for Four Point Bending Beam (FBBB) test) were prepared with one rubber size (#40 mesh), two aggregate sources, two WMA additives (Aspha-min and Sasobit) and tested at 20°C. It was indicated that compaction and mixing temperatures of the crumb rubber asphalt concretes significantly reduces with the WMA additives. Additionally, inclusion of the WMA additives extended the fatigue life and increased the stiffness of the rubberized WMA pavements with respect to control (HMA) pavements.

Based on the findings of past research, it is important to perform laboratory experiments on moisture susceptibility, rutting and fatigue cracking on the WMA specimens, in order to

predict the effect of foamed binder characteristics on the long-term performance of WMA pavements in the field.

CHARACTERIZATION OF FOAMS IN VARIOUS DISCIPLINES

Foam is described as a thermodynamically unstable colloidal dispersion in which a gas is dispersed in a continuous liquid phase (Schramm, 2005). Foams are investigated in various disciplines because of its widespread application in life. For instance, food industry (champagne, soda heads, whipped cream etc.), detergent industry (dishwashing and clothes-washing), personal care products (shaving cream, bubble bath foam, hair shampoo suds), process industry (foam blankets, fire extinguishing foams, mineral and oil flotation froths) are the common foam application areas in everyday life (Schramm, 1994).

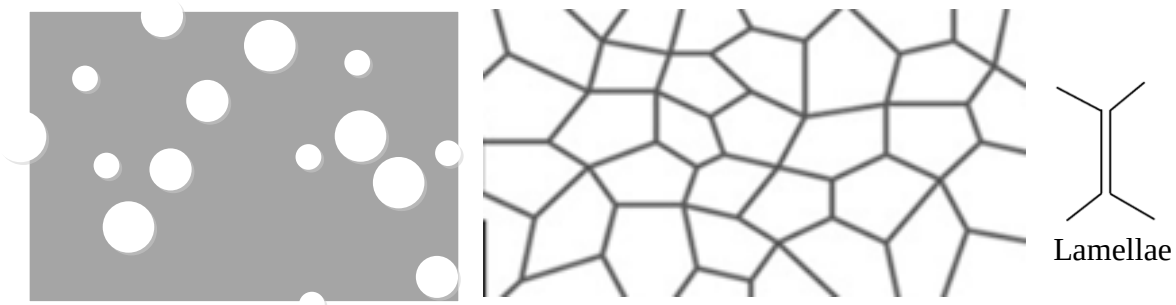

Figure 3:The structure of foams a) Type 1: Kugelschaum or wet foam b) Type 2: Polyederschaum or dry foam.

Foams in different disciplines are typically classified as Type-1 and Type-2 due to their structures (shapes) as shown in Figure 3 (Sebba, 1987; Schramm, 2005). Type-1 foams have well separated spherical bubbles in the liquid, where the liquid volume is the same or larger than the bubbles. This type is also known as Kugelschaum or wet foam, gas emulsion or ball foam. Type-

2 foams have non-spherical (polyhedral) bubbles separated by almost flat liquid films called lamellae. This type of foams is referred as Polyederschaum or dry foam. Jenkins (2000) indicated that the foamed asphalts used in base stabilization applications are more close to Type-2 foam. However, Kutay and Ozturk (2012) showed that the bubbles in foamed WMA binders made using a laboratory foamer are spherical and similar to Type-1. This study is discussed in Chapter 6.

The characterizations of the foams are commonly assessed in terms of their stability. The foam stability is evaluated against: (i) film thinning and (ii) film rupturing (Schramm and Wassmuth, 1994). In the film thinning process, the bubbles are separated with thin films (liquid-films) and no change in the total surface area of the foam is observed when the bubbles touch each other. On the other hand, in the film rupturing process, the bubbles are turned to one single larger bubble when the bubbles coalesce. Therefore, the total surface area decreases with time.

As referred in the description, foams are thermodynamically unstable and it is crucial to quantify their evolution with time. Typical tests for characterization of foam stability are divided into three major categories: (i) lifetime of individual bubbles, (ii) static foam tests and (iii) dynamic foam tests (Schramm, 2005). The measurement of bubble lifetime is not commonly used since small contaminations and vibrations influence the results and reproducibility is not good (Schramm, 2005). In static foam tests, typically a constant volume of foaming solution in a pipette is allowed to fall a specified distance with recording the time into a separate volume of the same solution that is contained in a vessel. Decay of the volume of the foam as well as the initial volume (right after draining of the fluid above) is measured (ASTM D1173-53: Ross and Miles Test) as shown in Figure 4a. There are simpler tests such as ASTM D3601-88 (Bottle

Test), D3519-88 (Blender Test) and DIN 53902 Part 1 (Perforated disk test), which are also variations of the static foam tests where reduction in height of the foam over time are measured. The main difference is how the foam is generated such as poring, shaking, beating and stirring (Barel et al., 2005). In dynamic foam tests, foam is generated by flowing gas through a porous orifice into the fluid as shown in Figure 4b. The volume of the foam is measured when steady-state flow is achieved. Examples of such tests include ASTM D892-92, D1881-86 (Diffuser Stone Test) and D3427-86 (Gas Bubble Separation Test). The difference between the tests is the foam generation method such as air injection and circulation (Barel et al., 2005). It should be noted that unlike foams in many other disciplines, there is typically no static foam layer on the surface of the binder in foamed WMA applications. The bubbles rising to the surface typically collapse and disappear. Therefore, dynamic foam tests are probably not applicable to foamed WMA binders.

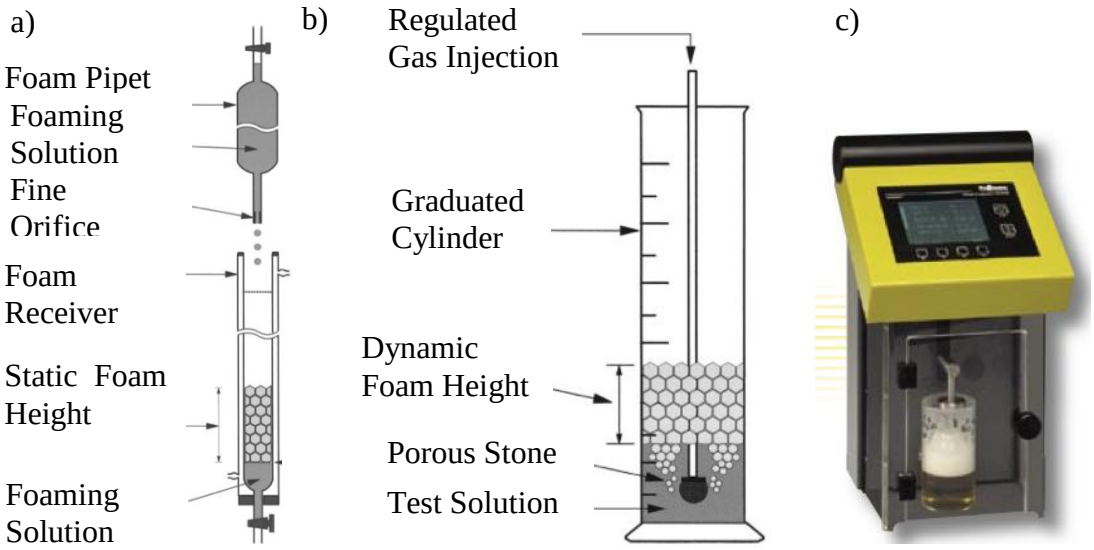

Figure 4: (a) Static and (b) dynamic foam tests (Source: Schramm 2005) and (c) NIBEM-T foam stability system.

In most of the ASTM tests described above, the foaming characteristics of the fluid are measured for individual foaming method (e.g., pushing air through the porous stone). However, there are various methods of making foam in WMA applications. Therefore, the test method for foamed WMA should be such that the foamed WMA specimen sampled at the plant or laboratory device can be measured and compared to a baseline method. As a result, some kind of static foam test is needed, where the reduction in height of the overall foamed asphalt is measured.

The NIBEM-T foam stability instrument (Haffmans, 2012) is an equipment typically used to measure the reduction in foam height of beers (Figure 4c). In this system, a movable plate with three electrodes is lowered to make contact with the surface of the foam. As the foam collapses, contact between the electrodes and the foam is lost. The instrument continuously moves the plate down to restore contact. The measured rate at which the plate is lowered quantifies the rate of collapse of the foam. However, in its present configuration, this system has operation temperature range between -5 and 40^{o}C, which will not allow testing of foamed binder. Guillerme et al. (1993) developed an apparatus to analyze the formation and stability of foams that is coupled with a video camera. The system evaluates the foam texture as well as the physical characteristics, such as foam volume and the liquid in the foam. However, the overall system is not applicable for WMA because of its opaque nature.

The other methods to determine foam stability also include the physical properties of the foam such as density and viscosity. German and McCarthy (1989) utilized MRI imaging to measure the dissipation rate of the foam. The variation in the proton signal across the imaging plane with time meets the change in density and indirectly the dissipation pattern for every point

in the foam. However, this method cannot be applied to foamed binder since the rate of the dissipation with time is variable due to temperature decrease of the foam and rapid density change. Hutzler et al. (1995) used AC Capacitance method to measure the density of the non-ionic detergent solution (foam). A trial was done to measure with the capacitance of foam binder in Advanced Characterization Asphalt Laboratory at Michigan State University. However, it was observed that the foam dissipates before the capacitance stabilizes. Therefore, it is not applicable and practical for foamed binder.

Neu (1960) presented various methods of foam measurement and defined several parameters to characterize foam. The focus of this research was on the foams generated by shampoo and toothpaste. He developed a method using Sunbean mixer to assess the foaming profile. He defined parameters such as (i) Specific Foam Volume (ml/g), (ii) Density= Mass of Foam/Volume, (iii) Viscosity = measured using Modified Techne Viscometer, (iv) Light Transmission: The loss of light transmission through a layer of foam is a function of the degree of dispersion of air, (v) Photomicrography: The particle size distribution and specific surface area of the foam measured on a 100 cm^2 area, and (vi) Foam Drainage. Among these methods, most appropriate parameters that may apply foamed binder are probably the particle (bubble) size distribution and specific surface area.

FOAMED WMA BINDER PROPERTIES BASED ON THE CONVENTIONAL BINDER TESTS

As stated before, there are various foamed binder technologies. Therefore, the foam characteristics are scattered in a wide range because of the technology, temperature, water content, air pressure, additive content, etc. The preliminary studies and discussions stated that the

test methods for the foams summarized in section 0 are not applicable to the WMA foamed binders because of their temperature, opaque nature etc. On the other hand, many researchers in the pavement area have attempted to characterize foamed binder properties by modifying or utilizing traditional HMA binder tests.

Saleh (2006) used Brookfield viscometer to measure the change in viscosity of the foamed asphalt with time. As an alternative measure of the quality of the foamed asphalt, he suggested that the average foam viscosity over the first 60 seconds of foaming could be used. It should be noted that foams are typically non-Newtonian fluids (Schramm 2005). Therefore, their viscosity depends on the applied shear rate. Also, steady-state shearing motion is needed to measure a correct viscosity. It is important to evaluate the repeatability and accuracy of viscosity measurements in highly dynamic (unsteady) foamed asphalt, which is typically, collapses quickly. While the method may be promising, care should be taken while defining and interpreting the viscosity measurements.

Gandhi and Amirkhanian (2007) used Brookfield viscometer and Dynamic Shear Rheometer (DSR) to analyze the variation in the binder properties right after binder modification and after aging to simulate the plant shutdown. The samples were prepared by two different WMA modification methods were used foaming additive (Aspha-min) and non-foaming additive (Sasobit). The initial viscosity tests were run at 135 and 120°C at 30, 60 and 90 minutes of adding the WMA additives. The $|G^*|/\sin\delta$ at the PG temperature and at the failure temperature were measured. Then, the binders were aged at 120°C for 3 days. Their viscosities were measured at 135°C and PG grade of the aged binders were determined. It was clearly observed that the effect of WMA additives significantly is dependent on the chemical properties of the

asphalt binders. Additionally, it was noted that Aspha-min increased the viscosity of the base binder. On the other hand, Sasobit significantly decreased the viscosity of the binder.

Wasiuddin et al. (2007) studied the rheological properties of two binders (PG64-22 and PG70-28) with Sasobit and Aspha-min. The additives were added 2%, 3% and 4% by weight of the binder. It was concluded that the change in the amount of Sasobit had no effect on the mixing temperature of PG64-22. On the other hand, the mixing temperature of PG70-28 decreased by 10°C, 12°C, 13°C for added 2%, 3% and 4%, respectively. Moreover, it was observed that the amount of Aspha-min had no effect on the mixing temperatures. The G*/sin(δ) measurement indicated that both Aspha-min and Sasobit had no negative effect on binder grading due to high temperature viscosity reduction. In addition, the authors performed rutting measurements on the WMA mixtures. It was stated that that rutting potential decreases with decreasing mixing and compaction temperatures.

Binder lubricity test for DSR was introduced to evaluate the workability of asphalt binder (Hanz et al., 2010). It was stated that internal friction of asphalt binders decreased by the inclusion of additives. Hence, this provided the aggregates to compact at lower temperatures. The setup that Hanz et al. (2010) used is composed of three balls mounted on a ball assembly and a fourth ball placed on the tip of rotating chuck. A thin film of lubrication fluid is spread in between the ball assembly and chuck .Then, the chuck is rotated in one direction. The testing temperatures are selected in between 80-100°C due to the limitation of the DSR apparatus. The normal forces are suggested to be 20 and 30 N to maintain the contact between the assembly and the chuck under 50 revolutions per minute (rpm). The measured coefficient of friction is used to evaluate the effect of binder grade and WMA additive. It was stated that the viscosity reduction

is not the only factor to reduce the production temperatures since no dependence on the shear rate was observed.

Nazzal and Qtaish (2013) utilized Atomic Force Microscopy (AFM) to evaluate the moisture susceptibility and healing characteristics of WMA pavements. Various AFM technologies such as tapping mode imaging and force spectroscopy were performed on two types of binders using four WMA technologies (Advera, Evotherm, Sasobit, and foamed WMA). AFM images introduced the dimensional changes in the foam structure (bee-like) within the virgin and polymer modified asphalt binders. Sasobit additive decreased the size of the bee-like structures within the neat and polymer modified asphalt binders. On the other hand, no significant difference in the structure dimensions was observed in other WMA technologies. Therefore, the stiffness of binders with Sasobit measured to higher than the other binders as the higher shear modulus values obtained in the DSR test. In addition, it was observed that nano-scale adhesive forces increased in all binders in the utilization of WMA technologies before the moisture conditioning. The forces measured to be highest in Advera and foamed WMA and lowest in Sasobit. Therefore, Sasobit mixture can have lower indirect tensile strength value than the other mixtures. In addition, the AFM analysis showed that these adhesive forces significantly decrease after moisture conditioning in both the control (HMA) and mixtures produced with different WMA technologies. However, the stress reduction was the least in the Evotherm WMA and the control mixtures and the highest in the Advera WMA. Therefore, it was expected that Advera WMA can have the least TSR value in overall mixtures. In addition, the AFM force spectroscopy experiments stated that TSR value depends on the adhesive forces between the aggregates and the binder. Moreover, AFM healing experiments indicated that WMA

technologies except the Sasobit improved the micro-crack closure rate. It was concluded that AFM measurement is feasible to study the moisture damage and healing phenomena in WMA mixtures.

Huang et al. (2012) used neutron scattering technology to determine the microscopic structure of asphalt and for determining the presence of moisture and its distribution in foamed binder. The resolution varies from 200 nm to 1 nm under the small angle neutron scattering (SANS) in the vector transfer range from 0.003 Å-1to 0.5 Å-1. Two types of asphalt binder (PG64-22 and one from Korea) and ordinary and heavy water (deuterium oxide, D2O) at 4% by weight of binder were used to make samples at 150°C via a laboratory foaming device. However, the sampling of the foamed binder was poor and water dissipated through the sampling. Therefore, the authors' conclusions were debatable since no water entry less than 0.1 µm was observed in the foamed asphalt and it was claimed that if water greater than 0.1 µm exists, no micro-structural changes were detected less than 0.1 µm.

SYNTHESIS OF PREVIOUS RESEACHES AND MOTIVATION OF CURRENT STUDY

While the WMA technologies are appealing, the long-term performance of WMA as compared to HMA is not well-known in U.S and Europe. WMA's disadvantages are mainly related to rutting and moisture susceptibility issues as referred. Premature rutting failure has been reported for surface asphalt concrete in different studies. This has been mostly related to decreased ageing at lower production temperatures and increased moisture content for foaming technologies. In addition, it is early to rely on the long term performance of WMA pavements based on the laboratory studies. It should be recalled that the first field sections constructed in U.S. are less than nine years old. The first sections constructed in Europe (Germany and

Norway) are about fourteen years old. Since water is injected in most of the WMA foaming technologies during the initial mixing process. Residual water in the mixture can cause premature rutting and stripping due to incomplete vaporization. Therefore, the moisture susceptibility of mixtures should be carefully evaluated. Moreover, most of the current design methodologies of WMA foamed asphalt pavements are based on the WMA plant manufacturers' recommendations and past experience of the contractors. Such design approach has lead to premature WMA pavement failures (Kim et al., 2011).

NCHRP 09-43 Final Report is the most recent study in U.S. This report suggests a WMA mixture design specification which is primarily based on limited empirical data (Bonaquist, 2011). In addition, most of the current knowledge on WMA is based on empirical data and there is a significant lack of understanding of the fundamental behavior of the foamed binder used in WMA pavement. Understanding the WMA foamed binder characteristics that affect the mechanical behavior of pavements, is crucial to accurately predict and improve its long term performance. Therefore, there is a growing need for understanding the WMA pavements from binder production to mixture performance.

There are four major challenges in understanding the foamed WMA pavement. First, the foamed binder quality indicators should be determined such as expansion ratio, half-life and foam index etc. Secondly, a repeatable testing method should be developed to repeatedly and precisely measure and calculate these quality indicators. Thirdly, the foam structure should be observed with time to understand the workability of the binder as well as the physical properties of the binder such as residual water. Finally, the performance of the WMA pavements should be consistent with the foam binder quality indicators.

To respond to these needs, this research; (1) identified various parameters as foam binder quality indicators, (2) developed a practical laboratory device to measure these parameters, (3) validated the device by comparing with nondestructive 3D imaging methods (i.e., x-ray microtomography), (4) investigated the relationship between the binder quality indicators proposed and the mixture performance tests, (5) investigated foaming characteristics of different kinds of binders, (6) investigated the effects of air pressure and water content on the foamed binder and mixture performance.

CHAPTER 3

FOAMED BINDER PARAMETERS FOR WMA

Making foamed binder is relatively simple process where hot binder is mixed with a limited amount of water (typically 2-3% by weight of the binder). However, the rheology of the foamed binder is not way simple. The quality of the foamed binder depends various factors such as the binder type, grade and modification, the foaming technology used, amount of water, temperature etc. Moreover, the quality of the binder plays a crucial role during the mixing, laying and compaction stages of warm mix asphalt pavement production.

Typically, the mixing and compaction temperatures of the asphalt pavements are determined by the viscosity of the binder, which is an indicator of the mixture workability. However, measuring the viscosity of the foamed binder leads to disturbance to bubbles and unreliable values. It should be also noted that the viscosity of the foamed binder is time dependent, in which the viscosity of the foamed binder varies with both time and temperature. Therefore, researchers developed parameters such as expansion ratio, half-life and foam index, as a measure of the quality of foamed binders. These parameters are discussed in detail in the fallowing section. In addition, the factors influencing the foam quality have been studied by various researchers.

Abel (1978) concluded that the silicone content in bitumen reduces the foaming abilities of binder. Binders with relatively low viscosity had a tendency to foam more than those with

high viscosity. Thus, they had more expansion and shorter half-life. On the other hand, it was observed that the higher viscosity binders resulted better aggregate coating due to longer half-life. Abel (1978) also suggested that the temperature should be above 147°C for acceptable foaming quality.

Barinov (1990) proved that the increase in the concentration of asphaltenes increases the expansion ratio and half-life of the binders. Asphaltenes act as surfactants reducing the surface tension in the bubbles, which result in the delay of foam collapse. On the other hand, Lesueur et al. (2004) concluded that bitumen composition did not significantly influence foam characteristics. It should be noted that very limited research data is available on the effects of binder composition on foam characteristics. Castedo-Franco and Wool (1983) indicated that any binder independent from its type, grade and source could be foamed with the proper combinations of the nozzle type, water content, air and bitumen injection pressure.

Namutebi et al. (2011) studied the affect of the foaming process on the chemistry of the binders. It was hypothesized that the injected air and water may cause oxidative aging to the binder. Fourier Transform Infrared spectrometry (FTIR) method was utilized to analyze the different components of the foamed and unfoamed binder. The carbonyls and sulphoxides compounds are the major indicative of binder aging. It was concluded that the foaming caused no change in the binder chemistry because of the short term exposure to water and air. In addition, it was concluded that the foam characteristics were affected by the penetration grade rather than the source of bitumen.

EXPANSION RATIO, HALF-LIFE AND FOAM INDEX

Asphalt foams used in base stabilization applications were typically characterized using following three parameters: Expansion Ratio, Half-life and Foam Index. Expansion ratio (ER) is the ratio of the expanded volume to the initial volume of the binder (Brennen et al., 1983). Figure 5 shows an illustration of reduction in ER with time, which is equivalent to reduction in height of a foamed binder with time.

The ER can be defined as:

$$ER = \frac{V^0}{V^f} \quad [1]$$

where V^0 and V^f are overall foam volume at time t=0 and final binder volume after all foam dissipates, respectively (Figure 5). The ER is a measure of relative volume of the steam bubbles.

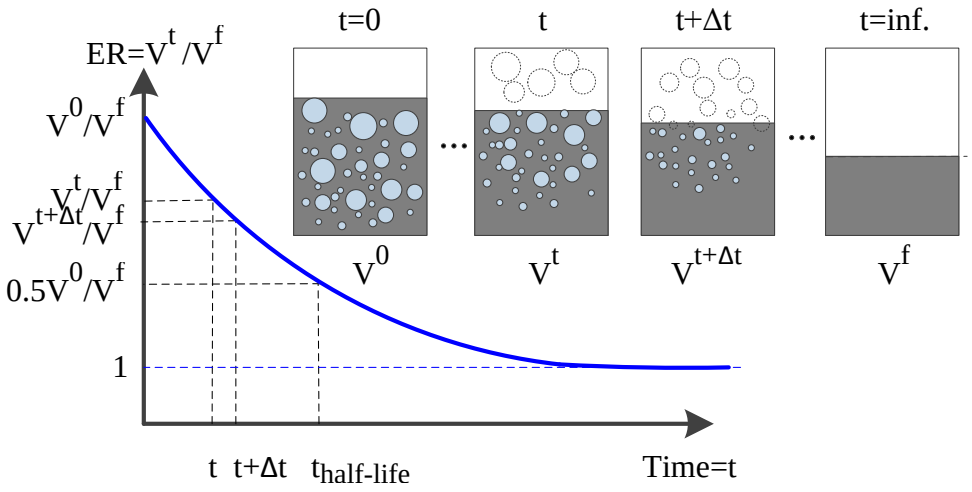

Figure 5: Typical Expansion Ratio (ER) versus time graph. (V^t= overall foam volume at t)

The rate of dissipation of moisture, on the other hand, is typically quantified using the parameter called half-life (HL). HL is defined as the elapsed time between the time at which the foamed binder reaches its maximum volume and the time it reaches to half of the maximum volume (Brennen et al., 1983). HL can be determined as follows in Equation 2:

$$HL = t_{0.5(V^0 - V^f)/V^f} \quad [2]$$

where $t_{0.5V^0/V^f}$ is the time at which the overall foam volume is reduced by half, as shown in Figure 5.

Brennen et al. (1983) stated that the expansion ratio and the half-life are affected by the amount of foamed asphalt prepared, water content used and the temperature at which the foaming took place. Ruckel et al. (1983) indicated that the foam parameters are affected by the size of the container, in which the binder is foamed.

Typically expansion ratio increases with foaming temperature and water content; whereas, half-life decreases with increasing temperature and water content (Kim et al., 2006). Moreover, the decrease in the half life causes the film thinning of the foam as well as the reduction in the viscosity as temperature increases (Wirtgen, 2004). As the viscosity decreases, the surface tension of the bitumen films decreases, and the steam pressure within the bubbles exceeds the surface tension of the bitumen and bubbles and the bubbles collapse.

Researchers have been working to determine optimum combinations to increase both the quality of the foamed binder and foamed based WMA asphalt pavements. For instance, Brennen et al. (1983) reported that a foaming temperature of 160°C and water content of 2% were measured to be the best combination for optimum expansion ratio and half-life. Ruckel et al.

(1983) recommended the range of the expansion ratio from 8 to 15 and at least 20 seconds for half-life. Maccarrone et al. (1995) proved that highly expandable and stable binder has optimum quality with expansion ratio greater than 15 and half-life greater than 60 seconds by adding certain surface active additives. Maccarrone et al. (1995) also suggested that the high expansion of the foamed binder improved the aggregate coating and mix properties. The optimum condition achieved with 2.6 % of water content and 0.7% of surface active additives. Similarly, Bowering and Martin (1976) showed that the cohesion and compressive strength of stabilized base mixes were significantly greater when high expansion (15:1) foamed bitumen was used. Muthen (1998) suggested the minimum expansion ratio to be 10 and the minimum half-life to be 12s. Nataatmadja (2001) suggested the water content to be in the range of 2% to 2.5%. On the other hand, Mohammad et al. (2003) used an optimum water content of 2.75% for PG58-28 binder at 160°C. Marquis et al. (2003) used an optimum water content of 3.0% for PG64-28 binder, which measured an expansion ratio of 11 and half-life of 8.5 s at 160°C. Kim and Lee (2006) determined the optimum foaming for the PG52-34 with 1.3 % water content at 170°C under air pressure of 400 kPa and water pressure of 500 kPa. Leek ad Jameson (2011) recommended the ER to be between 8 and 20 and the half-life to be minimum 6 seconds for foams used in base stabilization applications. Jenkins (2000) related the half life of foamed asphalt to the binder/mixture temperature (i.e., higher temperatures cause shorter half-life).

Foam Index (FI), the area under the ER versus time curve, is another parameter introduced by Jenkins (2000) and it is a measure of a combination of ER and half-life. The FI can simply be calculated via a discrete integration as follows:

$$FI = \sum_{t=0}^{t(ER=1)} 1/2 * \left(E_R + E_{R+1}\right) * \left(t_{t+1} - t_t\right) \quad [3]$$

where ER_t and ER_{t+1} are the expansion ratios at times t and t+1 respectively. The original FI equation, presented by Jenkins (2000), was developed for base stabilization applications where the binder content in the asphalt mixture is much less (2-3%) than the binder content of WMA (4-6%) pavements (Namutebi, 2011). As a result, its applicability to WMA needs to be investigated. Attempts by researchers to apply the foam index in foam characteristics optimization has been partially succeeded (Sunarjono, 2008). Even though it is not mentioned and investigated in Jenkins (2000), FI is an indirect indicator of the total surface area of the bubbles. The bubble size distribution as well as the total surface area of the bubbles can be computed from the ER versus time data.

As summarized from the literature, there is no common ground between the researchers to select optimum ER, HL and FI values, and there is no accurate method to measure these parameters. In addition, the recommendations are based on the performance of stabilized based not on WMA. Therefore, these parameters are investigated and new parameters are introduced to better relate the foam quality to asphalt performance in this study.

The practice of the foam height measurements of the foamed asphalt

There are challenges in the conventional method for measuring the foam height reduction, as a result, accurately calculating the foamed binder parameters. During asphalt foam testing in base stabilization applications (for ER and HL), measurements were facilitated by use of a fudicial marker (e.g., ruler) attached to the side of a container. This container is then filled

with foamed binder and the height of the binder is recorded over time (Muthen, 1998; Maine DOT, 2004). Although this method is simple and practical, it is inaccurate due to the foamed binder opacity and results can be highly dependent on the operator (He and Wong, 2006).

Jenkins (2000) proposed to measure the foam height reduction in 10 second intervals to calculate the FI. However, typically only two measurements, volume at the beginning of the foaming for the calculation of ER and the time when the height reduced to half of the initial for the calculation of HL are taken. As a result, the time dependent ER curve, which is needed for Foam Index (FI) calculation, cannot be obtained. Namutebi (2011) used a video camera to capture the images of the foamed asphalt in a container during collapse of the bubbles with the aid of a dipstick with marks. However, the method was only used to collect data to measure the ER and HL and the entire ER versus time data was not measured. He and Wong (2006) utilized a video camera to record the foam generation and dissipation process. Then, they visually determined the height values at different times from the recorded video and generated ER versus time graphs.

An automated procedure is needed for repeatable and accurate measurement of reduction in height of foamed asphalt. A novel and practical method based on image analysis is developed in this study and explained in CHAPTER 4.

An exercise to observe the effect of ER and HL on morphology of bubbles

In WMA applications, HL and ER may be important parameters that indirectly relate the workability and coating, respectively. For example, if the half-life is long (i.e., the foam collapses in a long period of time), overall viscosity of foam will remain relatively low and good workability can be expected. On the other hand, the expansion ratio is an indicator of total

volume of bubbles. It can be claimed that as the bubble volume increases, the surface area will also increase. However, ER cannot provide the size distribution of the bubbles, which is very important for surface area calculation. High surface area is desirable because more surfaces will be available for fine and coarse aggregates for better coating. Table 3 shows a comparison of surface areas of several bubbles with different sizes, as well as their illustrations in Figure 6. All have the same total bubble volume (i.e., 523.6 mm^3), which would lead to same expansion ratio if they were in a foamed binder. However, since surface area is inversely related to the radius, when the radius reduced from 5 mm to 0.25 mm, the total surface increased 20 times (even though volume, i.e., ER is same).

It should be emphasized that the small bubbles will collapse much slower than large bubbles, which may affect the long term performance of the pavement if encapsulated small moisture bubbles exist after the pavement construction. Therefore, an optimum size range should be specified in foamed WMA applications.

Table 3: Comparison of surface areas of bubbles with different sizes

Number of bubbles (n)	1	125	1000	8000
Radius (R), mm	5.00	1.00	0.50	0.25
Volume ($V_B = n*4/3\ \pi R^3$), mm^3	523.6	523.6	523.6	523.6
Surface area ($S_B=n*4\pi R^2$), mm^2	314.2	1570.8	3141.6	6283.2
Surface area ratio (with respect to R=5 mm), i.e., S_B / $S_{B(R=5mm)}$	1	5	10	20

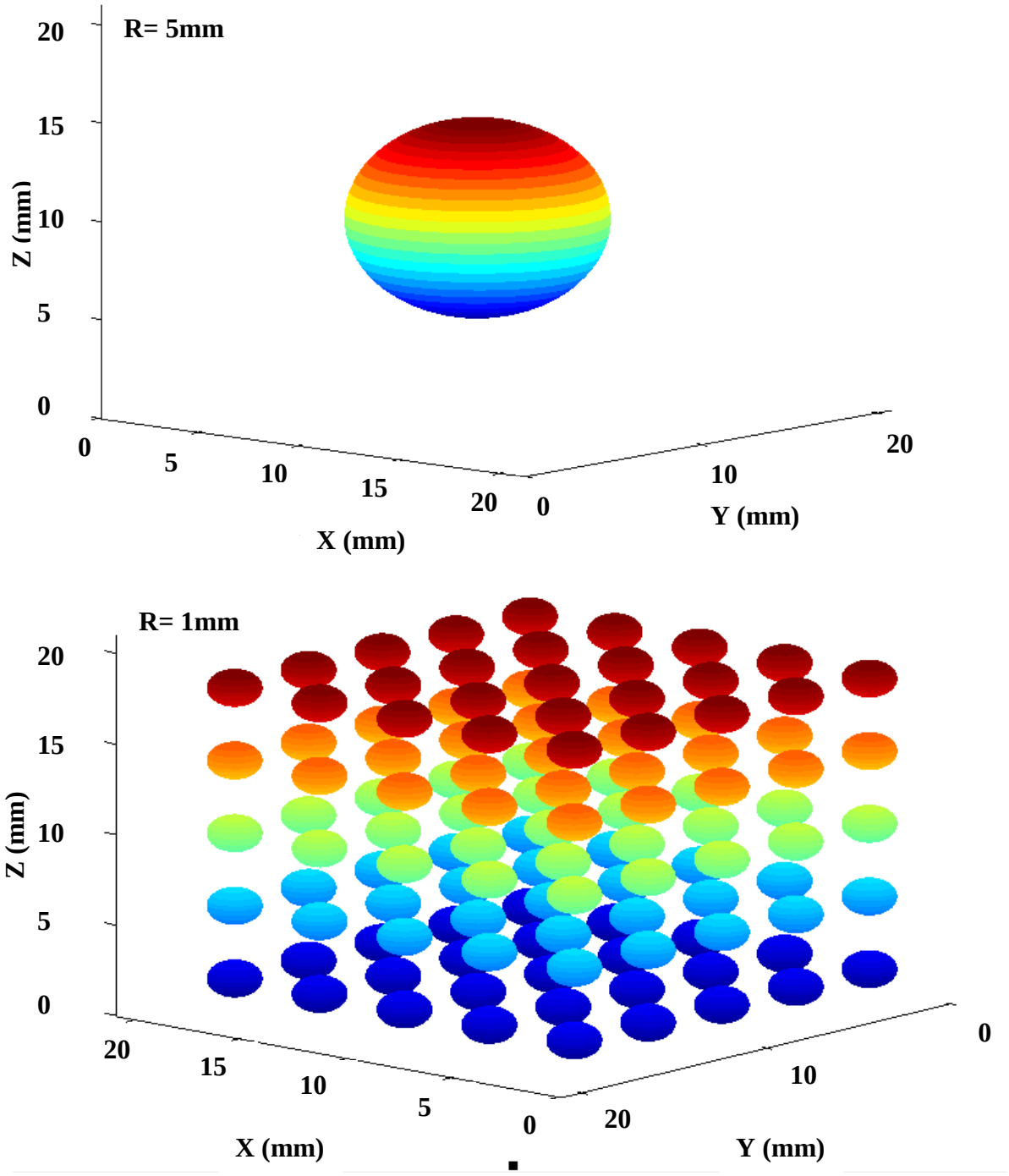

Figure 6: Illustration of comparison of surface areas of bubbles with different sizes

Figure 6 (cont'd)

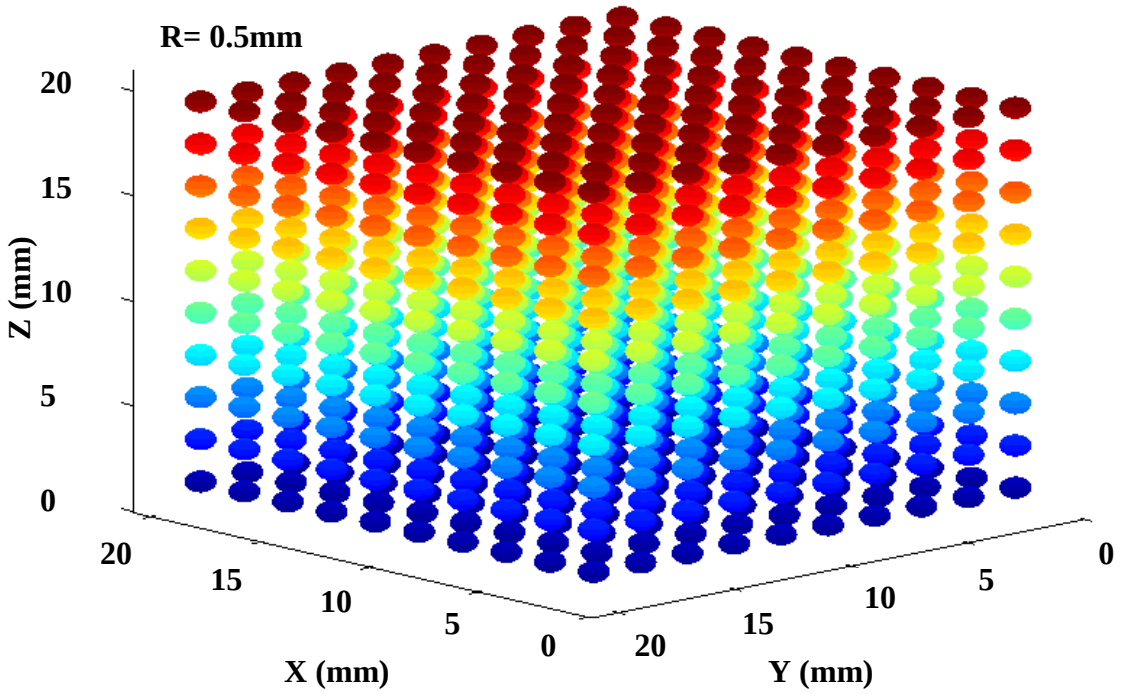

BUBBLE SIZE DISTRIBUTION

Bubble Size Distribution (BSD) is potentially a very important parameter, since it can directly relate to the ability of the foamed binder to coat the aggregates as well as the workability. The BSD is also an indicator of the total surface area of the bubbles. It is hypothesized that as the surface area of the bubbles increase, more interfaces are available for interaction of binder and aggregates. As a result, better coating can be achieved. It has been already mentioned that small-size bubbles collapse (or dissipate) much slower than large size bubbles, which leads to longer half-life. This can potentially aid in workability during placement and compactability. However, there is a danger that encapsulated moisture bubbles remaining

after construction may lead to moisture damage. Therefore, an optimum size range or an optimum surface area range should be defined.

Theoretically, BSD can be computed from the rate of reduction of the volume of the foam with time. This can be accomplished by using the Stoke's law (Lamb, 1932), similar to the method used in the traditional Hydrometer test, which is commonly used in geotechnical engineering for measurement of grain size distribution of the fine soils (Das, 2009). One major difference is that the hydrometer apparatus is not used since it is not practical because of the high temperature of the foamed binder and binder's opaque nature (one cannot see the hydrometer). A method to measure the reduction in the volume of the foamed asphalt is presented in CHAPTER 4. Once the BSD is computed, total surface area of the bubbles can be computed as explained in the next section.

Figure 7 shows an illustration of rising and collapsing of the bubbles in a cylindrical container as well as the reduction in overall height of the foamed binder during this process. It is well known (based on Stoke's law) that the bubbles with large volume (diameter) will rise to the surface faster than those with smaller diameter. Stoke's law for rising bubbles in a fluid can be expressed in Equation 4 (Lamb 1932):

$$D=\sqrt{\frac{18\,\mu v}{(\rho_f-\rho_b)g}} \qquad [4]$$

where v = velocity of bubble (m/s), g = gravitational acceleration (9.81 m/s^2), D = diameter of bubble (m), ρ_f = density of fluid (kg/m^3), ρ_b = density of the bubble (kg/m^3), μ= dynamic viscosity of the fluid (Pa.s=kg/(m.s)). The viscosity of the foamed binder is assumed to be

constant through the calculations since the temperature of the container (±3°C) is kept constant during the measurements. In addition, the viscosity change with time is neglected as the overall measurements take less than 4 minutes.

Equation 5 shows that if the velocity of a bubble rising in a fluid is known, its diameter is calculated using the density and viscosity of the fluid (bubble density may be neglected since it is much lower than the fluid density). In order to calculate the average diameter of bubbles escaping within a time interval (Δt), average velocity of the bubbles is needed. At any time interval Δt, the rate of reduction of the height of the foamed fluid is the same as the average velocity of the bubbles escaped within that time interval. Average velocity can be obtained from the reduction in height of the foamed fluid in the container as follows:

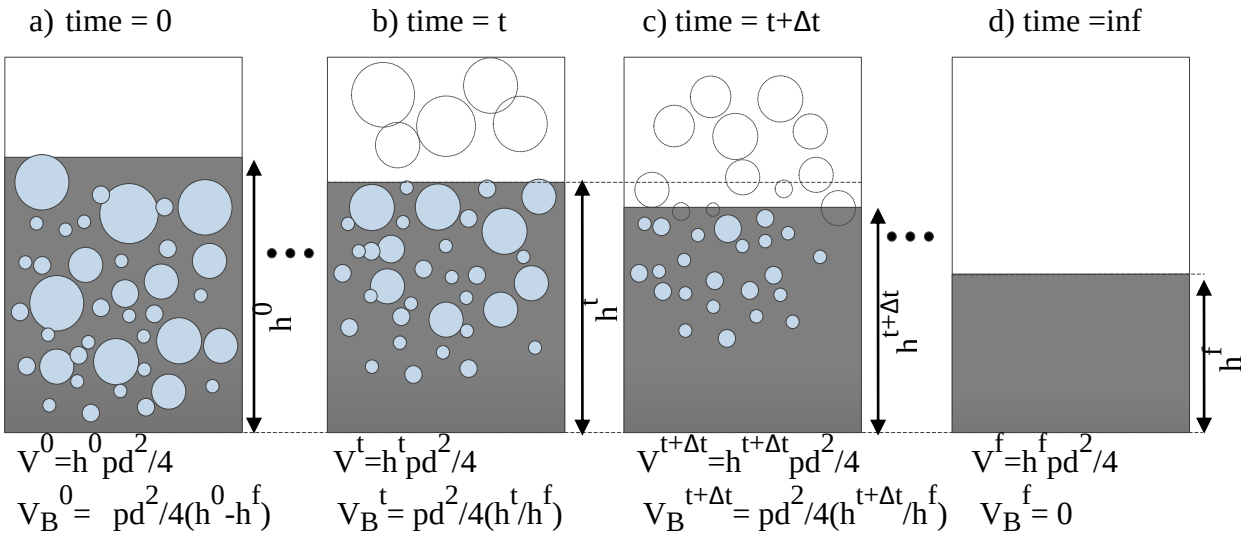

Figure 7: Illustration of the reduction of foamed binder volume with time.

$$v^t = \frac{h^t - h^{t+\Delta t}}{\Delta t} \quad [5]$$

where v^t=average velocity of the bubbles escaped at time t, Δt = time interval, h^t and $h^{t+\Delta t}$ are the height of the foamed fluid at t and t+Δt, respectively.

For the foamed binder in

Figure 7, percentage of the bubbles escaped (PBE) from the binder (i.e., bubbles that have risen to the surface) at an intermediate time (Δt) interval can be obtained as follows:

$$PBE^t = \frac{V_B^t - V_B^{t+\Delta t}}{V_B^0} \times 100 \quad [6]$$

where PBE^t = percentage of bubbles escaped at time interval Δt, V_B^0 = (initial) volume of the bubbles at t=0, V_B^t and $V_B^{t+\Delta t}$ = volume of the bubbles at t and t+Δt, respectively. Equations of V_B^t and $V_B^{t+\Delta t}$ are shown in Figure 7. It is noted that PBE^t is analogous to percent retained in each sieve, which is calculated during sieve analysis of aggregates. As a result, PBE^t can be used to calculate the percent passing (PP) as follows:

$$PP^t = 100 \sum_{i=0}^{t_i = t} PBE^{t_i} \quad [7]$$

where PP^t is percent passing at time t.

SURFACE AREA INDEX

The number of the bubbles and the total surface area of the bubbles can be computed, from the bubble size distribution, as follows:

$$N_B = \frac{V_B^t}{V_B^{single}} \quad [8]$$

$$S_B^t = N_B S_B^{single} \quad [9]$$

where N_B = number of bubbles, V_B^t = total volume of the bubbles escaped at time t, V_B^{single} =volume of a single bubble = $4/3\,\pi R^3$, S_B^t = total surface area of the bubbles escaped at time t, S_B^{single} = surface area of a single bubble = $4\pi R^2$, R= average radius of bubbles escaped at time t. Combining equations 8 and 9 and plugging the values of $V_B^{single} = 4/3\,\pi R^3$, $S_B^{single} = 4\pi R^2$ and R=D/2 reveals:

$$S_B^t = \frac{6V_B^t}{D^t} \quad [10]$$

where S_B^t = surface area and D^t = average diameter of bubbles escaped from the foam at time t.

Total bubble surface area of all the bubbles can be calculated by adding the S_B^t values at different times:

$$BSA = \sum_{i=0}^{\infty} S_B^{t_i} \quad [11]$$

where BSA = total surface area of all bubbles (in mm^2) in the foam at time = 0. A dimensionless parameter can be obtained by dividing the BSA by the surface area of the fluid (i.e., the asphalt binder) in the container as follows:

$$SAI = \frac{BSA}{\pi d(h^f + \frac{d}{2})} \quad [12]$$

where SAI =surface area index (dimensionless), d=diameter of the container and h^f = final height of the binder after all the bubbles dissipate (in

Figure 7). The SAI can be a useful dimensionless parameter for quantifying total surface generated by the foaming action and will influence the effectiveness of aggregate coating in WMA applications. It is also anticipated to relate to workability since small bubbles will lead to large SAI. Small bubbles typically do not collapse as fast as the large bubbles therefore the foam viscosity will stay low longer. This potentially leads to improved workability during placement and compaction.

CHAPTER 4

DEVELOPMENT OF THE ASPHALT FOAM COLLAPSE TEST (AFCT) AND VERIFICATION USING X-RAY MICROTOMOGRAPHY

An accurate and repeatable testing method is needed for the measurement of the rate of reduction in the height of foamed asphalt in order to calculate the foam binder quality parameters precisely. As part of this study, an automated test device (called Asphalt Foam Collapse Test (AFCT) was developed to measure the reduction in the height of the foam binder over time. As discussed in CHAPTER 3, once the reduction in height of the asphalt foam with time is measured, the foamed binder's quality parameters (i.e., the expansion ratio, foam index, half-life, bubble size distribution and surface area index) can be calculated. In addition, the absence of an accurate and repeatable testing method in measuring the foam quality in the current practice can be filled with AFCT, which is also practical and affordable test for the practitioners.

AFCT SETUP

The major components of the AFCT setup are: (i) a camera, (ii) a light source (preferably a light table),(iii) two steel rods, (iv) two aluminum custom made pulleys with precision bearings, (v) fishing line and weights, (vi) a plastic bobber, (vii) a steel floating ball and (viii) a stopper. The conceptual drawing of the main components of the setup is illustrated in Figure 8 (except the light table and camera). The actual picture of the overall setup, including the camera and light source (which are not shown in Figure 8) is given in Figure 9. Each component of the setup was determined after various trials with different designs.

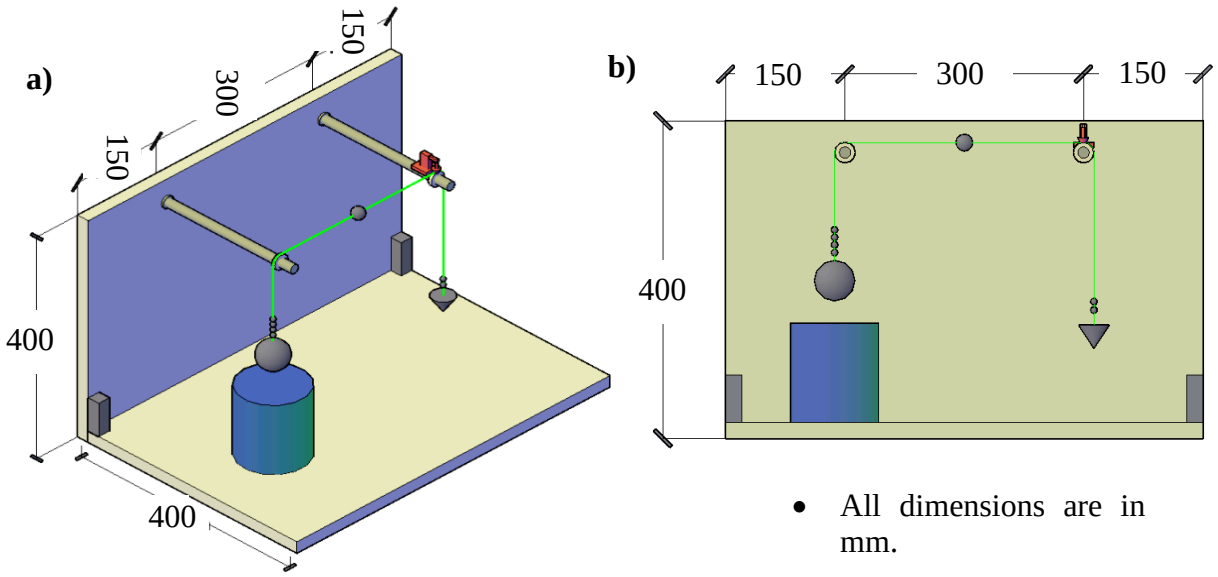

Figure 8: A sketch of the main component of the AFCT setup a) side-view b) front-view

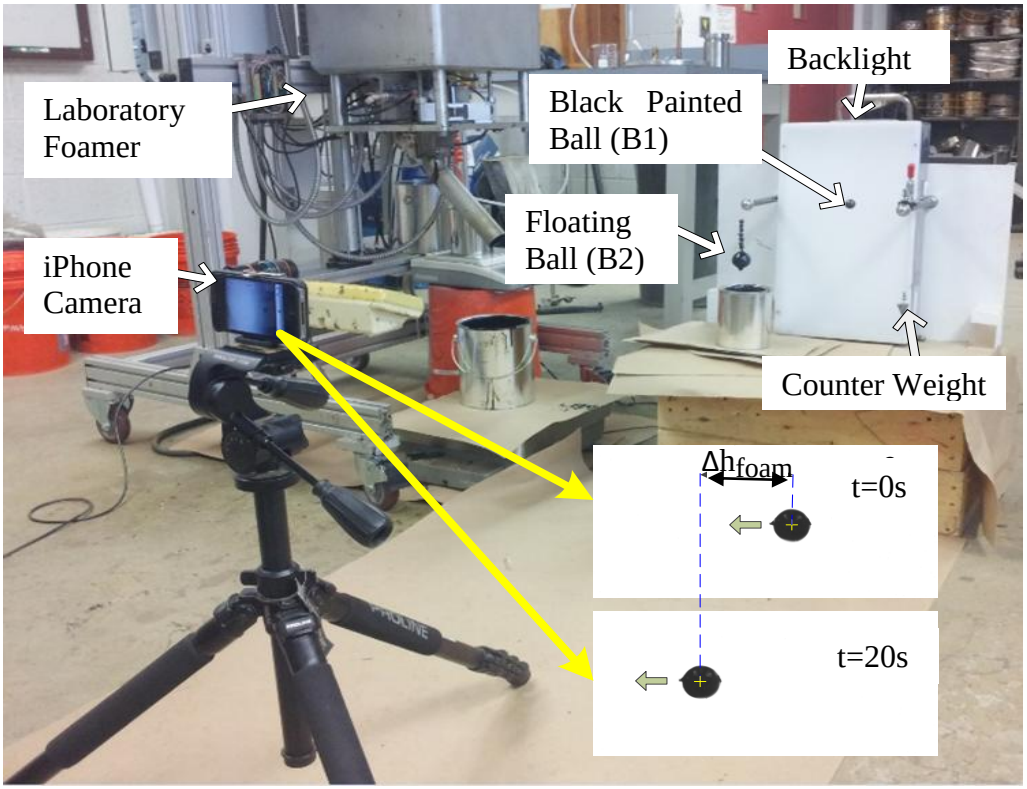

Figure 9: Picture of the AFCT test setup

The costly part of the AFCT setup was the digital camera. However, the trials indicated that the test could be performed both using non-industrial and industrial cameras to capture images. In this study, two different cameras (an iPhone camera and a high speed industrial camera) were used and compared with respect to each other. The details of the image capturing and analysis were discussed in the later sections. The back light source was a fluorescent light table.

The other components such as rods, bearings and stopper were all mounted or attached to the L-shaped white painted wooden block as shown in the isometric view in Figure 8. Initially, the rods (Rod 1 and Rod 2) were bolted to the wooden block. Then, custom-made aluminum pulleys with precision bearings were attached to the rods. The precision bearings provided close to frictionless rotation of the pulleys during the experiment. In addition, a lubricant (i.e. WD40) was also sprayed to minimize the friction. Finally, a stopper was mounted on Rod 2 in Figure 8, and used as a triggering mechanism.

The rest of the components of the test setup were glued or tied to the fishing line. The fishing line was the most convenient, abrasion resistant and almost frictionless material that provided free rotation of the pulleys during the test. A black painted plastic bobber (B1) with 2 cm diameter was initially drilled with a hand driller (2 small holes slightly larger than the diameter of the fishing line - 180° apart). Then, B1 was glued to the middle of the fishing line using superglue. The floating ball (B2) was attached to one side of the fishing line. B2 is a temperature-resistant steel floating ball that has a diameter of 2” (50.8mm). Before tieing the fishing weights to the other end of the fishing line, B2 was dipped into hot binder and fully coated with binder. Thus, the change in the weight of B2 during the test was minimized. Then,

the weight of the binder coated bobber (B2) was balanced with the weights as shown in Figure 8. Finally, an extra weight of 1 -2 grams was attached onto the B2 to ensure the free flow when the stopper was released at the trigger of the experiment. The test starts by releasing the stopper and starting the acquisition of the images by the camera. The cost analysis of AFCT setup is given in

Table 4, where the overall cost was approximately $389. The camera price was estimated based on the cost of a smart phone.

Table 4: Overall cost estimate of AFCT setup

AFCT Setup Components:	Unit	Unit Price	Total
Camera	1 ea	$200	$200
8x Optical Zoom Lens	1 ea	$20	$20
Light Table	1 ea	$52	$52
Aluminum Rods	2 ea	$5	$10
Pully + Precision Bearing	2 ea	$21	$42
Stopper	1 ea	$13	$13
Fishing Line	1 ea	$10	$10
Fishing Weight	2 box	$5	$10
Bobber (B1)	1 ea	$0.5	$0.5
Floating Ball (B2)	1 ea	$13	$13
2000 ml beaker	1 ea	$18	$18
		Total	$389

AFCT PROCEDURE

The AFCT test is designed to be convenient for both laboratory and field practices. Initially, the binder is foamed into a beaker, which is heated to the binder temperature in a conventional oven or in a heating mantle. The size of the binder sampling dish is selected to be

2000 ml glass beaker for 200±20 gr. of foamed binder after various trials (i.e., quart aluminum can, 1000 ml beaker etc). However, the users can change the size of the beaker as well as the binder amount depending on the properties of the foam binder, if the binder expends excessively and overflows from the beaker. It is crucial to keep the size of the beaker and the amount of the binder same while comparing the quality of different foamed binders. As summarized in CHAPTER 3, the foam quality parameters depend on the amount of the binder and the size of the beaker (Brennen et al. 1983, Ruckel et al. 1983), except the SAI introduced in this study.

The beaker filled with the foamed binder needs to be rapidly placed under the floating ball (B2), and B2 is leveled to the surface of the foam, then quickly, the stopper that fixes the fishing line is released. As foam collapses, B2 goes down with the surface of the foamed binder, but does not sink into the foamed binder. This is a crucial step during test and can be ensured by balancing the two sides of the fishing line. If B2 sinks into the foamed binder, the test is discarded and repeated. Meanwhile, a camera simultaneously captures the movement of the black-painted ball (B1) as the foam collapses (Figure 9). Since B1 and B2 are on the same line, they move as the same amount. In Figure 9, sub-images with white background and black circle (which is B1) are the images captured by the camera and shows the movement of bobber B1 from t=0 sec to t=20 sec towards left (as B2 goes down). The details of the image analysis is explained in the following section

AFCT IMAGE ANALYSIS

Image analysis is used to calculate the movement of B1 with time, which corresponds to the change in the foam height. Since both B1 and B2 are attached to the same fishing line, they

move the same distance within the equivalent time intervals. However, B1 moves horizontally while B2 moves vertically.

In order to record the video images, as it was stated previously, a non-industrial (iPhone) camera and a high speed industrial camera were used (Figure 9). The non-industrial camera allows the system to be easily transported to the field as well as being less costly. Initially, the accuracy of the iPhone camera was validated against a high-speed industrial camera. The high-speed industrial camera captures 400 frames per second (fps), whereas the iPhone camera captures 30 fps. In order to validate the frame rate, a timer was placed at the top of the setup and included in the video images. It was observed that the non-industrial (iPhone) camera has adequate accuracy to measure the height reduction of foamed binders. In addition, an 8x Optical Zoom Lens was mounted to the iPhone camera to capture the foam collapse from approximately 2m distance. This facilitated the overall operation by providing sufficient space to work with the foaming device and AFCT setup. The frame rate of the camera for the AFCT test can be as low as 1 fps, which provides sufficient data interval.

Once a video is captured, first, the frame rate is verified using non-commercial video editing software (e.g., VirtualDub). Then, a sequence of images was extracted from the video file every 1 second. The centroid of the black painted ball (B1) in each image was computed using an algorithm developed in MATLAB®. In this algorithm, first, each image is converted to a binary (black/white) image through a thresholding operation such that only the bobber is black and the rest of the image (background) is white (see sub-images in Figure 9). It is noted that, since the fishing line is relatively transparent, with the aid of the background lighting (light table in Figure 9), it disappears when the original image is converted to binary image. As a result, in each

image, only a black circle (i.e., B1) is visible. The center coordinate of the black circle is determined using a morphological labeling operation (Kutay et al. 2010, 2011). This procedure is repeated for all consecutive images. The change in the x-coordinate of the center of B1 in consecutive images corresponds to the change in the height of the foam (B2). The displacement of B2 with recorded time is equal to the reduction of the foam height with time. Thus, the foamed binder parameters explained in CHAPTER 3 can be easily and precisely calculated with these data.

AFCT TEST RESULTS

After developing the AFCT procedure, the effects of the injected air pressure and water content on the binder quality indicators were investigated. A virgin (non-modified) binder (PG58-28) was utilized in this study. The foaming temperature was 155 °C. The viscosity of non-foamed binder at this temperature is approximately 300 mPa.s. The laboratory Foamer utilized in this study had an air injection capacity varying from 0 to 30 psi. However, the trials indicated that the repeatability of the foaming became poor after 20 psi. It was observed that if a feedback system is mounted just before the foaming nozzle to better control the injection process, it can increase the foamer's repeatability. Due to this deficiency, the maximum injected pressure in this study was limited to 20 psi. It should also be noted that the pressure levels of laboratory foamers are significantly lower than the field foamers.

In this study, the water content range was selected to be in the range of 1% to 5%, which simulates a wide range of the current field applications. The accuracy of the injected water content was approximately ± 0.5-1% in the laboratory foamer used in this study. Since the overall water amount is relatively low, even one drop of water may affect the quality of the

foamed binder. For example, 1% water content, 2 grams of water is injected to 200 grams of binder.

Effect of Injected Water Content on the Foam Properties

The foam quality parameters of foams were initially analyzed for the binder prepared with constant injected air pressure (15 psi) and three different water contents (1%, 2%, and 4% by weight of the binder). Figure 10 and Figure 11 show the foamed binder characteristics of these water contents. Based on these figures, the following conclusions can be drawn:

- Expansion ratio of the foamed binders increased with the increases in the water content.
- Half-life of the foamed binders decreased with the increase in the water content. The half-life of the foamed binder prepared with 1% water content was approximately twice of the half-life of the one with 4% water content.
- Foam Index, which is the area under the expansion ratio versus time, decreased with the increase in the water content.
- As the injected water content in the foamed binder increased, the maximum diameter of the bubbles increased. This leads to the short half-life and high expansion ratio.
- The diameter of foamed binder at 50% of passing (D50), which was calculated from bubble size distribution, increased with the increase in the water content.
- Surface area index, which is dimensionless parameter, is an indicator of the surface area of the bubbles. The SAI decreased as the water content increases.

- Bubble size distribution of the foamed binders plotted in Figure 11 clearly shows the effect of water content on the internal microstructure of the foamed binders. As the water content increases the bubble size distribution becomes coarser. On the contrary, the low water content resulted finer bubble gradation.

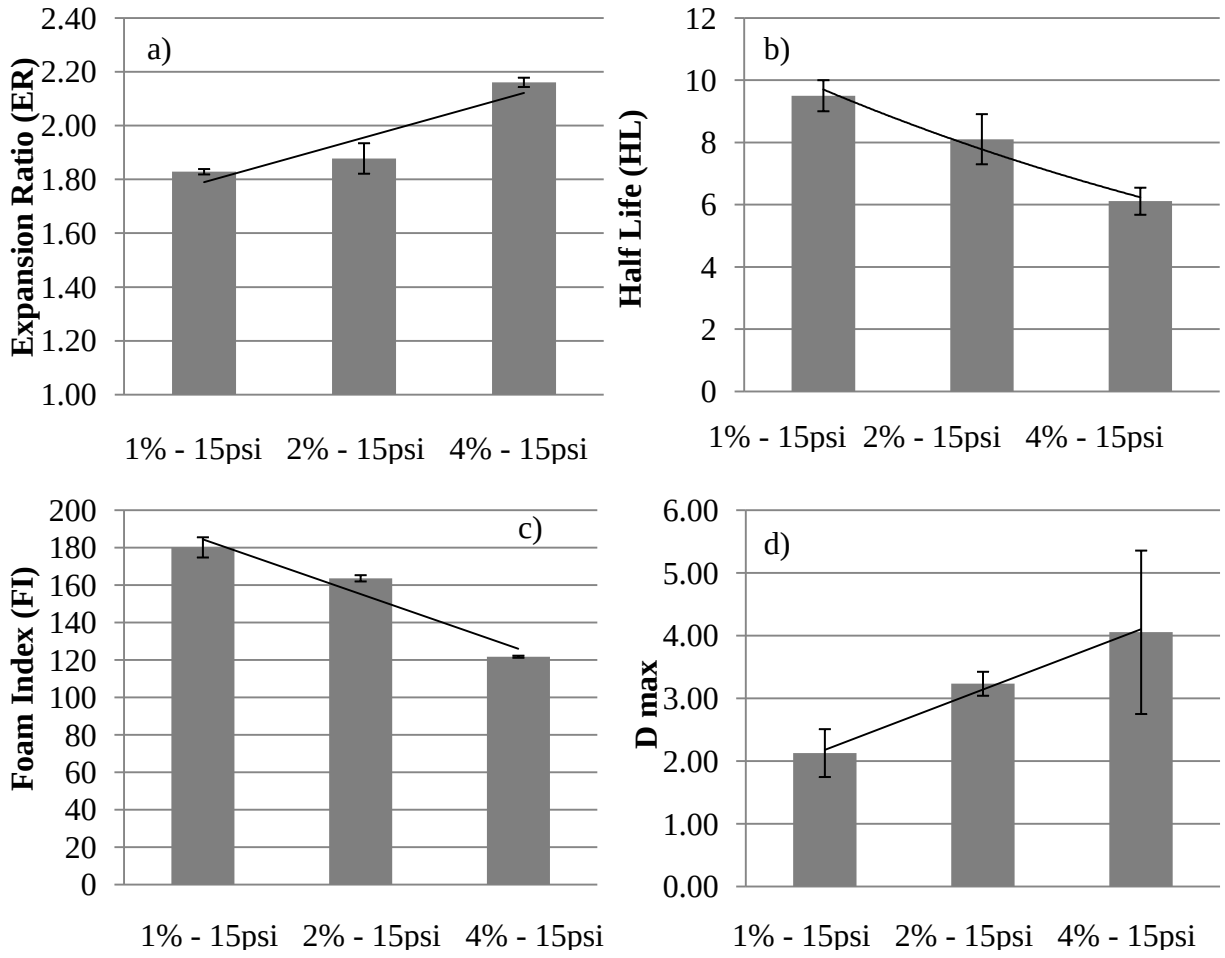

Figure 10: Foam quality analysis of the binders prepared with constant air pressure and different water contents

Figure 10 (cont'd)

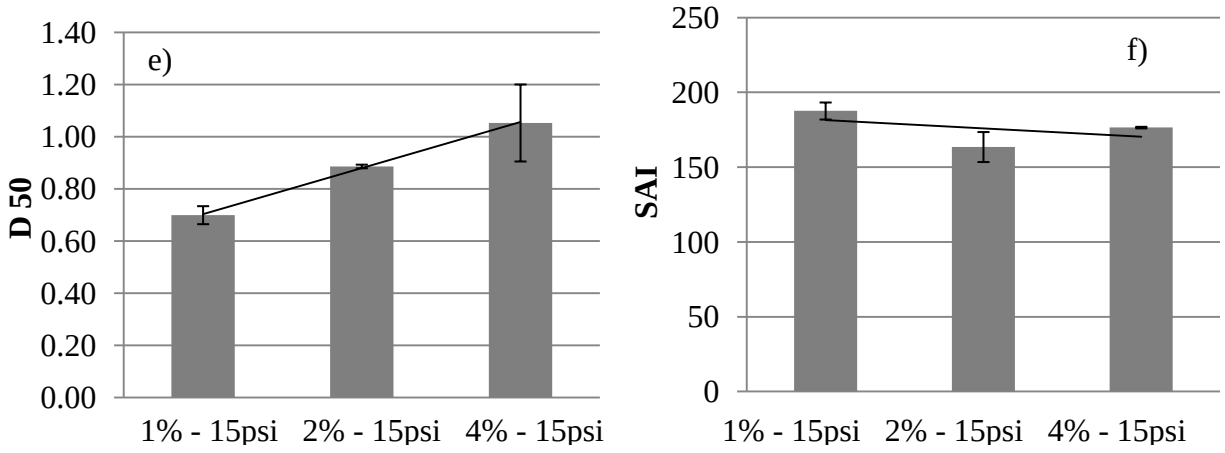

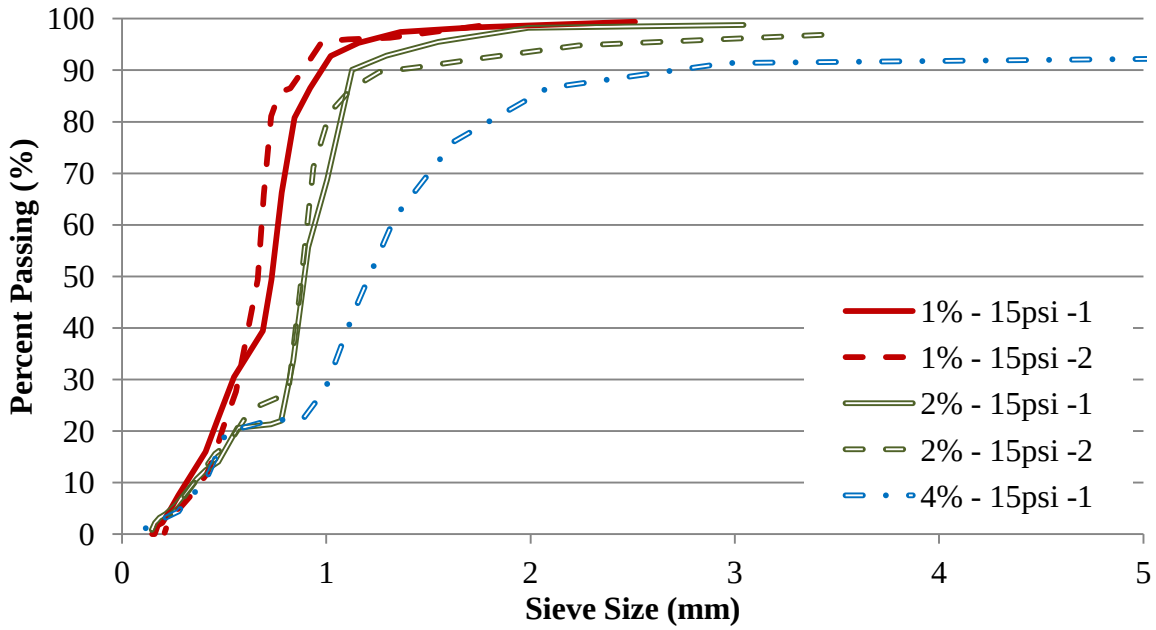

Figure 11: Bubble size distribution of the binders prepared with constant air pressure and different water contents

Effect of Injected Air pressure on the Foam Properties

In this section, foamed binder quality indicators were studied for constant water content (1% by weight of the binder) and three different injected air pressures (10psi, 15psi, and 20psi).

Figure 12 and Figure 13 show the variation of ER, FI, HL, D_{max}, D_{50} and SAI at different air pressures. Based on these figures, the following conclusions can be drawn:

- The ER increased with increasing the air pressure.
- Half-life of the binders decreased exponentially with the increase in the injected air pressure. As shown in Figure 12b, the half-life of the foamed binder prepared under 10 psi air pressure was approximately 6 times longer than the one prepared under 20 psi air pressure.
- Foam Index of the binders linearly decreased with the increase in the injected air pressure.
- D_{max} and D_{50}, which were calculated from the bubble size distribution curves given in Figure 13, were clear indicators of how the air pressure influenced the bubble sizes. It was revealed that the bubble size increased with the injected air pressure.
- As plotted in Figure 13, the variability in the bubble size distribution of the replicates is relatively high. However, it is clear that the gradations of the bubbles for different air pressures are significantly different. This bubble size distribution can affect the workability and coating, as well as the performance of the pavements.

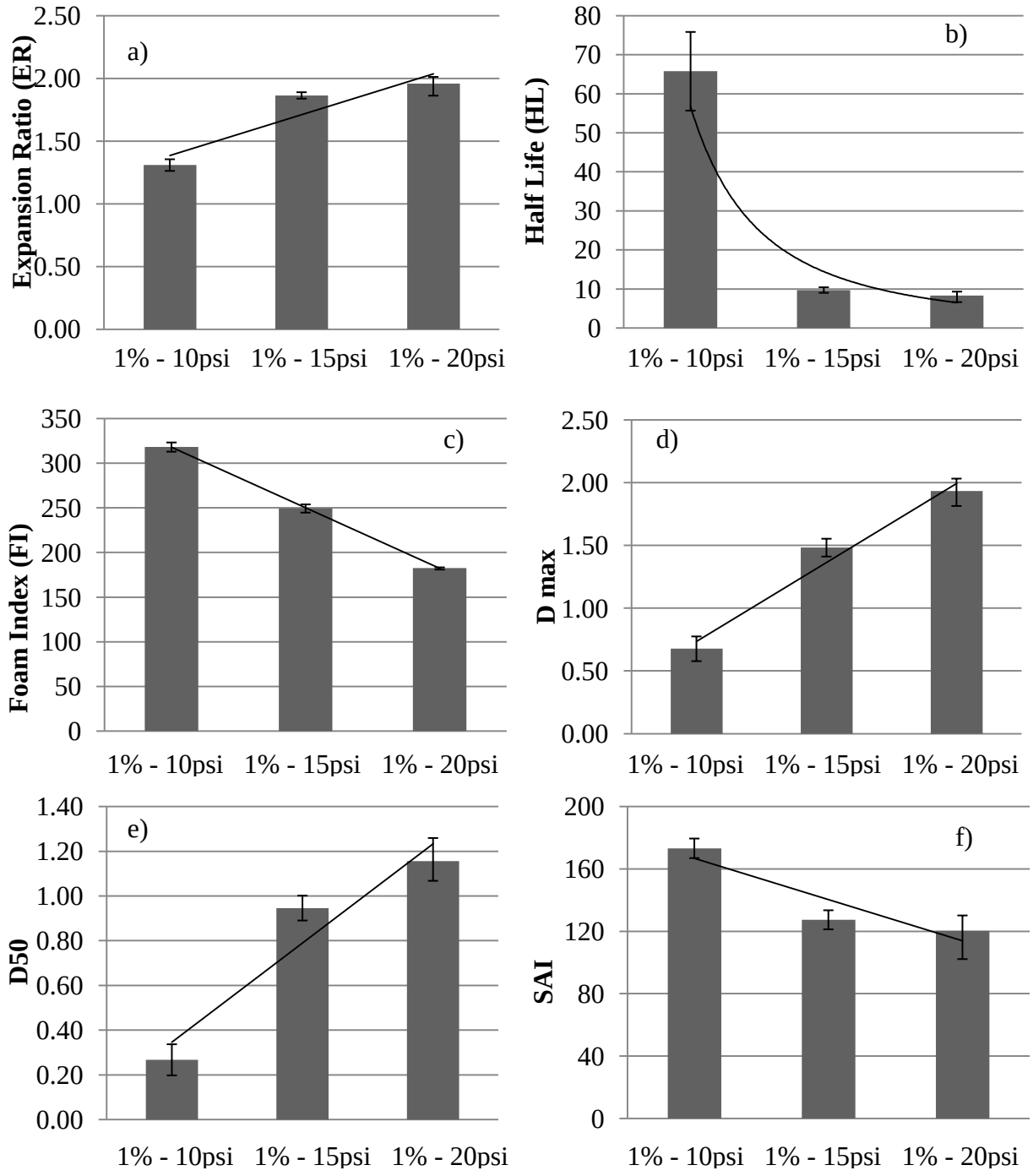

Figure 12: Foam quality analysis of the binders prepared with constant water content and different air pressures

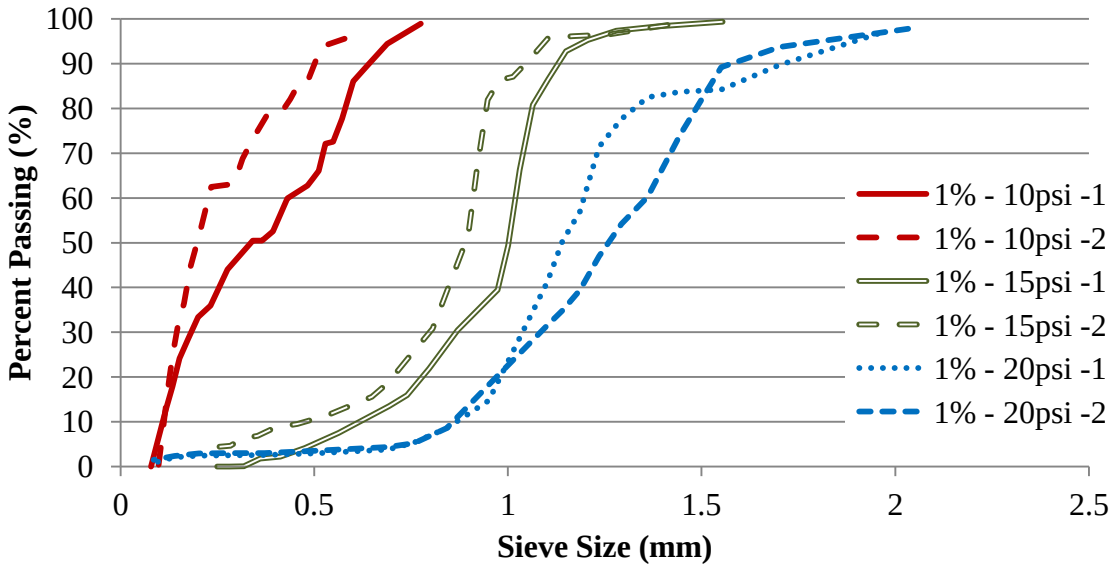

Figure 13: Bubble Size Distribution of the binders prepared with constant water content and different air pressures

Analysis of Foamed Binder Properties under Different Injected Air Pressure and Water Content Combinations

The effects of water content and air pressure were investigated individually in the previous sections. In this section, results of three combinations (1% - 10psi, 3% - 15psi, and 5% - 20 psi) presented. These trials were called as "1st Trial" in the Figure 14 and Figure 15. As shown, there are clear trends, where ER, D_{50} and D_{max} increase with water content and air pressure. In order to increase the number of combinations of water content and air pressure, tests were planned to be repeated at 2% - 12.5psi and 4% - 17.5psi. However, because of known variability of the laboratory foamer, the entire set of combinations was re-tested on the same day. This set is called as "2nd Trial" in the Figure 14 and Figure 15. Based on these figures, the following conclusions can be drawn:

- Although the magnitudes of the parameters are different when 1st and 2nd trials are compared, overall trends are the same.
- ER increased as the injected water content and air pressure increased (Figure 14a).
- As shown in Figure 14b, the half-life decreases with increasing water content and air pressure. The half-life of the foamed binder prepared with injecting 1% water content and 10psi air pressure varied increased 15 seconds to 76 seconds in between the 1st and 2nd trials, which illustrates the variability of the laboratory foamer.
- It can be clearly be observed from Figure 14b that the foam index decreases with the increase of the injected water content and air pressure.
- Bubble size distributions of the foamed binders for both 1st and 2nd trials are shown in Figure 15a and Figure 15b. For each trial, the size distribution for each combination significantly diverged from each other.
- D_{max} and D_{50} increased with the increases of the injected air pressure and water content.
- The SAI, which was calculated from the bubble size distribution, decreased with increasing water content and air pressure combinations.

The AFCT analysis showed that the foam quality indicators significantly depend on the water content and air pressure. However, it is still unknown how these foam quality indicators

relate to aggregate coating, as well as the mixture performance. Therefore, in CHAPTER 5, the relation between the foam quality indicators and mixture performance are presented.

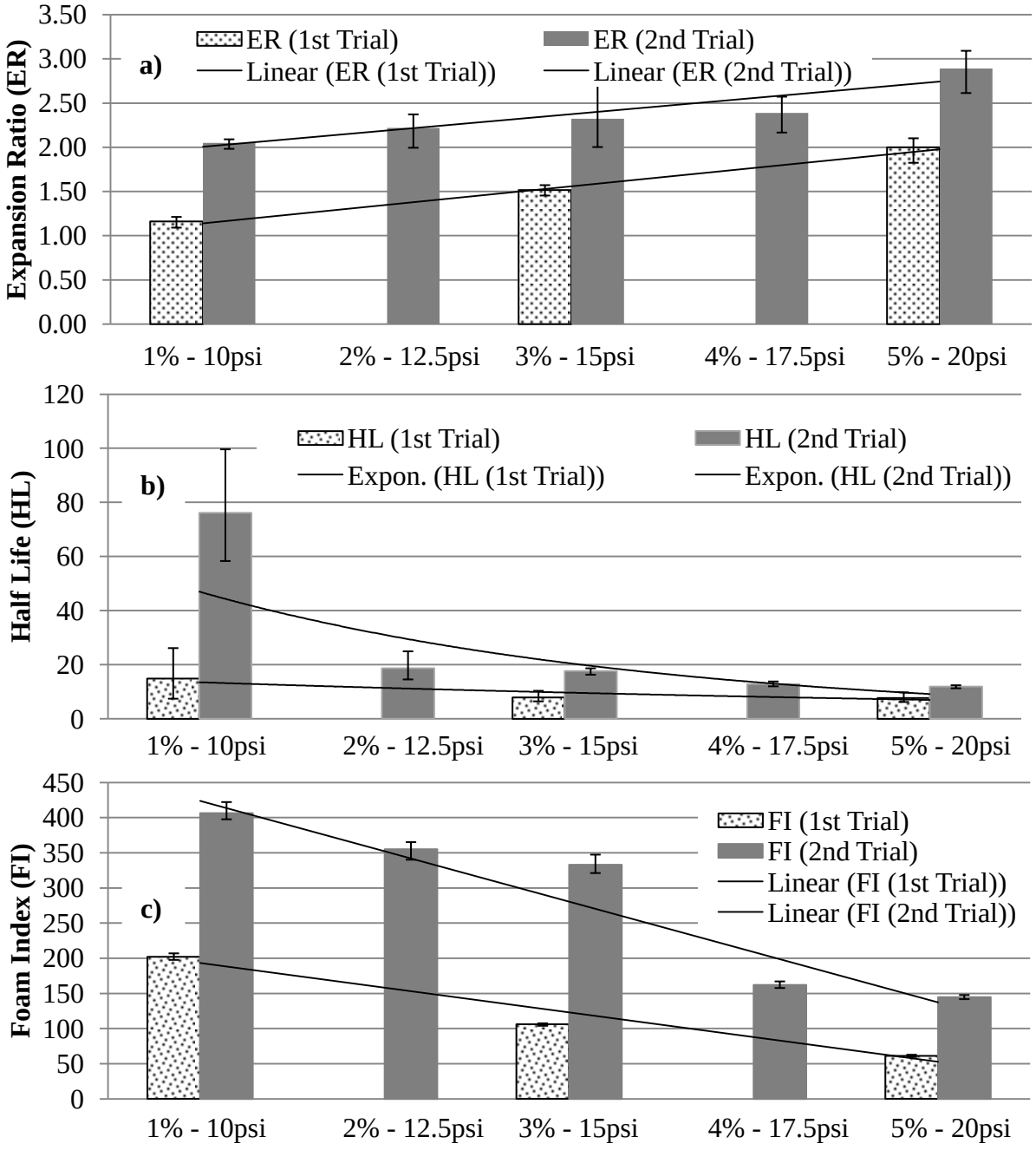

Figure 14: Foam quality analysis of the binders prepared with different water content and air pressure combinations

Figure 14 (cont'd)

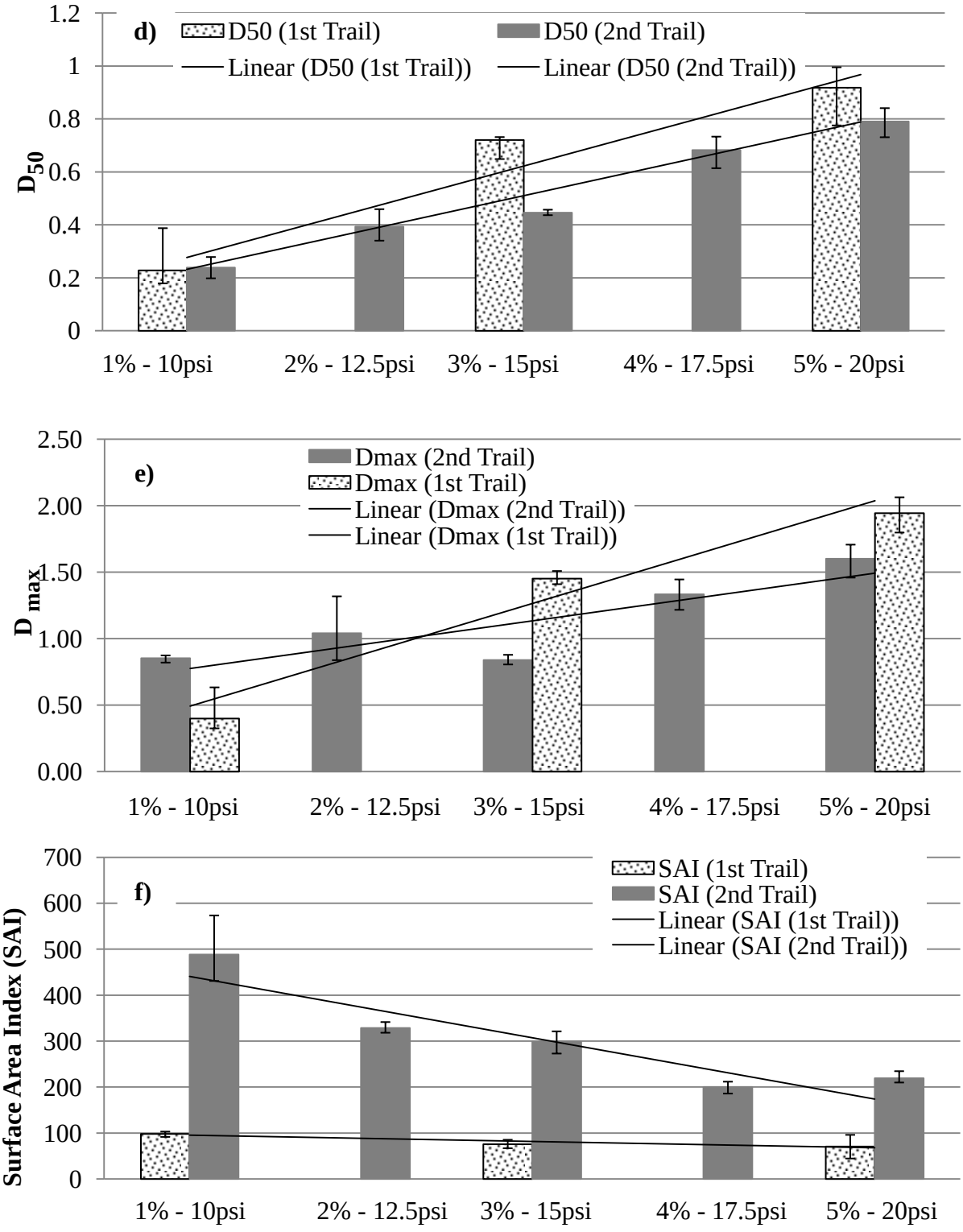

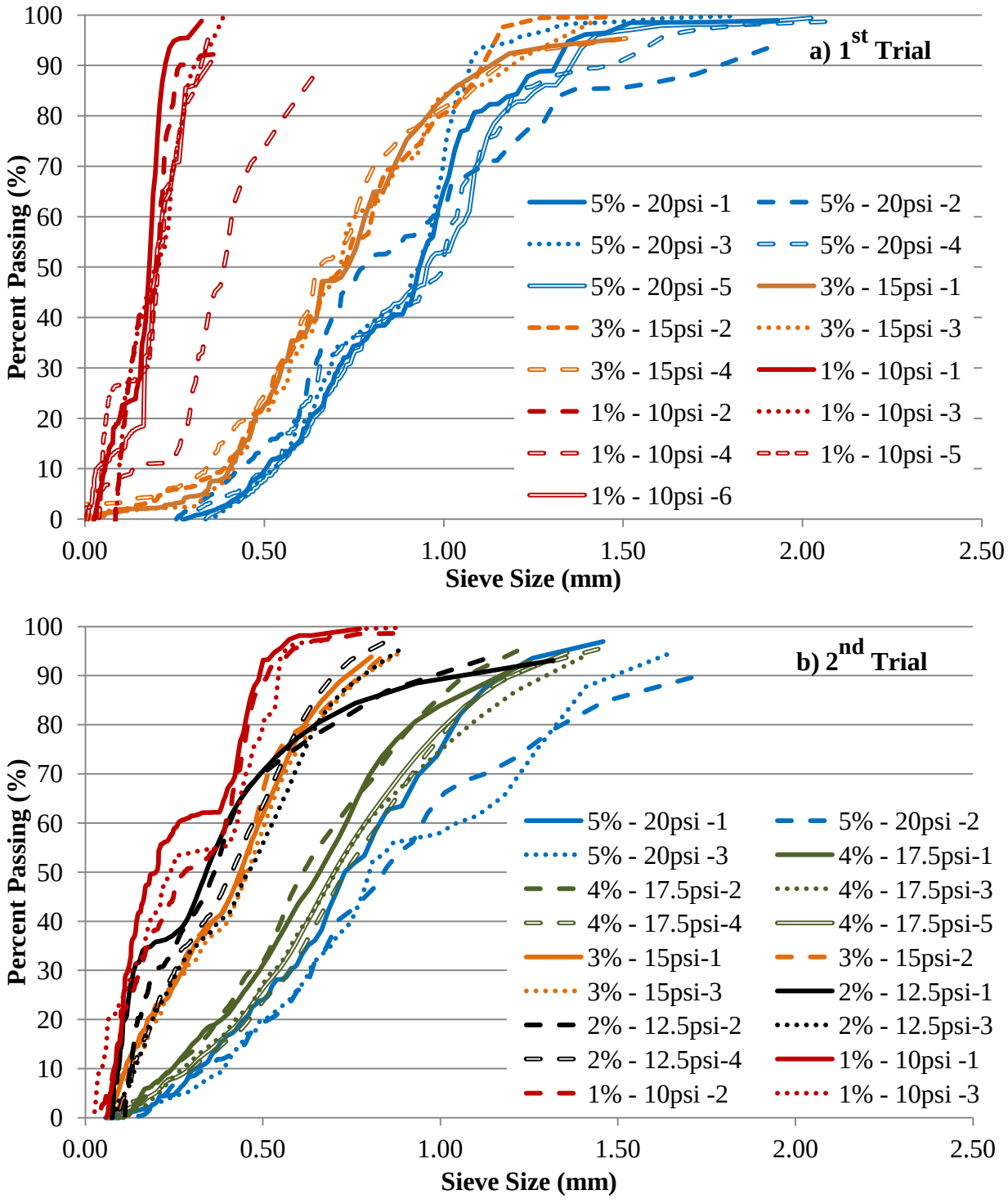

Figure 15: Bubble Size Distribution of the binders prepared with different water content and air pressure combinations a) 1st Trial, b) 2nd Trial

VERIFICATION OF AFCT USING X-RAY MICROTOMOGRAPHY IMAGING

In order to verify the AFCT procedure to compute the bubble size distribution, 3D images of foamed binders were acquired using X-Ray microtomography technique. Then, 3D image-based bubble size distribution was compared against bubble size distribution computed from the AFCT. The verification process is described below.

X-Ray Microtomography Sample Preparation Procedure

Careful sampling of the foamed binder was very crucial in order not to disturb the specimens during the process. Initially, the binder was foamed into a beaker at approximately same temperature with the binder, as shown in Figure 16a. Then, the binder was poured into 13x75 mm (11 mm inner diameter) polypropylene tubes, which were heat resistant (melting point ~170°C). After pouring, each specimen was instantly frozen using liquid nitrogen, as shown in Figure 16b. The frozen PP tubes are shown in Figure 16c. The foamed binders were sampled at the 1st, 15th, and 30th minutes. In between the sampling intervals, the beaker with the binder was kept in the conventional oven at 155°C.

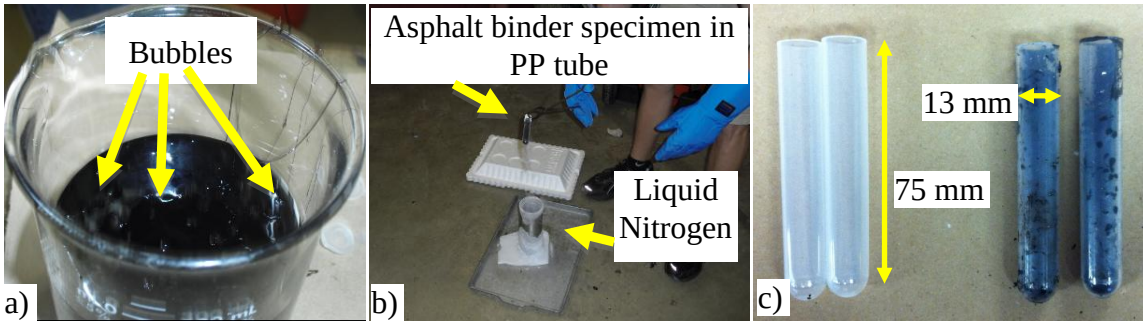

Figure 16: Picture of (a) the foamed asphalt where bubbles are visible at the surface, (b) illustration of freezing of asphalt binder using liquid nitrogen, c) PP tubes w and w/o foamed binder

The purpose of this study was: (1) to verify the bubble size distribution computed by the AFCT as soon as the foam is generated, and (2) to monitor the change in microstructure at different times using 3D XRM images. It was observed that the instant freezing procedure did not damage the binder samples. This observation was further validated when the 3D XRM images were analyzed, where there were no visible cracks within the specimens. For the XRM analysis, the frozen tubes were transported to Argonne National Laboratory (ANL). 3D internal images were generated using the synchrotron based X-ray Microtomography device (5-BM-C beam line at Advanced Photon Source (APS)).

3D Imaging using Synchrotron-Based X-ray Microtomography

The 3D image acquisition of the specimens was done at the 5-BM-C Microtomography beam line at the Advanced Photon Source (APS) facility in ANL. The illustration of the equipment is given in Figure 17. This XRM system uses a cryo-cooled CCD system and optics, which permit a range of spatial resolutions from 3 microns to about 100 microns (depending on the sample size). In this research, 20keV parallel beam was utilized, which provided a volume scan of 13x13 mm area, 5.5 mm tall cylinders. This size was the maximum scan range for the camera and optical system (i.e., the X-ray detector). Parallel beam herein is defined as a beam where photon particles travels through linear accelerator with 20keV energy. The final image size was 1299 by 1299 by 550 pixels. This corresponded to 12.9 mm/ 1299 pixels = 0.01 mm/pixel (10 micron) image resolution. The PP tubes (10.89 mm inner diameter and 75 mm tall) were convenient for this study since the maximum sizes of the bubbles were much smaller (~2.5 mm calculated from AFCT analysis).

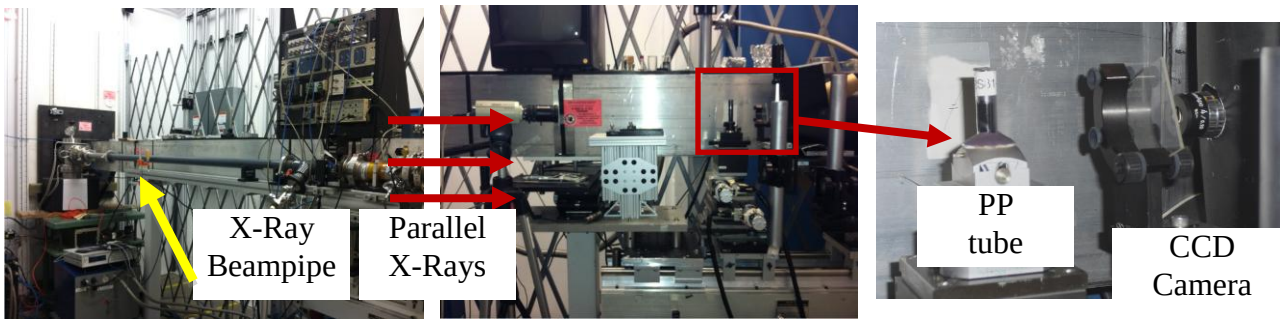

Figure 17: Picture and illustration of Synchrotron-based X-ray Microtomography setup used in this research. This setup is at Advanced Photon Source (APS) located in Argonne National Lab (ANL).

X-Ray CT Microtomography Image Analysis

The scanned images are reconstructed with the inbuilt software of the X-Ray Microtomography device and saved in "*.img" format. An algorithm was developed in MATLAB® to convert these images to "*.tif" format as given in Figure 18a. The sequence of images was then imported to a non-commercial video editing software (ImageJ), in order to crop the binder medium to improve the computational efficiency during analysis (each image was initially about 1.6 MB after cropping it was reduced to 760KB). Before beginning the 3D analysis, it was observed that most images has ring artifact problem, which would affect the overall analysis. Therefore, a ring artifact removal algorithm was developed in this study.

Ring Artifact Removal

In X-Ray images, the ring artifacts appear to be a number of dark concentric rings or semi-rings on the scanned surface as shown in Figure 18b. These artifacts may be formed due to slight movement of the tubes during the scanning or due to the temperature change in the samples. The samples were kept in a freezer and taken out just before scanning. Each scan took

about three hours, which resulted huge temperature variability in between the beginning and end of the scan. However, this was essential because the binder (PG58-28) used in this study was very soft and bubbles may be disturbed even before scanning.

The ring artifact removal algorithms available in literature are typically applicable to the sinograms (a visual representation of the raw data obtained in a computed axial tomography scan) of the raw XRM data (Prasad et al, 2011; Munch et al., 2009). However, these data was not accessible in this study. Since most of the ring artifacts in the scanned images were semi-circular, initially, the images were transformed from Cartesian to Polar, as shown in Figure 18c. The semi-circular artifacts became dark lines in the images. Then, a 2D median filter of size 5 pixels by 30 pixels was applied to these images. Median filter was selected since it is a common noise reduction filter, which preserves the edge structure while smoothing the non-uniform regions. As shown in Figure 18d, the most of the rings were eliminated with this filter. Then, Polar images were converted back to Cartesian coordinates (Figure 18e). When it was zoomed in the bubbles, as shown in the subimage of Figure 18e, it was observed that some noise occurred in the bubbles. Therefore, a second median filter (4x4) was applied to the image, as shown in Figure 18f. When it was zoomed in to the bubbles as illustrated in the subimage, it was clear that the noise was reduced in the bubbles.

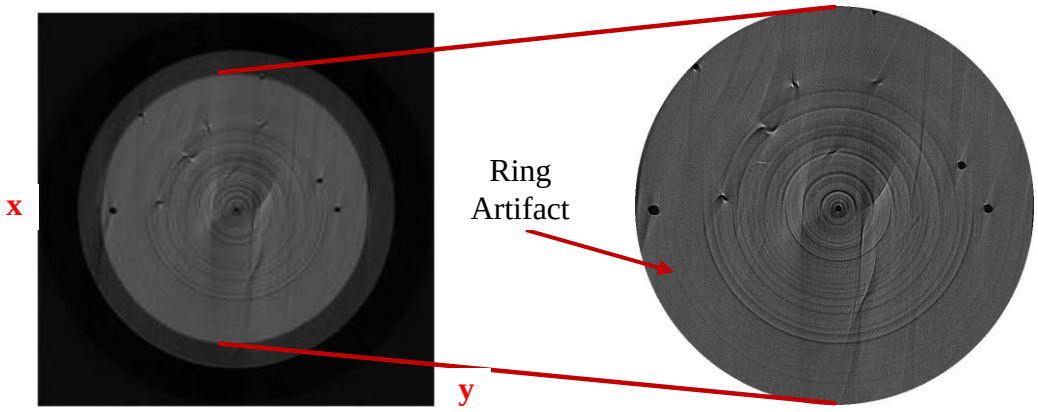

a) Original Image (1299x1299) b) Cropped Image (878x878)

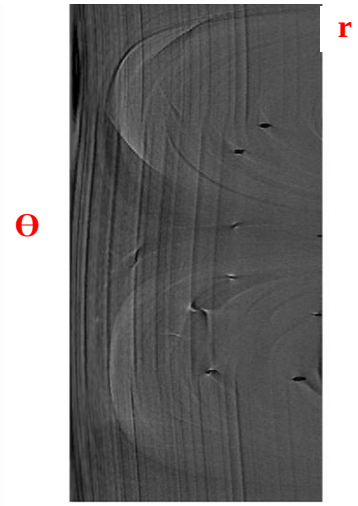

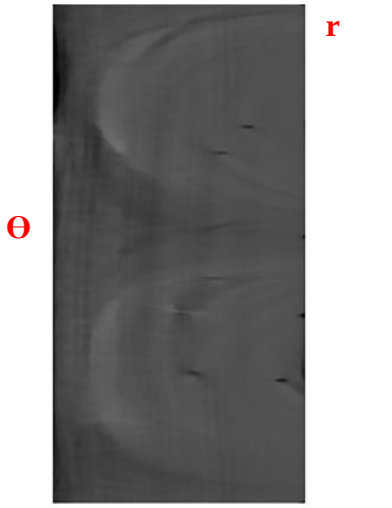

c) Cartesian to Polar Coordinate d) Median Filtered Image (5x30)

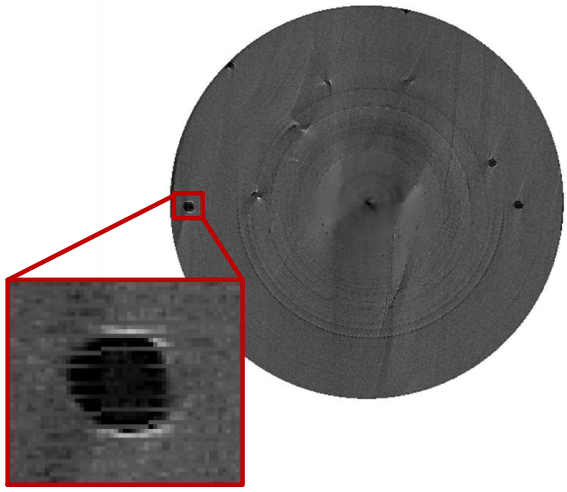

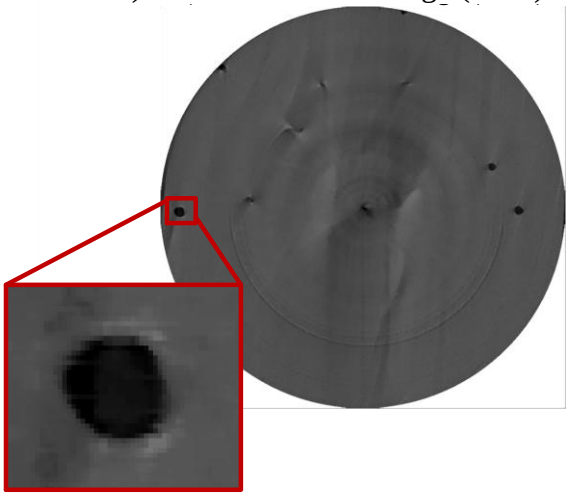

e) Polar to Cartesian Coordinate f) Median Filtered Image (4x4)

Figure 18: Ring artifact removal algorithm

3D XRM Analysis Procedure

The analysis of 3D XRM images was relatively straightforward since the bubbles had distinctly darker color in the images as compared to the binder medium, as shown in Figure 18. In addition, they were occupying separate locations within the binder (i.e., they were not touching each other). However, the image size was to concern due to the computational limitations. Initially, the images (878x878) were resized to half (439x439). Then, the resized images were converted to binary (black/white) images using a thresholding algorithm. Then, a connected components algorithm was utilized to label individual bubbles. After each bubble was labeled, the volumes and equivalent diameters (i.e., the diameter of a sphere of equivalent volume) of the bubbles were computed. In order to quantify the change in the structure of bubbles, their volume and size distribution were computed using algorithms developed in Matlab®.

3D temporal view of bubbles in the foamed binder prepared with 1% water content and 10psi air pressure at the 1^{st}, 15^{th} and 30^{th} minutes was given in Figure 19. As shown in the subimages, there were distorted bubbles at the border of the binder and the PP tube. Therefore, before further analysis, each bubble was individually visualized and grouped as accepted and rejected subsets. The accepted bubbles were in sphere or in ellipsoid shape, as shown in Figure 19.

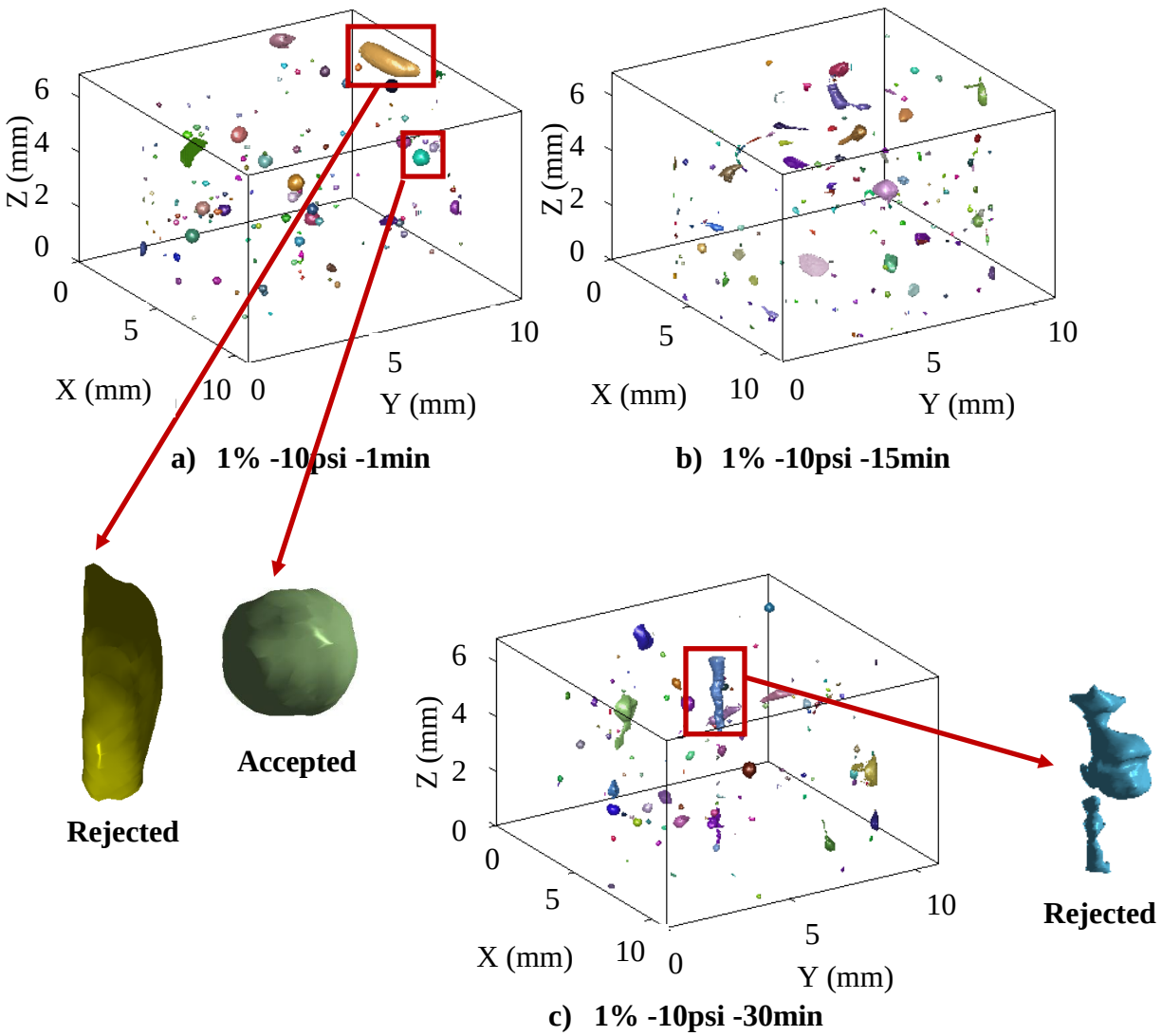

Figure 19: 3D temporal view of bubbles in the foamed binder prepared with 1% water content and 10psi air pressure a)1min, b)15min, c)30min

3D XRM Analysis and Comparision with Respect to AFCT

For each foamed binder, two replicates (PP tubes) were prepared at the 1st, 15th and 30th minutes. It took about 1 minute to fill two replicates at a time. Therefore, some larger bubbles may collapse during the sampling process. In order to limit the error, two foamed binders were

selected for XRM scanning and analyzing: i) 1% water content and 10 psi air void (1%-10psi), ii) 2% water content and 12.5 psi air void(2%-12.5psi), since it had been already revealed that both these combinations had the longest half-life, low average bubble size, and low expansion ratio.

The bubble size comparison of the samples were performed with respect to the equivalent diameters, as given in Figure 20 and Figure 21. Initially, the average bubble size for each replicate at the 1^{st}, 15^{th} and 30^{th} minutes were calculated and plotted in Figure 20a and Figure 21a. It was clearly observed that the bubbles collapse with time. In addition, it was also verifed that the rate of foam collapse was relatively high for the foamed binder prepared with high water content and air pressure (2%-12.5psi) than the one with relatievly low water content and air pressure (1%-10psi). In other words, the foam dissipates more rapidly from the binder with high expansion ratio and short half-life. As plotted in Figure 20b and Figure 21b, the maximum bubble sizes also decreased from the 1^{st} min to 30^{th} minute. However, it can be misleading to compare the maximum bubble size in between 1%-10psi and 2% -12.5psi by analyzing a single bubble. Similarly, the number of bubbles decreased as the time passes, as given in Figure 20c and Figure 21c. Since the bubbles were not distributed homegenous within the binder, the sampling may affect the number of bubbles in each replicate.As it was hypothesized before, the bubble size distribution of the samples were plotted in Figure 20d and Figure 21d, in which the gradation became finer as time passes, since larger bubbles dissipates quicker than the smaller bubbles. This observation validates the use of Stoke's Law in analyzing the AFCT height reduction data.

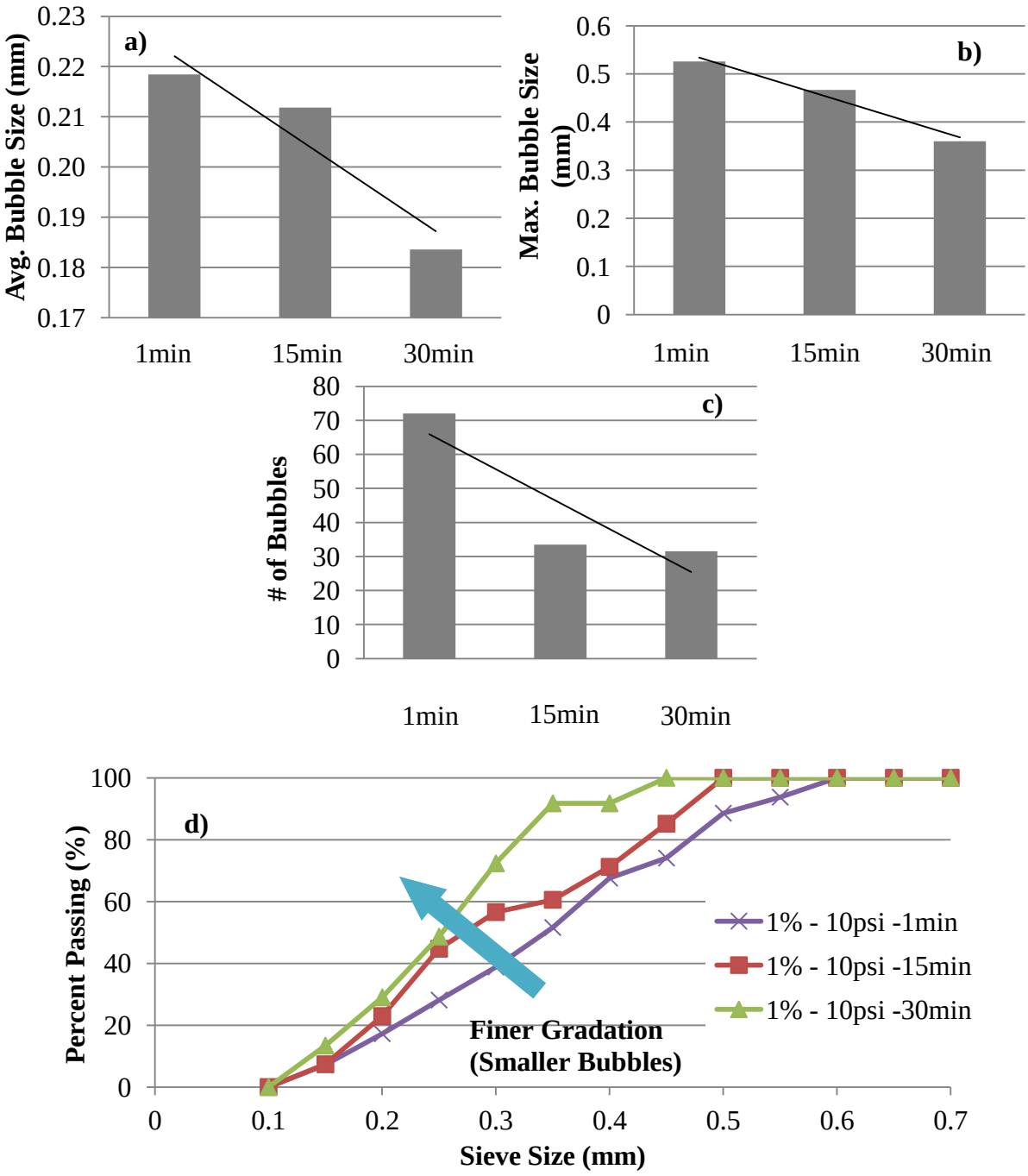

Figure 20: Bubble size comparison of X-Ray Microtomography images foamed binder prepared with 1% water content and 10psi air pressure a) Average, b)Maximum, c) Minimum, d) Number of bubbles, e) Bubble Size Distribution

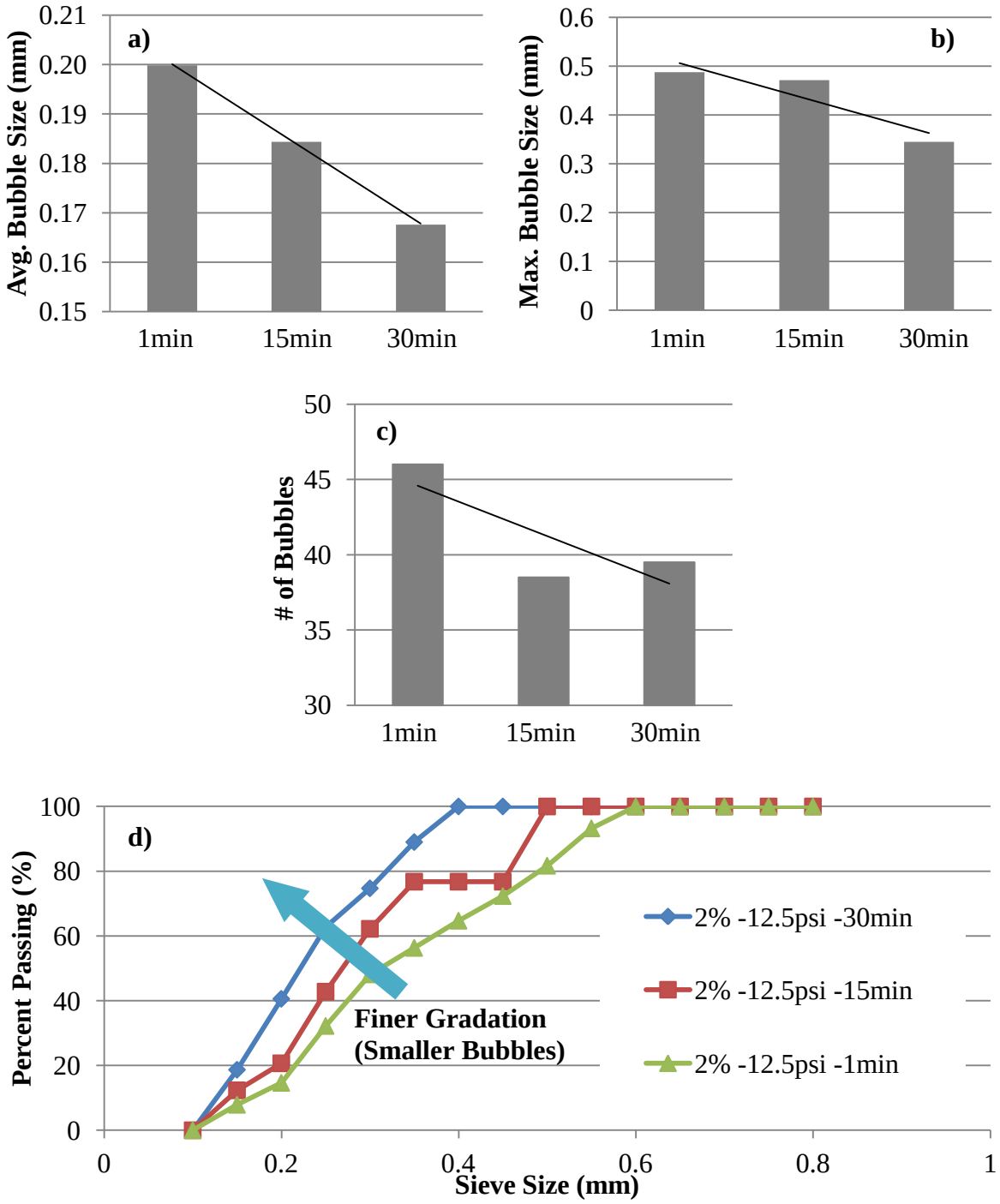

Figure 21: Bubble size comparison of X-Ray Microtomography images foamed binder prepared with 2% water content and 12.5psi air pressure a) Average, b)Maximum, c) Minimum, d) Number of bubbles, e) Bubble Size Distribution

The bubble size distributions calculated from the XRM images at the 1st minute and the AFCT were plotted for the 1%-10psi and 2%-12.5psi in Figure 22 and Figure 23. The bubble size distributions of three replicates from AFCT data and two replicates from XRM data were given in Figure 22. In addition, the average D_{50} were calculated and given in Table 5. Although both the analysis had relatively high variability, the gradations from both analyzes matched very well, except the very fine side of the gradation (smaller size). This variability was also expected since the bubble size distribution calculated from AFCT analyses takes into the change in first 5 minutes. On the other hand, the XRM samples were taken in the 1 minute and the sample size is comparably small. Also, after 5 minutes during AFCT test, the rate of reduction becomes very small and cannot be measured accurately with the camera used in this research. Perhaps a higher resolution camera and longer measurement of heights would have lead to better match. Considering all the variability, it can be claimed that the Bubble Size Distribution from AFCT matches very well with the Bubble Size Distribution from XRM images.

The bubble size distributions of four replicates from AFCT data and two replicates from XRM data for 2%-12.5psi were given in Figure 23. The gradations from both analyzes were varied in the same range although the difference was relatively high in the coarse gradations. This could be because of collapse of larger bubbles during sampling of XRM. It may be occurred because of the relatively rapid collapse of the large bubbles while sampling for XRM. It was also clearly observed from the calculated D_{50} from AFCT and XRM, given in Table 6.

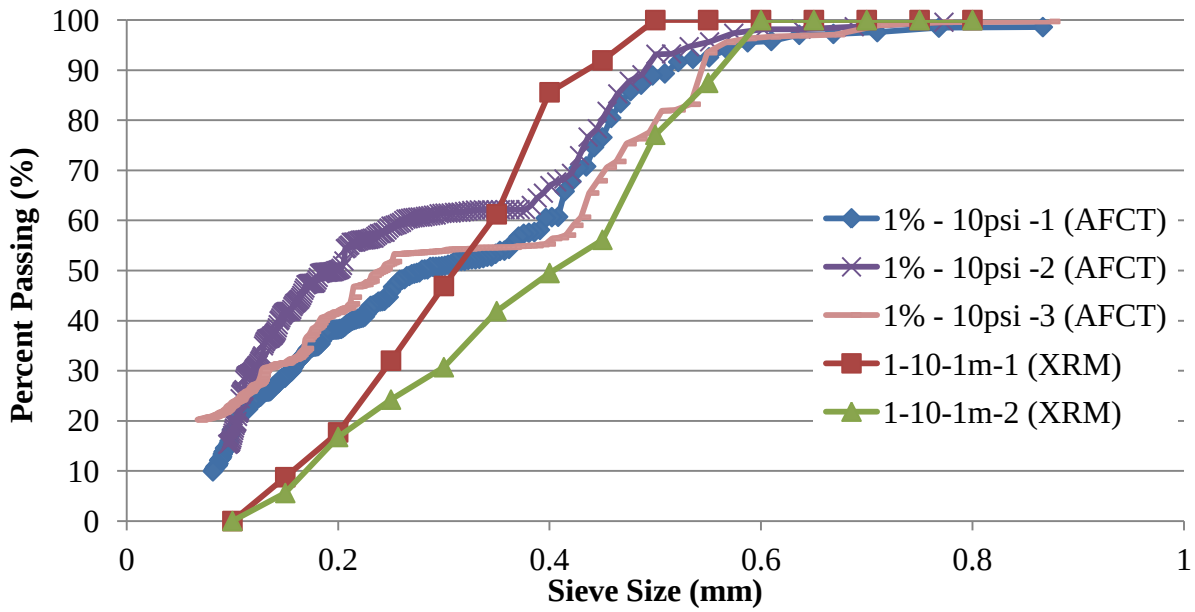

Figure 22: Comparison of Bubble Size Distribution from X-Ray Microtomography and AFCT.

Table 5: Comparison of Average Bubble Size from X-Ray Microtomography and AFCT imaging

	Bubble Size(mm)	Avg. Bubble Size (mm)	StDev. Bubble Size (mm)
1% - 10psi -1 (AFCT)	0.198		
1% - 10psi -2 (AFCT)	0.279		
1% - 10psi -3 (AFCT)	0.239	0.239	0.040
1% - 10psi -1 (XRM)	0.311		
1% - 10psi -2 (XRM)	0.404	0.357	0.066

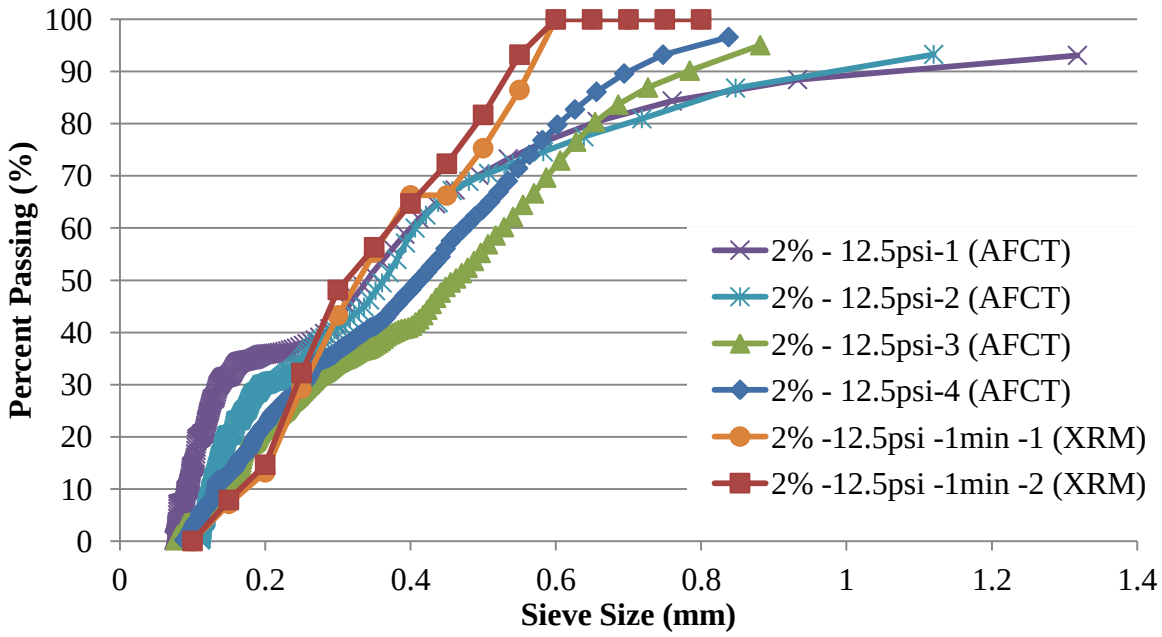

Figure 23: Comparison of Bubble Size Distribution form X-Ray Microtomography images and AFCT.

Table 6: Comparision of Average Bubble Size from X-Ray Microtomography and AFCT.

	Bubble Size (mm)	Avg. Bubble Size (mm)	StDev. Bubble Size (mm)
2% - 12.5psi -1 (AFCT)	0.340		
2% - 12.5psi -2 (AFCT)	0.363		
2% - 12.5psi -3 (AFCT)	0.459		
2% - 12.5psi -4 (AFCT)	0.412	0.394	0.053
2% - 12.5psi -1 (XRM)	0.328		
2% - 12.5psi -2 (XRM)	0.292	0.310	0. 026

CHAPTER 5

LABORATORY PERFORMANCE TESTS ON WMA MIXTURES PREPARED WITH FOAMED BINDER

The current WMA pavement design procedures are based on limited empirical data and recommendations of the WMA technology suppliers. WMA design procedures do not consider the foam quality since its importance has not been fully understood. Therefore, the long term performance of the WMA mixtures prepared with different foamed binders (the ones in CHAPTER 4) in the laboratory was evaluated via performance tests and compared with the foamed binder quality parameters presented earlier.

WMA ASPHALT MIXTURE DESIGN

Draft Appendix of AASHTO R 35: Special Mixture Design Considerations and Methods for WMA, was followed in this study for the WMA mix design. The aggregate gradation of the WMA mixtures was a dense graded mixture as shown in Figure 24. This design was previously used in a traditional HMA and crumb rubber modified asphalt (terminal blend) pavement sections in Lansing, Michigan. The performance of these mixtures was evaluated by the author of this thesis. All mixtures were prepared with PG58-28 virgin binder, which was provided by a local petroleum supplier. The properties of the binder were given in CHAPTER 4.

The standard Superpave mix design procedure, as suggested in the draft Appendix of AASHTO R 35, was utilized in this study to obtain the optimum asphalt content and to evaluate the volumetrics of the mix design. The optimum binder content of the HMA mix was 4.53% by

weight of the mixture. The WMA mixtures were initially prepared with the same binder content as the HMA to calculate the volumetrics and if needed to adjust the binder content. The first trial with WMA resulted in the mix properties (i.e., air void at N_{design}, VFA, VMA) that were within the Superpave limits. The target air void at N_{design} for WMA mix was within the limits 4±0.5% as suggested in Superpave Mix Design, though it was close to the lower limit, 3.54%. The voids in mineral aggregates (VMA) at N_{design} was 15%, which is higher than the minimum, 14%. The voids filled with asphalt (VFA) was 78%, which is in the range of 70-80, as specified by Superpave specification. Thus, the WMA mix design was almost identical to that of HMA/

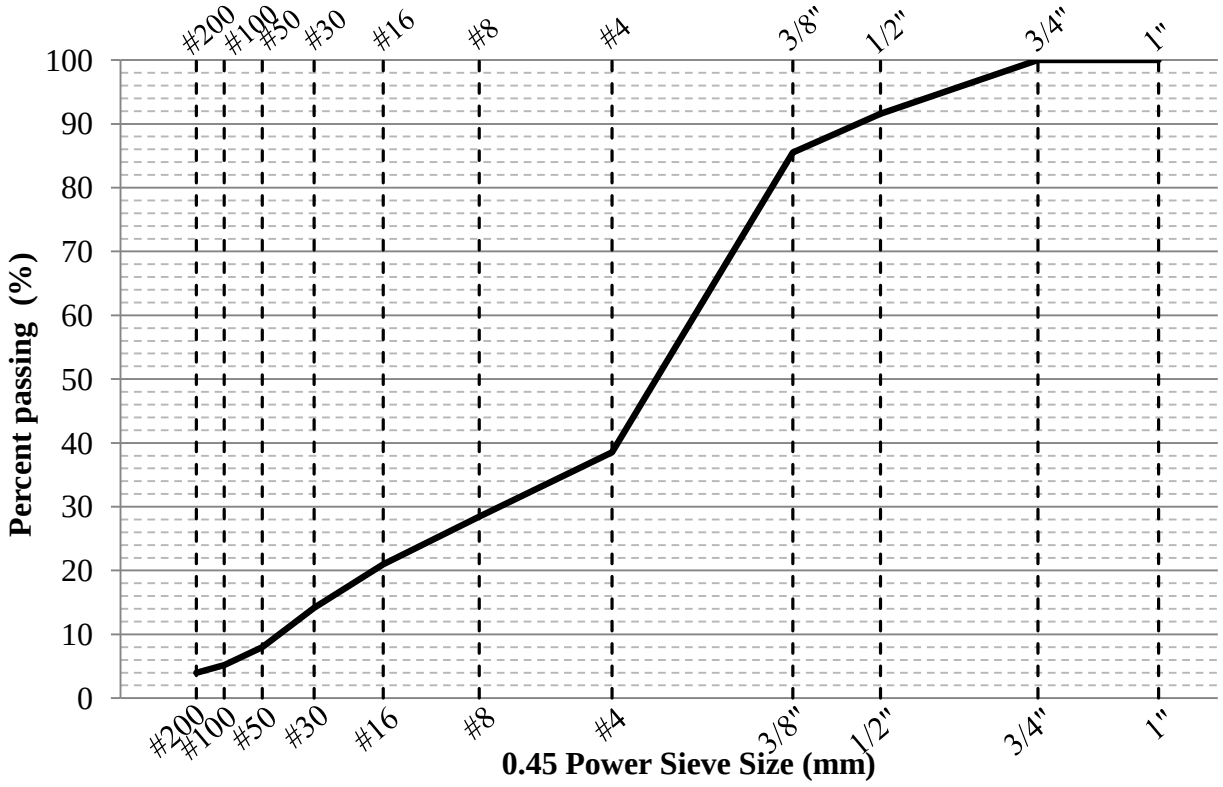

Figure 24: Aggregate gradation of WMA mixtures

PERFORMANCE TEST SAMPLE PREPARATION

The WMA samples for performance testing were prepared based on the suggestions of NCHRP Reports 691 and 714, which were the most recent studies on WMA design and performance analysis.

Flow chart of the WMA asphalt mixture design and performance tests is illustrated in Figure 25. Initially, the foamed binder temperature (FT) was determined based on the viscosity of the non-foamed binder. The viscosity of the binder should be approximately 300 mPa.s at the foaming temperature for successful foaming. The rate of flow of 200 grams of binder took 15 seconds at this viscosity under the gravity (manufacturer's calibration). FT was 155°C for the PG58-28 binder used. Then, the aggregate temperature (AT) was determined to be approximately 20°C lower than the FT, which was 135°C. This was also based on the experience of the states and current practice.

The preparation process for WMA and conventional HMA are very similar. Initially, the aggregates were batched and heated to AT. The binder is heated about 5°C more than FT (FT+5°C) in order to compensate the temperature loss of the binder while pouring it to the chamber of the foamer. It should be noted that it was crucial to calibrate and verify the water content and air pressure of the foamer, frequently. Once the binder temperature equilibrated, the aggregates were transferred to the mixing bucket and placed on a scale that is located under the foamer. The binder was directly foamed into the mixing bucket. If excessive binder was foamed, it was gently moved with a piece of paper towel. The loose mixture was mixed in a bucket mixer approximately 2 minutes till a homogenous mix was accomplished. Then, the mixtures were conditioned for short term (two hours) at compaction temperature (CT) before compaction. CT

was determined to be 10°C lower than AT, which was 128°C in this study. The samples were compacted with a Superpave Gyratory Compactor (SGC). After overnight cooling of the samples at the room temperature, the samples were cut and cored to the specific sizes for the performance tests. The cored and cut samples were accepted for performance testing if percent of the air void was in the range of 7±0.5%.

The performance test samples in this chapter were named based on the foamed binder's injected water content and air pressure, as given in Table 7. For instance, a WMA sample prepared with 1% water content and 10 psi air pressure injected foamed binder was called as "1% - 10psi".

Table 7: Performance test sample descriptions

Foamed Binder		Name of the WMA Sample
Water Content (% of the binder)	Air Pressure (psi)	
1%	10 psi	1% - 10psi
2%	12.5 psi	2% - 12.5psi
3%	15 psi	3% - 15psi
4%	17.5 psi	4% - 17.5psi
5%	20 psi	5% - 20psi

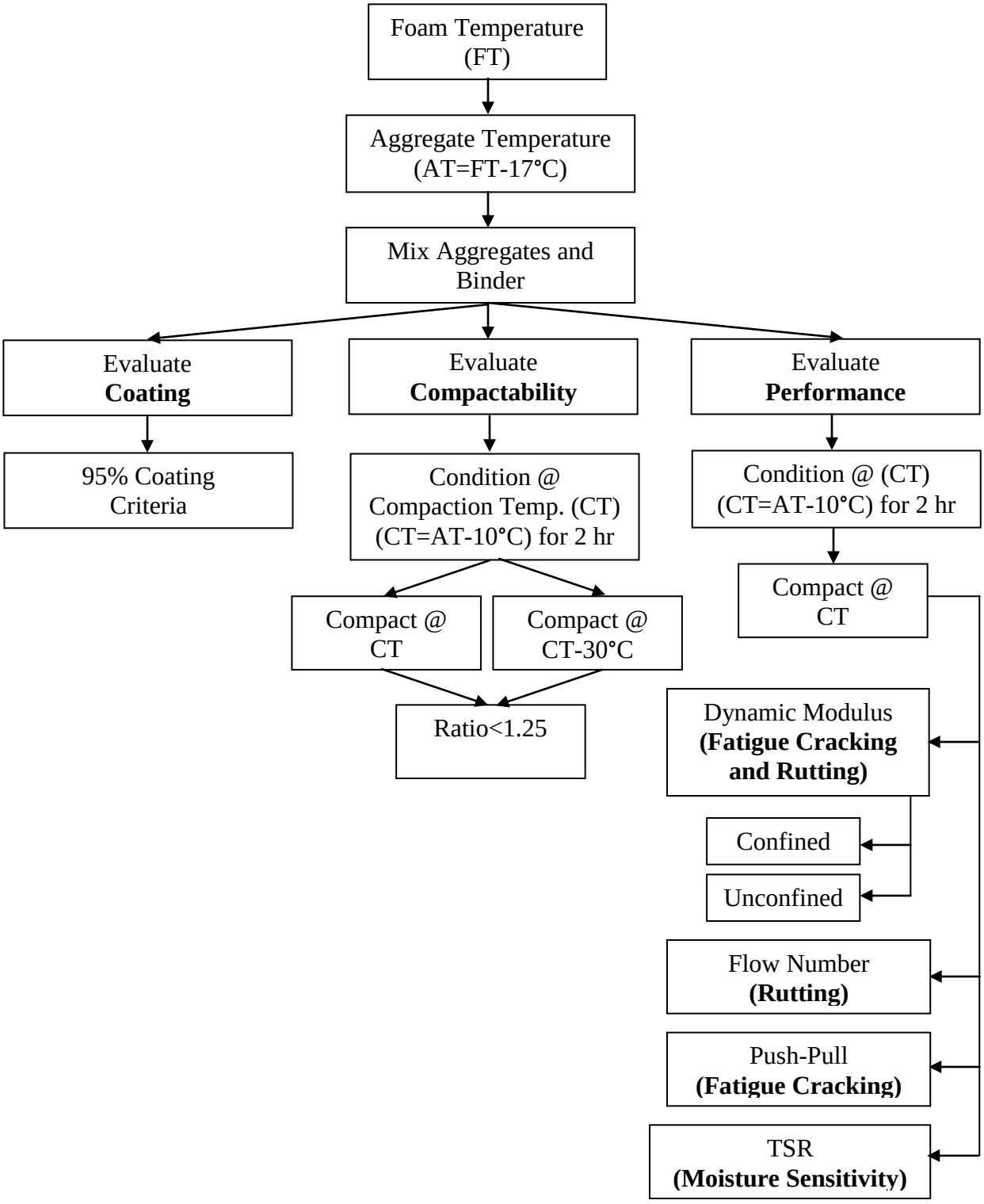

Figure 25: Flow chart of the WMA performance evaluation study

STATISTICAL EVALUATIONS OF LABORATORY TEST RESULTS

This study was designed with the mixtures with identical aggregate gradations with different foamed binders (i.e., injected air pressure and water content) to understand the influence of the foam quality on the pavement response (see Table 7). Both correlation and regression analyses were used in this study since the data set was limited with five different mixtures. Initially, the measured data was ranked according to the Kendall rank correlation coefficient (tau (τ) coefficient), which is a distribution free/non-parametric, ranking correlation parameter for small data sets (Gibson, 2012). The set of data pairs are initially ordered in the increasing rank of the first column. Then, the observations are specified as concordant and discordant pairs based on the rank of the second column. The data pairs are compared with respect to the first row. If the value of the pair is greater than the first row, it is specified as a concordant pair. On the contrary, if the value of the pair is smaller than the first row, it is classified as discordant pair. The same process is repeated for each consequent row till the last row. The tau coefficient is calculated as follows:

$$\tau = \frac{n_c - n_d}{\frac{n(n-1)}{2}} \quad [13]$$

where n_c and n_d are the total number of concordant and discordant pairs and n is the total number of points. The tau coefficient ranges from -1 to 1. If the coefficient is equal to 1, it indicates perfect agreement between two rankings. On the contrary, if the coefficient is equal to -1, it designates the disagreement between two rankings (i.e., one ranking is in the reverse of the other). A coefficient of 0 signifies the lack of association or complete independence between

two different data sets. The significance of correlation is also assessed based on the (n_c-n_d) and n using Kendall's Tau significance table (Kendall and Gibbons, 1996). A detailed Kendall's Tau coefficient calculation is given in the next section.

Regression analysis was also used to study the relation between the foamed binder parameters and performance of mixtures. Linear regression lines were fitted using the least squares approach. In addition, polynomial regression was fitted for characterizing the nonlinear relationships as a 2^{nd} order polynomial. The regression lines were coupled with the coefficient of determination (R^2), in which the goodness of the regression fit is evaluated.

COATING OF AGGREGATES

Coating of the WMA mixtures is a concern due to low production temperatures. The degree of particle coating is typically determined using AASHTO T195, Standard Method of Test for Determining Degree of Particle Coating of Bituminous-Aggregate Mixtures. In NCHRP Reports 691 and 714, the coating criterion for the WMA mixtures was recommended as 95%.

AASHTO T195 requires sieving the loose mixture through 3/8" sieve, right away after mixing while it is still hot. Then, the aggregates retaining on the sieve are laid on a wax paper in a single layer without further mixing. The aggregates are separated into two subgroups: as coated and uncoated aggregates.

Figure 26 shows the percentage of uncoated aggregates at different combinations of water content and air pressures of foaming. As shown, percent of uncoated aggregates are similar in 1% - 10psi, 2% - 12.5psi, and 3% - 15psi, and then it increases significantly at 4% -17.5psi and

5% - 20psi. Statistical analysis of the relation between the injected water content/air pressure of the foamed binder and the percent of uncoated aggregates are given in Table 8. In addition, Kendall's tau coefficient, which is explained in the previous section, is illustrated in Table 8a. The tau coefficient is relatively low at 0.4 and the (n_c-n_d) is 4. For single tailed significance test, the proportion of rankings is 0.242 (24.2%). It can be concluded that the ranking correlation is significant as a level of 0.758 (75.8%) while statistical significance is typically at 95%. The coefficient of determination of the linear fit is 0.673 and its significance is 0.911 (91%).

Based on the findings in CHAPTER 4, low water content and air pressure leads to small bubbles. For example, 1% water content and 10 psi air pressure injected foamed binder was anticipated to be composed of relatively small bubbles and the collapse of the foamed binder takes longer, which allowed the binder to be more workable and coat the aggregates better. On the other hand, the foamed binder prepared with 5% water content and 20 psi injected air was composed of large bubbles and the foam collapsed relatively quick. The findings indicated that the time interval of the binder was too short to coat the aggregates. Based on the suggested criteria in NCHRP reports, only three mixes (i.e., 1% - 10psi, 2% -12.5psi and 3% - 15psi) passed the coating criteria.

According to the coating tests, following conclusions can be drawn:

(i) As the expansion ratio of the foamed binder increased and its half-life decreased, degree of coating decreased.

(ii) As the bubble sizes in the foamed binder increased, the coating of aggregates became poor. On the contrary, as the surface area of the bubbles increased because of the small bubbles, the aggregates were coated better.

As it was observed in Figure 26, while the trend is clear, the variability within the same mixtures was relatively high. The coarse aggregates used in this study had limited number of ironstones, which had partially coating problems. Clay-ironstone is a widespread a yellowish-brown to dark brow aggregate (siderite) composed of $FeCO_3$ in Michigan. These aggregates are soft and porous and there are limitations of their usage in asphalt pavements in MI (MDOT Procedures for aggregate inspection, 2009).

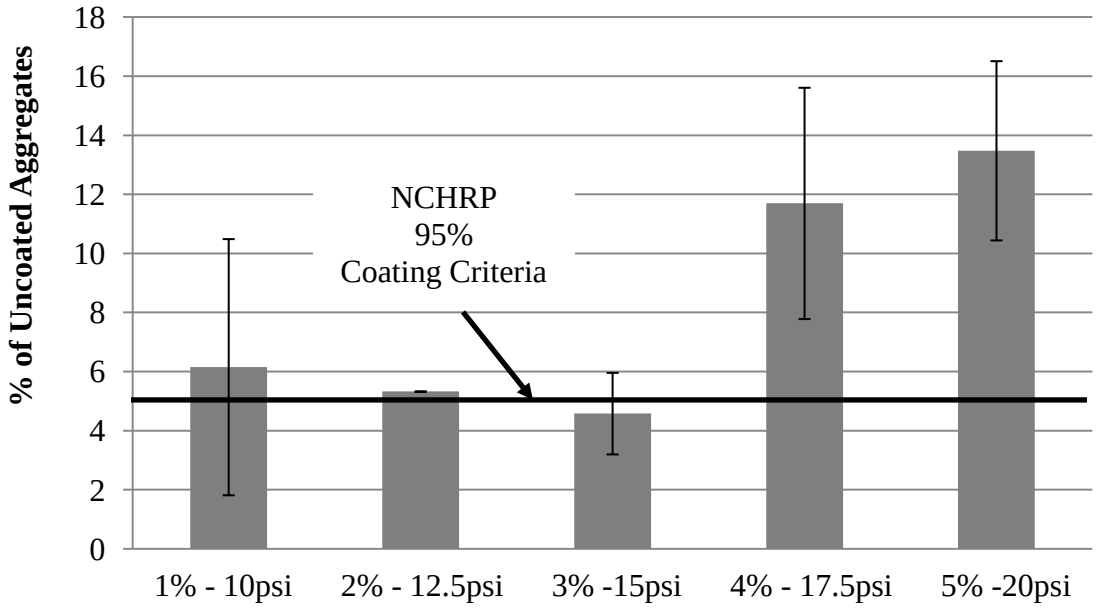

Figure 26: Percent (%) of uncoated aggregates

Table 8: Statistical analysis for percent of uncoated aggregates: a) Illustration of Kendall's Tau Correlation Coefficient calculation b) Correlation and Linear Regression Summary

a) Illustration of Kendall's Tau Correlation Coefficient calculation

Row	Water Content/Air Pressure	% of Uncoated Aggregates	2nd Row		3rd Row		4th Row		5th Row	
			C*	D**	C	D	C	D	C	D
1st Row	1	6.15	-	-	-	-	-	-	-	-
2nd Row	2	5.33	-	+	-	-	-	-	-	-
3rd Row	3	4.58	-	+	-	+	-	-	-	-
4th Row	4	11.70	+	-	+	-	+	-	-	-
5th Row	5	13.48	+	-	+	-	+	-	+	-
n	5									
Σn_C	7									
Σn_D	3									
$n_C - n_D$	4.00									
τ	0.40									
Significance	0.76									

C*= Concordant

D**= Discordant

b) Correlation and Linear Regression Summary

	Correlation		Linear Regression		
	Kendall's Tau	Kendall's Tau Significance (1- pvalue)	R	R^2	Regression Significance (1-pvalue)
% of Uncoated Aggregates vs. Water Content/Air Pressure	0.400	0.758	0.821	0.673	0.911

COMPACTABILITYOF WMA MIXTURES

Compactability of the WMA mixtures is another concern due to low production and laying temperatures. Compactability of WMA mixtures was determined using the procedure described NCHRP Reports 691 and 714. The procedure compares the number of gyrations to reach 92% relative density (i.e., 8% air voids) at compaction temperature (CT) and 30°C lower

than CT, which is designated as the temperature loss in between the production and construction. Then, the compactability ratio (CR) is calculated using:

$$CR = \left(N_{92}\right)_{CT-30\,^{\circ}C} / \left(N_{92}\right)_{CT} \quad [14]$$

where $\left(N_{92}\right)_{CT-30\,^{\circ}C}$ = the number of gyrations to reach 92% relative density at 30°C below the CT and $\left(N_{92}\right)_{CT}$ = the number of gyrations to reach 92% relative density at CT. The mixture is deemed compactable if the compactability ratio is less than 1.25 (NCHRP Report 691 and 714).

Three air voids and water content combinations were selected based on the foam quality parameters: i) 1% water content and 10 psi air pressure, ii) 3% water content and 15psi air pressure, and iii) 5% water content and 20 psi air pressure. Three replicates were compacted for each mixture set at 128°C and 98°C for this study. Then, the average number of gyrations was computed to achieve the 8% air voids as shown in Figure 27a. The statistical analysis of the relation between the number of gyrations and the injected water content/air pressure of the foamed binder is given in Table 9. Since the data pairs are limited with three different mixtures and the ranking is poor and not linear, the tau coefficient is calculated to be 0.333, which is relatively low. Thus, the significance of the ranking correlation is 0.5, which is significantly lower than the typical level 0.95. In addition, the linear regression shows similar trend with respect to ranking correlation. The coefficient of determination and significance are both relatively low.

The compactability ratios for the selected samples were significantly lower than 1.25 (suggested limit) as shown in Figure 27b, no further testing was performed for the other foamed binder combinations, since compactability was not a concern for the selected mix design and not directly related with the pavement performance. It appears from Figure 27b that the water content/air combinations did not indicate a trend. However, different foaming technologies used in the field may or may not result in such a trend, which is not investigated in this study.

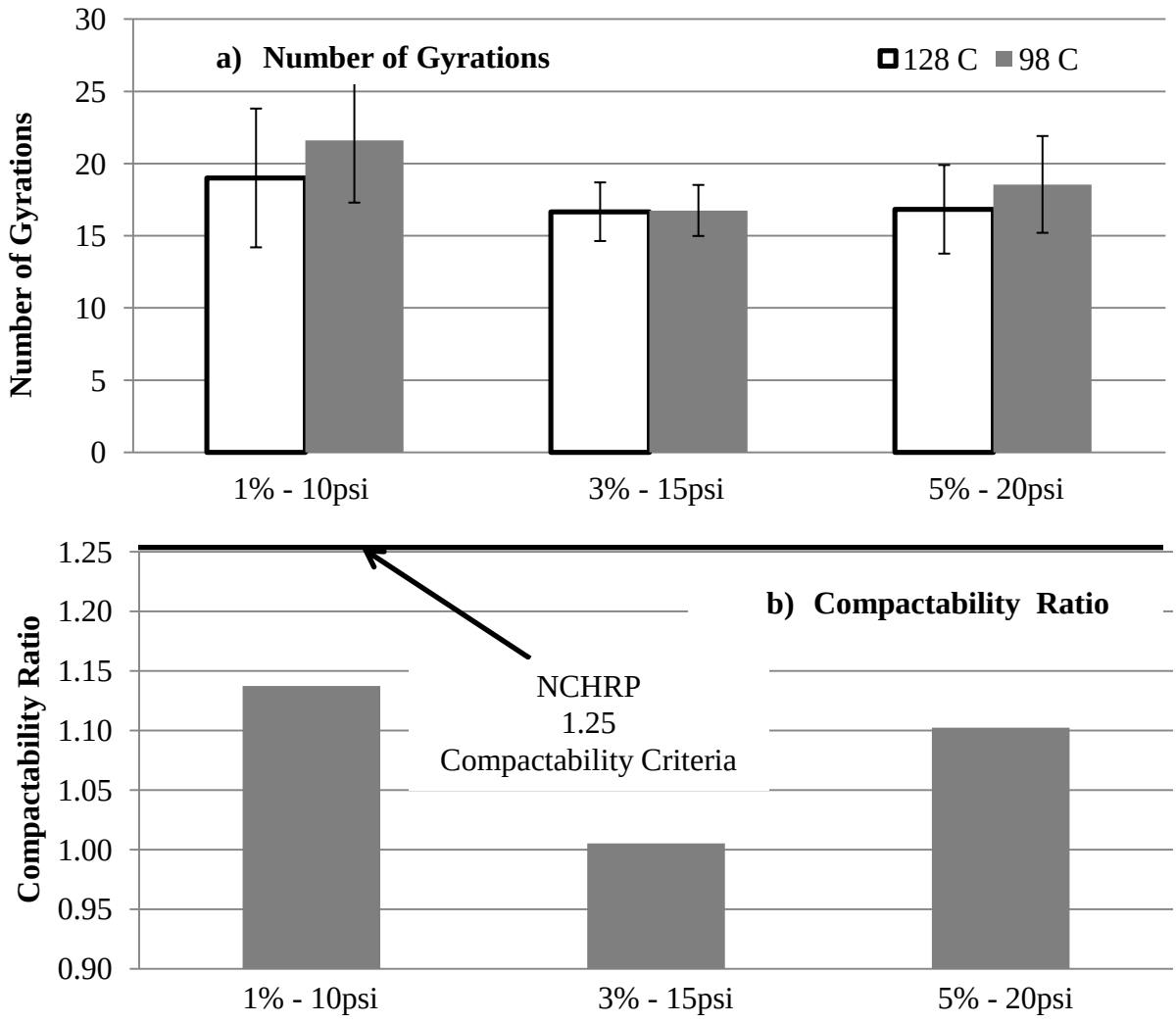

Figure 27: Compactability of WMA mixtures: a) number of gyrations, b) compactability ratio

Table 9: Statistical analysis for number of gyrations and compactability ratio

	Correlation		Linear Regression		
	Kendall's Tau	**Kendall's Tau Significance (1- pvalue)**	**R**	**R^2**	**Regression Significance (1-pvalue)**
Number of Gyrations @ 128°C versus Water Content/Air Pressure	0.333	0.500	0.832	0.693	0.626
Number of Gyrations @ 98°C versus Water Content/Air Pressure	0.333	0.500	0.622	0.387	0.427
Compactability Ratio versus Water Content/Air Pressure	0.333	0.500	0.255	0.065	0.164

MIXTURE PERFORMANCE TESTS

After the coating of the aggregates and compactability of the mixtures were assessed, the next step was evaluating the long-term performance of WMA mixes via laboratory tests. The performance tests included in this study were: (i) Dynamic Modulus, (ii) Flow Number, (iii) Compression-Tension Fatigue, and (iv) Moisture Susceptibility (TSR).

Dynamic Modulus Test

Dynamic Modulus (|E*|) test is a non-destructive test to determine the stiffness and the viscoelastic primary responses (i.e., undamaged, low-strain response) of asphalt mixtures at different temperatures and loading frequencies. In addition, this test is useful for preliminary estimation of rutting and fatigue cracking of asphalt pavements at design stage, and also major input to the Mechanistic Empirical Design Guide (MEPDG) software.

Dynamic Modulus Test Procedure

The |E*| tests were conducted according to AASHTO TP79: Determining Dynamic Modulus and Flow Number of Hot Mix Asphalt (HMA) by using the Asphalt Mixture Performance Tester (AMPT), shown in Figure 28, though it should be noted that the sample preparation for WMA mixes is different than HMA mixes. Initially, the short-term (2 hours) conditioned loose mixtures (long-term conditioning (4 hours) is an obligation for HMA mixtures) were compacted at a diameter of 150mm to a height of 180mm. Then, the compacted samples were cored at a diameter of 100mm and the ends were cut to a final height of 150mm. The final samples were accepted for testing if percent of the air void was in the range of 7±0.5%. Then, the LVDT tabs were glued using two components high strength epoxy (120° apart from each other). LVDT gauge lengths were about 70 mm and the top and bottom tabs were about 37.5 mm away from the top and bottom edges of the samples. The |E*| tests were performed at -10, 10, 21, 37, and 54°C at loading frequencies of 0.1, 0.5, 1.0, 5, 10, and 25 Hz for at each temperature in two different modes: (a) unconfined, and (b) confined.

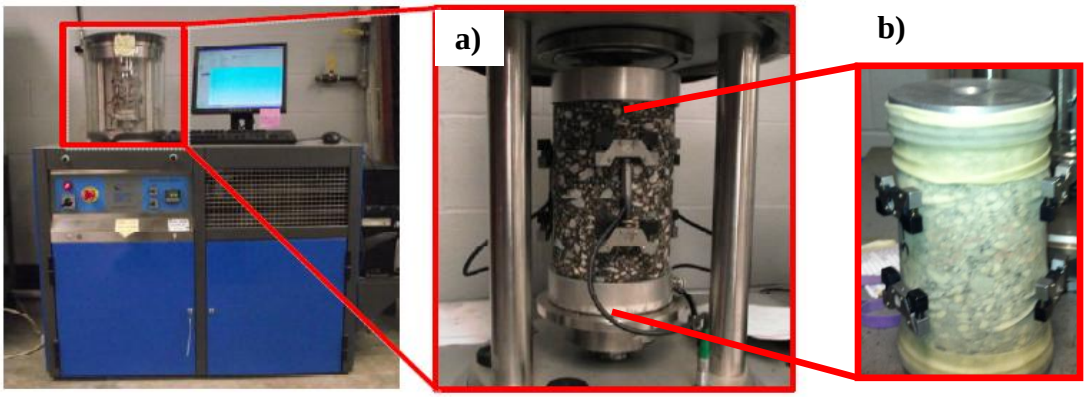

Figure 28: Asphalt Mixture Performance Tester (AMPT): a) Unconfined test sample, b) Confined test sample

Brief Summary of Dynamic Modulus Master Curve

After determining |E*| values and phase angles at each temperature and frequency, |E*| master curves are generated using the time temperature superposition principle, in which both the effects of temperature and frequency on the asphalt mixture is combined. The raw |E*| data at different temperatures and frequencies and its master curve generated by shifting the data at different temperatures along the loading frequency are given in Figure 29. The resulting parameter in x-axis is called the reduced frequency (f_R), which is defined as follows:

$$f_R = f\ a(T) \quad \text{or} \quad \log(f_R) = \log(f) + \log(a(T)) \qquad [15]$$

where a(T) is the shift factor coefficient which is a function of temperature (T) and f is the loading frequency. The temperature dependency of the asphalt mixture is measured by the amount of the shifting of the raw |E*| data. The shift factor is determined by fitting a second order polynomial as function of T and the reference temperature (T_{ref}), as follows:

$$a(T) = 10^{a_1(T^2 - T_{ref}^2) + a_2(T - T_{ref})} \qquad [16]$$

where a_1 and a_2 are the shift factor coefficients. Finally, the following sigmoid function is fitted to the measured |E*| data to generate the master curve as shown in Figure 29.

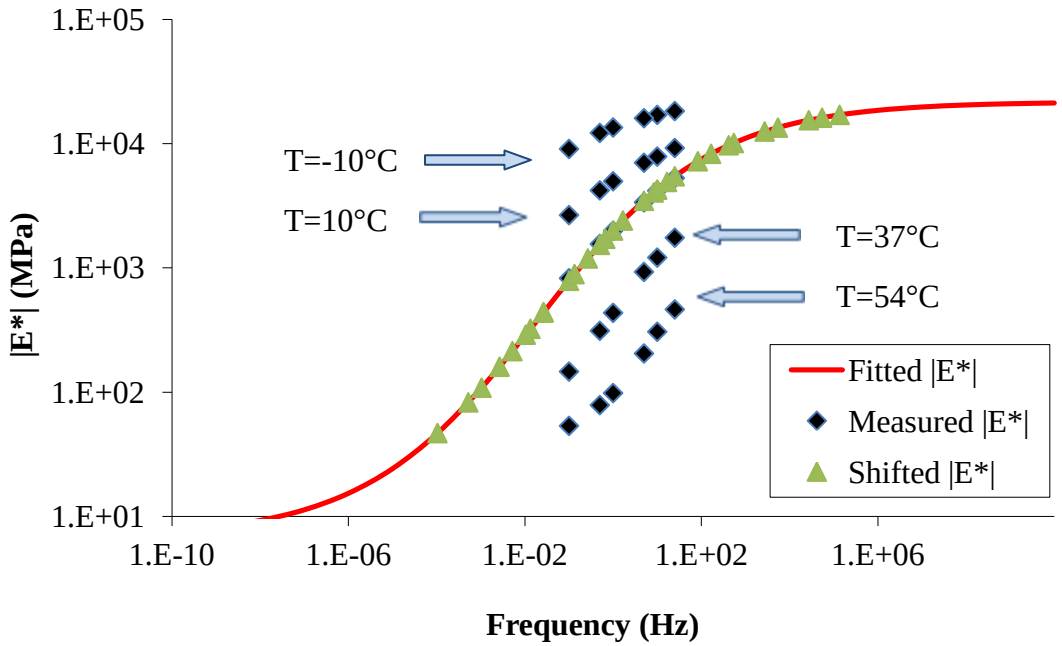

Figure 29: Illustration of shifting |E*| data at different temperatures to obtain the |E*| master curve

$$\log(|E^*|) = b_1 + \frac{b_2}{1 + \exp(-b_3 - b_4 \log(f_R))} \quad [17]$$

where b_1, b_2, b_3 and b_4 are the sigmoid coefficients. |E*| increases with the increase in the loading frequency and decreases with the increases of the testing temperature. |E*| master curve is useful for estimating the behavior (i.e., rutting and fatigue cracking) of mixtures over a range of temperatures and rates of loading. Typically, mixtures with relatively low |E*| values at low temperatures/high frequencies are more flexible (and less brittle), therefore more resistant to fatigue cracking. On the other hand, mixtures with high |E*| at high temperatures/low frequencies are stiffer and are more resistant to rutting.

In order to better interpret the master curves, they can be plotted in log-log scale (to better see the difference between the curves at low reduced frequencies) and in linear-log scale (to better see the difference between the curves at high reduced frequencies). Less cracking is typically expected when the |E*| is low at high reduced frequencies (high reduced frequency = high test frequency/low test temperature combination). On the other hand, less rutting is expected when |E*| is high at low reduced frequencies (low reduced frequency = low test frequency/high test temperature combination).

Unconfined Dynamic Modulus Test Results and Discussions

The effect of the foamed binder parameters on the rutting and fatigue cracking performance has not been studied before. Therefore, three foamed binders with different injected air pressure and water content (i.e., 1% - 10psi, 3%- 15psi, 5% - 20psi) were initially selected to prepare WMA samples. Two replicates for each WMA mixture set were tested according to AASHTO TP79, as given from Table 17 to Table 22 in APPENDIX A. Figure 30a shows the |E*| versus reduced frequency plots in log-log scale. As shown, the curves of three different mixtures are very similar. Therefore, it is hard to estimate the relative rutting susceptibilities of these WMA mixtures. Figure 30b shows the |E*| versus reduced frequency plots in linear-log scale. As shown, the fatigue cracking potential of WMA mixtures decreased with the increase in the injected water content and air pressure to foam the binder. On the contrary, the fatigue cracking susceptibility increased with the decrease in the injected water content and air pressure of the foamed binder. This may be explained by the long half-life and the small bubbles that may have gotten stuck in the 1% - 10psi mixture, causing fatigue cracking susceptibility. The 2 hours of curing time may not be adequate for the collapse of all the micro bubbles. Although |E*|

master curve is a good ‘indicator’ of performance of asphalt mixtures, the conventional dynamic modulus test (unconfined) was not sufficient to discuss the rutting and cracking potential of different WMA mixtures for this study. Additionally, the measured |E*| (not the sigmoid fitted) at 10 Hz at 10, 21 and 54°C versus the foam quality indicators (i.e., ER, HL, FI, D_{50} and SAI) were plotted in Figure 31, in order to investigate if any relation exists in between the measured |E*| and the foam quality. It was clear that |E*| decreases with the increase in the temperature as explained in the previous section. However, there was negligible variability in the measured |E*| of WMAs. Thus, no relation was founded in between the foam quality and |E*| as shown in Figure 31 and Table 10. Since the dataset is limited with three different mixes, the tau coefficient and its significance is relatively low, 0.333 and 0.5. In addition, the linear regression fit indicates the lack of the relation between unconfined |E*| and foamed binder parameters. Therefore, in the following section, the dynamic modulus tests under confinement were performed using the same samples, in order to be able to establish relation between the confined |E*| and foam binder quality.

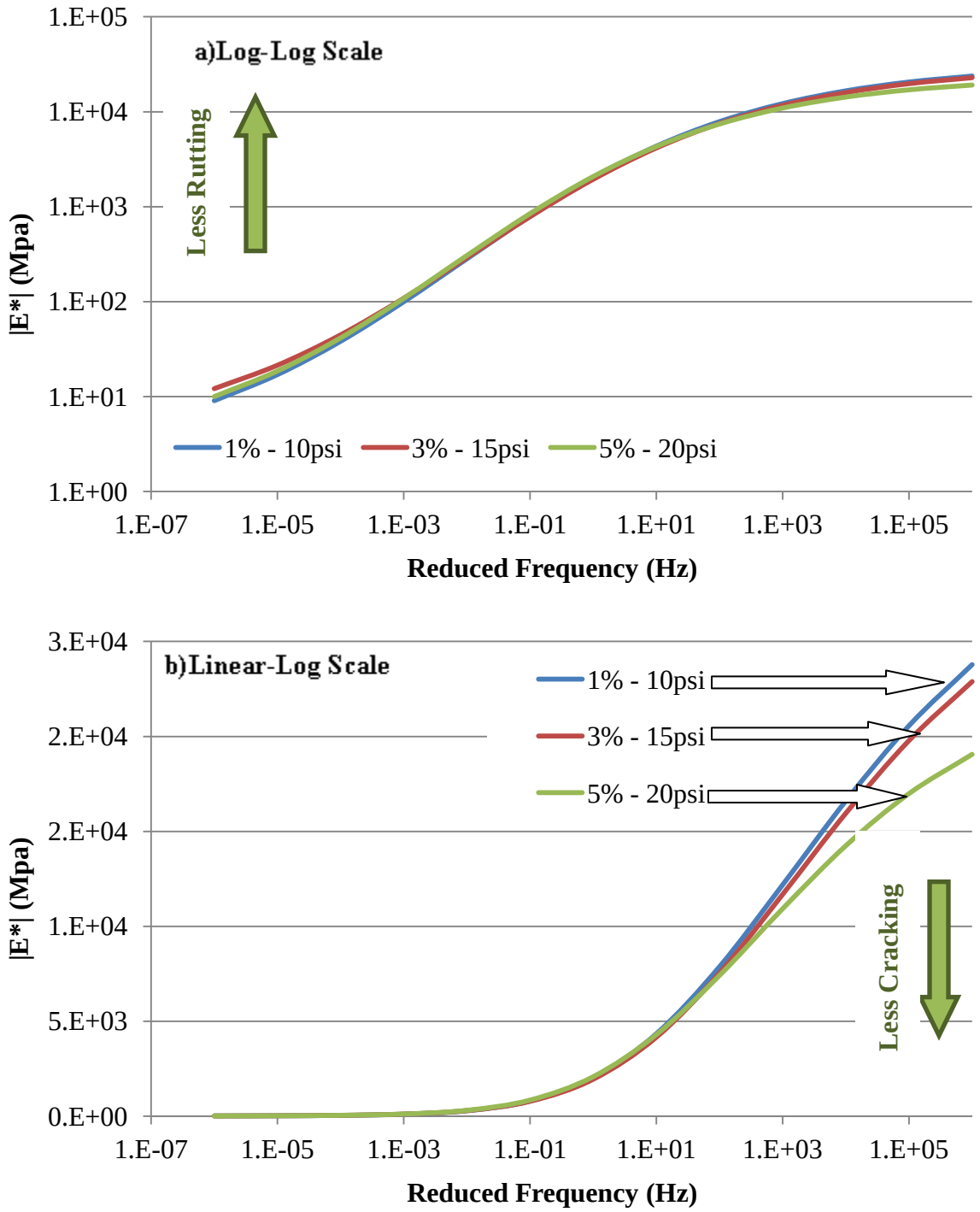

Figure 30: Unconfined Dynamic Modulus: a) log-log, b) linear –log.

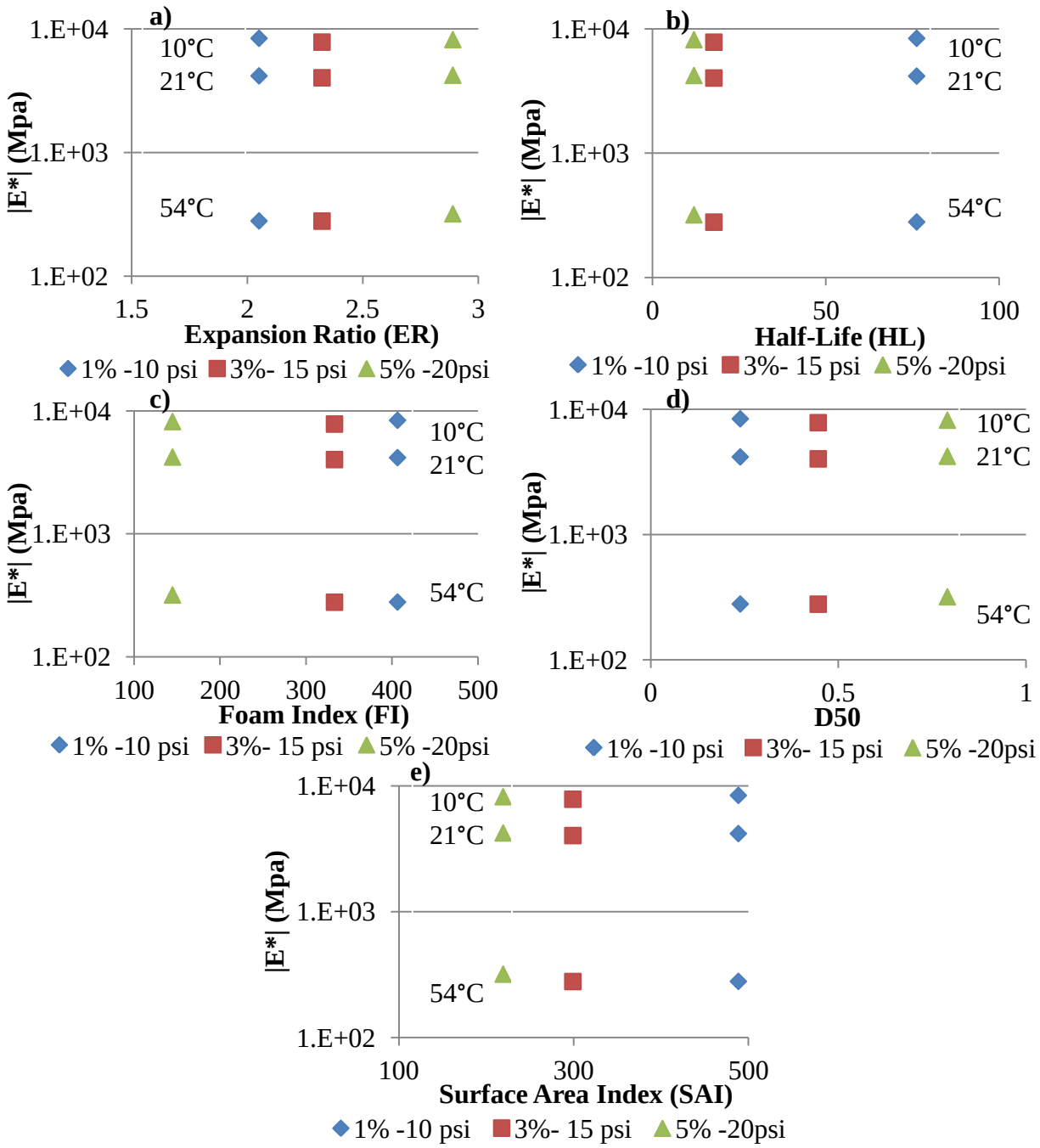

Figure 31: The comparison of Unconfined Dynamic Modulus at 10 Hz and Foam Binder Quality Parameters a) Expansion Ratio (ER), b) Half-Life (HL), c) Foam Index (FI), d) D50, e) Surface Area Index (SAI)

Table 10: Statistical analysis between unconfined dynamic modulus at 10 Hz and foam binder quality parameters

	Correlation		Linear Regression		
	Kendall's Tau	**Kendall's Tau Significance (1- pvalue)**	**R**	**R^2**	**Regression Significance (1-pvalue)**
Unconfined E* vs. Expansion Ratio	0.333	0.500	0.427	0.182	0.281
Unconfined E* vs. Half-Life	-0.333	0.500	0.199	0.040	0.128
Unconfined E* vs. Foam Index	-0.333	0.500	0.471	0.222	0.312
Unconfined E* vs. D50	0.333	0.500	0.374	0.140	0.244
Unconfined E* vs. SAI	-0.333	0.500	0.0107	0.0001	0.007

Confined Dynamic Modulus Test Results and Discussions

The confined dynamic modulus is generally not performed due to the complexity of the testing procedure. Zeiada et al. (2011) studied the different level of confining stresses (10, 20, 30 and 40 psi) on the moduli with respect to the unconfined stress. It was observed that the confining stress higher than 20 psi did not increase the moduli of the mixtures. In addition, it was concluded that the mixtures were less affected form the confinement at lower temperatures due to the stiffness of the mixtures at lower temperatures. On the other hand, the confining pressure at higher temperatures significantly affects the moduli due to loss of stiffness at high temperatures. Therefore, 20 psi confined stress was determined to be used in this study. The measured and predicted |E*| and phase angle data is available for each test from Table 23 to Table 28 in APPENDIX A.

The |E*| versus reduced frequency curves were plotted in log-log scale in Figure 32a and in linear-log scale in Figure 32b. The confined dynamic modulus tests indicated that there was slight difference in the rutting potential of WMA mixtures prepared with different foamed binders. It was observed that |E*| decreased (i.e., the rutting potential increased) as the injected water content and air pressure increased in the foamed binder (see 5% - 20psi versus 1% -10psi and 3% - 15psi). However, this may be misleading as the difference in the |E*| was limited and varied in a small range. Therefore, the difference may be caused by the sample to sample variability. Figure 32b shows the |E*| master curve in the linear-log scale, where a clear trend is not visible. WMA prepared with 3% - 15psi has the highest |E*| as compared to the WMAs with 1% - 10psi and 5% - 20psi. In order to further investigate the relations in between the measured |E*| and the foam quality, the measured |E*| (not the sigmoid fitted) at 10 Hz at 10, 21 and 54°C versus the foam quality indicators (i.e., ER, HL, FI, D_{50} and SAI) were plotted in Figure 33. It was clearly observed that there is no linear trend in between the |E*| and foam quality. The statistical analysis is also provided in Table 11. Kendall's correlation and linear regression are both relatively low due to nonlinear ranking. In addition, it was not possible to fit a polynomial regression since the dataset is less than four mixtures. It was concluded that the WMAs prepared with 3% -15psi was the optimum mix design due to confined dynamic modulus. However, It should be noted that |E*| is only an "indicator" of performance. Actual performance tests are Flow Number (for rutting) and Push-Pull fatigue (for fatigue cracking).

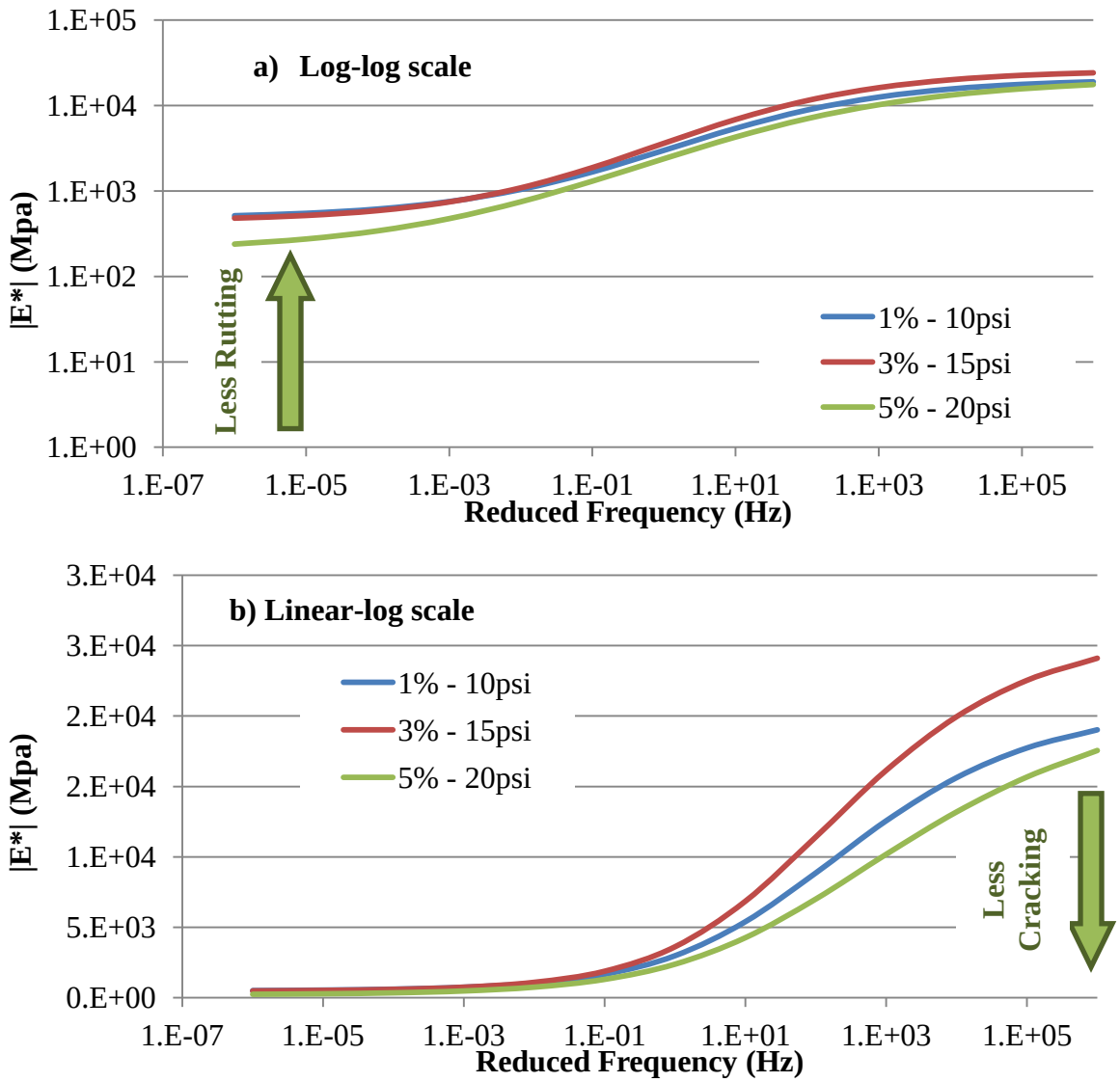

Figure 32: Confined Dynamic Modulus: a) log-log, b) linear –log.

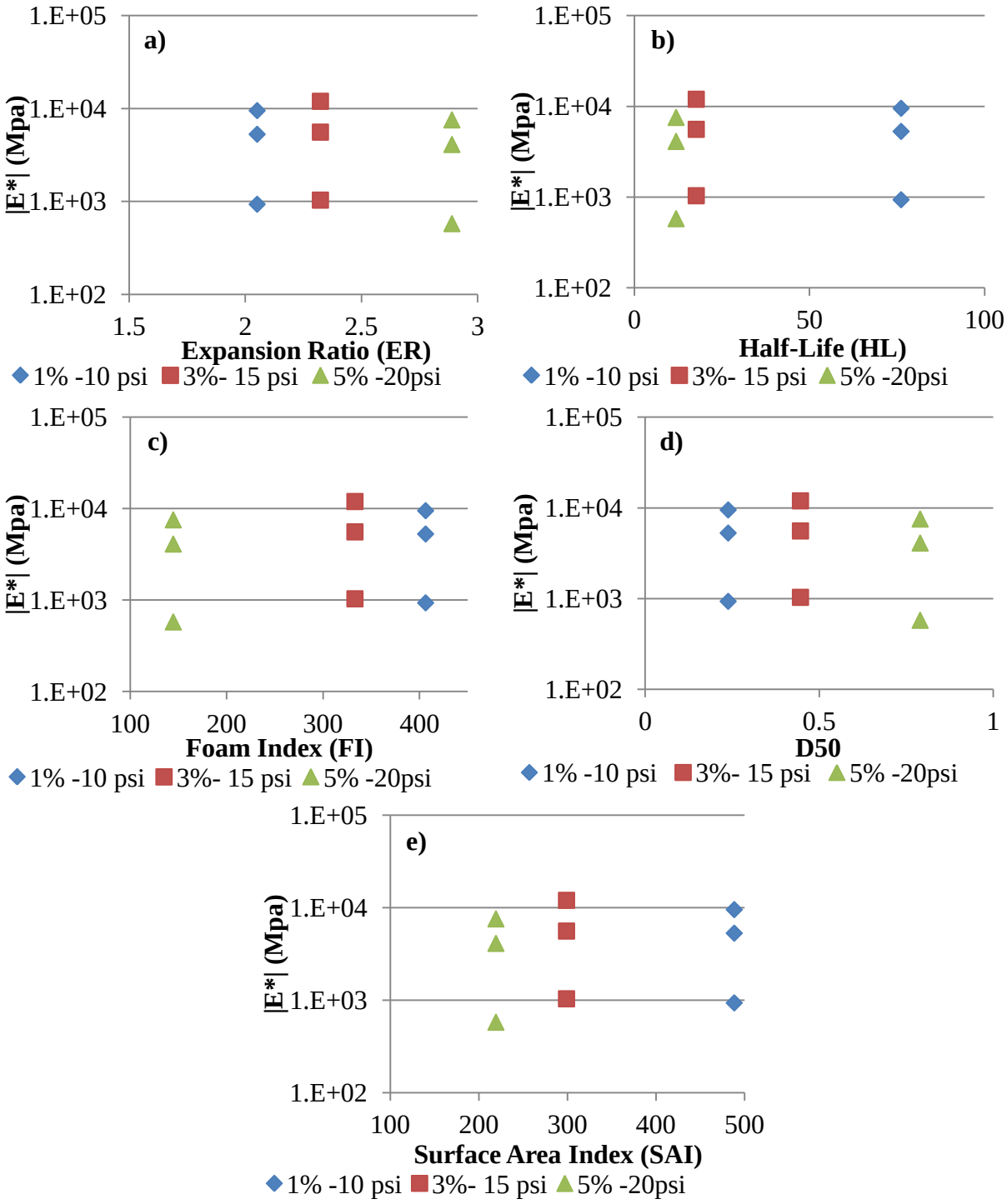

Figure 33: The comparison of Confined Dynamic Modulus at 10 Hz and Foam Binder Quality Parameters a) Expansion Ratio (ER), b) Half-Life (HL), c) Foam Index (FI), d) D50, e) Surface Area Index (SAI)

Table 11: Statistical analysis between confined dynamic modulus at 10 Hz and foam binder quality parameters

	Correlation		Linear Regression		
	Kendall's Tau	**Kendall's Tau Significance (1- pvalue)**	**R**	**R^2**	**Regression Significance (1-pvalue)**
Confined E* vs ER	-0.333	0.500	0.873	0.762	0.676
Confined E* vs HL	0.333	0.500	0.407	0.166	0.267
Confined E* vs FI	0.333	0.500	0.896	0.803	0.707
Confined E* vs D50	-0.333	0.500	0.843	0.711	0.639
Confined E* vs SAI	0.333	0.500	0.590	0.348	0.402

Flow Number (FN)

Rutting, depression of pavement surface along the wheel path, is one of the major pavement distress types. One of the ways to determine rutting potential on pavement surface is the Flow Number Test, where the flow number is associated to the resistance of the pavement to permanent deformation.

Flow Number Test Procedure and Analysis

The tests were conducted according to AASHTO TP79: Determining Dynamic Modulus and Flow Number for Hot Mix Asphalt (HMA) by using the Asphalt Mixture Performance Tester (AMPT) shown in Figure 28. The loose mixtures were subjected to the short-term (2 hours) aging before compacting in a Superpave gyratory compactor at a diameter of 150mm to a height of 180mm. Then, the compacted samples were cored to a diameter of 100mm and the ends

were cut to obtain a final height of 150mm. The final samples were accepted for testing if percent of the air void is in the range of 7±0.5%.

Flow Number Test is a repeated load test conducted at relatively high temperatures (35-54^{o}C). The test procedure (i.e., test temperature, axial deviator stress, confining stress, contact stress, duration of stress pulse, duration of rest period and the shape of stress pulse) is not determined in the AASHTO TP79. However, the deviator stress is generally applied in haversine shape, 0.1 seconds of loading (stress) followed by 0.9 seconds of unloading (recovery) periods, in which each loading and unloading periods create one cycle. These repeated stress pulses and recovery periods through the Flow Number test result a continuously growing permanent strain in the asphalt mix. These strain values are plotted with respect to each cycle and analyzed.

Since WMA mixture testing experience is very limited, the test parameters were selected based on the recommendations of NCHRP reports 691 and 714. The flow number test temperature was 45^{o}C, which is equal to the 50% reliability of 7 day maximum pavement temperature in Michigan. This was computed at a depth of 20 mm (suggested depth for surface course mixes) using LTPPBind Version 3.1beta. The tests were conducted under 87 psi (600 kPa) axial deviator stress and 4.4psi (30 kPa) contact stress at 0 psi confining stress (unconfined mode).

Flow Number Test Results and Discussions

Initially, three foamed binders with different injected air pressures and water contents (i.e., 1% - 10psi, 3%- 15psi, 5% - 20psi) were selected to prepare WMA samples. Since there was no significant difference determined from both the confined and unconfined dynamic

modulus tests, the other samples (2%-12.5psi and 4-17.5psi) in the test matrix were not prepared initially. As shown in Figure 34a, the initial test set was identified as "1". For the simplicity, the average of two to four replicates was plotted in Figure 34. The data for each replicate is available in Figure 59 in the APPENDIX B. It was observed that the rutting resistance of the mixes increased with the increase of the injected air pressure and water content of the foamed binder in the preparation of WMA mixtures. This may have caused by higher aggregate-to-aggregate friction, possibly because of poor coating of the aggregates. In addition, relatively quick failure of the WMA mixtures with low water content and air pressure injected samples may also be the micro bubbles captured in the samples because of the longer half-life.

In order to further investigate these hypotheses, two more WMA samples with different foamed binders (i.e., 2%-12.5psi and 4%-17.5psi) were prepared and tested under the same conditions shown as "2" in Figure 34. It was expected to be that the fatigue behavior of these two transition samples will follow the similar curves and lay in between 1%-10psi, 3%-15psi and 5%-20psi. However, the "2" set was failed relatively quickly as compared to the "1" set. The trend in the relation of the rutting and foam binder parameters was same, i.e., rutting potential increased with increasing the water content and air pressure. In order to better illustrate the trend, the permanent microstrains were plotted at 50 cycles, as shown in Figure 34b. The trend lines for the two data sets ("1" and "2") were separately plotted to illustrate the overall trend. As clearly shown in Figure 34b, the trends were same. It had been already known that the laboratory foamer has been having repeatability problems within each trial on the same day and even worse between the days. Since the samples "1" and "2" were not prepared on the same day, the variability of the tests was expected. The results shown in Figure 34 clearly show the influence

of the foam binder parameters on the rutting susceptibility. Therefore, the permanent strain at 50^{th} cycle versus the foam quality indicators (i.e., ER, HL, FI, D_{50} and SAI) was plotted in Figure 35, in order to investigate these relations individually. The statistical analysis was given in Table 12. Kendall's tau coefficients are +1 and -1 and their significances are 100%. In addition, the linear regression significantly fit the data. As shown in Figure 35a and d, Expansion Ratio (ER) and D_{50} increase with the increase in the injected water content and air pressure of the binder as the permanent microstrain at50^{th} cycle decreases. On the contrary, half-life (HL), foam index (FI), and Surface Area Index (SAI) increase with the decrease in the injected water content and air pressure of the binder as the permanent microstrain at50^{th} cycle increases. The relation of rutting and foam binder parameters was determined in this section as follows:

(i) As the expansion ratio of the foamed binder increases, its half-life decreases (Figure 35a and b). This improves the rutting resistance of WMA pavements.

(ii) As the surface area index decreases, the higher aggregate-to-aggregate friction as a result of the poor coating improves the rutting resistance of the WMA pavements.

(iii) As the bubble sizes in the foamed binder (see D50 in Figure 35d) increases and the surface area index (see SAI in Figure 35e) decreases, the coating of aggregates becomes poor. The poor coating increases the shear strength in between the aggregates. This improves the rutting resistance of WMA pavements at high temperatures.

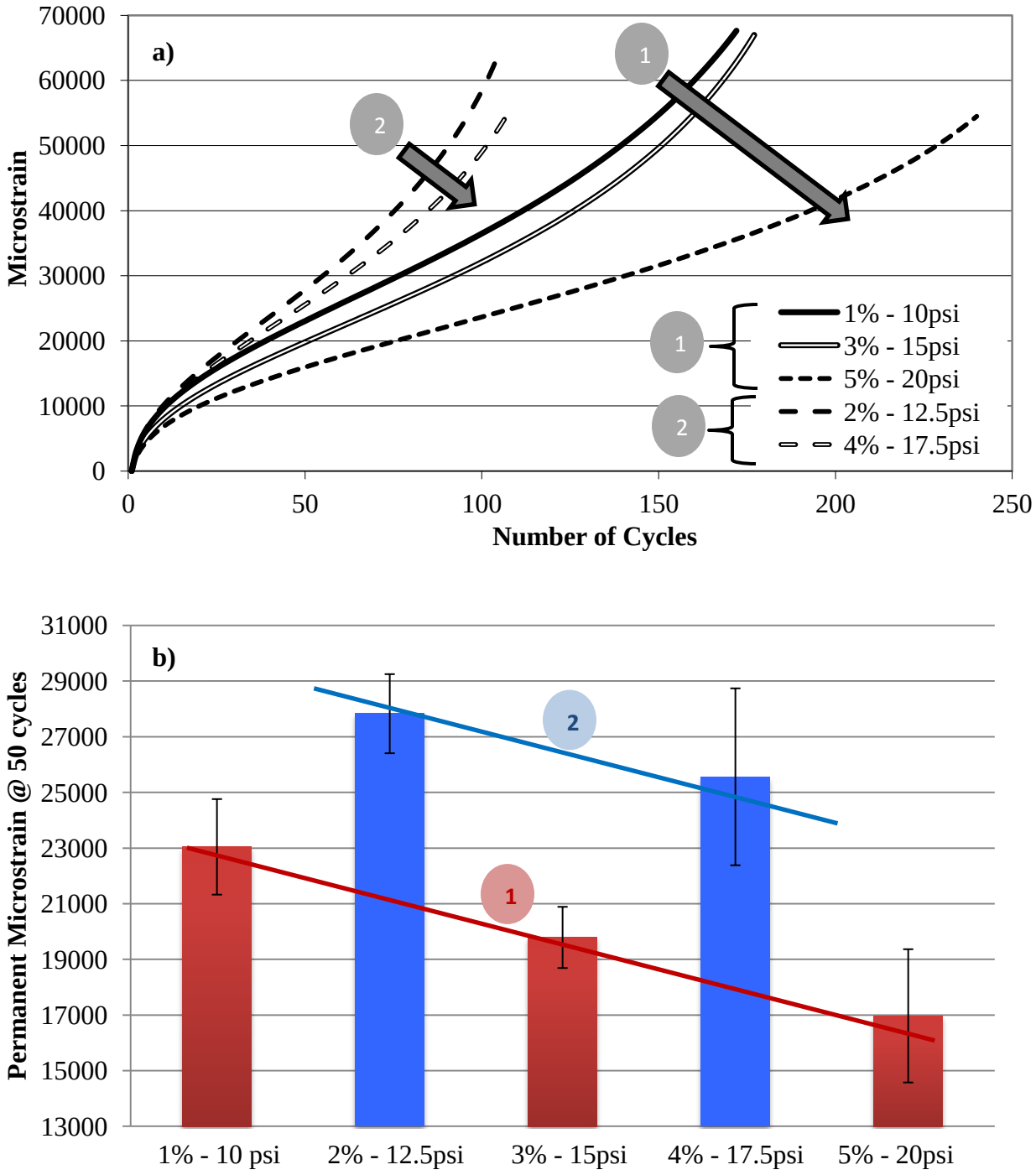

Figure 34: a) Permanent (plastic) strain with cycles obtained from unconfined FN tests, b) Permanent strain at 50 cycles

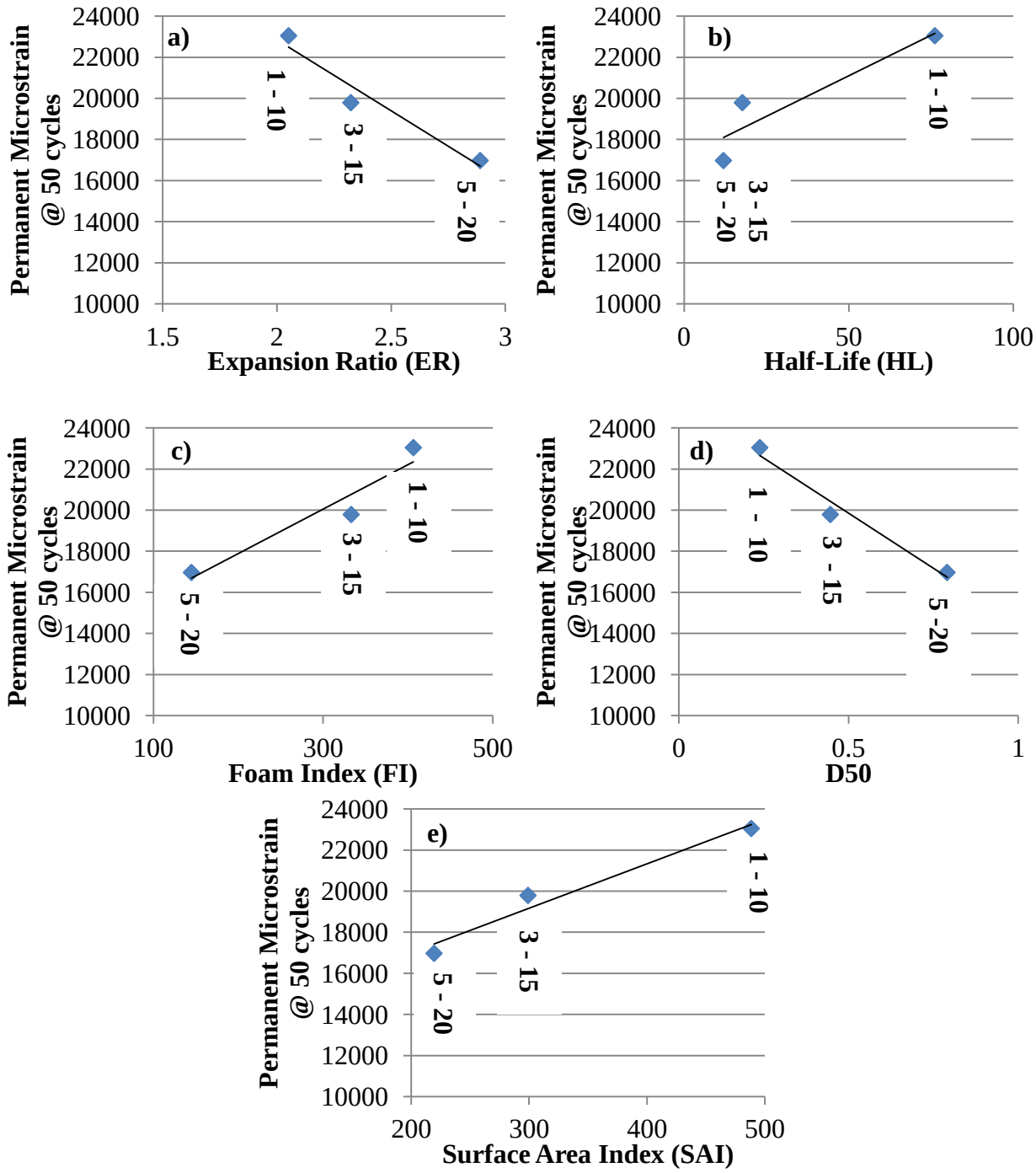

Figure 35: The comparison of permeate strain at 50 cycles and foam binder quality parameters a) Expansion Ratio (ER), b) Half-Life (HL), c) Foam Index (FI), d) D50, e) Surface Area Index (SAI)

Table 12: Statistical analysis between the permeate strain at 50 cycles and foam binder quality parameters

	Correlation		Linear Regression		
	Kendall's Tau	**Kendall's Tau Significance (1- pvalue)**	**R**	**R^2**	**Regression Significance (1-pvalue)**
Permanent Microstrain @ 50 cycles vs. Water Content/Air Pressure	-1.000	1.000	0.999	0.998	0.974
Permanent Microstrain @ 50 cycles vs. ER	-1.000	1.000	0.971	0.943	0.847
Permanent Microstrain @ 50 cycles vs. HL	1.000	1.000	0.921	0.847	0.745
Permanent Microstrain @ 50 cycles vs. FI	1.000	1.000	0.958	0.918	0.815
Permanent Microstrain @ 50 cycles vs. D50	-1.000	1.000	0.983	0.967	0.884
Permanent Microstrain @ 50 cycles vs. SAI	1.000	1.000	0.983	0.964	0.879

Push-Pull (Compression-Tension) Fatigue Test

Fatigue cracking is typically caused by many repetitions of the heavy traffic load, inadequate support in between the pavement layers and subgrade, very stiff binder in the surface layer and poor drainage. Laboratory cyclic push-pull (tension-compression) test is one of the common methods to predict field fatigue life of the pavements. In addition, this test was preferred in lieu of Four Point Bending Beam (FPBB) test (AASHTO T 321: Standard Method of Test for Determining the Fatigue Life of Compacted Hot Mix Asphalt (HMA) Subjected to Repeated Flexural Bending) since this test is much easier to conduct as well as the use of less material, energy and time, and it provides more information than the FPBB test. The fatigue performance

of the pavements is quantified by the number of cycles to failure (N_f) in Push-Pull test at a given strain level, temperature and loading frequency.

Push-Pull Test Procedure

Laboratory samples were prepared in the Superpave gyratory compactor to a height of approximately 180 mm and then cut and cored to a cylindrical sample, 76 mm in diameter and 150 mm tall. The samples were accepted for testing if air void was in acceptable range (7±0.5%). Initially, LVDT tabs were mounted with two components high strength epoxy (120° apart from each other). LVDT gauge lengths were about 70 mm and the top and bottom tabs were about 37.5 mm away from the top and bottom edges of the samples. Then, the specimens were glued with steel epoxy to aluminum top and bottom plates using a custom made gluing jig to provide perfectly parallel specimen ends, as shown in Figure 36. Finally, the tests were conducted using Asphalt Mixture Performance Tester (AMPT). Samples were carefully mounted to AMPT to eliminate eccentricity during the test, which may cause non-uniform stress distribution and thus localized failure (in general close to one of the end platens), as shown in Figure 36c.

Push-pull test can be conducted in both stress controlled and strain controlled loading mode. However, the push-pull tests in this study were performed only at strain controlled mode at 10 Hz frequency at both 10°C and 20°C. For both temperatures, two replicates of each sample were prepared and tested. However, some tests were removed from the analysis due to localized failures at the top and bottom of the samples during testing, as shown in Figure 36c. The samples with the mid-failure as shown in Figure 36d were used for the analysis. The analysis were performed

using viscoelastic continuum damage concept (VECD) and using non-commercial software developed by Dr. M. Emin Kutay, called PP-VECD v0.1.

Brief summary of Viscoelastic Continuum Damage (VECD) concept

Viscoelastic Continuum Damage (VECD) theory is based on Schapery's elastic-viscoelastic correspondence principle and the work potential theory. Schapery (1999) divided the total strain (ε_{tot}) as viscoelastic (ε_{ve}) and viscoplastic (ε_{vp}) strains, as follows:

$$\varepsilon_{tot} = \varepsilon_{ve} + \varepsilon_{vp} \quad [18]$$

The viscoelastic strain is the sum of both the linear viscoelastic strains and the strains due to the microcracks. The time dependent viscoelastic behavior can be simplified into a linear elastic solution through the pseudostrain using convolution integral, as follows:

$$\varepsilon^R = \frac{1}{E^R} \int E(t-\tau) \frac{\partial \varepsilon}{\partial \tau} d\tau \quad [19]$$

where ε^R is the pseudostrain, E^R is the reference modulus, E(t) is the linear viscoelastic relaxation modulus, t is time and τ is the time variable of integration. When E^R is taken as unity, ε_R is equal to the linear viscoelastic stress (σ) as follows:

$$\sigma = \varepsilon^R E^R \quad [20]$$

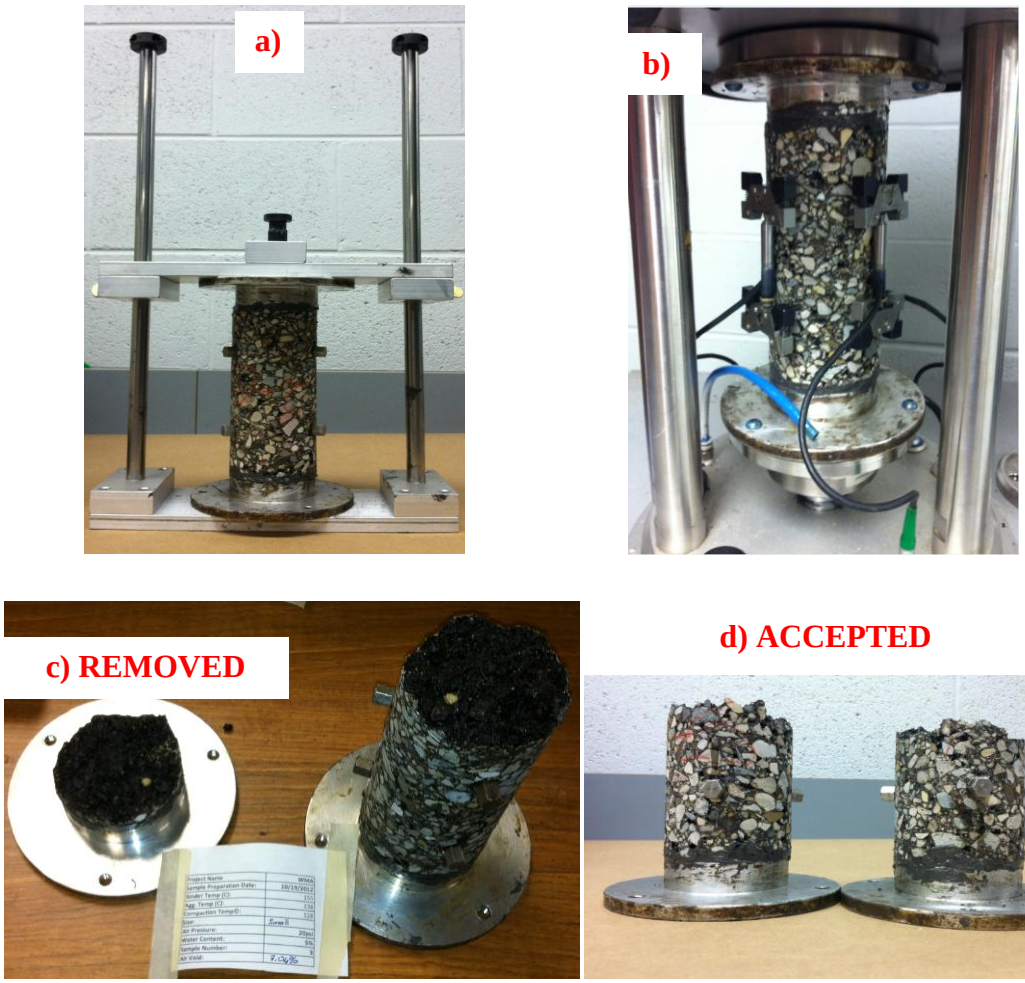

Figure 36: Push-Pull Test: a) Custom made gluing jig, b) AMPT fixture, c) Non-accepted tests (end failure), d) Accepted tests (mid failure)

However, this simplified equation does not consider the nonlinear behavior due to the continuum damage of micro cracks. Therefore, the stress-strain behavior of the viscoelastic material is determined based on the time dependent damage growth. The following equations utilize the pseudostrain energy density function and the damage parameter (S):

$$\sigma = IC(S)\varepsilon^{R} = \frac{\partial W^{R}}{\partial \varepsilon^{R}} \qquad [21]$$

$$W^R = \frac{I}{2} C(S) \varepsilon^{R\,2} \quad [22]$$

$$\frac{dS}{dt} = (-\partial W^R / \partial S)^{\alpha} \quad [23]$$

where W^R is the pseudostrain energy density function, C(S) is the pseudostiffness, I is the initial stiffness parameter (0.9-1.1), which eliminates the sample to sample variability, α is the material constant related to the damage growth.

Independent of loading history, testing mode (stress or strain controlled), magnitude or rate of the loading, and testing temperature, all C versus S curves for each PP test for the same mixture should collapse on a single curve. Once C versus S from different tests (on the same type of WMA) seems to collapse on a single curve, an exponential best fit line is as follows:

$$C = \exp(aS^b) \quad [24]$$

where a and b are the constants defining the best fit. However, this C versus S curves are not sufficient to determine the fatigue performance. The number of cycles to failure (N_f) was determined based on the 50 % reduction in pseudostiffness (i.e., *C*=0.5).

Push-Pull Test Result and Discussions

As it was stated before, the push-pull tests were performed at strain controlled mode at 10 Hz frequency at both 10°C and 20°C. Although the best fitted C versus S curves were given in Figure 37, the individual C versus S curves for each test were plotted from Figure 60 to Figure 64 in APPENDIX C.

As shown in Figure 38, the fatigue cracking performance of the tested mixtures under constant strain (300 microstrain) were compared at different temperatures (5, 10, 15, 20, 25 and 30°C) using the VECD theory. As the temperature increased, the fatigue resistance of the asphalt mixtures increased (as expected). In addition the fatigue performance of the WMA mixtures at 20°C calculated under different traffic loads (strain levels) (100, 200, 300, 400 and 500 microstrain). As shown in Figure 38 and Figure 39, the best fatigue performance was observed at 3% - 15psi and 4% -17.5psi mixtures. The worst performance was in 5% - 20psi, which is consistent with coating analysis. It was also mentioned during FN data analysis that 5% - 20psi might have "exposed" uncoated aggregates causing more friction between the aggregates. These "exposed" aggregates can lead to increased fatigue cracking potential. On the other hand, the 1% - 10psi and 2% - 12.5psi samples also showed worse performance as compared to 3% - 15 psi and 4% - 17.5psi mixes. This could be due to trapped moisture bubbles in 1% - 10psi and 2% - 12.5psi since these samples had small foam bubbles. Therefore, it can be concluded that the "optimum" water content and air pressure is around 3% -15psi and 4% -17.5 psi. The number of cycles to failure at 300 microstrain, 10 Hz, and 20°C versus the foam quality indicators (i.e., ER, HL, FI, D_{50} and SAI) was plotted in Figure 40 and the statistical analysis were studied individually. Although the expansion ratio (ER) increases as the water content and air pressure increases, the there is no trend in between ER and fatigue resistance. As shown in Figure 40a, 3% - 15 psi showed the best performance as compared to the other mixes. In addition, the other graphs (i.e., HL, FI, D_{50}, SAI) were analyzed from Figure 40b to Figure 40e, in which the best fatigue performance was observed at 3% - 15psi and 4% -17.5psi mixtures. The statistical

analysis, in which the correlation and linear regressions studied in Table 13, indicated that the lack of linearity. Therefore, polynomial regression is fitted to the data as given in Table 13. The coefficient of determination (R^2) and significance of the polynomial fit are relatively high for ER, FI and D_{50}. However, the significance of the relation with SAI and HL is relatively low. As a result, it is crucial to consider foam quality in the WMAs design for the optimum performance.

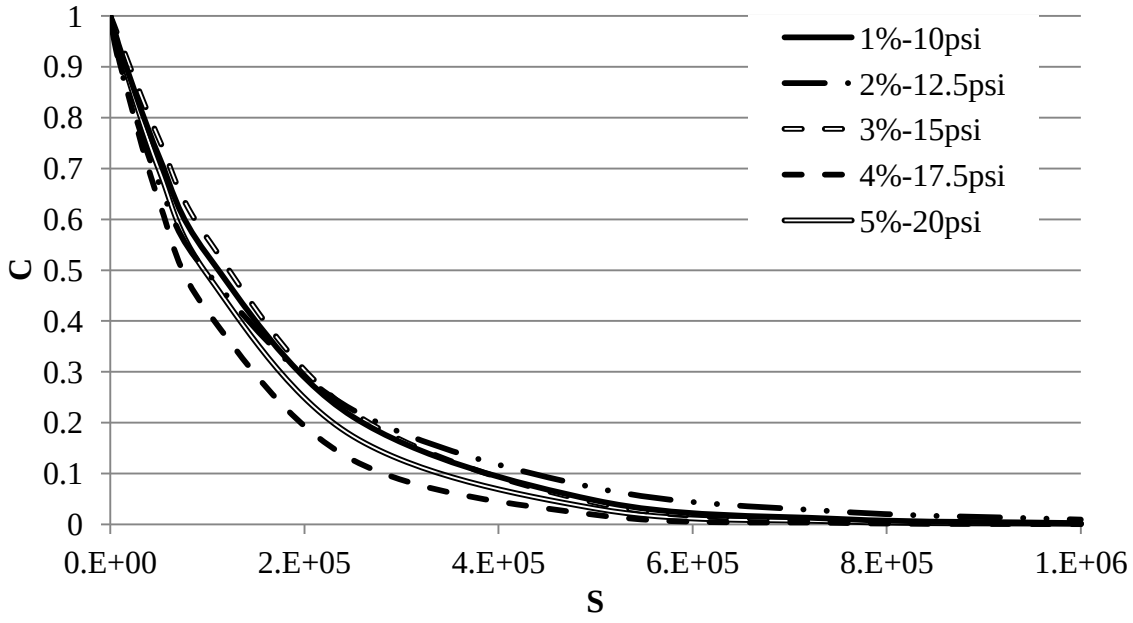

Figure 37: C versus S curves of different WMAs

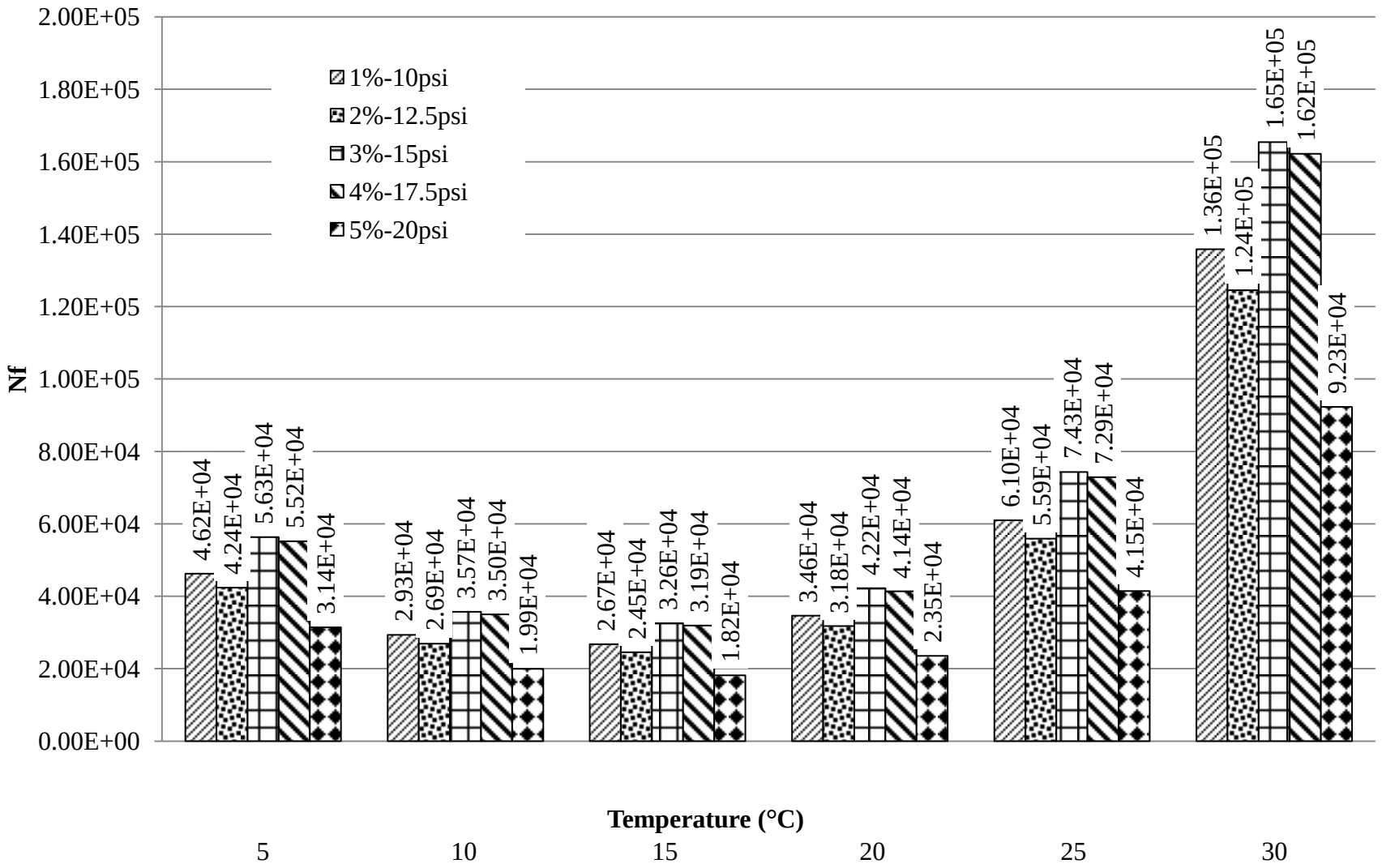

Figure 38: Number of cycles to failure at 300 microstrain.

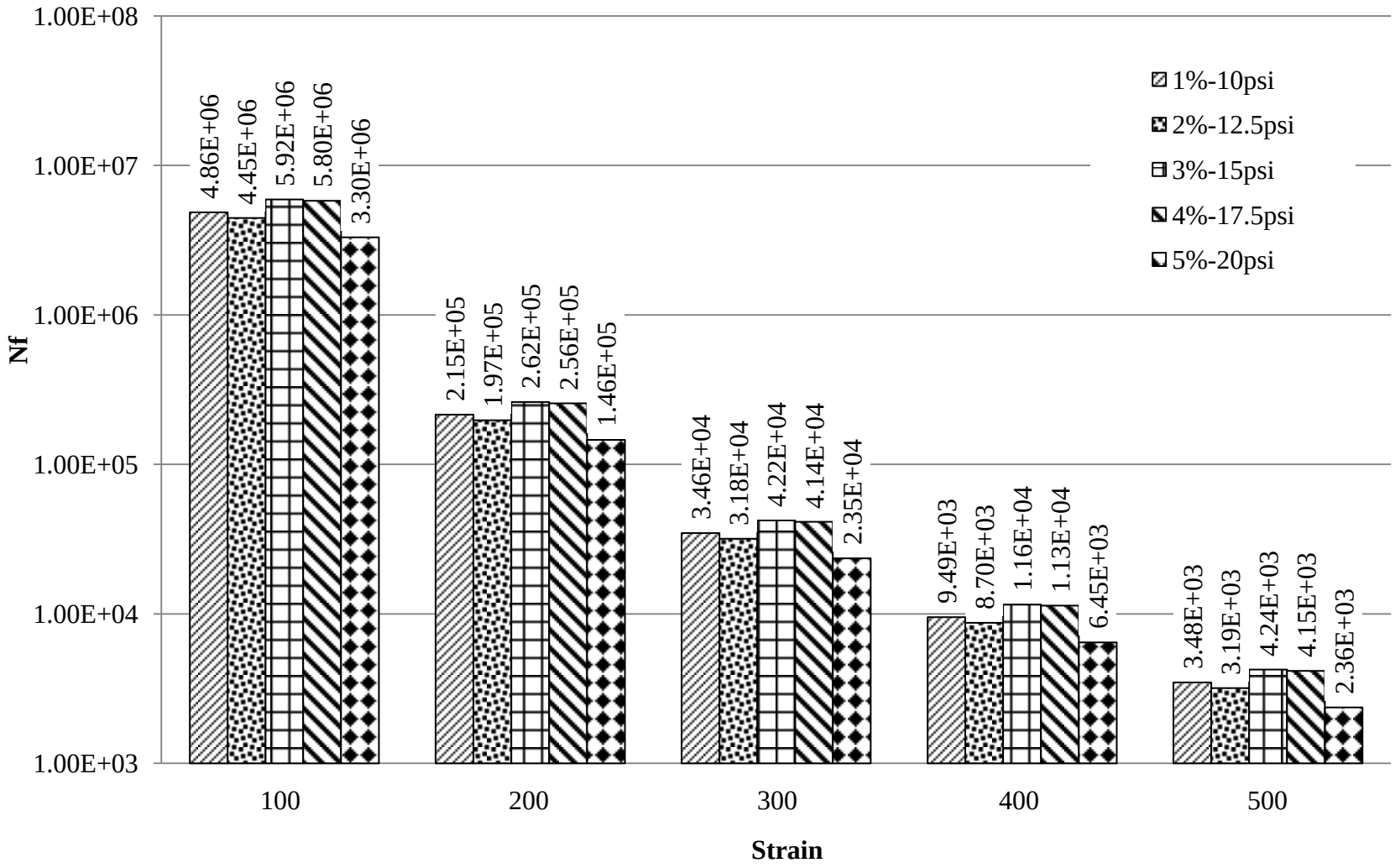

Figure 39: Number of cycles to failure at 20°C

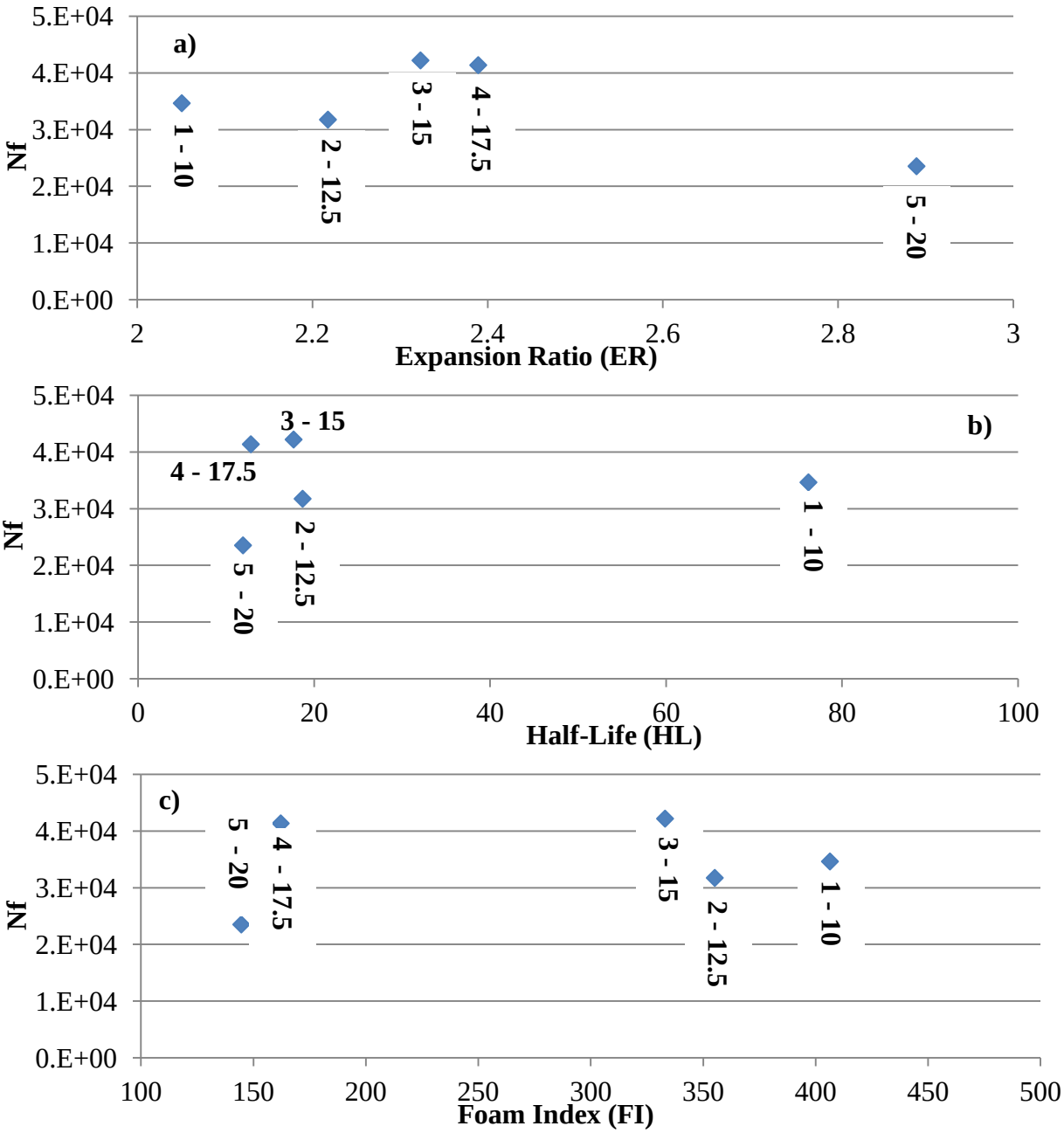

Figure 40: The comparison of Number of Cycles to failure at 300 microstrain, 10 Hz, 20°C and Foam Binder Quality Parameters a) Expansion Ratio (ER), b) Half-Life (HL), c) Foam Index (FI), d) D50, e) Surface Area Index (SAI)

Figure 40 (cont'd)

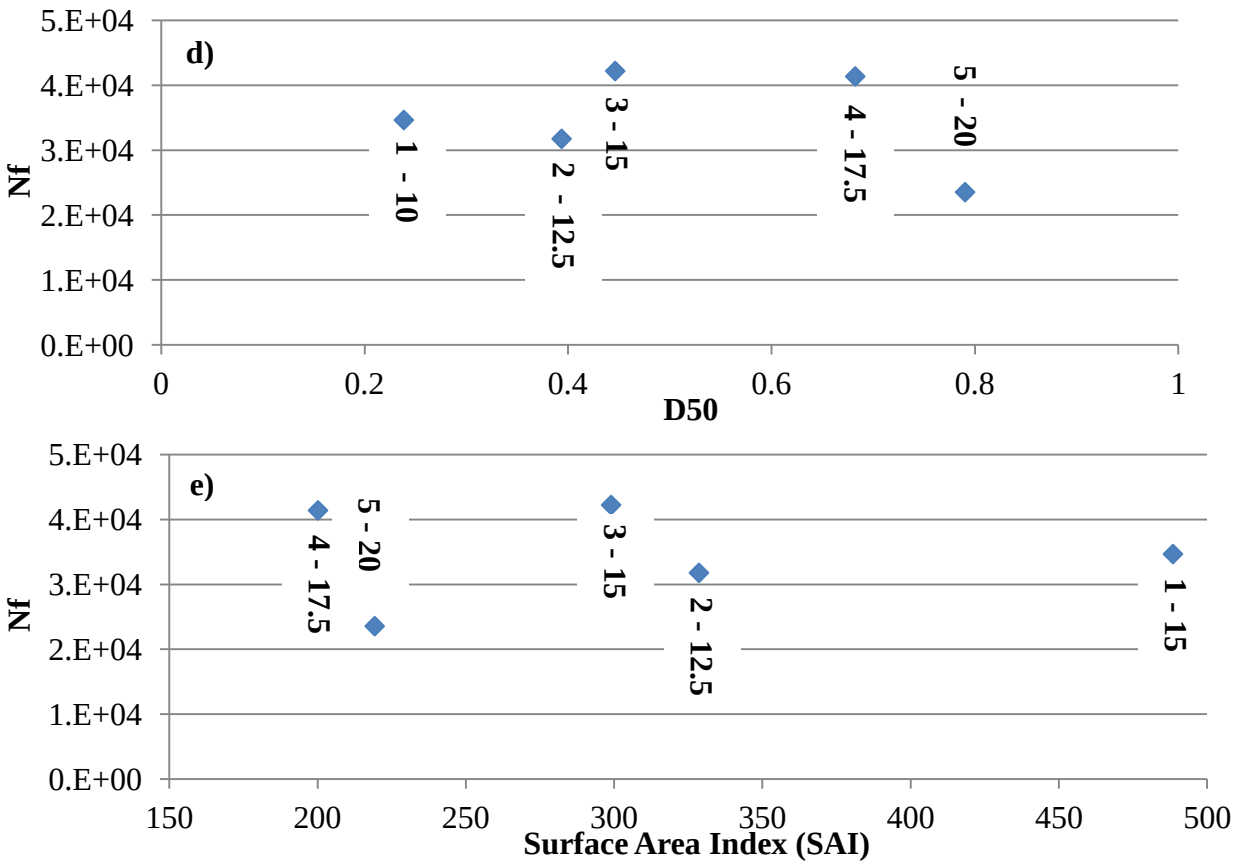

Table 13: Statistical analysis between Number of Cycles to failure at 300 microstrain, 10 Hz, 20°C and Foam Binder Quality Parameters

	Correlation		Linear Regression			Polynomial Regression	
	Kendall 's Tau	Kendall's Tau Significance (1- pvalue)	R	R^2	Regression Significance (1-pvalue)	R	R^2
Nf vs. ER	-0.200	0.592	0.602	0.363	0.412	0.881	0.776
Nf vs. HL	0.200	0.592	0.264	0.070	0.170	0.335	0.112
Nf vs. FI	0.200	0.592	0.523	0.273	0.350	0.526	0.277
Nf vs. D50	-0.200	0.592	0.478	0.228	0.317	0.688	0.473
Nf vs. SAI	0.000	0.5	0.387	0.150	0.253	0.0837	0.007

Tensile Strength Ratio (TSR)

Moisture susceptibility is another major concern related to the WMA pavements. Moisture damage can occur due to the loss of cohesion within the binder film, the failure of adhesive bond between the binder and the aggregate and the degradation of aggregates. There are various test methods for evaluation of moisture susceptibility of mixtures. These include Tunnicliff & Root (ASTM D4867), Lottman (ASTM D4867), Immersion Compression, Boiling water test (ASTM D3625), Texas freeze-thaw pedestal test, Marshall Stability index, Environmental Conditioning System (ECS), Standard Method of Test for Resistance of Compacted Hot Mix Asphalt (HMA) to Moisture-Induced Damage (AASHTO T283).

In this study, AASHTO T283, which is a typical method for determining the moisture susceptibility of HMA pavements, was performed. It was also suggested methodology for WMA mixtures in NCHRP Reports 691 and 714. The test measures the change of the tensile strength of the mixtures resulting from the freeze-thaw cycle of the conditioned mixes, relative to the unconditioned mixes.

TSR Test Procedure

The sample preparation for the AASHTO T283 is significantly different than the previous performance tests discussed. For each mixture, six to eight samples are prepared to achieve the target air void range (7.0% ± 0.5%). As soon as the loose mixture is prepared, it is left in the room temperature for 2±0.5 hours in order to cool down. Then, the loose mixture is placed into a conventional oven at 60±3°C for 16 hours. Finally, the sample is transferred to another oven at CT±3ºC for 2±10 minutes hours before the compaction. The mixture is compacted to at a size of 150 mm diameter to 95±5 mm height (see Figure 41). After overnight cooling, the maximum

bulk specific gravity of the sample should be checked and grouped into two subsets (three samples each), which has approximately same average air voids.

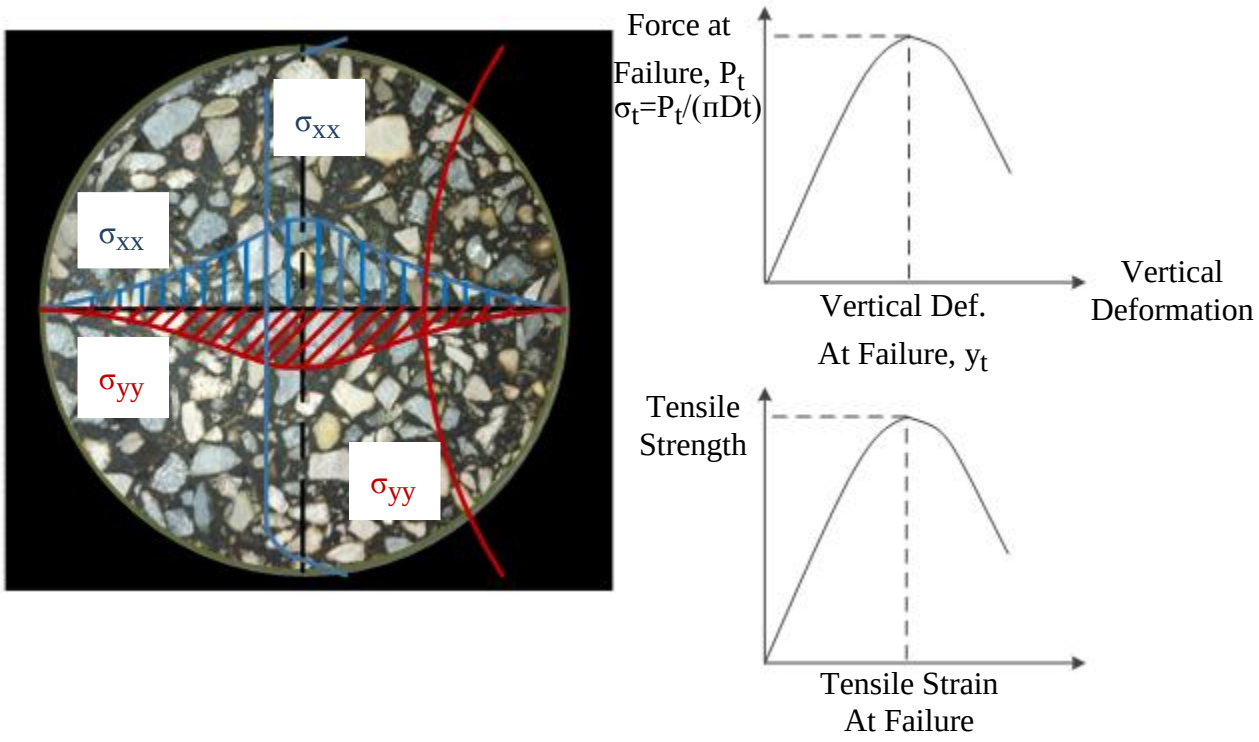

Figure 41: Indirect tensile strength test specimen and stress distribution

The first subset, called as unconditioned set, is left for drying and stored at room temperature. This set should be kept at 25 ± 0.5ºC for 2 h ± 10 min before testing. The second subset, called as conditioning set, saturated in the range of 70% to 80% in a vacuum container. The saturated samples are covered with a plastic film and placed into separate sealed bags with 10 ± 0.5 ml of extra water. These bags are kept in an environmental chamber at –18 ± 3°C for a minimum of 16 hours. After the freezing cycle, the samples are rapidly transferred to a water bath at 60± 1°C for 24±1 h without the seal bags and plastic films. Following the thaw cycle, the samples are transferred to a water bath at 25 ± 0.5°C for 2 h ± 10 min. The tests are

conducted using the Material Testing System (MTS) and loaded at a constant rate (50 mm/min). The maximum load achieved at failure is used to compute the tensile strength, as follows:

$$S_t = \frac{2P}{\pi tD} \quad [25]$$

where S_t is tensile strength in psi and P is the maximum load in lbf. D and t are the sample diameter and thickness in inches, respectively. Tensile Strength Ratio (TSR) is defined as the ratio of conditioned to unconditioned indirect tensile strength of mixes, as follows:

$$TSR = \frac{S_1}{S_2} \times 100\ \% \quad [26]$$

where S_1 and S_2 are the average conditioned and unconditioned tensile strength, respectively. If this ratio is greater than 80 percent, the mixtures are not considered to be susceptible to moisture damage. If low TSR values for WMA mixes are obtained, antistripping agents such as hydrated lime and liquid additives can be used.

TSR Test Result and Discussions

The samples for AASHTO T283 were prepared for each injected water content and air pressure combinations. The detailed data analysis for each mixture is available from Table 29 and Table 33 in APPENDIX D.

The conditioned and unconditioned strength of the mixtures were given in Figure 42. The change in the conditioned strength did not follow any trend with the change of the mixture. On the other hand, as shown in Figure 42b, the unconditioned strength of the mixtures decreased as

the water content and air pressure increases. The highest strength in the conditioned set was achieved in 3%-15psi mixture. As stated before, the lower water content and air pressure injected foamed binder was anticipated to be composed of relatively small bubbles and the collapse of the foamed binder takes longer. Therefore, it was observed that these mixtures had better aggregate coating, which also increased the strength between the aggregate and binder bonds. Thus, the tensile strength of these mixes was relatively high. On the contrary, the higher water content and air pressure injected foamed binder was anticipated to be composed of relatively large bubbles and foamed binder collapse more rapidly. Therefore, the bubbles evaporate quickly from the mixture, as well as resulting poor coating during mixture production. The poor bond between the aggregate and binder resulted relatively lower tensile strength. The statistical analysis between the sample strength and the injected water content and air pressure relation is given in Table 14. The Kendall's tau coefficient is 0.8 and its significance is equal to 0.958 for the unconditioned strength. This indicated that there is strong correlation between the unconditioned strength of the mixtures and foamed binder. In addition, the linear regression fitted well for this relation. Therefore, the coefficient of determination and significance of the regression are relatively high. However, both Kendall's tau and linear regression were poor for the conditioned strength.

TSR value is a function of both the conditioned and unconditioned tensile strength of mixtures. As given in Figure 43, the trend in the TSR increased with the increase in the water content and air pressure of the binder, mixture prepared. The statistical analysis between the TSR and foamed binder is given in Table 14. The Kendall's tau correlation and significance was relatively low, the coefficient of determination for the linear regression is 0.78 and its

significance is 69%. However, the mixture prepared with 3%-15psi foamed binder had the highest moisture resistance as well as the highest conditioned and unconditioned strengths. The outcomes of the moisture susceptibility tests were very similar to the fatigue cracking. The optimum mix design was observed to be 3%-15psi.

The unconditioned and conditioned tensile strength versus the foam quality indicators (i.e., ER, HL, FI, D_{50} and SAI) was plotted in Figure 44 due to high variability in the strength only in order to briefly investigate these relations individually. As shown in Figure 44a and d, Expansion Ratio (ER) and D_{50} increase with the increase in the injected water content and air pressure of the binder as the unconditioned strength decreases. On the contrary, half-life (HL), foam index (FI), and Surface Area Index (SAI) increase with the decrease in the injected water content and air pressure of the binder as the unconditioned strength increases as shown in Figure 44b, Figure 44c and Figure 44e. However, the conditioned strength has a different trend as stated earlier, where the highest strength in the conditioned set was achieved in 3%-15psi mixture with respect to the other WMAs. In addition, tensile strength ratio (TSR) versus the foam quality indicators (i.e., ER, HL, FI, D_{50} and SAI) was plotted in Figure 45, in which the optimum mix was determined to be 3%-15psi mix. It can be also concluded that similar to the performance tests discussed previously, the moisture resistance of the WMA mixtures can also be controlled with foamed binder quality.

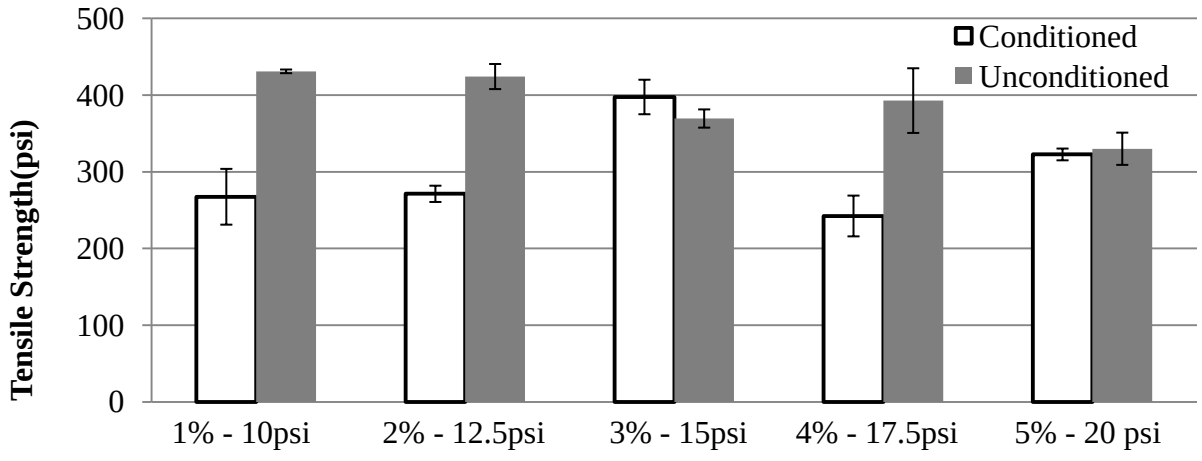

Figure 42: Unconditioned and conditioned tensile strength

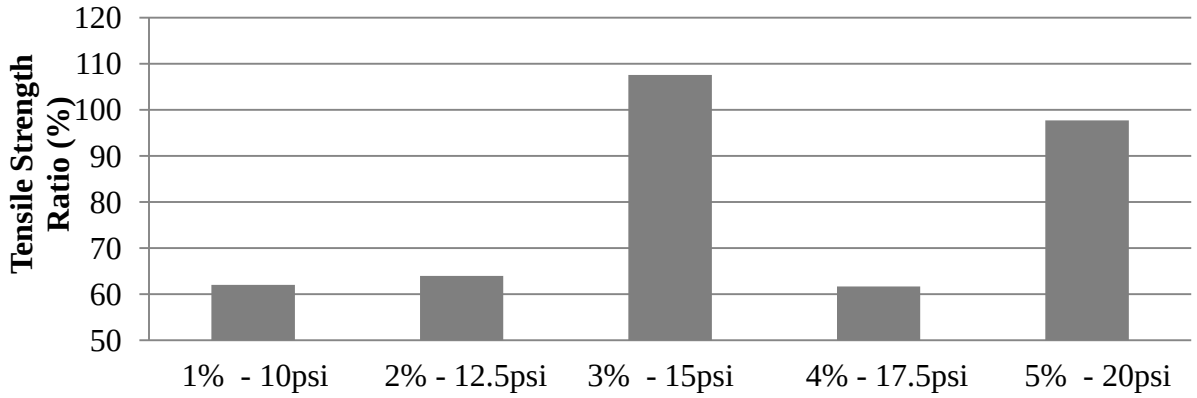

Figure 43: Tensile Strength Ratio (%)

Table 14: Statistical analysis of unconditioned strength, conditioned strength and TSR with respect to water content and air pressure

	Correlation		Linear Regression		
	Kendall's Tau	Kendall's Tau Significance (1- pvalue)	R	R^2	Regression Significance (1-pvalue)
Uncondotioned Strength vs. Water Content/Air Pressure	-0.8	0.958	0.912	0.832	0.731
Condotioned Strength vs. Water Content/Air Pressure	0.2	0.592	0.879	0.772	0.683
TSR vs. Water Content/Air Pressure	0.2	0.592	0.884	0.782	0.690

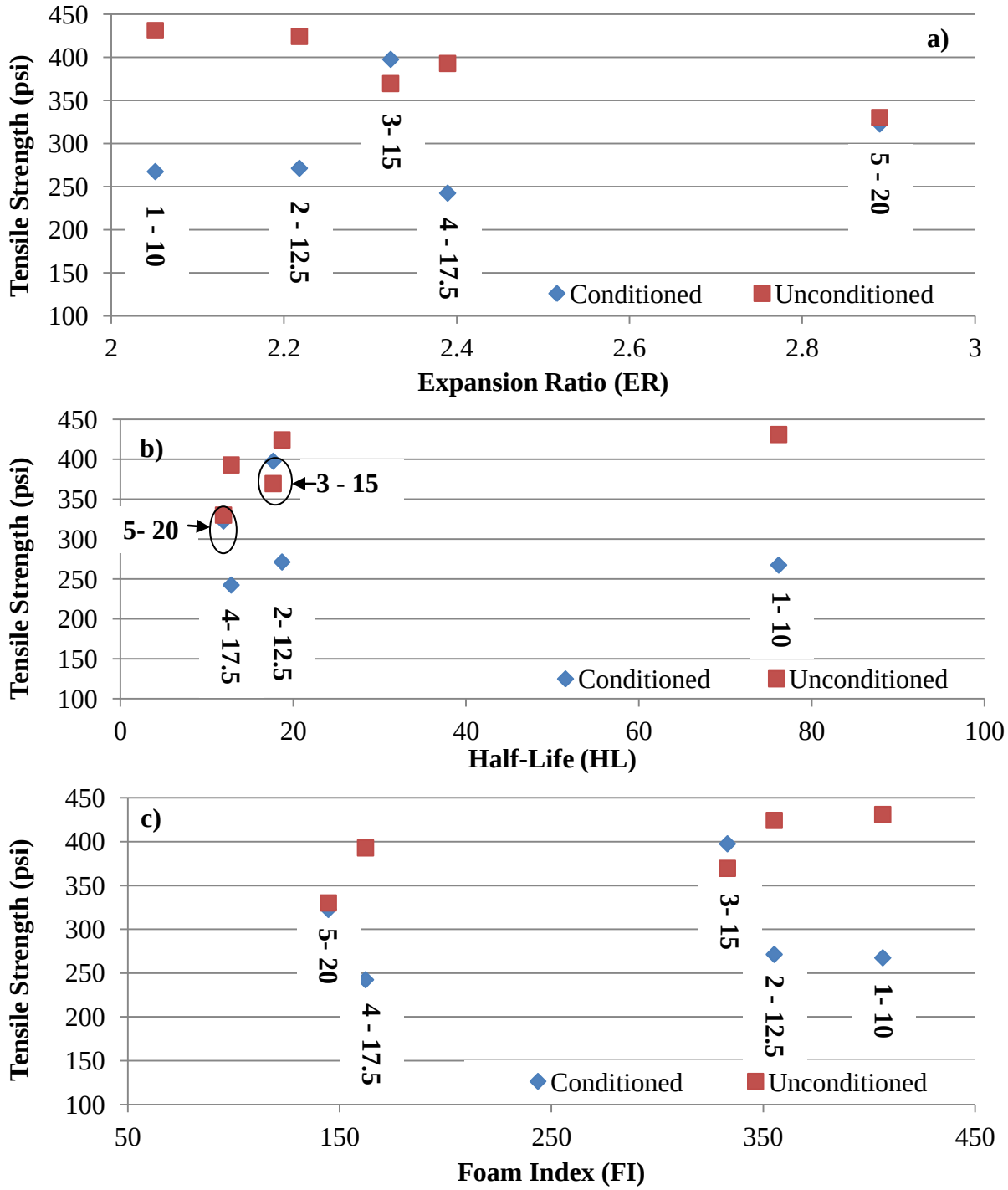

Figure 44: The comparison of Unconditioned/Conditioned Tensile Strength and Foam Binder Quality Parameters: a) Expansion Ratio (ER), b) Half-Life (HL), c) Foam Index (FI), d) D50, e) Surface Area Index (SAI)

Figure 44 (cont'd)

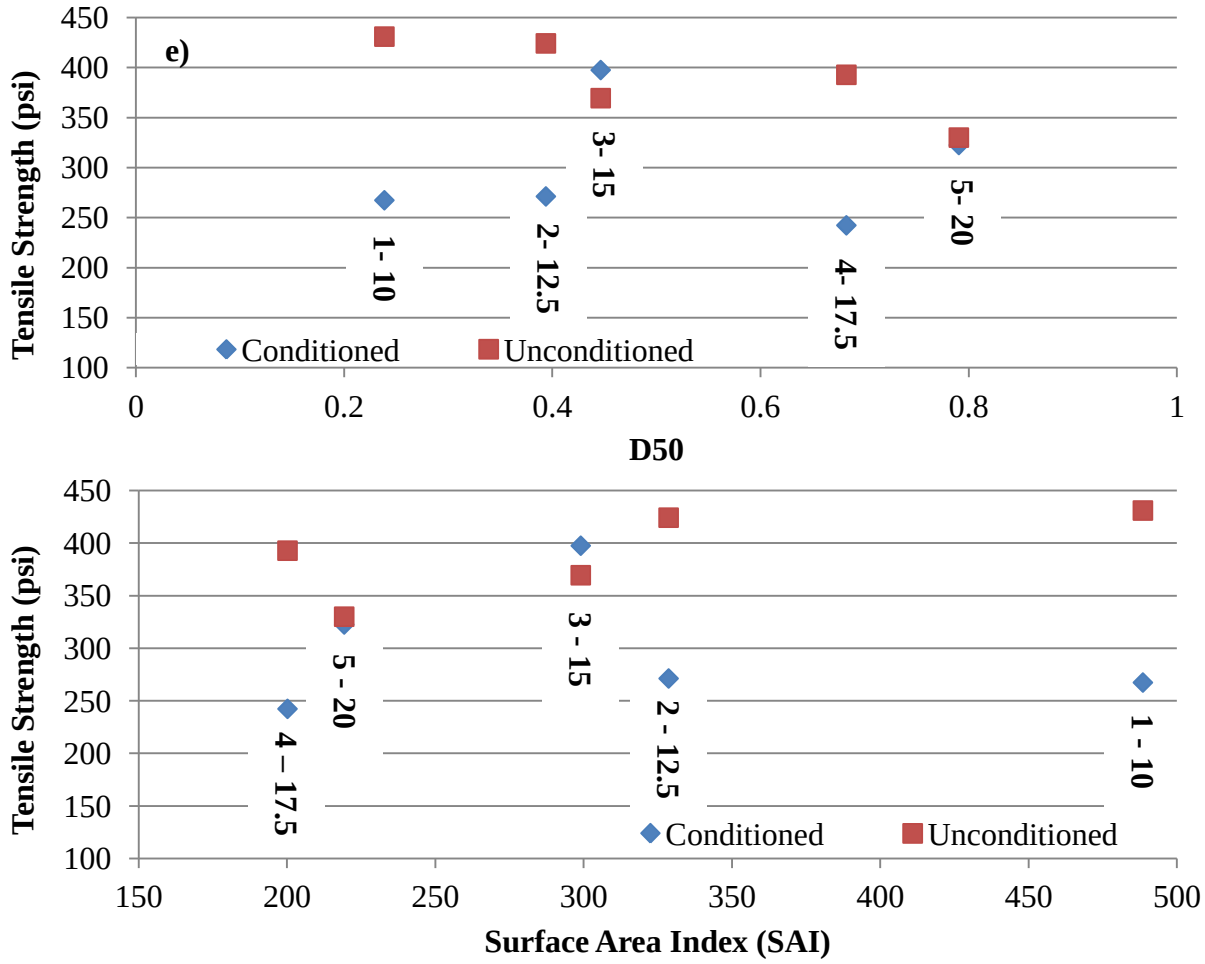

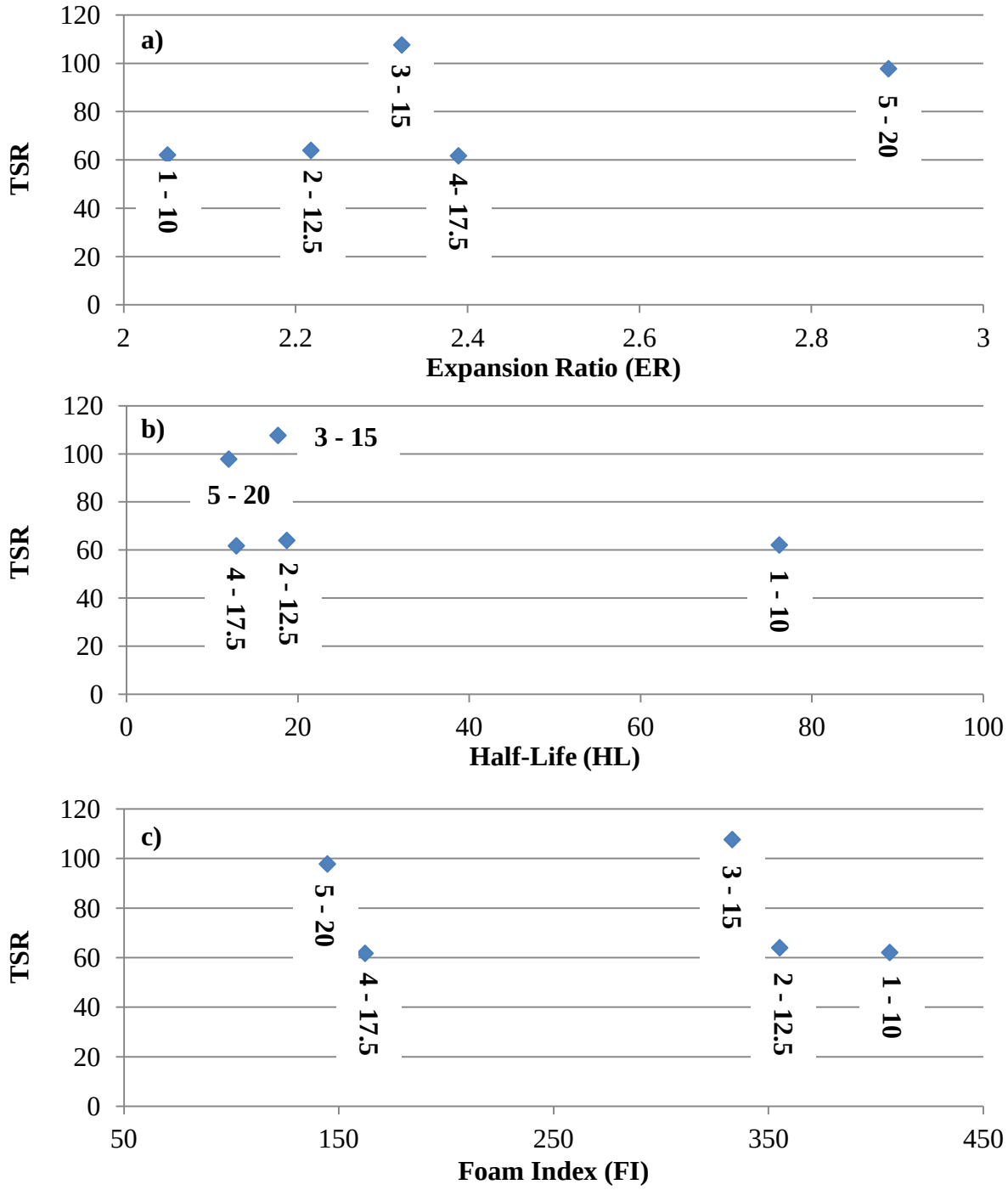

Figure 45: The comparison of Tensile Strength Ratio (TSR) and Foam Binder Quality Parameters a) Expansion Ratio (ER), b) Half-Life (HL), c) Foam Index (FI), d) D50, e) Surface Area Index (SAI)

Figure 45(cont'd)

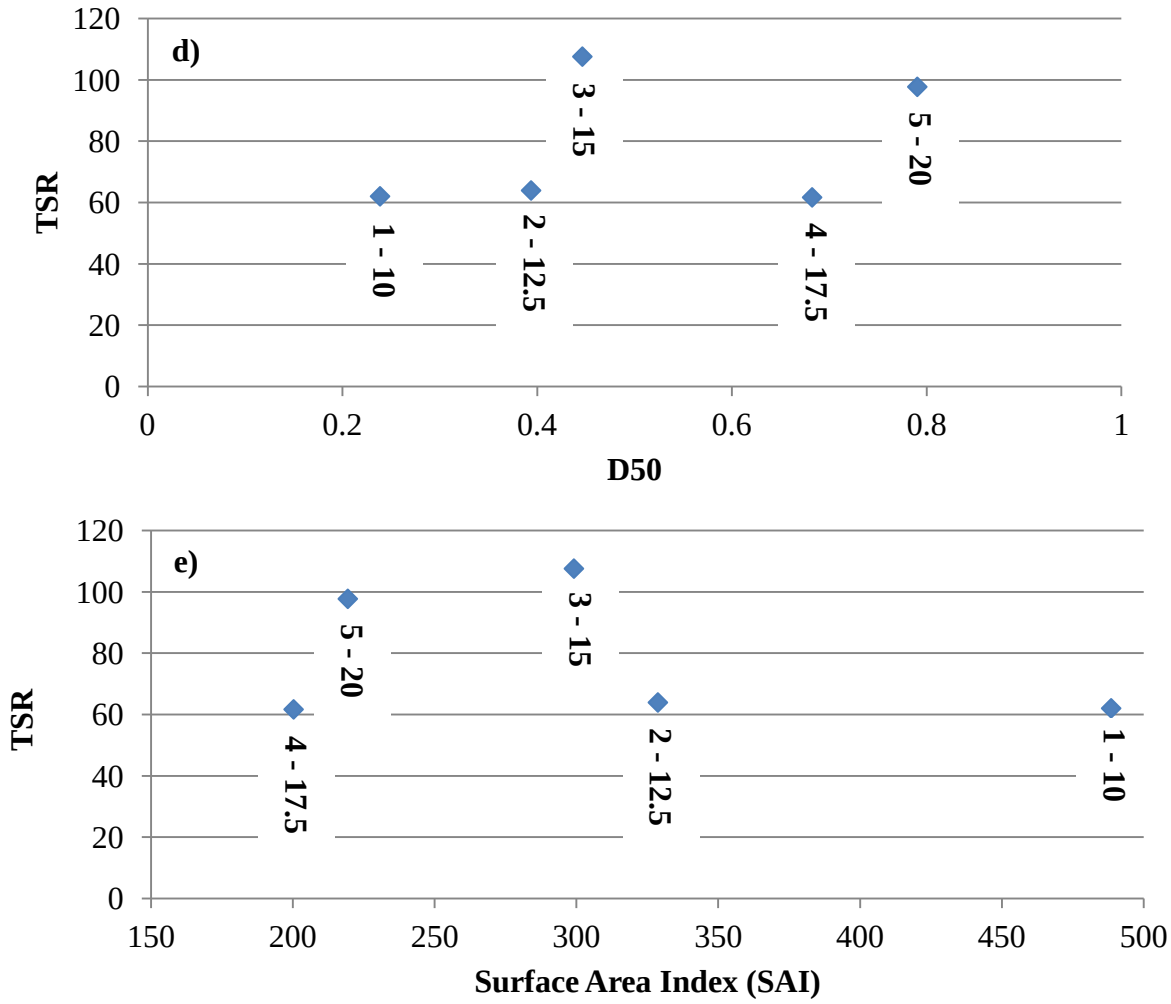

CHAPTER 6

INVESTIGATION OF FOAM DISIPATION USING SYNHROTRON-BASED X-RAY MICROTOMOGRAPHY

The quality of the foamed binder depends various factors such as the binder type, grade and modification, the foaming technology used, amount of water, temperature etc. AFCT analysis, which was verified with X-ray Microtomography (XRM) imaging technique, proved the foamed binder parameters depends on the injected water content and air pressure in CHAPTER 4. In order to further investigate the effects of some of the other characteristics such as the binder type and foaming technology on the generation and evolution of the foam, XRM imaging technique was also utilized to frozen foamed binder samples. Change in overall volume of the moisture bubbles as well as the size distribution of the bubbles was computed using 3D image processing methods. Variation of volume and size distributions of the bubbles in different types of asphalt binders as well as a mastic specimen was discussed in this chapter.

MATERIALS AND METHODS

Four different types of binders and a mastic sample were investigated by XRM as given in Table 15. Two of the selected binders were unmodified binders with PG grades of 58-28 (the binder source was different than the binder used in CHAPTER 4) and 64-22. One of the other binders was a polymer (Elvaloy) modified binder and the last one was a Crumb Rubber (CR) modified binder. The CR modified binder had 15 % CR (by weight of binder), which was

prepared using a technique called Wet Process. The binder was mixed with CR at 190^{o}C using a mixer at a rate of 2000±100 rpm (revolutions per minute) for 60 ± 5 minutes.

Table 15: Description of the specimens utilized in this study.

Identification	Binder Modification	Warm Mix Method
PG58-28F	Unmodified	Laboratory Foaming
PG70-22F	Elvaloy	Laboratory Foaming
PG64-22F	Unmodified	Laboratory Foaming
PG70-22CRMF	Crumb Rubber Wet Process	Laboratory Foaming
PG58-28A	Unmodified	Advera (Synthetic Zeolite)
PG70-22A	Elvaloy	Advera (Synthetic Zeolite)
PG70-22CRMA	Crumb Rubber Wet Process	Advera (Synthetic Zeolite)
PG58-28SANDF	PG 58-28+ fine aggregate	Laboratory Foaming

Each binder was foamed using two methods: (i) a laboratory foaming device (Wirtgen WLB 10) and (ii) Advera, a synthetic Zeolite additive (details were given in CHAPTER 2). The nozzle-based foamed binders were prepared by injecting air (5%), water (1.5%) and asphalt binder (93.5%) at 160°C.The zeolite based foamed binders were prepared with Advera at 120°C. 4.5% Advera by weight of the binder was added to the asphalt binder, where the crystallized water in the Advera transforms into moisture bubbles and foams the binder. The same binder foaming procedure was followed independent of the independent of the binder type.

In order to observe the effect of foaming on the microstructure when aggregates are present, mastic specimens were prepared by mixing the foamed PG58-28 binder with fine aggregates retained on #200 sieve (passing #100 sieve). Binder content for the mastic specimens were selected to be 10% by weight of the mix. The mixing temperature was approximately 150°C because of rapid cooling of the foamed binder after the foaming process.

3D IMAGING USING SYNCHROTRON BASED X-RAY MICROTOMOGRAPHY

The 3D image acquisition of the specimens was done at the 5-BM-C Microtomography beam line at the Advanced Photon Source (APS) facility in Argon National Laboratory (ANL), similar to the analysis in CHAPTER 4. In this part of the research, 20keV parallel beam was utilized, which provided a volume scan of 7 mm diameter, 7 mm tall cylinders. This size was the maximum size sample that can be scanned with the default camera and optical system (i.e., the X-ray detector). The final image size was 1299 by 1299 by 1299 pixels. This corresponded to 7 mm/ 1299 pixels = 0.0054 mm/pixel (5.4 micron) image resolution. Same procedure explained in CHAPTER 4 used in the analysis of 3D XRM images in this chapter.

The 7 mm diameter and 7 mm tall specimens were appropriate for this study because the maximum sizes of the bubbles were much smaller (~0.4mm) than the overall sample size, as shown in Figure 50 and Figure 51. The maximum size of the bubbles was larger in binders made with Zeolite (Figure 52); however, it was still smaller than the overall size of the specimen. As shown in Figure 56 and Figure 57, the bubbles in mastic specimens were also very small (maximum size ≈ 0.2mm), therefore the 7 mm diameter tubes were appropriate in this study.

BINDERS PREPARED USING DIRECT FOAMING

Figure 46 shows the 3D visualization of the labeled (with different colors) bubbles for two of binders frozen at different times. These views were generated from XRM images after thresholding and labeling operations described in CHAPTER 4. Figure 46qualitatively shows the reduction in bubble size and density in about 10 minutes for both of the binder specimens PG58-28F and PG70-22F. However, the rate of reduction in the bubble density and size seems to be slower in PG70-22F as compared to PG58-28F specimen. This phenomenon might be due to (i)

smaller diffusion coefficient of PG 70-22 binder as compared to PG 58-28 and PG 64-22 binders, and/or (ii) PG70-22 is a stiffer binder than others, which perhaps slows down the movement of the bubbles within the binder. The reduction in size of the bubbles is quantified in the following section.

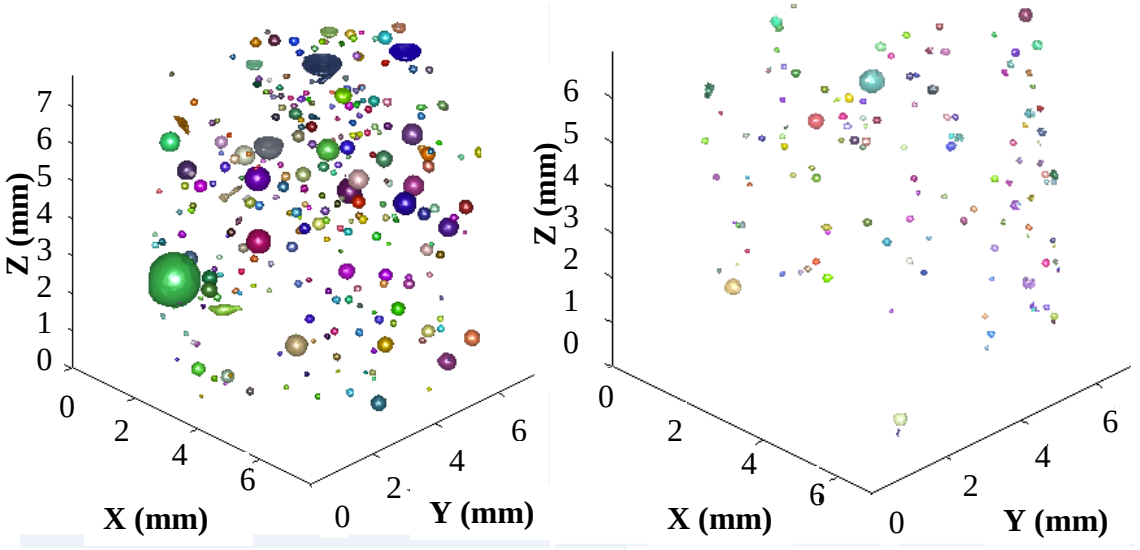

a) t=0.4min (PG58-28F unmodified binder)

b) 10min (PG58-28F unmodified binder)

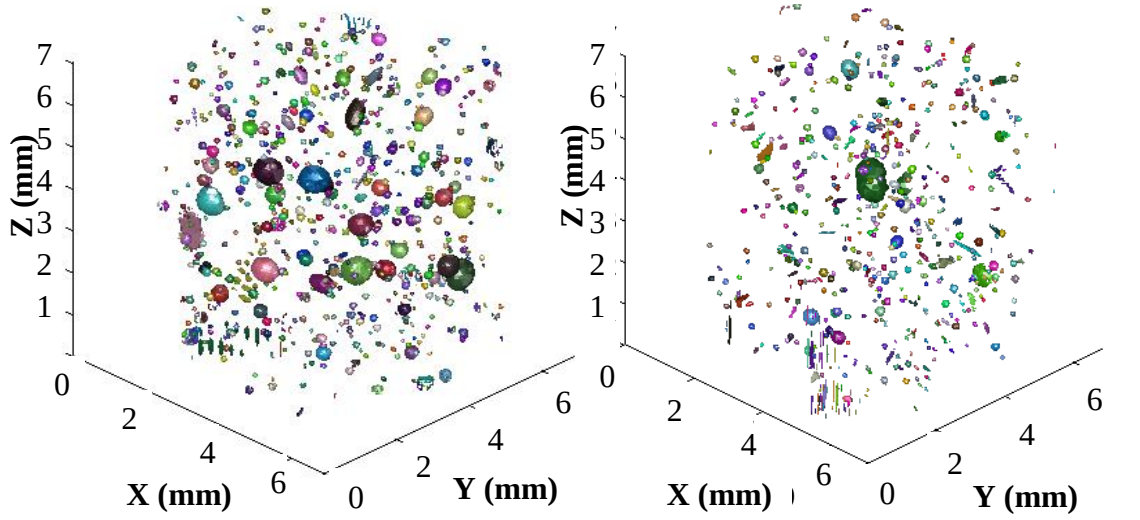

c) t= 1min (PG70-22F Elvaloy modified binder)

d) t=13min (PG70-22F Elvaloy modified

Figure 46: 3D temporal view of bubbles in two asphalt binder specimens: (a) & (b) PG58-28 unmodified binder and (c) & (d) PG70-22 Elvaloy polymer modified binder.

Temporal change in the total volume of the bubbles

Figure 47 shows the reduction in the volumetric proportion of the bubbles with time. The volumetric proportions of the bubbles were calculated from the 3D XRM binary images using the Matlab® algorithms, explained in CHAPTER 4. The volumetric percentage of the bubbles is the ratio of the total volume of the bubbles to the total scanned volume. As shown in Figure 47a, rate of change of volumetric percentage of bubbles varies in different binders. Figure 47b shows that curves follow approximately linear trend when plotted in log-log scale. In order to quantify the change in the total bubble volume, a parameter called moisture dissipation index (MDI) is defined to quantify the speed of dissipation of moisture within the binder. The MDI is anticipated to correlate well with the amount of time that takes for moisture to dissipate in the field after foam mix asphalt is placed. The MDI is defined as the slope of the linear best-fit line equation fitted to logarithm of volumetric bubble percentage versus time graph (Figure 47b) as follows:

$$\log(V) = -(c_1 \log(t) + c_2) \quad [27]$$

$$MDI = c_1$$

where V = volumetric percentage of bubbles (%) at any time t (min), c_1 and c_2= are the fit coefficients as shown in Figure 47. Figure 48 shows the MDI values for different binders investigated in this study. As seen from the Figure 48, MDI values are higher for unmodified binders as compared to the polymer and crumb rubber modified binders. As it was hypothesized before, this phenomenon can be attributed either to the (relatively high) stiffness of the polymer modified binders or (possibly to) their low diffusion coefficient.

On the other hand, the volume of the bubbles in the crumb rubber modified binder (PG70-22CRMF) seemed to have increased with time. While this may be because of a measurement or sampling error, it may also be an artifact of the existence of crumb rubber (CR) particles in the binder as shown in Figure 49. It is hypothesized that, while mixing within the foaming nozzle, the CR particles caused the bubbles to be even smaller than the resolution (i.e., 5.4 micron) of the XRM images. The bubbles in CR specimens might have diffused and disappeared in a much longer period of time.

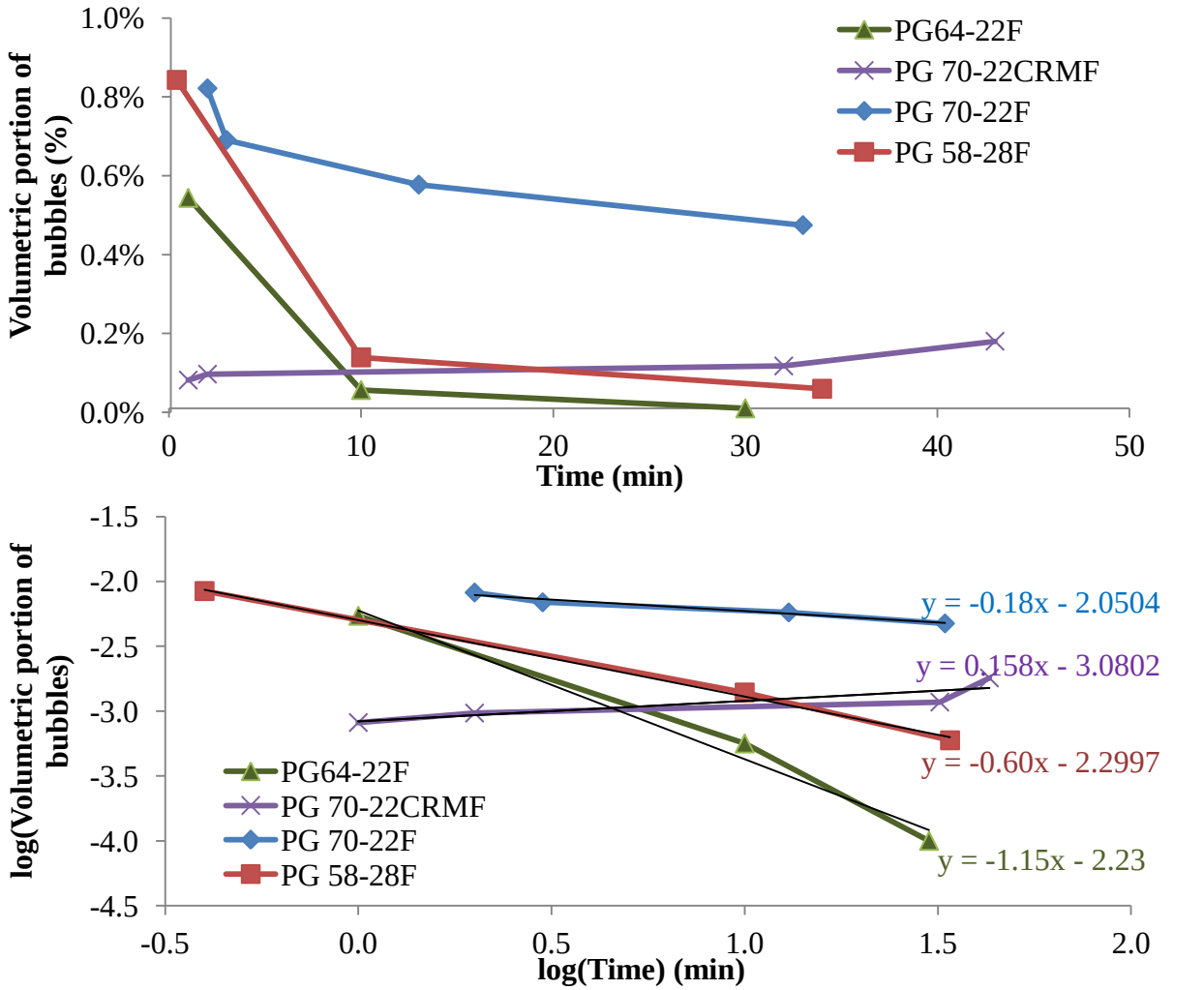

Figure 47: Reduction in the volume of bubbles with time; (a) in linear x-y scale and (b) logarithmic x-y scale.

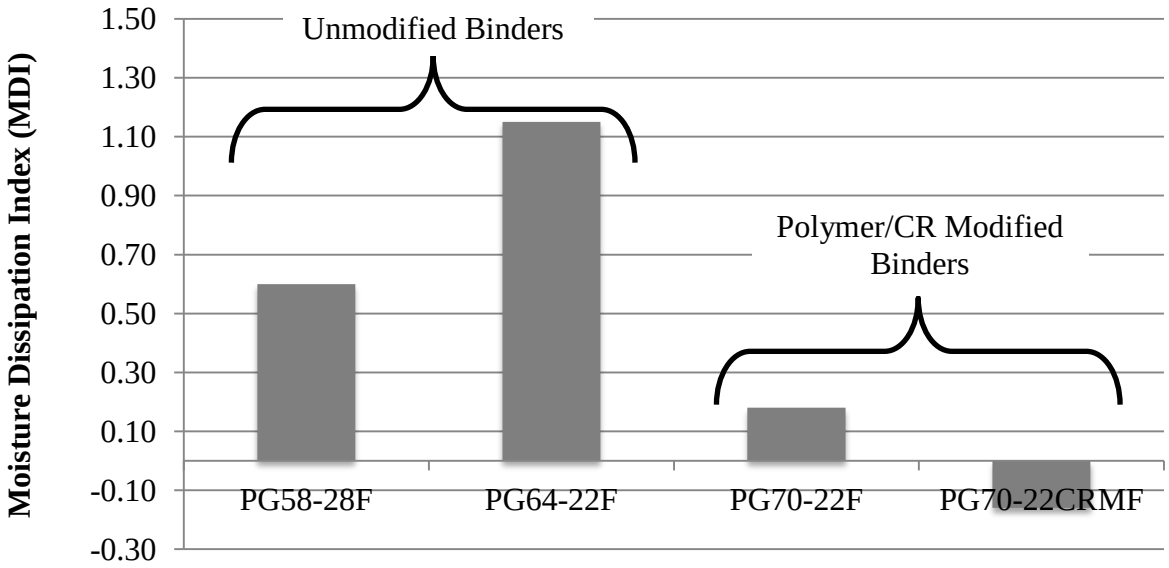

Figure 48: Moisture Dissipation Index (MDI) values for different binders.

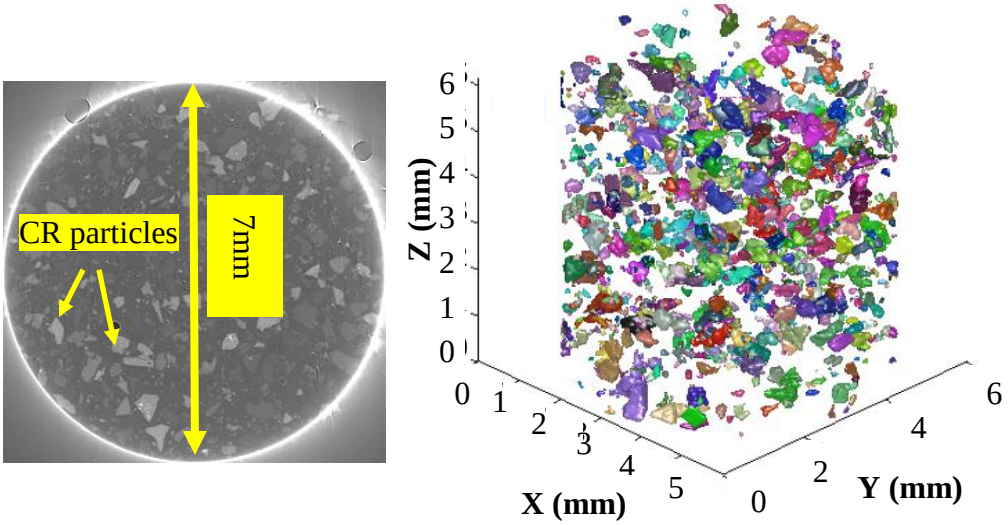

Figure 49: (a) 2D slice XRM image of PG70-22CRMF and (b) 3D visualization of crumb rubber particles.

Temporal change in the size distribution of the bubbles

In addition to the total volume of the bubble, size distribution of the bubbles was also analyzed. In order to calculate the size distribution, first, equivalent diameters of each bubble were computed using the labeled binary XRM images. The equivalent diameter is herein defined

as the diameter of the equivalent sphere that has the same volume as a given bubble. Then cumulative frequency distribution of the bubble sizes was computed. Figure 50 and Figure 51 show the change in bubble size distribution with time for the specimens utilized in this study. In general, the size of the bubbles reduces with time and they become more uniformly graded. Figure 50a and Figure 50b, the size distribution in t=30 min is not shown because there were only few bubbles left in the binder and illustration of size distribution would not have been realistic. In Figure 51c and Figure 51d, size distribution of the bubbles in PG70-22CRMF seems to indicate that at 43 min, the sizes are larger (in general) than t=32 min. This may be due to an error in the sampling in PG70-22CRMF.

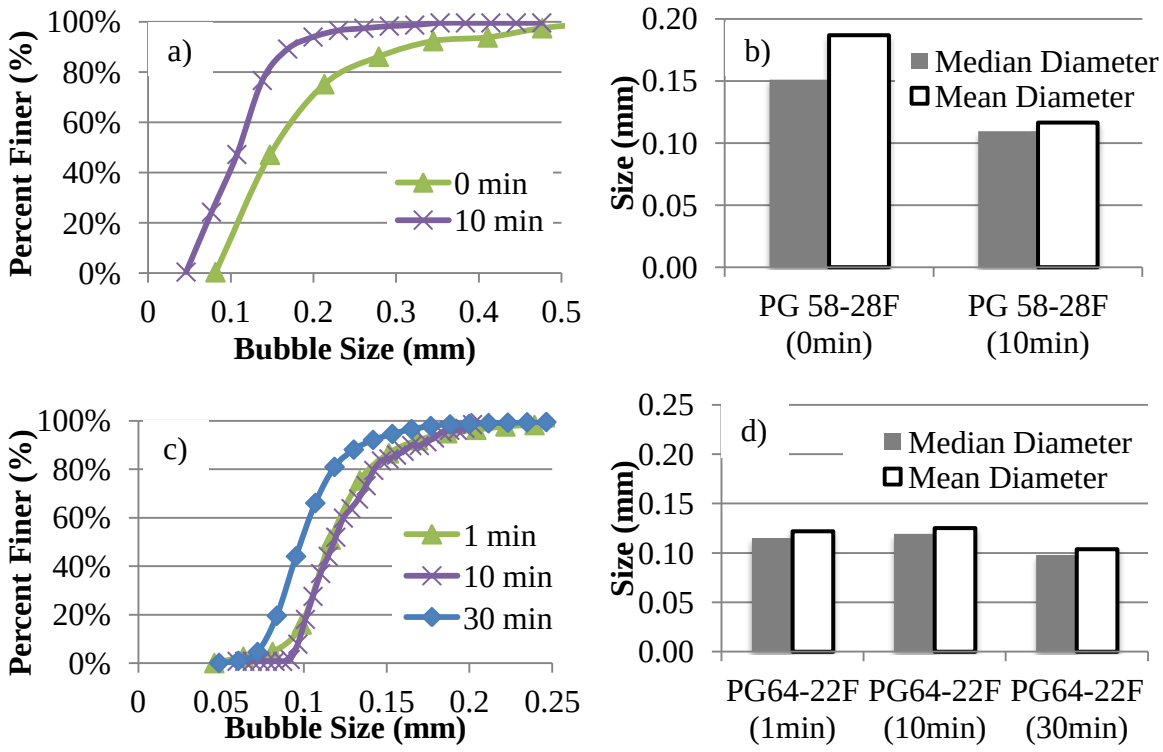

Figure 50: The change in size distribution of bubbles over time for: (a) & (b) PG58-28F and (c)&(d) PG64-22F.

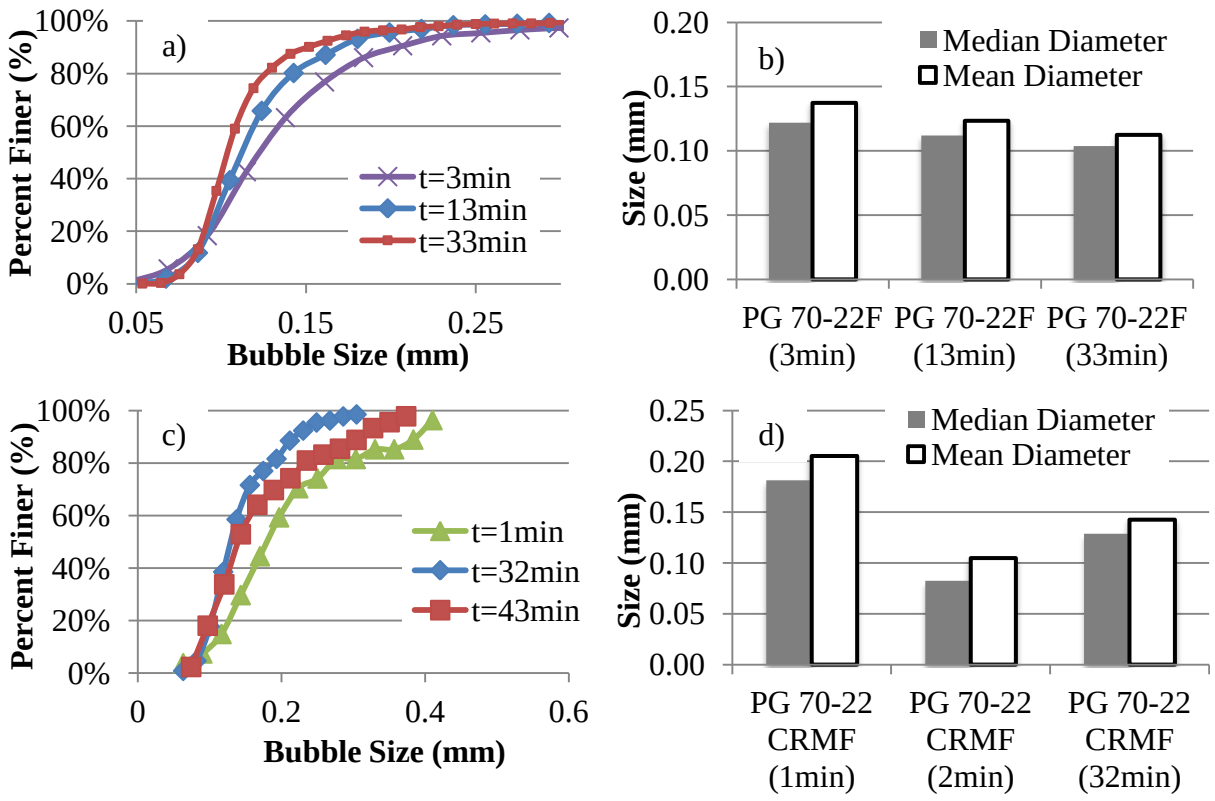

Figure 51: Change in size distribution of the bubbles with time for binder (a) & (b) PG70-22 and (c)&(d) PG70-22CRMF.

BINDERS PREPARED USING SYNTHETIC ZEOLITE

It was observed that binders foamed using Zeolite additive (Advera) exhibited quite different bubble size distribution as shown in Figure 52. Bubbles were larger and more scarce. This indicates that different foaming methods can exhibit different bubble volume and size distribution. Figure 53 shows the change in the overall volume of the bubbles in specimens prepared with synthetic Zeolite. Typically, the rate of dissipation of moisture was larger as compared to the foamed specimens. Figure 54 shows the comparison between the MDI values of specimens prepared using direct foaming and Zeolite additive, where MDI values are larger in binders prepared with Zeolite. This (with the limited data available) indicates that the moisture

disspates faster in Zeolite as compared to direct foaming process. In these figures, PG58-28A is not shown because no air bubble was observed within the XRM images of this specimen. This was attributed to the insufficient mixing of the Zeolite during sample preparation. An example image of PG58-28A is shown in Figure 55, where a clear bright spot in the center is visible. This bright area is probably the Zeolite additive, which is not mixed with the binder.

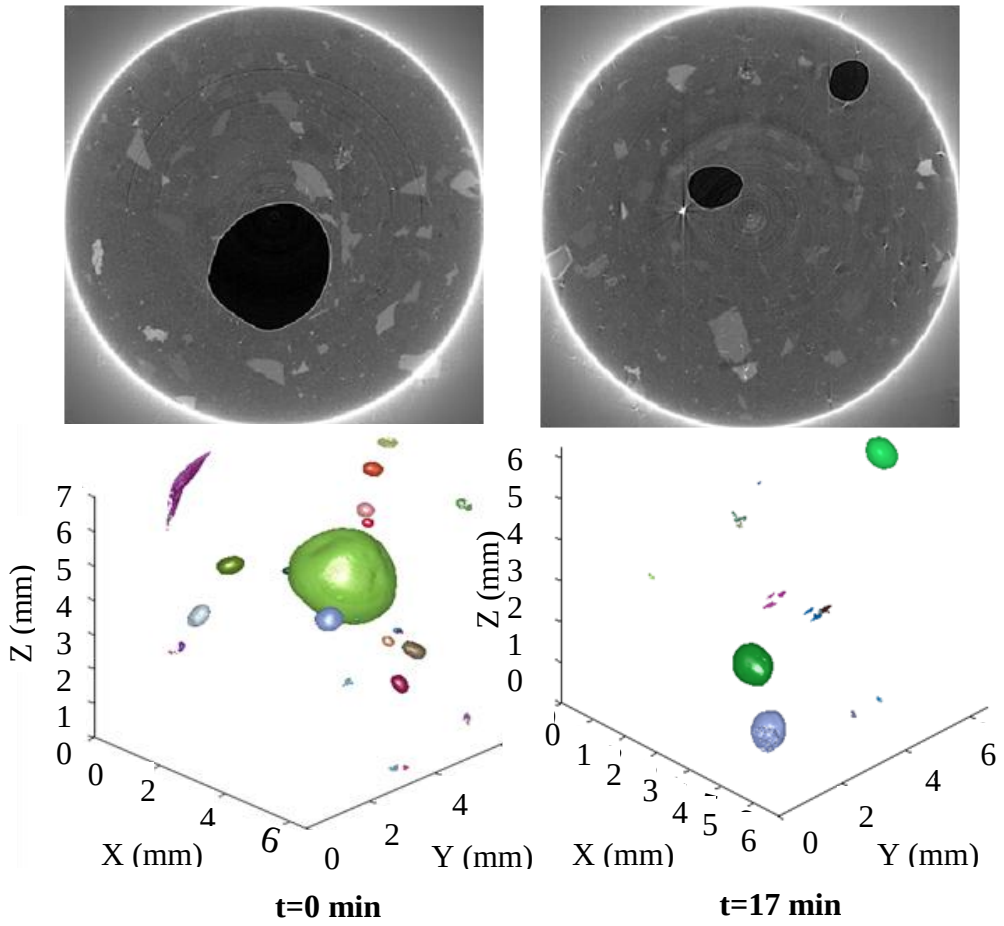

Figure 52: 3D XRM image of PG70-22CRMA binder foamed using Zeolite additive.

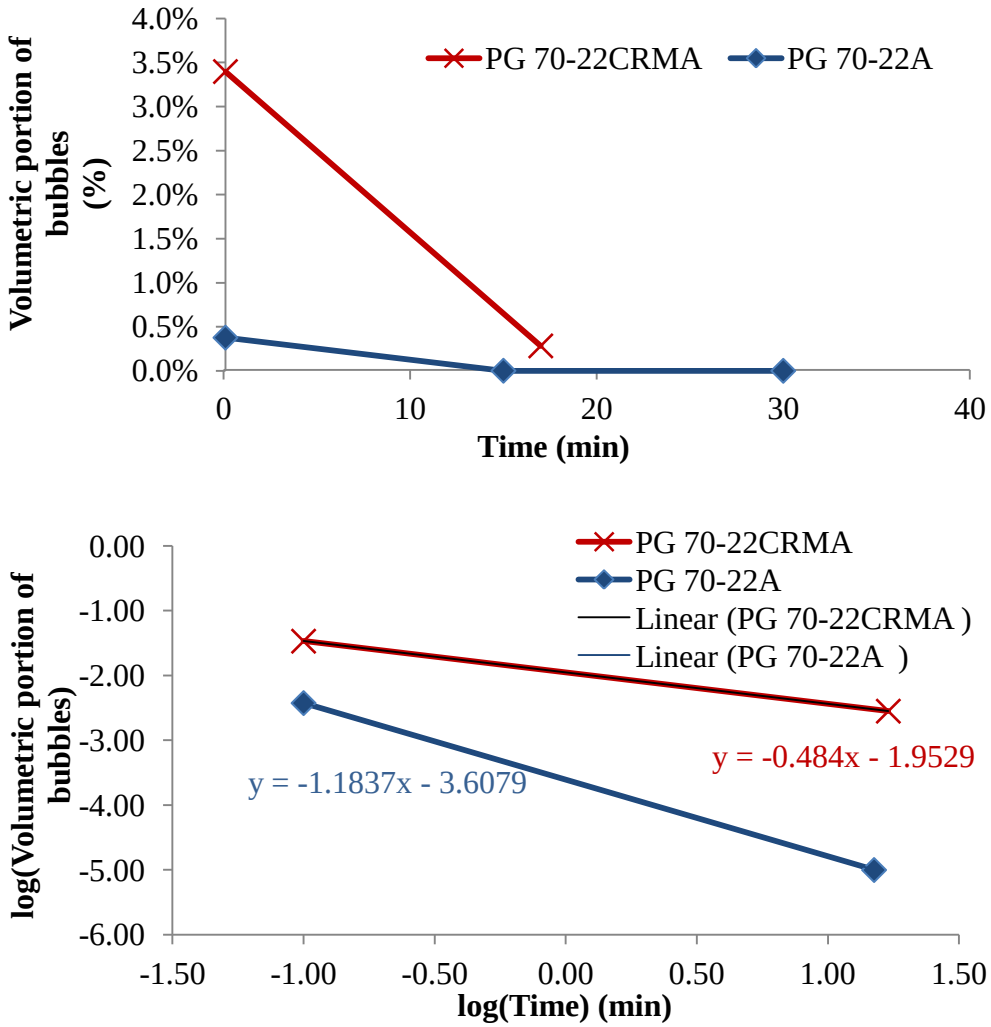

Figure 53: Reduction in the volume of bubbles with time in specimens prepared with Zeolite.

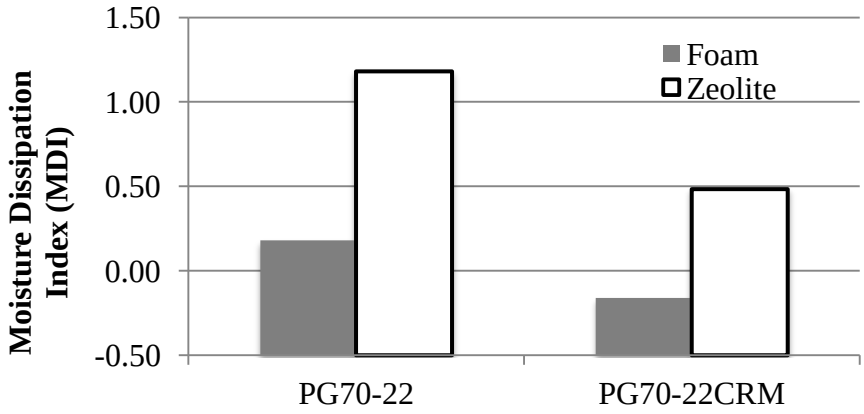

Figure 54: Moisture Dissipation Index (MDI) comparison of binders prepared with foam and Zeolite binders.

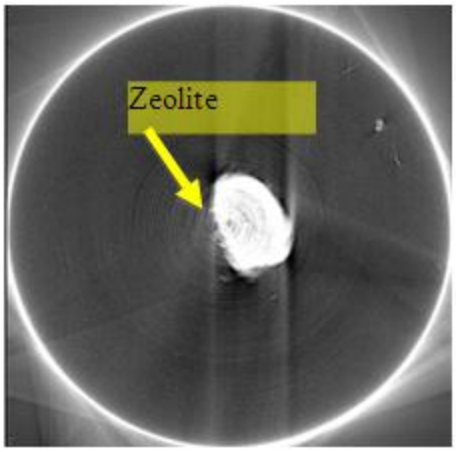

Figure 55: 2D XRM image slice of PG58-28A, which was prepared with Zeolite.

INVESTIGATION OF FOAMED MASTICS

In addition to the asphalt binders, mastics (asphalt binder + fine aggregate) were also included in the research program. It is hypothesized that morphology and type of fine aggregate can play a crucial role in the moisture retention and dissipation in the mixture. Similar to the procedure for binders, the mastic specimens were poured into the 7 mm diameter tubes, frozen using liquid nitrogen and scanned using XRM. Figure 56 shows example XRM image slices of these two specimens as well as 3D visualization of the bubbles. It was observed that large elongated voids appeared in mastic specimens. This may be due to (i) fracturing during freezing using liquid nitrogen or (ii) distortion of the bubbles because of the fine aggregate grains. Figure 57 illustrates the change in the size distribution as well as mean and median size of the bubbles where reduction in bubble size was observed between times 6 min and 34 min. However, as shown in Figure 58, overall volume of the bubbles actually increased with time. It may be a sampling problem or non-homogenous mixing. Therefore, further specimen preparation and testing are needed to better understand the actual behavior.

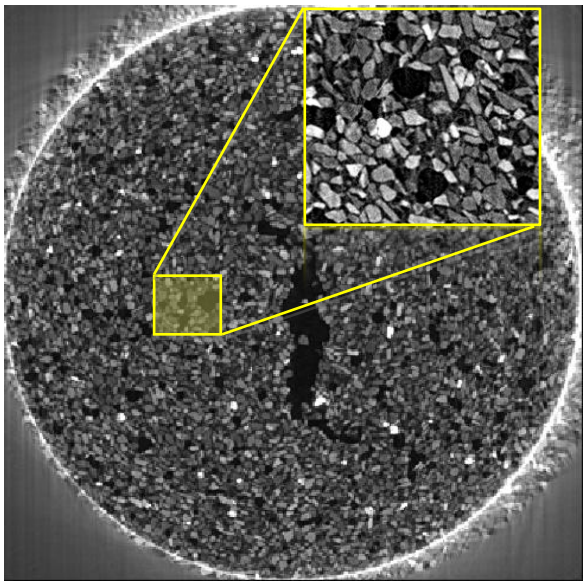

(a) 2D slice of mastic specimen (t = 6min)

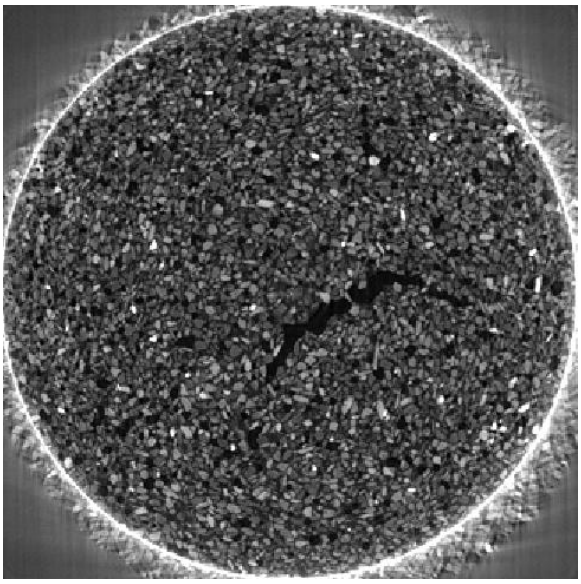

(b) 2D slice of mastic specimen (t = 34min)

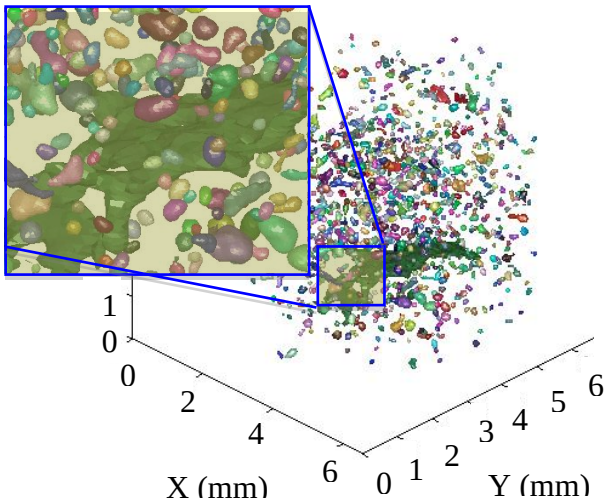

(c) Voids of the mastic at t=6 min.

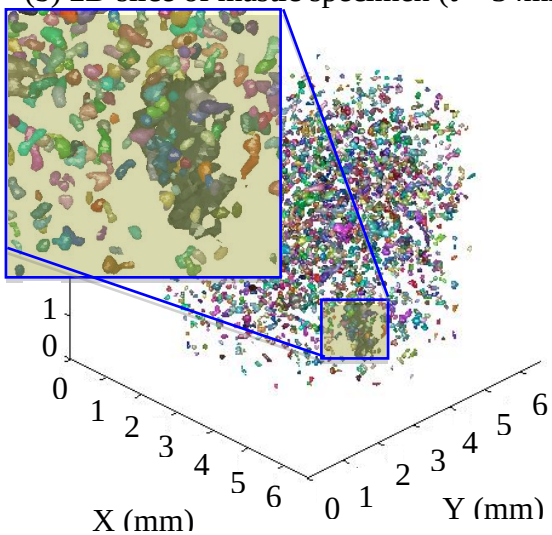

(d) Voids of the mastic at t=34 min.

Figure 56: (a) & (b) 2D slices from XRM images and (c) & (d) 3D visualization of pores of foamed asphalt mastics.

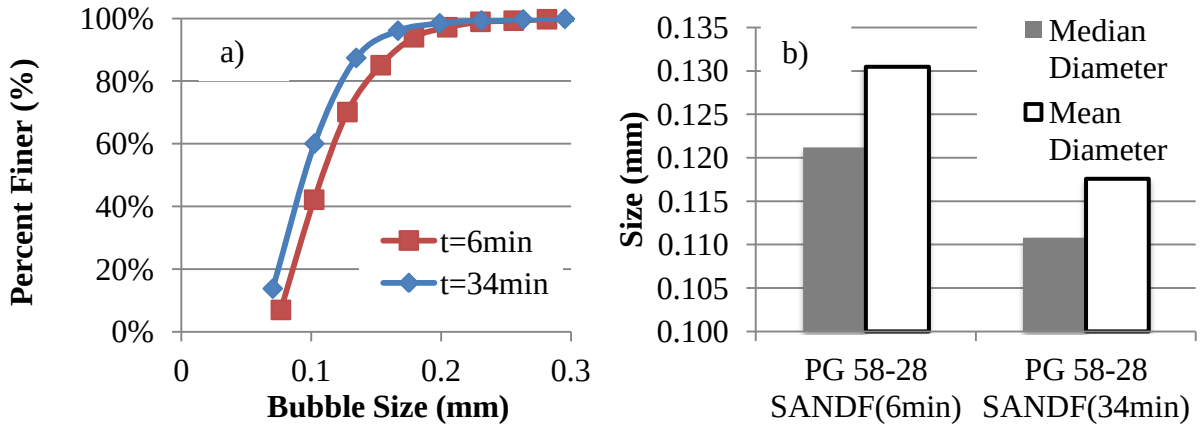

Figure 57: Change in (a) size distribution and (b) mean & median size of the bubbles in PG58-28SANDF

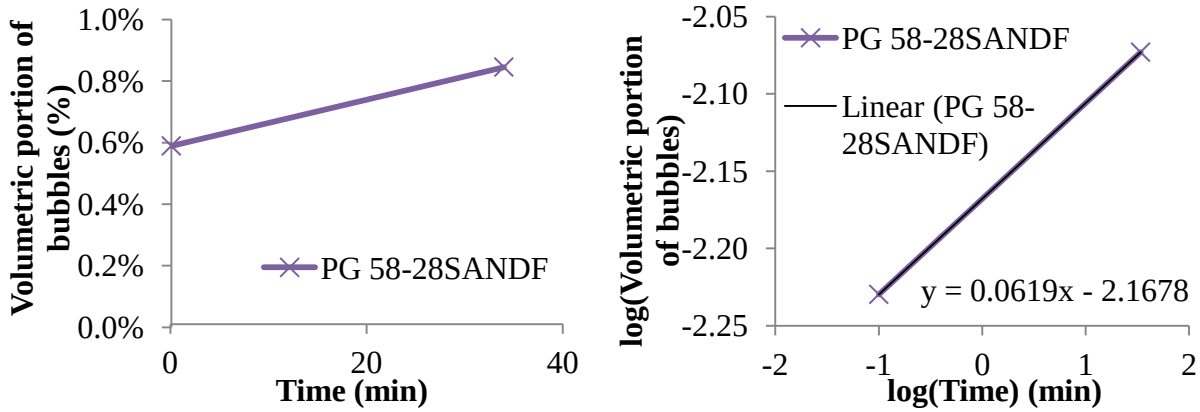

Figure 58: Change in the overall volumetric percentage of the bubbles with time in specimen PG58-28SANDF.

CHAPTER 7

CONCLUSION AND RECOMEDATIONS

SUMMARY

Most of the current knowledge on foamed Warm Mix Asphalt (WMA) is based on limited empirical studies and there is a significant lack of understanding of the behavior of the foamed binder used in WMA pavements. Understanding the WMA foamed binder characteristics, which affect the mechanical behavior of pavements, is crucial to accurately predict and improve their long-term performance. Therefore, there is a growing need for understanding the WMA pavements' behavior, from binder production to mixture performance.

As of today, the importance of foam quality has never been considered in WMA pavement design. It has been hypothesized that the quality of the foamed binder depends various factors such as the binder type, grade and modification, the foaming technology used, amount of water, air pressure and temperature. The quality of the foamed binder plays a crucial role during mixing, laying and compaction stages of WMA pavement production. However, there is no study that came up with foamed binder quality indicators for WMA applications. Even though there are some candidate foamed binder quality indicators that were developed for stabilized base applications (i.e., Expansion Ratio (ER), half-life (HL), Foam Index (FI)), their relation to WMA performance have never been investigated. Furthermore, there is no available method to precisely measure the potential foamed binder quality indicators. Therefore, an accurate and repeatable procedure is needed for the measurement of reduction in height of foamed asphalt in order to calculate these indicators. In this research, an automated test device, called as Asphalt

Foam Collapse Test (AFCT), was developed to measure the reduction in the height of the foamed binder over time. Once the reduction in height of the asphalt foam with time is measured, the foamed binder's quality parameters can be precisely calculated. Tracking the change of the foam structure with time helps to understand the workability of the binder as well as the physical properties of the binder such as the residual water. In addition, in this research, new parameters (i.e., Bubble Size Distribution (BSD) and Surface Area Index (SAI)) are introduced to assess the quality of the foamed binder. These indicators are potentially very important parameters, since they directly relate to the ability of the foamed binder to coat the aggregates, the workability of the mix and the mixture performance. The AFCT test and associated BSD computation method was verified using X-Ray Microtomography imaging technique. Moreover, both AFCT and X-Ray Microtomography imaging were utilized to investigate foaming characteristics of different kinds of binders prepared at different levels of injected air pressure and water content. As part of this research, the relationship between various binder quality indicators and the mixture performance tests were investigated and the effects of air pressure and water content on the foamed binder and mixture performance were also observed.

CONCLUSIONS

This research presented a novel testing methodology called Asphalt Foam Collapse Test (AFCT) for determining foamed binder parameters such as expansion ratio, half-life and foam index. The AFCT is an automated, accurate and repeatable test method for measuring the height reduction of the foamed binder as it collapses. A new procedure utilizing the AFCT data is also introduced to calculate the bubble size distribution and bubble surface area of the foamed binder from AFCT measurements. As a result of this new approach, a new dimensionless parameter

called Surface Area Index (SAI), which was directly related to the mixture coating, workability as well as the performance, was introduced.

Based on the study on the foamed binder characteristics, the following major conclusions were drawn:

- The expansion ratio (ER) is an indicator of overall volume of bubbles, but it can be a misleading parameter for the size distribution of the bubbles, which affects the coating and workability.
- Water content and air pressure have significant effect on the ER, half-life (HL) and foam index (FI). ER increases with the increase of water content and air pressure, whereas HL and FI decreases with the increase of water content and air pressure.
- The size distribution of the bubbles in foamed binder becomes coarser (i.e., the bubbles become larger and larger) as the water content and air pressure increase.
- As the injected water content and air pressure in the foamed binder increased, the maximum diameter of the bubbles increased. This leads to the short half-life and high expansion ratio.
- SAI, which is an indication of total surface area of the bubbles, increased with decreasing water content and air pressure. Also, better mixture coating was observed at high SAI values.
- AFCT procedure to compute the bubble size distribution was validated using 3D X-Ray microtomography (XRM) imaging. 3D image-based bubble size

distribution was compared against bubble size distribution computed from the AFCT and a good match (within the sample to sample variability) was observed.

Scope of this study also included evaluation of the performance of the WMA mixtures prepared at different foaming water contents and air pressures. Testing program included unconfined and confined dynamic modulus (|E*|), Flow Number (FN), Push-Pull Fatigue (PPF), and Tensile Strength Ratio (TSR) tests. Based on the laboratory tests, the performance of the mixtures are ranked as given in Table 16, in which the rank is 1 to 3 or 1 to 5 from better to relatively worse performance. Additionally, the following conclusions were drawn:

Table 16: Performance ranking of mixtures based on the laboratory tests

Performance Tests	**Performance test sample descriptions**				
	1% - 10psi	2% - 12.5psi	3% - 15psi	4% - 17.5psi	5% - 20psi
Unconfined |E*|	No Ranking				
Confined |E*|	3	NA	1	NA	2
Flow Number	5	4	3	2	1
Push-Pull Fatigue	4	3	1	2	5
Tensile Strength Ratio	3	3	1	3	2

- The unconfined |E*| of different WMA mixtures prepared at different foaming water content/air pressure combinations were very similar. Therefore, it is hard to estimate the relative rutting or fatigue cracking susceptibilities (as estimated using ME-PDG) of these WMA mixtures, as well as their relation to the foamed binder quality indicators through unconfined |E*| tests for this study.

- The confined |E*| tests revealed differences in |E*|s of mixtures made at different foaming water content/air pressure combinations. The confined |E*| is perhaps a more appropriate test as the pavements in the field is in 'confined' state.
- FN increased (i.e., better rutting performance was observed) as the SAI decreases. It is hypothesized that this is because of 'poorer' coating at low SAI values, allowing the aggregate-to-aggregate friction to be relatively large, which is in-turn helping towards the rutting performance.
- The fatigue analysis indicated the importance of the foamed binder characteristics on the mix performance. As a result of the high-injected water content and air pressure in the binder, higher percentage of uncoated aggregates increased the fatigue cracking potential. On the other hand, small foam bubbles trapped in the mix due to the relatively low water content and air pressure in the foamed binder also increased the fatigue cracking resistance. Therefore, there is an optimum range of bubble sizes (and the surface area) and D_{50} that maximizes the resistance to fatigue cracking.
- The unconditioned strength of the mixtures decreases as the injected water content and air pressure in the foamed binder increases. However, a similar trend was not observed on the conditioned strength of the WMA mixtures.
- The lower water content and air pressure results better aggregate coating, which also increase the strength between the aggregate and binder bonds. Thus, the tensile strength of these mixes is relatively high. On the contrary, the higher water

content and air pressure caused poor bond between the aggregate and binder results relatively lower tensile strength.

As part of the study, further analyses with XRM imaging were performed. Several types of asphalt binders were prepared using two different foaming methods: (i) direct foaming and (ii) using synthetic Zeolite. Once the images of these samples were obtained, image processing and analysis techniques were utilized to quantify the change in the microstructure of the moisture bubbles with time. The findings of this study are summarized as follows:

- High quality 3D images of foamed binder specimens can be captured using the synchrotron based XRM system. Quantitative information such as the speed of reduction in the volume of bubbles can be obtained from the XRM images.
- Rate of moisture dissipation in foamed asphalt binders depends on the type and PG of asphalt. It was observed in this study that high PG (stiff) asphalt binders dissipated moisture slower than low PG (soft) binders. This is meaningful because the stiffer binders possibly have lower diffusion coefficient. Therefore, high PG binders might be more susceptible to moisture damage in foamed asphalt pavements.
- Foaming process (i.e., direct foaming versus use of foaming agents such as Synthetic Zeolite) influences the moisture retention and dissipation. It was observed that Zeolite dissipated moisture faster than the direct foaming method. Therefore, mixtures prepared with Zeolite will probably be less susceptible to moisture damage. However, quick dissipation of bubbles may also lead to reduced workability during construction.

- Moisture dissipation in mastic (binder + fine aggregate) is different from the dissipation of moisture from the binder. Size distribution and overall volume of the moisture bubbles in binders decrease with time. However, limited data obtained in this study suggests that even though sizes of the bubbles decrease, overall volume of the bubbles initially increase in mastics. It is hypothesized that this phenomenon is because of coalescence of the micro-bubbles and these coalesced bubbles dissipate in a longer period of time.

RECOMMENDATIONS

The AFCT test and the described methodologies for calculating the foam quality indicators are valuable. The absence of an accurate and repeatable testing method in measuring the foam quality in the current practice can be filled with AFCT, which is also practical and affordable test that can be used by the practitioners. In addition, the findings of the performance tests indicate the importance of foam quality in the performance of the pavement.

The majority of this research was limited with one type of binder and one aggregate gradation. In the further studies, it is recommended to change the binder type and gradation to increase the data range. In addition, this research was limited with the laboratory study. It is recommended to study the relation in between the foam binder quality and field performance.

The crumb rubber (CR) usage in the asphalt pavements is very widespread and beneficially reuses the scrap tires. There are numerous laboratory and field studies that showed superior performance of CR modified asphalt pavements over traditional HMA. However, the initial cost of the CR modified pavements is comparably high than HMA, partially because of the high production temperatures. Constructing CR modified WMA can compensate for the cost

associated with high temperatures (~190^{o}C) used during mixing CR with asphalt binder. However, effect of moisture content/air pressures, in the presence of CR particles can be different and should be investigated.

APPENDICES

APPENDIX A

Table 17: Unconfined Dynamic Modulus for the first replicate of 1% - 10psi WMA mixture

Shift Factor Coefficients:	
a1=	0.00082
a2=	-0.15022
Reference Temperature:	
Tref=	21

Sigmoid Coefficients:	
b1=	0.12275
b2=	4.47288
b3=	0.90776
b4=	0.40460

Gaussian Model (phase angle fit):	
a=	33.35002
b=	-2.42217
c=	5.07082

Total Error:	0.5403
Σ Error1	0.2724
Σ Error2	0.2679

Measured Data				Shift Factor	Reduced Frequency		Predicted Data		Error	
T (C)	**f (Hz)**	**|E*| (Mpa)**	**Phase angle**	**log(aT)**	**f_R (Hz)**	**Log f_R (Hz)**	**Sigmoid Fit, |E*| Mpa**	**Predicted Phase Angle**	**Error1 (|E*|)**	**Error2 (Phase Angle)**
10	25	9809	15.10	1.373	590.260	2.771	11909.128	19.74	0.021	0.031
10	10	8460	16.93	1.373	236.104	2.373	9936.447	21.33	0.018	0.026
10	5	7237	18.60	1.373	118.052	2.072	8535.660	22.52	0.019	0.021
10	1	5040	23.02	1.373	23.610	1.373	5687.247	25.20	0.014	0.009
10	0.5	4305	24.53	1.373	11.805	1.072	4662.058	26.30	0.010	0.007
10	0.1	2778	28.65	1.373	2.361	0.373	2777.269	28.65	0.000	0.000
21	25	5217	23.53	0.000	25.000	1.398	5777.513	25.11	0.012	0.007
21	10	4140	25.99	0.000	10.000	1.000	4435.721	26.56	0.008	0.002
21	5	3420	27.56	0.000	5.000	0.699	3570.583	27.59	0.005	0.000
21	1	2065	31.15	0.000	1.000	0.000	2041.093	29.75	0.002	0.004
21	0.5	1658	31.73	0.000	0.500	-0.301	1568.405	30.56	0.007	0.004
21	0.1	875.4	32.53	0.000	0.100	-1.000	813.318	32.06	0.011	0.001

Table 17 (cont'd)

Measured Data				Shift Factor	Reduced Frequency		Predicted Data		Error	
T (C)	**f (Hz)**	**|E*| (Mpa)**	**Phase angle**	**log(aT)**	**f_R (Hz)**	**Log f_R (Hz)**	**Sigmoid Fit, |E*| Mpa**	**Predicted Phase Angle**	**Error1 (|E*|)**	**Error2 (Phase Angle)**
37	10	1163	36.22	-1.643	0.227	-0.643	1145.193	31.36	0.002	0.013
37	5	880.1	36.05	-1.643	0.114	-0.944	858.592	31.96	0.004	0.011
37	1	402.5	34.83	-1.643	0.023	-1.643	425.987	32.96	0.009	0.005
37	0.5	282.9	33.67	-1.643	0.011	-1.944	312.150	33.20	0.017	0.001
37	0.1	150.9	30.08	-1.643	0.002	-2.643	150.900	33.32	0.000	0.011
54	25	495	38.92	-2.930	0.029	-1.532	477.343	32.84	0.006	0.016
54	10	316.9	35.06	-2.930	0.012	-1.930	316.815	33.19	0.000	0.005
54	5	211.5	33.74	-2.930	0.006	-2.231	231.634	33.33	0.017	0.001
54	1	101.3	29.33	-2.930	0.001	-2.930	112.344	33.18	0.022	0.013
54	0.5	82.8	26.85	-2.930	0.001	-3.231	82.837	32.93	0.000	0.023
54	0.1	53.7	22.99	-2.930	0.000	-3.930	42.115	31.91	0.061	0.039

Table 18: Unconfined Dynamic Modulus for the second replicate of 1% - 10psi WMA mixture

Shift Factor Coefficients:	
a1=	0.000465
a2=	-0.12891
Reference Temperature:	
Tref=	21

Sigmoid Coefficients:	
b1=	0.475519
b2=	3.908692
b3=	0.951278
b4=	0.475207

Gaussian Model (phase angle fit):	
a=	34.71557
b=	-1.330173
c=	3.257148

Total Error:	0.4187
Σ Error1	0.2573
Σ Error2	0.1613

Measured Data				Shift Factor	Reduced Frequency		Predicted Data		Error	
T (C)	**f (Hz)**	**|E*| (Mpa)**	**Phase angle**	**log(aT)**	**f_R (Hz)**	**Log f_R (Hz)**	**Sigmoid Fit, |E*| Mpa**	**Predicted Phase Angle**	**Error1 (|E*|)**	**Error2 (Phase Angle)**
-10	25	18797	6.16	3.838	172064.979	5.236	18310.230	4.551	0.003	0.026
-10	10	17651	6.91	3.838	68825.992	4.838	17311.789	5.779	0.002	0.016
-10	5	16639	7.71	3.838	34412.996	4.537	16476.661	6.855	0.001	0.011
-10	1	14235	9.78	3.838	6882.599	3.838	14282.714	9.860	0.000	0.001
-10	0.5	13013	10.98	3.838	3441.300	3.537	13240.334	11.368	0.002	0.004
-10	0.1	9770	15.13	3.838	688.260	2.838	10665.334	15.309	0.010	0.001
10	25	9745	15.27	1.260	454.459	2.657	9982.793	16.408	0.003	0.007
10	10	8320	17.46	1.260	181.784	2.260	8481.256	18.913	0.002	0.008
10	5	7235	19.27	1.260	90.892	1.959	7372.819	20.852	0.002	0.008
10	1	5126	23.85	1.260	18.178	1.260	5009.052	25.308	0.003	0.006
10	0.5	4422	25.58	1.260	9.089	0.959	4122.902	27.121	0.008	0.006
10	0.1	2765	29.86	1.260	1.818	0.260	2451.035	30.817	0.015	0.003

Table 18 (cont'd)

Measured Data				Shift Factor	Reduced Frequency		Predicted Data		Error	
T (C)	f (Hz)	|E*| (Mpa)	Phase angle	log(aT)	f_R (Hz)	Log f_R (Hz)	Sigmoid Fit, |E*| Mpa	Predicted Phase Angle	Error1 (|E*|)	Error2 (Phase Angle)
21	25	5418	24.45	0.000	25.000	1.398	5446.218	24.445	0.001	0.000
21	10	4197	26.91	0.000	10.000	1.000	4239.406	26.877	0.001	0.000
21	5	3401	28.65	0.000	5.000	0.699	3436.818	28.592	0.001	0.000
21	1	1974	32.46	0.000	1.000	0.000	1973.061	31.938	0.000	0.002
21	0.5	1593	33.17	0.000	0.500	-0.301	1511.068	33.025	0.007	0.000
21	0.1	817	34.15	0.000	0.100	-1.000	769.975	34.538	0.009	0.001
37	25	1715	35.8	-1.631	0.584	-0.233	1606.587	32.802	0.009	0.008
37	10	1141	36.07	-1.631	0.234	-0.631	1108.359	33.926	0.004	0.006
37	5	837.1	36.23	-1.631	0.117	-0.932	824.239	34.458	0.002	0.005
37	1	377.9	35.4	-1.631	0.023	-1.631	399.444	34.567	0.009	0.002
37	0.5	262.9	34.58	-1.631	0.012	-1.932	289.808	34.127	0.017	0.001
37	0.1	127.2	31.61	-1.631	0.002	-2.631	137.943	32.053	0.017	0.001
54	25	388.5	38.26	-3.104	0.020	-1.706	368.974	34.485	0.009	0.010
54	10	241.7	35.81	-3.104	0.008	-2.104	241.237	33.750	0.000	0.006
54	5	160	34.85	-3.104	0.004	-2.405	175.073	32.876	0.018	0.006
54	1	75.4	30.27	-3.104	0.001	-3.104	85.008	29.931	0.028	0.001
54	0.5	63.3	27.14	-3.104	0.000	-3.405	63.300	28.341	0.000	0.004
54	0.1	44.7	22.31	-3.104	0.000	-4.104	33.692	24.157	0.074	0.008

Table 19: Unconfined Dynamic Modulus for the first replicate of 3% - 15psi WMA mixture

Shift Factor Coefficients:	
a1=	0.00055
a2=	-0.13572
Reference Temperature:	
Tref=	21

Sigmoid Coefficients:	
b1=	0.621746
b2=	3.752085
b3=	0.909983
b4=	0.468356

Gaussian Model (phase angle fit):	
a=	33.27342
b=	-1.23645
c=	3.275035

Total Error:	0.3378
Σ Error1	0.2017
Σ Error2	0.1361

Measured Data				Shift Factor	Reduced Frequency		Predicted Data		Error	
T (C)	**f (Hz)**	**|E*| (Mpa)**	**Phase angle**	**log(aT)**	**f_R (Hz)**	**Log f_R (Hz)**	**Sigmoid Fit, |E*| Mpa**	**Predicted Phase Angle**	**Error1 (|E*|)**	**Error2 (Phase Angle)**
-10.0	25	18416.0	5.9	4.019	261303.522	5.417	18116.011	4.225	0.002	0.029
-10.0	10	17385.0	6.7	4.019	104521.409	5.019	17187.807	5.368	0.001	0.019
-10.0	5	16535.0	7.3	4.019	52260.704	4.718	16410.465	6.372	0.001	0.013
-10.0	1	14343.0	9.2	4.019	10452.141	4.019	14361.502	9.181	0.000	0.000
-10.0	0.5	13259.0	10.3	4.019	5226.070	3.718	13383.229	10.595	0.001	0.003
-10.0	0.1	10212.0	14.0	4.019	1045.214	3.019	10947.846	14.304	0.008	0.002
10.0	25	9239.0	15.4	1.305	504.409	2.703	9802.605	16.141	0.006	0.005
10.0	10	8053.0	17.5	1.305	201.764	2.305	8363.851	18.544	0.004	0.006
10.0	5	7241.0	19.2	1.305	100.882	2.004	7300.530	20.396	0.001	0.006
10.0	1	5054.0	23.7	1.305	20.176	1.305	5024.480	24.624	0.001	0.004
10.0	0.5	4187.0	25.2	1.305	10.088	1.004	4165.845	26.332	0.001	0.004
10.0	0.1	2598.0	29.4	1.305	2.018	0.305	2530.358	29.785	0.003	0.001

Table 19 (cont'd)

Measured Data				Shift Factor	Reduced Frequency		Predicted Data		Error	
T (C)	f (Hz)	|E*| (Mpa)	Phase angle	log(aT)	f_R (Hz)	Log f_R (Hz)	Sigmoid Fit, |E*| Mpa	Predicted Phase Angle	Error1 (|E*|)	Error2 (Phase Angle)
21	25	5250	24	0.000	25.000	1.398	5306.757	24.077	0.001	0.000
21	10	4095	26.36	0.000	10.000	1.000	4155.530	26.353	0.002	0.000
21	5	3304	28.01	0.000	5.000	0.699	3388.408	27.942	0.003	0.000
21	1	1947	31.64	0.000	1.000	0.000	1981.390	30.985	0.002	0.002
21	0.5	1575	32.23	0.000	0.500	-0.301	1533.054	31.944	0.004	0.001
21	0.1	809	32.97	0.000	0.100	-1.000	804.340	33.187	0.001	0.001
37	25	1663	34.56	-1.660	0.547	-0.262	1586.485	31.832	0.006	0.008
37	10	1169	34.86	-1.660	0.219	-0.660	1109.594	32.761	0.007	0.006
37	5	849.9	35	-1.660	0.109	-0.961	835.294	33.156	0.003	0.005
37	1	377.5	34.27	-1.660	0.022	-1.660	418.825	32.997	0.018	0.004
37	0.5	264.8	33.38	-1.660	0.011	-1.961	309.004	32.470	0.028	0.003
37	0.1	138.3	30.29	-1.660	0.002	-2.660	153.395	30.275	0.021	0.000
54	25	444.6	35.34	-3.114	0.019	-1.716	395.790	32.919	0.019	0.007
54	10	289	32.24	-3.114	0.008	-2.114	264.711	32.101	0.015	0.000
54	5	193.6	31.32	-3.114	0.004	-2.415	195.579	31.188	0.002	0.000
54	1	92.5	27.75	-3.114	0.001	-3.114	99.065	28.232	0.015	0.002
54	0.5	75.1	25.82	-3.114	0.000	-3.415	75.093	26.670	0.000	0.003
54	0.1	45.9	22.59	-3.114	0.000	-4.114	41.548	22.620	0.026	0.000

Table 20: Unconfined Dynamic Modulus for the second replicate of 3% - 15psi WMA mixture

Shift Factor Coefficients:	
a1=	0.00058
a2=	-0.13696
Reference Temperature:	
Tref=	21

Sigmoid Coefficients:	
b1=	0.415353
b2=	4.155925
b3=	0.796877
b4=	0.417205

Gaussian Model (phase angle fit):	
a=	33.52415
b=	-1.206494
c=	3.205231

Total Error:	0.756343
Σ Error1	0.2549
Σ Error2	0.5015

Measured Data				Shift Factor	Reduced Frequency		Predicted Data		Error	
T (C)	**f (Hz)**	**|E*| (Mpa)**	**Phase angle**	**log(aT)**	**f_R (Hz)**	**Log f_R (Hz)**	**Sigmoid Fit, |E*| Mpa**	**Predicted Phase Angle**	**Error1 (|E*|)**	**Error2 (Phase Angle)**
-10.0	25	24226.0	24.2	4.048	279257.696	5.446	24363.112	3.890	0.001	0.084
-10.0	10	22654.0	35.7	4.048	111703.078	5.048	22653.609	4.995	0.000	0.086
-10.0	5	21349.0	25.3	4.048	55851.539	4.747	21276.864	5.973	0.000	0.076
-10.0	1	18120.0	32.8	4.048	11170.308	4.048	17858.283	8.745	0.001	0.073
-10.0	0.5	16598.0	33.8	4.048	5585.154	3.747	16322.264	10.156	0.002	0.070
-10.0	0.1	12726.0	21.8	4.048	1117.031	3.048	12735.514	13.892	0.000	0.036
10.0	25	8896.0	15.7	1.309	509.121	2.707	11034.439	15.910	0.024	0.002
10.0	10	7579.0	17.8	1.309	203.648	2.309	9147.617	18.372	0.021	0.003
10.0	5	6824.0	19.5	1.309	101.824	2.008	7816.359	20.276	0.015	0.004
10.0	1	4830.0	24.0	1.309	20.365	1.309	5139.194	24.639	0.007	0.003
10.0	0.5	4092.0	25.6	1.309	10.182	1.008	4188.485	26.407	0.003	0.003
10.0	0.1	2620.0	29.6	1.309	2.036	0.309	2465.313	29.979	0.008	0.001

Table 20 (cont'd)

Measured Data				Shift Factor	Reduced Frequency		Predicted Data		Error	
T (C)	f (Hz)	|E*| (Mpa)	Phase angle	log(aT)	f_R (Hz)	Log f_R (Hz)	Sigmoid Fit, |E*| Mpa	Predicted Phase Angle	Error1 (|E*|)	Error2 (Phase Angle)
21	25	5051	24.08	0.000	25.000	1.398	5444.640	24.098	0.009	0.000
21	10	3947	26.57	0.000	10.000	1.000	4165.391	26.452	0.007	0.000
21	5	3221	28.14	0.000	5.000	0.699	3344.949	28.094	0.005	0.000
21	1	1899	31.64	0.000	1.000	0.000	1905.711	31.231	0.000	0.001
21	0.5	1490	32.14	0.000	0.500	-0.301	1464.559	32.213	0.002	0.000
21	0.1	788.1	32.81	0.000	0.100	-1.000	764.040	33.455	0.005	0.002
37	25	1712	35.02	-1.653	0.555	-0.255	1525.227	32.080	0.016	0.008
37	10	1171	35.2	-1.653	0.222	-0.653	1061.407	33.029	0.014	0.006
37	5	850.9	35.11	-1.653	0.111	-0.954	798.247	33.421	0.009	0.005
37	1	406.3	33.86	-1.653	0.022	-1.653	402.208	33.200	0.002	0.002
37	0.5	297.9	32.6	-1.653	0.011	-1.954	297.900	32.624	0.000	0.000
37	0.1	149	29.16	-1.653	0.002	-2.653	149.158	30.277	0.000	0.004
54	25	412.9	36.94	-3.085	0.021	-1.687	388.974	33.150	0.010	0.010
54	10	267.8	33.99	-3.085	0.008	-2.085	261.535	32.288	0.004	0.005
54	5	177.2	33.14	-3.085	0.004	-2.386	193.947	31.329	0.017	0.005
54	1	86.9	29.48	-3.085	0.001	-3.085	98.625	28.234	0.028	0.004
54	0.5	72.1	26.59	-3.085	0.000	-3.386	74.648	26.605	0.008	0.000
54	0.1	46.9	21.24	-3.085	0.000	-4.085	40.769	22.399	0.036	0.005

Table 21: Unconfined Dynamic Modulus for the first replicate of 5% - 20psi WMA mixture

Shift Factor Coefficients:	
a1=	0.000517
a2=	-0.12781
Reference Temperature:	
Tref=	21

Sigmoid Coefficients:	
b1=	0.361519
b2=	4.012953
b3=	1.004746
b4=	0.458357

Gaussian Model (phase angle fit):	
a=	33.52834
b=	-1.232364
c=	3.2651

Total Error:	0.355764
Σ Error1	0.2035
Σ Error2	0.1523

Measured Data				Shift Factor	Reduced Frequency		Predicted Data		Error	
T (C)	**f (Hz)**	**|E*| (Mpa)**	**Phase angle**	**log(aT)**	**f_R (Hz)**	**Log f_R (Hz)**	**Sigmoid Fit, |E*| Mpa**	**Predicted Phase Angle**	**Error1 (|E*|)**	**Error2 (Phase Angle)**
-10.0	25	18303.0	6.6	3.786	152720.884	5.184	17476.096	4.863	0.005	0.026
-10.0	10	17051.0	7.3	3.786	61088.354	4.786	16484.016	6.133	0.003	0.016
-10.0	5	16030.0	8.1	3.786	30544.177	4.485	15660.903	7.238	0.002	0.011
-10.0	1	13492.0	10.3	3.786	6108.835	3.786	13523.385	10.291	0.000	0.000
-10.0	0.5	12207.0	11.5	3.786	3054.418	3.485	12518.746	11.807	0.003	0.003
-10.0	0.1	9067.0	15.6	3.786	610.884	2.786	10061.780	15.723	0.011	0.001
10.0	25	9229.0	15.6	1.230	424.241	2.628	9494.144	16.670	0.003	0.007
10.0	10	7875.0	17.7	1.230	169.696	2.230	8077.273	19.111	0.003	0.008
10.0	5	7022.0	19.4	1.230	84.848	1.929	7034.330	20.984	0.000	0.008
10.0	1	4981.0	23.8	1.230	16.970	1.230	4813.326	25.232	0.004	0.006
10.0	0.5	4207.0	25.4	1.230	8.485	0.929	3979.452	26.933	0.007	0.006
10.0	0.1	2661.0	29.4	1.230	1.697	0.230	2397.680	30.330	0.013	0.003

Table 21 (cont'd)

Measured Data				Shift Factor	Reduced Frequency		Predicted Data		Error	
T (C)	f (Hz)	|E*| (Mpa)	Phase angle	log(aT)	f_R (Hz)	Log f_R (Hz)	Sigmoid Fit, |E*| Mpa	Predicted Phase Angle	Error1 (|E*|)	Error2 (Phase Angle)
21	25	5282	24.23	0.000	25.000	1.398	5315.027	24.238	0.001	0.000
21	10	4183	26.59	0.000	10.000	1.000	4169.307	26.540	0.000	0.000
21	5	3374	28.21	0.000	5.000	0.699	3403.171	28.147	0.001	0.000
21	1	1990	31.81	0.000	1.000	0.000	1990.505	31.223	0.000	0.002
21	0.5	1559	32.42	0.000	0.500	-0.301	1537.903	32.192	0.002	0.001
21	0.1	825.3	33.2	0.000	0.100	-1.000	799.673	33.444	0.005	0.001
37	25	1750	34.85	-1.565	0.680	-0.167	1727.880	31.791	0.002	0.009
37	10	1211	35.02	-1.565	0.272	-0.565	1211.208	32.836	0.000	0.006
37	5	928.1	34.75	-1.565	0.136	-0.866	911.037	33.318	0.003	0.004
37	1	434.6	33.61	-1.565	0.027	-1.565	451.073	33.354	0.006	0.001
37	0.5	311.5	32.47	-1.565	0.014	-1.866	329.237	32.902	0.010	0.001
37	0.1	146.4	29.41	-1.565	0.003	-2.565	157.322	30.848	0.014	0.005
54	25	463.2	37.94	-2.938	0.029	-1.540	462.836	33.379	0.000	0.012
54	10	306.4	34.26	-2.938	0.012	-1.938	305.151	32.754	0.001	0.004
54	5	204.7	33.44	-2.938	0.006	-2.239	221.933	31.971	0.015	0.004
54	1	98.3	29.66	-2.938	0.001	-2.938	106.687	29.250	0.018	0.001
54	0.5	78.6	27.28	-2.938	0.001	-3.239	78.600	27.756	0.000	0.002
54	0.1	53.5	22.82	-2.938	0.000	-3.938	40.296	23.783	0.071	0.004

Table 22: Unconfined Dynamic Modulus for the second replicate of 5% - 20psi WMA mixture

Shift Factor Coefficients:	
a1=	0.000477
a2=	-0.12936
Reference Temperature:	
Tref=	21

Sigmoid Coefficients:	
b1=	0.457706
b2=	3.904656
b3=	1.028713
b4=	0.462209

Gaussian Model (phase angle fit):	
a=	33.47423
b=	-1.393113
c=	3.294088

Total Error:	0.332706
Σ Error1	0.1810
Σ Error2	0.1518

Measured Data				Shift Factor	Reduced Frequency		Predicted Data		Error	
T (C)	**f (Hz)**	**|E*| (Mpa)**	**Phase angle**	**log(aT)**	**f_R (Hz)**	**Log f_R (Hz)**	**Sigmoid Fit, |E*| Mpa**	**Predicted Phase Angle**	**Error1 (|E*|)**	**Error2 (Phase Angle)**
-10.0	25	17766.0	6.0	3.847	175941.202	5.245	17481.864	4.393	0.002	0.027
-10.0	10	16661.0	6.8	3.847	70376.481	4.847	16568.672	5.564	0.001	0.018
-10.0	5	15804.0	7.5	3.847	35188.240	4.546	15806.063	6.588	0.000	0.012
-10.0	1	13743.0	9.4	3.847	7037.648	3.847	13804.104	9.443	0.000	0.001
-10.0	0.5	12750.0	10.4	3.847	3518.824	3.546	12851.940	10.876	0.001	0.005
-10.0	0.1	10083.0	13.8	3.847	703.765	2.847	10490.297	14.617	0.004	0.006
10.0	25	9909.0	15.2	1.260	455.268	2.658	9829.581	15.712	0.001	0.003
10.0	10	8494.0	17.4	1.260	182.107	2.260	8437.170	18.097	0.001	0.004
10.0	5	7317.0	19.1	1.260	91.054	1.959	7401.276	19.944	0.001	0.005
10.0	1	5087.0	23.5	1.260	18.211	1.260	5159.003	24.200	0.002	0.003
10.0	0.5	4301.0	25.0	1.260	9.105	0.959	4301.948	25.940	0.000	0.004
10.0	0.1	2805.0	29.1	1.260	1.821	0.260	2646.355	29.512	0.007	0.001

Table 22 (cont'd)

Measured Data				Shift Factor	Reduced Frequency		Predicted Data		Error	
T (C)	f (Hz)	|E*| (Mpa)	Phase angle	log(aT)	f_R (Hz)	Log f_R (Hz)	Sigmoid Fit, |E*| Mpa	Predicted Phase Angle	Error1 (|E*|)	Error2 (Phase Angle)
21	25	5357	24.04	0.000	25.000	1.398	5575.598	23.379	0.005	0.003
21	10	4252	26.43	0.000	10.000	1.000	4413.164	25.710	0.004	0.003
21	5	3614	28.03	0.000	5.000	0.699	3627.820	27.360	0.000	0.002
21	1	2153	31.49	0.000	1.000	0.000	2158.409	30.611	0.000	0.003
21	0.5	1713	31.93	0.000	0.500	-0.301	1680.097	31.684	0.003	0.001
21	0.1	923.1	32.5	0.000	0.100	-1.000	888.597	33.237	0.006	0.002
37	25	1794	34.53	-1.627	0.590	-0.229	1785.946	31.449	0.001	0.009
37	10	1287	34.67	-1.627	0.236	-0.627	1259.256	32.582	0.003	0.006
37	5	960.4	34.41	-1.627	0.118	-0.928	951.625	33.143	0.001	0.004
37	1	463.5	33.37	-1.627	0.024	-1.627	476.783	33.390	0.005	0.000
37	0.5	340.5	32.01	-1.627	0.012	-1.928	349.942	33.035	0.005	0.003
37	0.1	168.9	28.72	-1.627	0.002	-2.627	169.573	31.206	0.001	0.009
54	25	524.8	34.91	-3.089	0.020	-1.691	446.828	33.338	0.026	0.005
54	10	331.2	33.23	-3.089	0.008	-2.089	296.343	32.736	0.019	0.001
54	5	216.8	33.37	-3.089	0.004	-2.390	216.785	31.977	0.000	0.004
54	1	95.5	30.89	-3.089	0.001	-3.089	106.098	29.321	0.023	0.005
54	0.5	75.9	27.78	-3.089	0.000	-3.390	78.907	27.857	0.009	0.000
54	0.1	50.7	22.97	-3.089	0.000	-4.089	41.476	23.950	0.051	0.004

Table 23: Confined Dynamic Modulus for the first replicate of 1% - 10psi WMA mixture

Shift Factor Coefficients:	
a1=	1.03E-05
a2=	-0.10815
Reference Temperature:	
Tref=	21

Sigmoid Coefficients:	
b1=	2.678669
b2=	1.610201
b3=	-0.092824
b4=	0.675849

Gaussian Model (phase angle fit):	
a=	28.49632
b=	-0.755005
c=	2.650591

Total Error:	0.428176
Σ Error1	0.2192
Σ Error2	0.2090

Measured Data				Shift Factor	Reduced Frequency		Predicted Data		Error	
T (C)	**f (Hz)**	**|E*| (Mpa)**	**Phase angle**	**log(aT)**	**f_R (Hz)**	**Log f_R (Hz)**	**Sigmoid Fit, |E*| Mpa**	**Predicted Phase Angle**	**Error1 (|E*|)**	**Error2 (Phase Angle)**
-10.0	25	17011.0	5.5	3.349	55846.894	4.747	16614.081	3.305	0.002	0.039
-10.0	10	16000.0	6.1	3.349	22338.758	4.349	15868.245	4.463	0.001	0.027
-10.0	5	15156.0	6.9	3.349	11169.379	4.048	15202.703	5.518	0.000	0.019
-10.0	1	13250.0	8.6	3.349	2233.876	3.349	13303.173	8.594	0.000	0.000
-10.0	0.5	12342.0	9.6	3.349	1116.938	3.048	12339.898	10.180	0.000	0.006
-10.0	0.1	9920.0	12.6	3.349	223.388	2.349	9859.927	14.354	0.001	0.014
10.0	25	10154.0	12.9	1.186	383.755	2.584	10721.016	12.888	0.006	0.000
10.0	10	8948.0	14.6	1.186	153.502	2.186	9255.675	15.397	0.004	0.005
10.0	5	8041.0	16.0	1.186	76.751	1.885	8142.133	17.352	0.001	0.008
10.0	1	5983.0	19.8	1.186	15.350	1.186	5724.346	21.794	0.005	0.010
10.0	0.5	5210.0	21.3	1.186	7.675	0.885	4819.255	23.532	0.009	0.010
10.0	0.1	3637.0	25.1	1.186	1.535	0.186	3140.772	26.756	0.018	0.006

Table 23 (cont'd)

Measured Data				Shift Factor	Reduced Frequency		Predicted Data		Error	
T (C)	f (Hz)	|E*| (Mpa)	Phase angle	log(aT)	f_R (Hz)	Log f_R (Hz)	Sigmoid Fit, |E*| Mpa	Predicted Phase Angle	Error1 (|E*|)	Error2 (Phase Angle)
21	25	6417	20.67	0.000	25.000	1.398	6417.837	20.489	0.000	0.001
21	10	5246	22.89	0.000	10.000	1.000	5152.719	22.887	0.002	0.000
21	5	4310	24.4	0.000	5.000	0.699	4312.791	24.516	0.000	0.000
21	1	2794	27.76	0.000	1.000	0.000	2795.308	27.363	0.000	0.001
21	0.5	2317	28.27	0.000	0.500	-0.301	2319.362	28.081	0.000	0.001
21	0.1	1412	29.56	0.000	0.100	-1.000	1544.280	28.375	0.012	0.004
37	25	2539	30.51	-1.721	0.475	-0.323	2288.550	28.120	0.013	0.008
37	10	1901	30.66	-1.721	0.190	-0.721	1805.625	28.494	0.007	0.007
37	5	1523	30.14	-1.721	0.095	-1.022	1526.142	28.352	0.000	0.006
37	1	965.9	28.07	-1.721	0.019	-1.721	1085.518	26.666	0.017	0.005
37	0.5	832.8	26.06	-1.721	0.010	-2.022	960.097	25.421	0.021	0.002
37	0.1	607.9	22.51	-1.721	0.002	-2.721	762.891	21.645	0.035	0.004
54	25	1144	26.19	-3.543	0.007	-2.145	916.773	24.833	0.031	0.005
54	10	918.2	22.62	-3.543	0.003	-2.543	803.113	22.695	0.020	0.000
54	5	789.1	20.26	-3.543	0.001	-2.844	737.986	20.886	0.010	0.003
54	1	634.3	15.58	-3.543	0.000	-3.543	634.189	16.386	0.000	0.005
54	0.5	606	13.32	-3.543	0.000	-3.844	603.836	14.447	0.001	0.008
54	0.1	550.9	10.26	-3.543	0.000	-4.543	554.605	10.261	0.001	0.000

Table 24: Confined Dynamic Modulus for the second replicate of 1% - 10psi WMA mixture

Shift Factor Coefficients:	
a1=	-0.00020
a2=	-0.10224
Reference Temperature:	
Tref=	21

Sigmoid Coefficients:	
b1=	2.674677
b2=	1.664104
b3=	-0.011619
b4=	0.619542

Gaussian Model (phase angle fit):	
a=	28.21331
b=	-0.774841
c=	2.637479

Total Error:	0.405294
Σ Error1	0.2062
Σ Error2	0.1991

Measured Data				Shift Factor	Reduced Frequency		Predicted Data		Error	
T (C)	**f (Hz)**	**|E*| (Mpa)**	**Phase angle**	**log(aT)**	**f_R (Hz)**	**Log f_R (Hz)**	**Sigmoid Fit, |E*| Mpa**	**Predicted Phase Angle**	**Error1 (|E*|)**	**Error2 (Phase Angle)**
-10.0	25	17829.0	5.8	3.237	43096.333	4.634	17725.916	3.444	0.001	0.041
-10.0	10	16775.0	6.5	3.237	17238.533	4.237	16792.655	4.640	0.000	0.028
-10.0	5	15912.0	7.1	3.237	8619.267	3.935	15984.807	5.726	0.000	0.019
-10.0	1	13783.0	8.9	3.237	1723.853	3.237	13781.021	8.875	0.000	0.000
-10.0	0.5	12711.0	9.9	3.237	861.927	2.935	12710.015	10.489	0.000	0.006
-10.0	0.1	10063.0	12.9	3.237	172.385	2.237	10061.692	14.702	0.000	0.014
10.0	25	11213.0	12.6	1.192	388.673	2.590	11416.915	12.506	0.002	0.001
10.0	10	10066.0	14.3	1.192	155.469	2.192	9889.066	14.988	0.002	0.005
10.0	5	9025.0	15.7	1.192	77.735	1.891	8740.208	16.931	0.004	0.008
10.0	1	6712.0	19.4	1.192	15.547	1.192	6257.497	21.367	0.008	0.010
10.0	0.5	5665.0	20.8	1.192	7.773	0.891	5322.773	23.114	0.007	0.011
10.0	0.1	3837.0	24.7	1.192	1.555	0.192	3558.343	26.381	0.009	0.007

Table 24 (cont'd)

Measured Data				Shift Factor	Reduced Frequency		Predicted Data		Error	
T (C)	f (Hz)	|E*| (Mpa)	Phase angle	log(aT)	f_R (Hz)	Log f_R (Hz)	Sigmoid Fit, |E*| Mpa	Predicted Phase Angle	Error1 (|E*|)	Error2 (Phase Angle)
21	25	6438	20.1	0.000	25.000	1.398	6951.046	20.095	0.009	0.000
21	10	5332	22.27	0.000	10.000	1.000	5651.048	22.497	0.007	0.001
21	5	4695	23.7	0.000	5.000	0.699	4780.814	24.135	0.002	0.002
21	1	3074	27.04	0.000	1.000	0.000	3176.105	27.022	0.004	0.000
21	0.5	2552	27.51	0.000	0.500	-0.301	2658.118	27.762	0.005	0.001
21	0.1	1620	28.81	0.000	0.100	-1.000	1788.678	28.111	0.013	0.002
37	25	2695	29.38	-1.818	0.380	-0.420	2479.022	27.959	0.011	0.005
37	10	2057	29.26	-1.818	0.152	-0.818	1975.727	28.210	0.005	0.004
37	5	1683	28.65	-1.818	0.076	-1.119	1678.822	27.974	0.000	0.002
37	1	1096	26.91	-1.818	0.015	-1.818	1198.182	26.090	0.013	0.003
37	0.5	954.4	24.95	-1.818	0.008	-2.119	1057.414	24.776	0.015	0.001
37	0.1	727.6	21.58	-1.818	0.002	-2.818	830.722	20.899	0.020	0.003
54	25	1184	23.96	-3.860	0.003	-2.462	931.466	22.992	0.034	0.004
54	10	948.9	20.65	-3.860	0.001	-2.860	820.498	20.640	0.021	0.000
54	5	817.4	18.3	-3.860	0.001	-3.161	755.667	18.737	0.012	0.002
54	1	656.9	13.19	-3.860	0.000	-3.860	649.665	14.234	0.002	0.008
54	0.5	617.8	11.21	-3.860	0.000	-4.161	617.798	12.374	0.000	0.010
54	0.1	563.2	8.5	-3.860	0.000	-4.860	564.822	8.501	0.000	0.000

Table 25: Confined Dynamic Modulus for the first replicate of 3% - 15psi WMA mixture

Shift Factor Coefficients:	
a1=	-0.00031
a2=	-0.08666
Reference Temperature:	
Tref=	21

Sigmoid Coefficients:	
b1=	2.696276
b2=	1.556474
b3=	0.023775
b4=	0.730306

Gaussian Model (phase angle fit):	
a=	28.63675
b=	-0.731871
c=	2.551689

Total Error:	0.385169
Σ Error1	0.1938
Σ Error2	0.1914

Measured Data				Shift Factor	Reduced Frequency		Predicted Data		Error	
T (C)	**f (Hz)**	**|E*| (Mpa)**	**Phase angle**	**log(aT)**	**f_R (Hz)**	**Log f_R (Hz)**	**Sigmoid Fit, |E*| Mpa**	**Predicted Phase Angle**	**Error1 (|E*|)**	**Error2 (Phase Angle)**
-10.0	25	15626.0	7.2	2.791	15459.103	4.189	15295.542	4.460	0.002	0.038
-10.0	10	14551.0	8.0	2.791	6183.641	3.791	14551.133	5.951	0.000	0.026
-10.0	5	13706.0	8.8	2.791	3091.821	3.490	13879.388	7.285	0.001	0.017
-10.0	1	11605.0	11.0	2.791	618.364	2.791	11943.884	11.040	0.003	0.000
-10.0	0.5	10677.0	12.2	2.791	309.182	2.490	10961.576	12.903	0.003	0.006
-10.0	0.1	8396.0	15.8	2.791	61.836	1.791	8466.335	17.564	0.001	0.012
10.0	25	11296.0	13.1	1.058	285.697	2.456	10844.926	13.123	0.004	0.000
10.0	10	9811.0	14.9	1.058	114.279	2.058	9439.720	15.753	0.004	0.006
10.0	5	8635.0	16.4	1.058	57.139	1.757	8340.743	17.797	0.004	0.009
10.0	1	6350.0	20.2	1.058	11.428	1.058	5875.002	22.392	0.009	0.011
10.0	0.5	5484.0	21.6	1.058	5.714	0.757	4930.048	24.155	0.012	0.012
10.0	0.1	3738.0	25.3	1.058	1.143	0.058	3163.931	27.297	0.020	0.008

Table 25 (cont'd)

Measured Data				Shift Factor	Reduced Frequency		Predicted Data		Error	
T (C)	f (Hz)	|E*| (Mpa)	Phase angle	log(aT)	f_R (Hz)	Log f_R (Hz)	Sigmoid Fit, |E*| Mpa	Predicted Phase Angle	Error1 (|E*|)	Error2 (Phase Angle)
21	25	6699	20.87	0.000	25.000	1.398	7041.839	20.214	0.006	0.003
21	10	5536	23	0.000	10.000	1.000	5685.684	22.745	0.003	0.001
21	5	4696	24.47	0.000	5.000	0.699	4759.783	24.471	0.002	0.000
21	1	3041	27.78	0.000	1.000	0.000	3046.238	27.483	0.000	0.001
21	0.5	2503	28.27	0.000	0.500	-0.301	2503.009	28.231	0.000	0.000
21	0.1	1581	29.46	0.000	0.100	-1.000	1623.611	28.479	0.004	0.003
37	25	2607	30.16	-1.671	0.533	-0.274	2548.095	28.178	0.003	0.007
37	10	1980	29.88	-1.671	0.213	-0.671	1977.782	28.629	0.000	0.004
37	5	1611	29.1	-1.671	0.107	-0.972	1649.779	28.510	0.003	0.002
37	1	1054	27.03	-1.671	0.021	-1.671	1141.358	26.760	0.011	0.001
37	0.5	923.9	24.98	-1.671	0.011	-1.972	1000.135	25.445	0.012	0.002
37	0.1	717.9	21.53	-1.671	0.002	-2.671	783.507	21.452	0.013	0.000
54	25	1138	25.51	-3.620	0.006	-2.222	907.868	24.150	0.032	0.005
54	10	926.9	21.76	-3.620	0.002	-2.620	795.572	21.781	0.022	0.000
54	5	808.3	19.41	-3.620	0.001	-2.921	732.326	19.823	0.015	0.002
54	1	639.3	15.09	-3.620	0.000	-3.620	633.784	15.095	0.001	0.000
54	0.5	605.7	13	-3.620	0.000	-3.921	605.675	13.117	0.000	0.001
54	0.1	553.5	10.5	-3.620	0.000	-4.620	561.097	8.972	0.002	0.015

Table 26: Confined Dynamic Modulus for the second replicate of 3% - 15psi WMA mixture

Shift Factor Coefficients:	
a1=	-9.7E-05
a2=	-
Reference Temperature:	
Tref=	21

Sigmoid Coefficients:	
b1=	2.591216
b2=	1.943639
b3=	0.119098
b4=	0.612476

Gaussian Model (phase angle fit):	
a=	29.37255
b=	-0.357151
c=	2.888489

Total Error:	1.274143
Σ Error1	0.3659
Σ Error2	0.9082

Measured Data				Shift Factor	Reduced Frequency		Predicted Data		Error	
T (C)	**f (Hz)**	**|E*| (Mpa)**	**Phase angle**	**log(aT)**	**f_R (Hz)**	**Log f_R (Hz)**	**Sigmoid Fit, |E*| Mpa**	**Predicted Phase Angle**	**Error1 (|E*|)**	**Error2 (Phase Angle)**
-10.0	25	26657.0	23.1	3.154	35614.754	4.552	27173.509	6.931	0.002	0.070
-10.0	10	25304.0	34.8	3.154	14245.902	4.154	25595.388	8.677	0.001	0.075
-10.0	5	24241.0	24.5	3.154	7122.951	3.853	24237.897	10.155	0.000	0.058
-10.0	1	21247.0	31.7	3.154	1424.590	3.154	20573.521	14.033	0.003	0.056
-10.0	0.5	19577.0	32.6	3.154	712.295	2.853	18813.189	15.841	0.004	0.051
-10.0	0.1	15113.0	20.1	3.154	142.459	2.154	14521.569	20.131	0.004	0.000
10.0	25	16097.0	37.2	1.140	345.416	2.538	16901.021	17.772	0.005	0.052
10.0	10	14136.0	6.8	1.140	138.166	2.140	14439.598	20.211	0.002	0.196
10.0	5	12655.0	28.1	1.140	69.083	1.839	12605.170	21.997	0.000	0.022
10.0	1	9407.0	37.4	1.140	13.817	1.140	8700.770	25.679	0.009	0.031
10.0	0.5	8184.0	38.6	1.140	6.908	0.839	7258.180	26.958	0.013	0.030
10.0	0.1	5620.0	32.8	1.140	1.382	0.140	4595.622	28.940	0.023	0.012

Table 26 (cont'd)

Measured Data				Shift Factor	Reduced Frequency		Predicted Data		Error	
T (C)	f (Hz)	|E*| (Mpa)	Phase angle	log(aT)	f_R (Hz)	Log f_R (Hz)	Sigmoid Fit, |E*| Mpa	Predicted Phase Angle	Error1 (|E*|)	Error2 (Phase Angle)
21	25	6855	20.71	0.000	25.000	1.398	10060.963	24.421	0.043	0.018
21	10	5617	22.75	0.000	10.000	1.000	8006.931	26.303	0.041	0.016
21	5	4590	24.13	0.000	5.000	0.699	6644.844	27.473	0.044	0.014
21	1	3002	27.27	0.000	1.000	0.000	4176.754	29.149	0.041	0.007
21	0.5	2496	27.62	0.000	0.500	-0.301	3398.830	29.367	0.039	0.006
21	0.1	1594	28.65	0.000	0.100	-1.000	2128.367	28.654	0.039	0.000
37	25	3644	49.76	-1.701	0.498	-0.303	3394.825	29.367	0.009	0.041
37	10	2774	45.41	-1.701	0.199	-0.701	2591.617	29.166	0.009	0.036
37	5	2122	44.22	-1.701	0.100	-1.002	2126.003	28.650	0.000	0.035
37	1	1367	32.21	-1.701	0.020	-1.701	1393.376	26.361	0.003	0.018
37	0.5	1188	31.17	-1.701	0.010	-2.002	1186.066	24.978	0.000	0.020
37	0.1	905.7	28.03	-1.701	0.002	-2.701	862.480	21.135	0.007	0.025
54	25	1141	26.26	-3.562	0.007	-2.164	1093.723	24.152	0.006	0.008
54	10	918.5	22.52	-3.562	0.003	-2.562	912.995	21.948	0.001	0.003
54	5	790.9	20.16	-3.562	0.001	-2.863	809.922	20.160	0.004	0.000
54	1	618.1	15.46	-3.562	0.000	-3.562	646.289	15.871	0.007	0.003
54	0.5	578.6	13.26	-3.562	0.000	-3.863	598.475	14.061	0.005	0.006
54	0.1	521.1	10.18	-3.562	0.000	-4.562	520.597	10.180	0.000	0.000

Table 27: Confined Dynamic Modulus for the first replicate of 5% - 20psi WMA mixture

Shift Factor Coefficients:	
a1=	0.00021
a2=	-0.11398
Reference Temperature:	
Tref=	21

Sigmoid Coefficients:	
b1=	2.478079
b2=	1.60413
b3=	-0.273441
b4=	0.713126

Gaussian Model (phase angle fit):	
a=	27.09391
b=	-0.246991
c=	2.64152

Total Error:	0.550183
Σ Error1	0.2576
Σ Error2	0.2925

Measured Data				Shift Factor	Reduced Frequency		Predicted Data		Error	
T (C)	**f (Hz)**	**|E*| (Mpa)**	**Phase angle**	**log(aT)**	**f_R (Hz)**	**Log f_R (Hz)**	**Sigmoid Fit, |E*| Mpa**	**Predicted Phase Angle**	**Error1 (|E*|)**	**Error2 (Phase Angle)**
-10.0	25	10624.0	8.3	3.462	72408.157	4.860	10445.031	4.181	0.002	0.050
-10.0	10	10061.0	9.2	3.462	28963.263	4.462	9981.899	5.531	0.001	0.040
-10.0	5	9560.0	9.2	3.462	14481.631	4.161	9563.088	6.733	0.000	0.027
-10.0	1	8356.0	10.1	3.462	2896.326	3.462	8346.743	10.111	0.000	0.000
-10.0	0.5	7713.0	10.6	3.462	1448.163	3.161	7721.542	11.789	0.000	0.011
-10.0	0.1	6038.0	12.7	3.462	289.633	2.462	6099.357	16.015	0.001	0.026
10.0	25	5794.0	15.2	1.182	380.290	2.580	6384.865	15.281	0.011	0.000
10.0	10	4959.0	17.6	1.182	152.116	2.182	5419.680	17.751	0.010	0.001
10.0	5	4344.0	19.8	1.182	76.058	1.881	4698.020	19.585	0.009	0.001
10.0	1	3201.0	25.8	1.182	15.212	1.182	3181.189	23.405	0.001	0.009
10.0	0.5	2931.0	30.5	1.182	7.606	0.881	2636.363	24.732	0.013	0.019
10.0	0.1	2052.0	20.7	1.182	1.521	0.182	1669.872	26.739	0.027	0.029

Table 27 (cont'd)

Measured Data				Shift Factor	Reduced Frequency		Predicted Data		Error	
T (C)	f (Hz)	|E*| (Mpa)	Phase angle	log(aT)	f_R (Hz)	Log f_R (Hz)	Sigmoid Fit, |E*| Mpa	Predicted Phase Angle	Error1 (|E*|)	Error2 (Phase Angle)
21	25	3615	19.92	0.000	25.000	1.398	3616.195	22.319	0.000	0.012
21	10	2908	22.12	0.000	10.000	1.000	2842.400	24.237	0.003	0.010
21	5	2421	23.71	0.000	5.000	0.699	2344.243	25.411	0.004	0.007
21	1	1507	27.65	0.000	1.000	0.000	1483.076	26.976	0.002	0.002
21	0.5	1225	28.27	0.000	0.500	-0.301	1225.154	27.088	0.000	0.004
21	0.1	763.5	28.7	0.000	0.100	-1.000	819.871	26.015	0.011	0.009
37	25	1281	27.98	-1.629	0.588	-0.231	1280.058	27.093	0.000	0.003
37	10	965.7	27.35	-1.629	0.235	-0.629	1006.038	26.812	0.006	0.002
37	5	773.3	26.55	-1.629	0.118	-0.930	850.775	26.204	0.014	0.001
37	1	535.2	23.63	-1.629	0.024	-1.629	611.784	23.629	0.021	0.000
37	0.5	477.9	21.67	-1.629	0.012	-1.930	545.255	22.118	0.021	0.002
37	0.1	374.5	18.97	-1.629	0.002	-2.629	442.311	18.044	0.028	0.005
54	25	708.3	22.95	-3.241	0.014	-1.844	562.629	22.571	0.035	0.002
54	10	567.2	20	-3.241	0.006	-2.241	491.981	20.374	0.022	0.002
54	5	482.6	18.1	-3.241	0.003	-2.542	452.056	18.573	0.011	0.003
54	1	391	14.08	-3.241	0.001	-3.241	389.533	14.250	0.001	0.001
54	0.5	371.6	12.05	-3.241	0.000	-3.542	371.589	12.442	0.000	0.003
54	0.1	339.8	9.67	-3.241	0.000	-4.241	342.959	8.636	0.002	0.011

Table 28: Confined Dynamic Modulus for the second replicate of 5% - 20psi WMA mixture

Shift Factor Coefficients:	
a1=	2.21E-06
a2=	-0.11398
Reference Temperature:	
Tref=	21

Sigmoid Coefficients:	
b1=	1.911767
b2=	2.587999
b3=	0.486123
b4=	0.418533

Gaussian Model (phase angle fit):	
a=	28.2353
b=	-1.038716
c=	2.990919

Total Error:	0.445971
Σ Error1	0.2387
Σ Error2	0.2073

Measured Data				Shift Factor	Reduced Frequency		Predicted Data		Error	
T (C)	**f (Hz)**	**|E*| (Mpa)**	**Phase angle**	**log(aT)**	**f_R (Hz)**	**Log f_R (Hz)**	**Sigmoid Fit, |E*| Mpa**	**Predicted Phase Angle**	**Error1 (|E*|)**	**Error2 (Phase Angle)**
-10.0	25	20047.0	5.6	3.533	85201.906	4.930	20524.429	3.854	0.002	0.031
-10.0	10	18922.0	6.2	3.533	34080.762	4.533	19105.683	4.981	0.001	0.019
-10.0	5	17977.0	6.8	3.533	17040.381	4.231	17971.772	5.978	0.000	0.012
-10.0	1	15639.0	8.5	3.533	3408.076	3.533	15188.635	8.781	0.003	0.004
-10.0	0.5	14370.0	9.4	3.533	1704.038	3.231	13952.450	10.190	0.003	0.008
-10.0	0.1	11111.0	12.8	3.533	340.808	2.533	11096.081	13.842	0.000	0.008
10.0	25	11558.0	13.2	1.253	447.636	2.651	11572.969	13.193	0.000	0.000
10.0	10	10134.0	14.9	1.253	179.054	2.253	9992.013	15.409	0.002	0.003
10.0	5	9040.0	16.4	1.253	89.527	1.952	8848.067	17.127	0.002	0.005
10.0	1	6565.0	20.2	1.253	17.905	1.253	6443.113	21.053	0.002	0.004
10.0	0.5	5529.0	21.6	1.253	8.953	0.952	5539.356	22.626	0.000	0.005
10.0	0.1	3723.0	25.4	1.253	1.791	0.253	3784.307	25.721	0.002	0.001

Table 28 (cont'd)

Measured Data				Shift Factor	Reduced Frequency		Predicted Data		Error	
T (C)	f (Hz)	|E*| (Mpa)	Phase angle	log(aT)	f_R (Hz)	Log f_R (Hz)	Sigmoid Fit, |E*| Mpa	Predicted Phase Angle	Error1 (|E*|)	Error2 (Phase Angle)
21	25	6567	20.65	0.000	25.000	1.398	6908.401	20.261	0.006	0.002
21	10	5299	22.78	0.000	10.000	1.000	5677.771	22.382	0.008	0.002
21	5	4466	24.22	0.000	5.000	0.699	4847.994	23.850	0.010	0.002
21	1	2901	27.43	0.000	1.000	0.000	3267.664	26.583	0.015	0.003
21	0.5	2394	27.85	0.000	0.500	-0.301	2730.776	27.389	0.017	0.002
21	0.1	1497	28.79	0.000	0.100	-1.000	1776.154	28.233	0.023	0.002
37	25	2694	29.09	-1.822	0.377	-0.424	2535.130	27.645	0.008	0.005
37	10	2034	28.63	-1.822	0.151	-0.822	1984.539	28.161	0.003	0.002
37	5	1645	27.8	-1.822	0.075	-1.123	1645.501	28.224	0.000	0.002
37	1	1125	25.3	-1.822	0.015	-1.822	1066.969	27.284	0.008	0.008
37	0.5	993.6	23.16	-1.822	0.008	-2.123	889.121	26.441	0.016	0.014
37	0.1	724	19.53	-1.822	0.002	-2.822	593.587	23.639	0.030	0.021
54	25	789.7	30.21	-3.756	0.004	-2.358	773.423	25.619	0.003	0.015
54	10	587.2	26.92	-3.756	0.002	-2.756	615.731	23.946	0.007	0.011
54	5	471.3	25.19	-3.756	0.001	-3.057	522.227	22.487	0.017	0.011
54	1	342.2	19.73	-3.756	0.000	-3.756	367.293	18.689	0.012	0.005
54	0.5	320.2	16.95	-3.756	0.000	-4.057	320.200	16.970	0.000	0.000
54	0.1	299	12.88	-3.756	0.000	-4.756	241.113	13.044	0.038	0.001

APPENDIX B

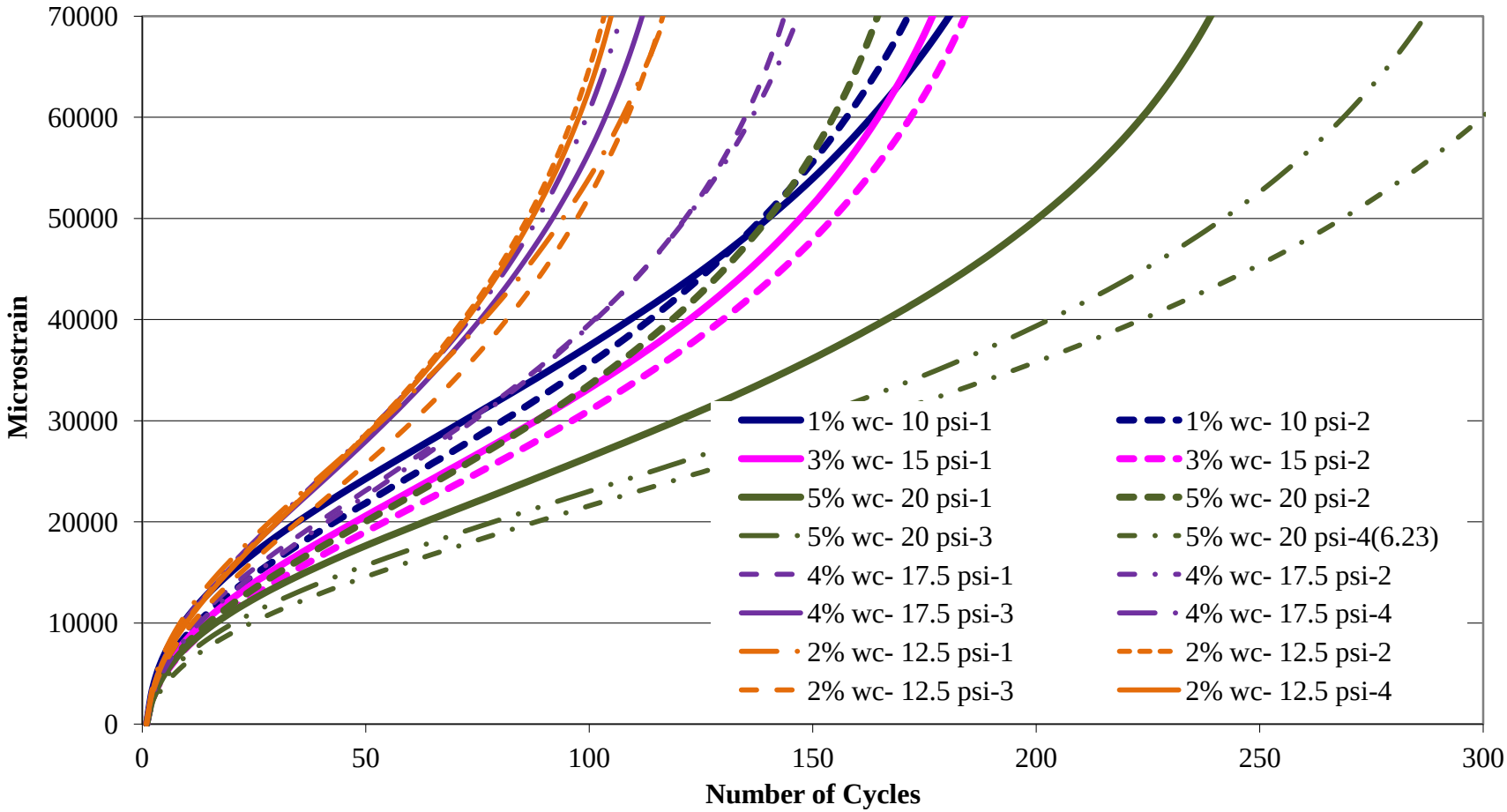

Figure 59: Raw Flow Number Data

APPENDIX C

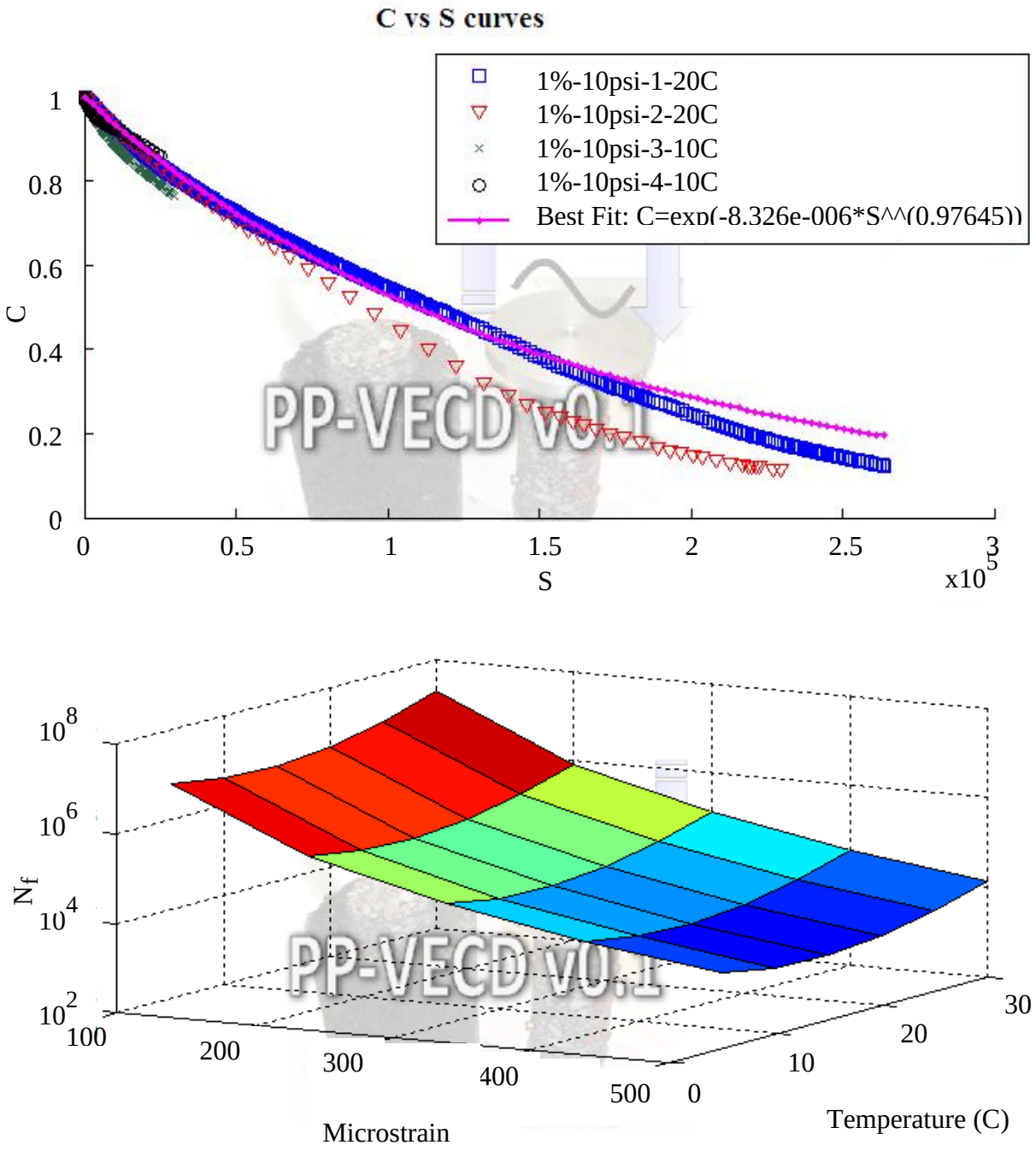

Figure 60: Push Pull Tests for WMA mixtures prepared with foamed binder - 1% water content -10 psi air pressure

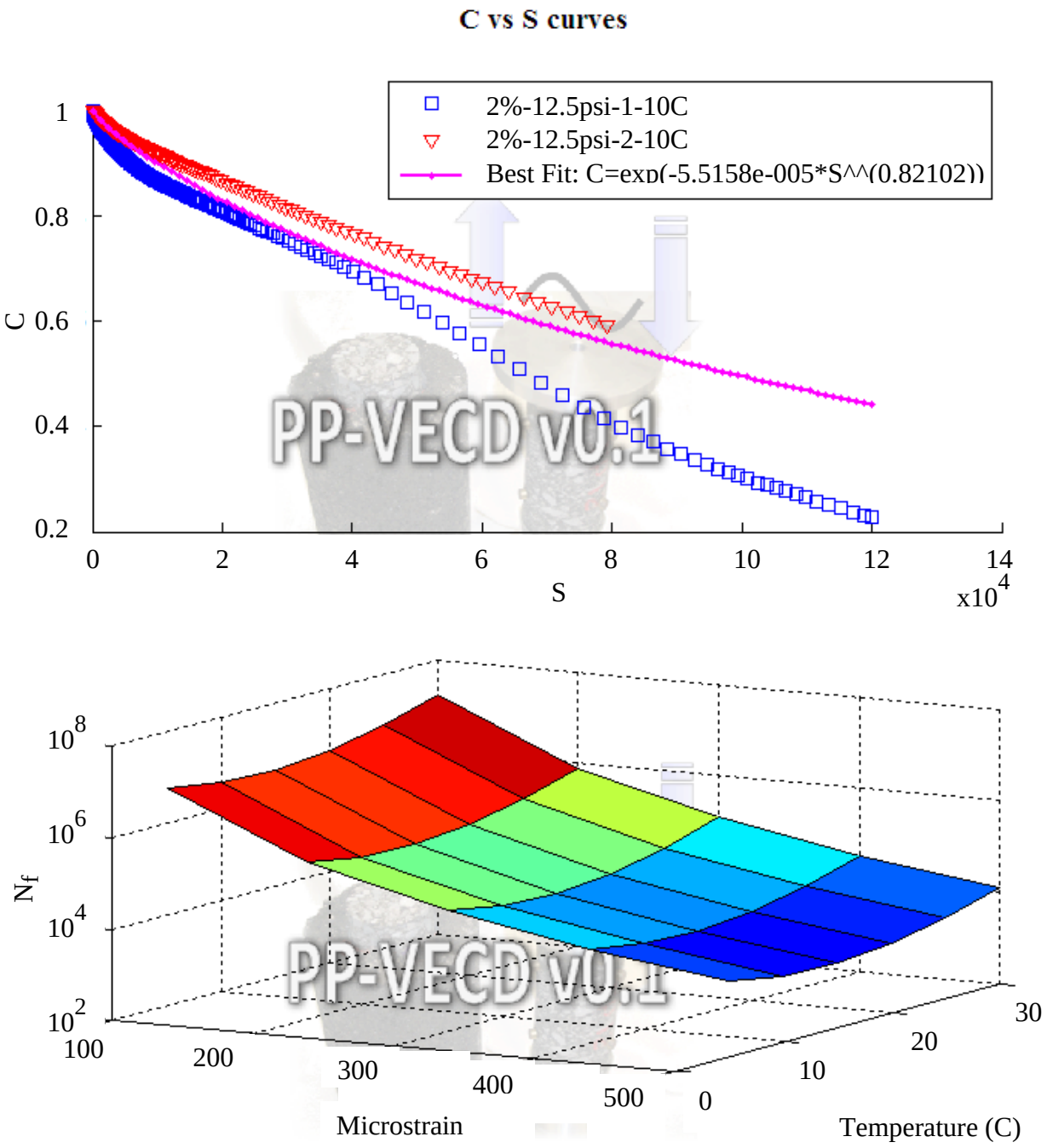

Figure 61: Push Pull Tests for WMA mixtures prepared with foamed binder - 2% water content -12.5 psi air pressure

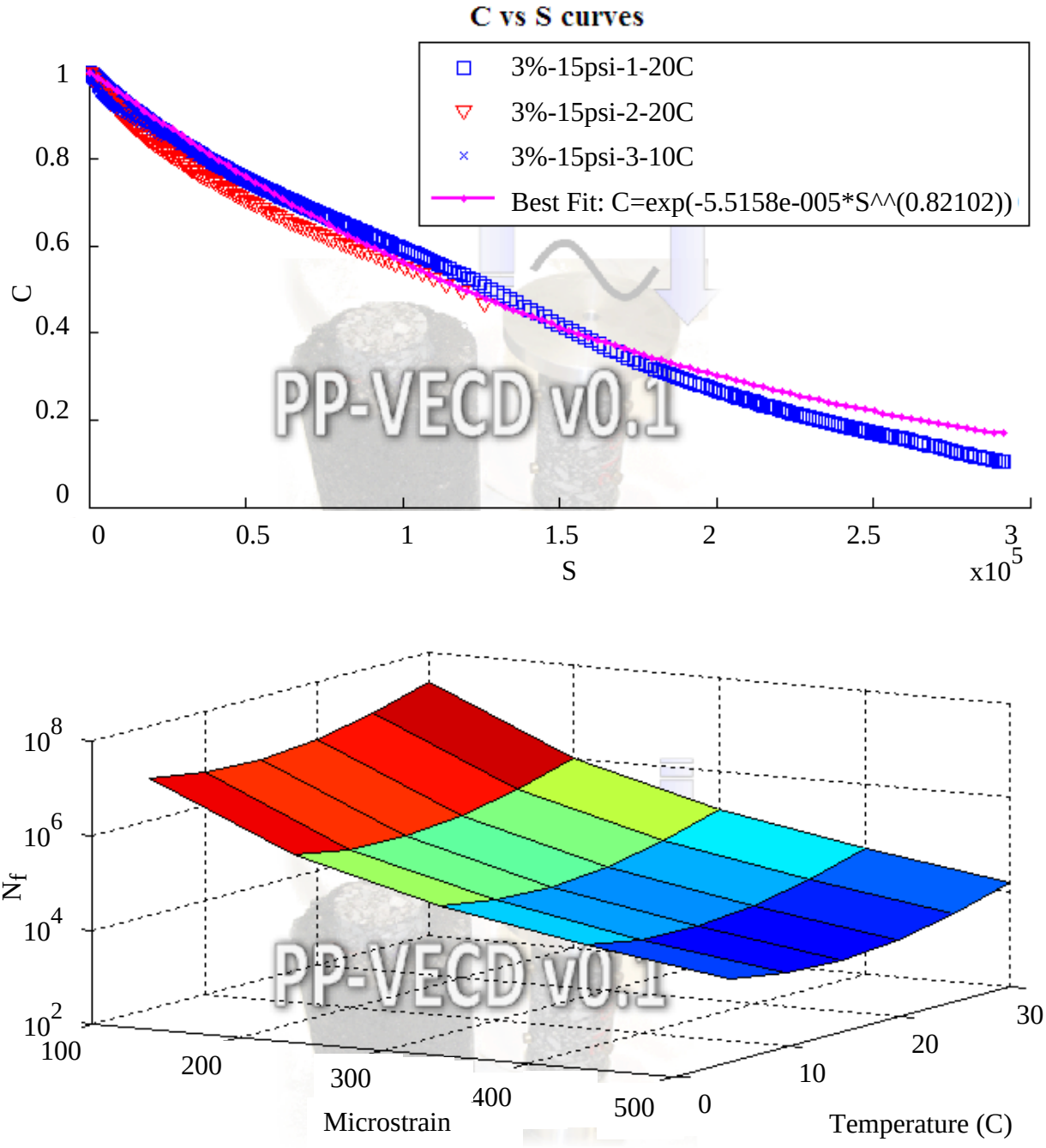

Figure 62: Push Pull Tests for WMA mixtures prepared with foamed binder - 3% water content -15 psi air pressure

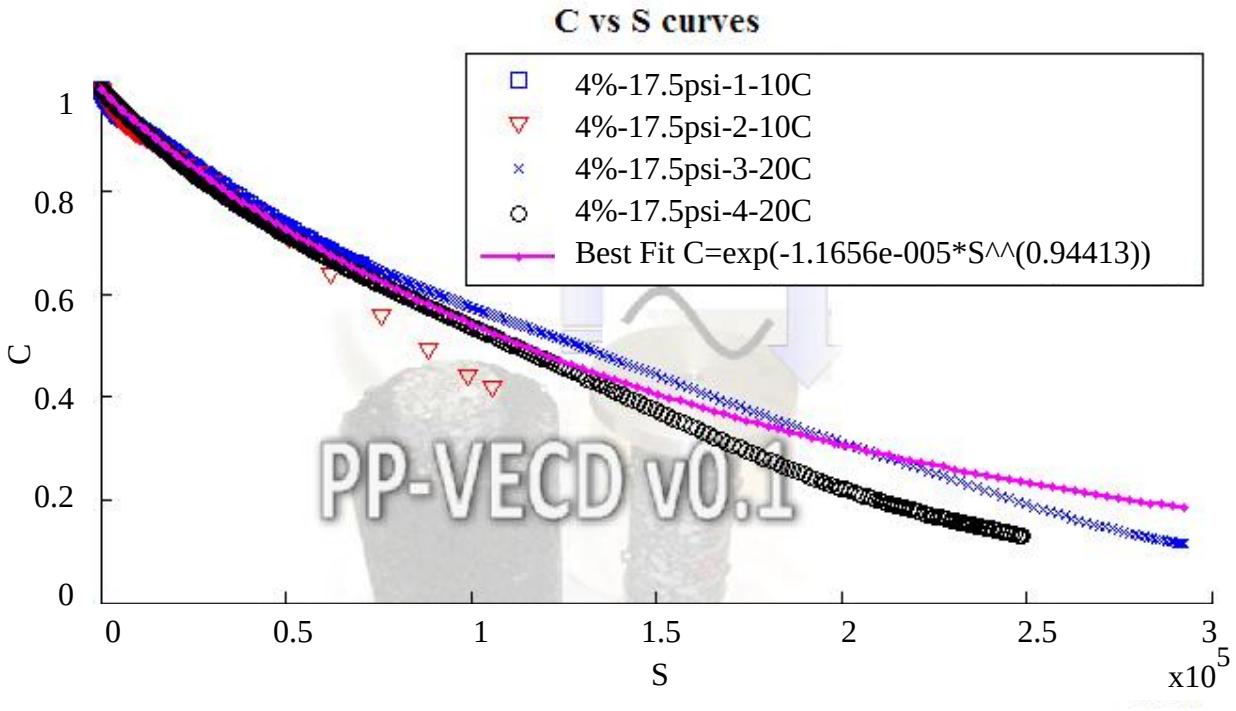

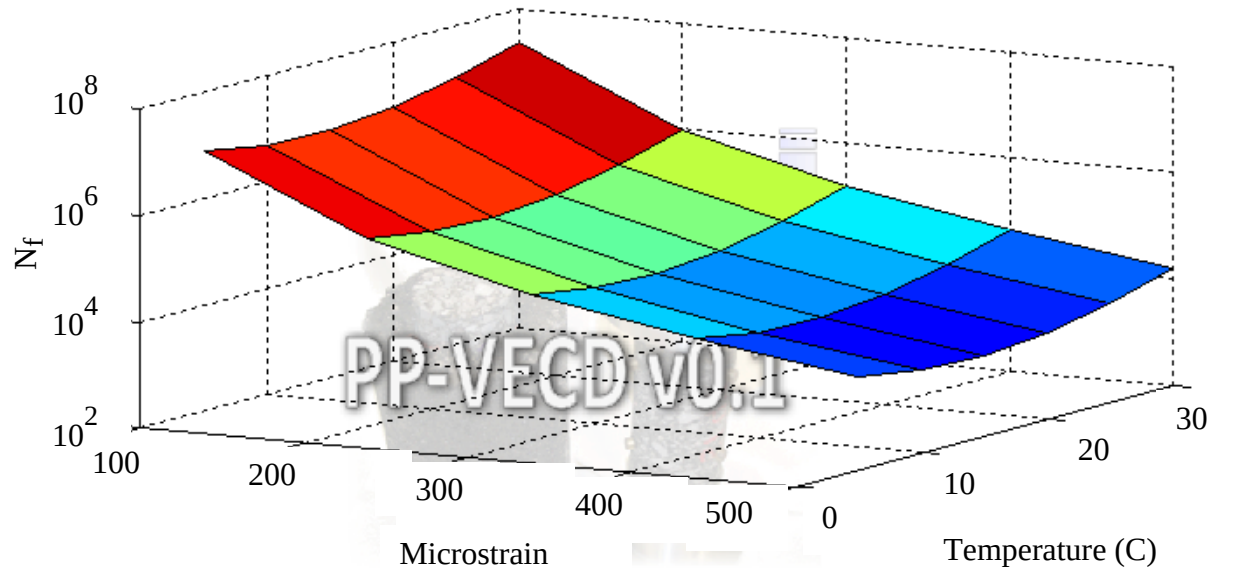

Figure 63: Push Pull Tests for WMA mixtures prepared with foamed binder - 4% water content -17.5 psi air pressure

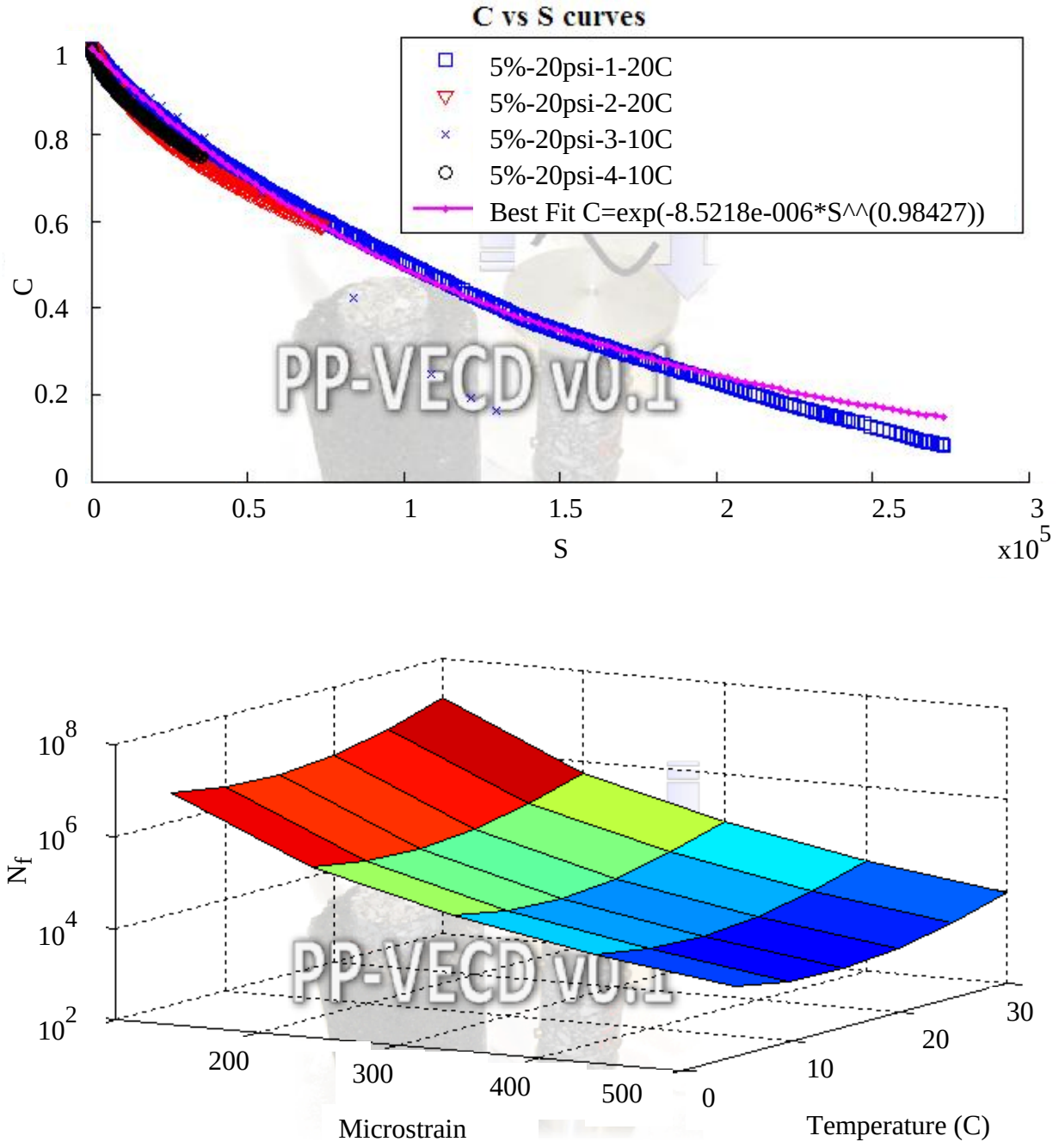

Figure 64: Push Pull Tests for WMA mixtures prepared with foamed binder - 5% water content -20 psi air pressure

APPENDIX D

Table 29: TSR test of the WMA mixtures prepared with foamed binder- 1% water content -10 psi air pressure

	A	B	C	D=(B-C)	E=(A/D)	F	G=(F-E)/F*100	H	I=H/25.4
Sample #	Weight in Air	SSD Weight	Weight in Water	Volume of Sample	Gmb	Gmm	Air Voids	Height (mm)	Height (inch)
1_10_1	3374.7	3428.6	1952.2	1476.4	2.286	2.442	6.40	88.85	3.50
1_10_2	3377.8	3438	1959	1479	2.284	2.442	6.48	89.07	3.51
1_10_3	3373.7	3434.9	1958.9	1476	2.286	2.442	6.40	89.29	3.52
1_10_4	3386.5	3439.1	1961	1478.1	2.291	2.442	6.18	88.45	3.48
1_10_5	3368.3	3427.6	1951	1476.6	2.281	2.442	6.59	89.03	3.51
1_10_6	3385.4	3450.9	1955.5	1495.4	2.264	2.442	7.29	89.18	3.51

CONDITIONED SET

	J= (G/100)*D	B	K	L=((K-B)/J)*100	M	N=2M/(3.14*5.9*I)	S1
Sample #	Volume of Air Voids	Initial Dry Weight	New SSD Weight	Percent Saturation	Load (Lbs)	Tensile Strength	Avg.Tensile Strength
1_10_1	94.46	3374.7	3442.5	71.78	9819.84	303.05	
1_10_2	95.79	3377.8	3452.3	77.77	8735.71	268.94	
1_10_5	97.28	3368.3	3437.8	71.44	7478.37	230.33	267.44

UNCONDITIONED SET

	M	N=2M/(3.14*5.9*I)	S2
Sample #	Load (Lbs)	Tensile Strength	Avg. Tensile Strength
1_10_3	13978.63	429.28	
1_10_4	13872.60	430.07	
1_10_6	14107.05	433.76	431.04

(S1/S2)*100
Tensile Strength Ratio (TSR)
62.0

Table 30: TSR test of the WMA mixtures prepared with foamed binder- 2% water content -12.5 psi air pressure

	A	B	C	D=(B-C)	E=(A/D)	F	G=(F-E)/F*100	H	I=H/25.4
Sample #	Weight in Air	SSD Weight	Weight in Water	Volume of Sample	Gmb	Gmm	Air Voids	Height (mm)	Height (inch)
2_12_1	3334.8	3397.7	1929.9	1467.8	2.272	2.442	6.96	88.655	3.49
2_12_2	3333.3	3399.7	1931.7	1468	2.271	2.442	7.02	89.105	3.51
2_12_3	3346.9	3412.3	1943.9	1468.4	2.279	2.442	6.66	88.95	3.50
2_12_4	3339.2	3397.7	1927.9	1469.8	2.272	2.442	6.97	89.555	3.53
2_12_5	3349.6	3417.4	1942.1	1475.3	2.270	2.442	7.02	88.6975	3.49
2_12_6	3341.5	3409.9	1936.6	1473.3	2.268	2.442	7.12	88.4425	3.48

CONDITIONED SET

	J=(G/100)*D	B	K	L=((K-B)/J)*100	M	N=2M/(3.14*5.9*I)	S1
Sample #	Volume of Air Voids	Initial Dry Weight	New SSD Weight	Percent Saturation	Load (Lbs)	Tensile Strength	Avg.Tensile Strength
2_12_3	97.84	3346.9	3424.7	79.52	9197.136	283.52	
2_12_5	103.64	3349.6	3426.8	74.49	8586.38	265.45	
2_12_6	104.95	3341.5	3423.9	78.51	8543.08	264.87	271.28

UNCONDITIONED SET

	M	N=2M/(3.14*5.9*I)	S2
Sample #	Load (Lbs)	Tensile Strength	Avg. Tensile Strength
2_12_1	14289.235	441.96	
2_12_2	13682.962	421.08	
2_12_4	13381.318	409.72	424.25

(S1/S2)*100
Tensile Strength Ratio (TSR)
63.9

Table 31: TSR test of the WMA mixtures prepared with foamed binder- 3% water content -15 psi air pressure

	A	B	C	D=(B-C)	E=(A/D)	F	G=(F-E)/F*100	H	I=H/25.4
Sample #	Weight in Air	SSD Weight	Weight in Water	Volume of Sample	Gmb	Gmm	Air Voids	Height (mm)	Height (inch)
3_15_1	3331.9	3398.7	1936.4	1462.3	2.279	2.442	6.69	88.50667	3.48
3_15_2	3338.0	3396	1933.6	1462.4	2.283	2.442	6.53	87.75333	3.45
3_15_3	3331.2	3395.2	1935.2	1460	2.282	2.442	6.57	89.21667	3.51
3_15_4	3340.8	3395.4	1934.1	1461.3	2.286	2.442	6.38	89.36667	3.52
3_15_5	3336.7	3391.3	1937.9	1453.4	2.296	2.442	5.99	89.00667	3.50
3_15_6	3357.2	3412.8	1945.8	1467	2.288	2.442	6.29	88.85667	3.50

CONDITIONED SET

	J= (G/100)*D	B	K	L=((K-B)/J)*100	M	N=2M/(3.14*5.9*I)	S1
Sample #	Volume of Air Voids	Initial Dry Weight	New SSD Weight	Percent Saturation	Load (Lbs)	Tensile Strength	Avg.Tensile Strength
3_15_1	97.89	3331.9	3409.5	79.28	11995.6	371.64	
3_15_2	95.49	3338	3405.5	70.69	13100.6	409.36	
3_15_5	87.02	3336.7	3405.7	79.29	1.34E+04	411.79	397.60

UNCONDITIONED SET

	M	N=2M/(3.14*5.9*I)	S2
Sample #	Load (Lbs)	Tensile Strength (TS)	Avg. Tensile Strength
3_15_3	12059.76	370.66	
3_15_4	11637.16	357.07	
3_15_6	12339.01	380.78	369.50

(S1/S2)*100
Tensile Strength Ratio (TSR)
107.6

Table 32: TSR test of the WMA mixtures prepared with foamed binder- 4% water content -17.5 psi air pressure

	A	B	C	D=(B-C)	E=(A/D)	F	G=(F-E)/F*100	H	I=H/25.4
Sample #	Weight in Air	SSD Weight	Weight in Water	Volume of Sample	Gmb	Gmm	Air Voids	Height (mm)	Height (inch)
4_17_1	3285.4	3352.7	1904.3	1448.4	2.268	2.442	7.11	88.3175	3.48
4_17_2	3326	3397.7	1927.9	1469.8	2.263	2.442	7.33	89.24333	3.51
4_17_3	3333.1	3404.7	1935.3	1469.4	2.268	2.442	7.11	88.6975	3.49
4_17_4	3340.8	3407	1939.5	1467.5	2.277	2.442	6.78	88.8475	3.50
4_17_5	3333	3398.6	1935.2	1463.4	2.278	2.442	6.73	88.325	3.48
4_17_6	3318.6	3385.9	1924.9	1461	2.271	2.442	6.98	89.3175	3.52

CONDITIONED SET

	J= (G/100)*D	B	K	L=((K-B)/J)*100	M	N=2M/(3.14*5.9*I)	S1
Sample #	Volume of Air Voids	Initial Dry Weight	New SSD Weight	Percent Saturation	Load (Lbs)	Tensile Strength	Avg.Tensile Strength
4_17_1	103.03	3285.4	3368.1	80.27	6857.16	212.90	
4_17_3	104.49	3333.1	3416.8	80.10	8127.94	249.74	
4_17_4	99.44	3340.8	3420.4	80.05	8520.68	264.53	242.39

UNCONDITIONED SET

	M	N=2M/(3.14*5.9*I)	S2
Sample #	Load (Lbs)	Tensile Strength (TS)	Avg. Tensile Strength
4_17_2	12797.44	395.63	
4_17_5	14048.82	433.59	
4_17_6	11380.32	349.38	392.87

(S1/S2)*100
Tensile Strength Ratio (TSR)
61.7

Table 33: TSR test of the WMA mixtures prepared with foamed binder- 5% water content -20 psi air pressure

	A	B	C	D=(B-C)	E=(A/D)	F	G=(F-E)/F*100	H	I=H/25.4
Sample #	Weight in Air	SSD Weight	Weight in Water	Volume of Sample	Gmb	Gmm	Air Voids	Height (mm)	Height (inch)
5_20_1	3305.4	3368.7	1917.2	1451.5	2.277	2.442	6.75	88.49667	3.48
5_20_2	3350.9	3410.7	1928.8	1481.9	2.261	2.442	7.40	89.09667	3.51
5_20_3	3342.2	3412.7	1933.4	1479.3	2.259	2.442	7.48	88.68333	3.49
5_20_4	3335.9	3401.3	1938	1463.3	2.280	2.442	6.65	88.15667	3.47
5_20_5	3333.3	3405.9	1939.5	1466.4	2.273	2.442	6.92	88.87333	3.50
5_20_6	3323.3	3385.6	1927.4	1458.2	2.279	2.442	6.67	88.76333	3.49

CONDITIONED SET

	J= (G/100)*D	B	K	L=((K-B)/J)*100	M	N=2M/(3.14*5.9*I)	S1
Sample #	Volume of Air Voids	Initial Dry Weight	New SSD Weight	Percent Saturation	Load (Lbs)	Tensile Strength	Avg.Tensile Strength
5_20_2	109.71	3350.9	3427.8	70.10	10403.7	322.36	
5_20_4	97.25	3335.9	3409.2	75.37	10738.21	330.49	
5_20_5	101.41	3333.3	3414.9	80.46	10214.06	315.14	322.66

UNCONDITIONED SET

	M	N=2M/(3.14*5.9*I)	S2
Sample #	Load (Lbs)	Tensile Strength	Avg. Tensile Strength
5_20_3	11009.98	340.43	
5_20_1	9872.10	305.89	
5_20_6	11132.43	343.91	330.07

(S1/S2)*100
Tensile Strength Ratio (TSR)
97.8

BIBLIOGRAPHY

BIBLIOGRAPHY

AASHTO Standard Specifications for Transportation Materials and Methods of Sampling and Testing (Part 2 – Tests), Twenty-Sixth Edition, American Association of State Highway and Transportation Officials, Washington D.C., 2011.

Abel, F., "Foamed asphalt base stabilization", 6th Annual Asphalt Paving Seminar, Colorado State University, 1978.

Acott, S.M., "Sand stabilization using foamed bitumen", Proceeding of 3rd Conference on Asphalt Pavements for South Africa, 155-172, 1979.

Asphalt Academy, "The Design and Use of Foamed Bitumen Treated Materials", Technical Guideline 2 (TG2), Pretoria, 2002.

Anderson, R. M., Baumgardner, G., May, R., and Reinke, G., "NCHRP 9-47: Interim Report: Engineering Properties, Emissions, and Field Performance of Warm Mix Asphalt Technologies", Transportation Research Board: National Highway Research Council, Washington, D.C., 2008.

ASTM Designation D1173-53 (Reapproved 1986), "Standard Test Method for Foaming Properties of Surface-Active Agents (a.k.a. Ross and Miles Test)", American Society for Testing and Materials: Philadelphia, PA, 1988.

ASTM Designation D1881-86, "Standard Test Method for Foaming Tendencies of Engine Coolants in Glassware", American Society for Testing and Materials: Philadelphia, PA, 1988.

ASTM Designation D3427 – 86, "Standard Test Method for Air Release Properties of Petroleum Oils", American Society for Testing and Materials: Philadelphia, PA, 1986.

ASTM Designation D3519-88, "Standard Test Method for Foam in Aqueous Media (Blender Test)", American Society for Testing and Materials: Philadelphia, PA, 1988.

ASTM Designation D3601-88, "Standard Test Method for Foam in Aqueous Media (Bottle Test)", American Society for Testing and Materials: Philadelphia, PA, 1988.

ASTM Designation D892-74 (Reapproved 1984), "Standard Test Method for Foaming Characteristics of Lubricating Oils", American Society for Testing and Materials: Philadelphia, PA, 1988.

Ayman, A., Abbas, A., Nazzal, M., Powers, D., "Laboratory Evaluation of Foamed Warm Mix Asphalt", International Journal of Pavement Research and Technology, 5(2), 93-101, 2012.

Bahia, H.U., Miller, T.D., "Establishing a Framework for Analyzing Asphalt Pavements Sustainability", Enviroad 2009 Conference, Warsaw, Poland, October 15-16, 2009.

Barel, A., Maib, B.P., Paye, M., Maibach, H.I., "Handbook of Cosmetic Science and Technology", Taylo r& Francis, 2005.

Barinov, E.N., "Formation and properties of bituminous foams", Chemistry and Technology of Fuels and Oils, 26(10), 544-548, 1990.

Bennert, T., "Evaluation of Warm Asphalt Technology –Feasibility Study", NJDOT Project 2008-1, Center for Advanced Infrastructure and Transportation, Rutgers University, 2008.

Bhusal, S., "A laboratory study of warm mix asphalt for moisture damage potential and performances issues", Ms. Thesis , Oklahoma State University, 2008.

Bissada, A.F., "Structural response of foamed-asphalt-sand mixtures in hot environments", Transportation Research Record: Journal of the Transportation Research Board, 1115, 134-149, 1987.

Blades, C., Kearney, E., "Asphalt Paving Principles", Cornell Local Roads Program, 2004.

Brennen, M.T., Altschaeffl, A.G. and Wood, L.E., "Laboratory Investigation of the use of Foamed Asphalt for Recycled Bituminous Pavements", Transportation Research Record: Journal of the Transportation Research Board, 911, 80-87, 1983.

Bonaquist, R., "Mix Design Practices for Warm Mix Asphalt", NCHRP Report 691, Transportation Research Board of the National Academies. Washington, D.C., 2011.

Bowering, R.H., "Properties and Behavior of Foamed Bitumen Mixtures for Road Building", AARB 5th Conference, 1970.

Bowering, R.H., Martin, C.L., "Foamed Bitumen: Production and Application of Mixture, Evaluation and Performance of Mixture", Proceedings of the Association of Asphalt Paving Technologists, 45, 453-477, 1976.

Castedo-Franco, L.H., Wood, E.L., "Stabilization with foamed asphalt of aggregates commonly used in low volume roads", In: Low-volume roads: 3rd international conference,

Washington, D.C., Transportation Research Record: Journal of the Transportation Research Board, 898, 297-302, 1983.

Cervarich, M., "Cooling Down the Mix – New "Warm Mix Asphalt", Technologies Developed in Europe"; Hot Mix Asphalt Technology, National Asphalt Pavement Association, Lanham, MD, March/April.13-16, 2003.

Cervarich, M., "Foaming the Asphalt: New Warm-Mix Technique Challenges Conventional Wisdom", Hot Mix Asphalt Technology, National Asphalt Pavement Association, Langham, MD. 12(4), 23-24, 2007.

Clark,M.F., Culley, R.W., "Evaluation of Air-Blown Asphalts to reduce Thermal Cracking of Asphalt Pavements", Proceedings of the Association of Asphalt Paving Technologists, 45,530-555, 1976.

Copeland, A., D'Angelo, J., Dongré, R., Belagutti,S., Sholar,G., "Field Evaluation of High Reclaimed Asphalt Pavement-Warm-Mix Asphalt Project in Florida", Transportation Research Record: Journal of the Transportation Research Board, 2179, 93-101, 2010.

Csanyi, L.H.. "Bituminous mixes prepared with foamed asphalt", Ames, IA: Iowa State University, Iowa Engineering Experiment Station, Bulletin 189, 1960.

D'Angelo, J., Harm, E., Bartozsek, J., Baumgardner, G., Corrigan, M., Cowsert, J., Harman, T., Jamshidi, M., Jones, W., Newcomb, D., Prowell, B., Sines, R. and Yeaton B., " Warm Mix Asphalt: European Practice", FHWA report no: FHWA-PL-08-007, 2008.

Das, B.M., "Principles of Geotechnical Engineering", Cengage Learning, Stamford, CT, 7th edition, 2009.

De Groot, P., Bowen, C., Koenders, B., Stoker, D., Larsen, O., and Johansen, J., "A Comparison of Emissions from Hot Mixture and Warm Asphalt Mixture Production", IRF World Meeting, Paris, 2001.

Diefenderfer, S. and Hearon, A., "Laboratory Evaluation of a Warm Asphalt Technology for Use in Virginia", Report No FHWA/VTRC 09-R11, Virginia Transportation Research Council, Charlottesville, VA., 2008.

Din 53902-Part 1, "Testing of Surface Active Agents; Determination of Foaming Power; Beating Method using A Perforated Disc", German Standards, Edition 81, 1992.

Engelbrecht, J.C., Roberts, F.L., Kennedy, T.W., " Cold Recycled mixtures, with emphasis on the curing of foamed specimens – a laboratory study", Annual Transportation

Convention, Session- Maintenance of Transport Infrastructure, Volume 350, Paper 7, 1985.

EPA, "Hot Mix Asphalt Plants Emission Assessment Report", United States Environmental Protection Agency, EPA-454/R-00-019, 2000.

FHWA, "Reclaimed Asphalt Pavement in Asphalt Mixtures: State of the Practice", Federal Highway Administration, FHWA-HRT-11-021, 2011.

Gandhi T, Amirkhanian S., "Laboratory investigation of warm asphalt binder properties-a preliminary analysis", The fifth international conference on maintenance and rehabilitation of pavements and technological control (MAIREPAV5), Park City, Utah, USA, p. 475–80. 2007.

German, B.J. and McCarthy, M.J., "Stability of Aqueous Foams: Analysis using Magnetic Resonance Imaging", Journal of Agricultural Food Chemistry, 37(5), 1321-1324, 1989.

Gibson, N., Qi, X., Shenoy, A., Al-Khateeb, G., Kutay, M.E.,. Andriescu, A., Stuart, K., Youtcheff, J., Harman,.T., "Full-Scale Accelerated Performance Testing for Superpave and Structural Validation", Report FHWA-HRT-11-045. FHWA, U.S. Department of Transportation, 2012.

Goh, S.W., You Z., "Mechanical Properties of Warm Mix Asphalt Using Aspha-min" Transportation Research Board (TRB), 87th Annual Meeting Compendium of Papers DVD, Washington, D.C., 2008.

Guillerme, C., Loisel, W., Bertrand, D., Popineau, Y., "Study of Foam Stability by Video Image Analysis: Relationship with the Quantity of Liquid in the Foams", Journal of Texture Studies, V.24-3, 287-302, 1993.

Haffmans, B.V. "http://www.ssco.com.tw/Haffmans/PDF_catalog/QC_instruments/E-NIBEMT.pdf ", 2012.

Hanz, A.J., Faheem, A., Mahmoud,E., Bahia, H.U., "Measuring Effects of Warm Mix Additives using a Newly Developed Asphalt Binder Lubricity Test for the Test", Transportation Research Record: Journal of the Transportation Research Board, 2180, 85-92, 2010.

Hassan, M.M., "Life-Cycle Assessment of Warm-Mix Asphalt: an Environmental and Economic Perspective", Transportation Research Board, 88th Annual Meeting Compendium of Papers DVD, Washington, D.C., 2009.

He, G. and Wong W., "Decay properties of the foamed bitumens", Construction and Building Materials, 20, 866–877, 2006.

Heitzman, M., "State of the Practice – Design and Construction of Asphalt Paving Materials with Crumb Rubber Modifier", FHWA-SA-92-022, Federal Highway Administration, Washington, D.C., May 1992.

Hossain, Z., Bhudhala, A, Zaman,M., O'Rear,E., Cross, S., and Lewis, S., "Evaluation of the Use of Warm Mix Asphalt as a Viable Paving Material in the United States", Report 06-H-0044, Federal Highway Administration, McLean, 2009.

Howard, I.L., Cooley, A., Doyle, J.D., "Laboratory Testing and Economic Analysis of High RAP Warm Mixed Asphalt", Mississippi Department of Transportation, FHWA/MS-DOT-RD-09-200, 2009.

Huang, B., Zhang,Y., Shu, X., Liu, Y., Ye, P. X., "Neutron scattering for moisture detection in foamed asphalt", Journal of Materials in Civil Engineering, 2012, in press.

Hurley, G.C. and Prowell, B.D., "Evaluation of Aspha-Min zeolite for use in warm mix asphalt", NCAT Report 05-04, 2005.

Hurley, G.C. and Prowell, B.D., "Evaluation of Sasobit for use in warm mix asphalt", NCAT Report 05-06, 2005.

Hurley, G., "Evaluation of New Technologies for Use in Warm Mix Asphalt", Master's Thesis, Auburn University, Auburn, AL, 2006.

Hurley, G. and Prowell, B., "Evaluation of Potential Processes for Use in Warm Asphalt Mixes," Journal of the Association of Asphalt Paving Technologists, Vol. 75, 41-85, 2006.

Hurley, G.C. and Prowell, B.D., "Field performance of warm mix asphalt", Transportation Research Board (TRB), 87th Annual Meeting Compendium of Papers DVD, Washington, D.C.,2008.

Hutzler, S., Verbist, G., Weaire, D. Van der Steen, J.A., "Measurement of foam density with AC capacitance", Europhysics Letters, 31 (8), pp. 497-502, 1995.

Jackson, S., "Application of Warm Mix Asphalt on Non-Typical Paving Projects", West Contracting, 2011.

Jenkins, K.J., "Mix Design Considerations for Cold and Half-warm Bituminous Mixes with emphasis on Foamed Bitumen", Ph.D. Dissertation, University of Stellenbosch, South Africa, 2000.

Jones, D., Fu, P., Harvey, J., Halles, F., "Full-Depth pavement reclamation with foamed asphalt: Final report.", California Department of Transportation Division of Research and Innovation Office of Roadway Research, UCPRC-RR-2008-07, 2008.

Jones, D., Wu, R., Tsai, B.W., and Harvey, J.T., "Warm-Mix Asphalt Study: First-Level Analysis of Phase 2 HVS and Laboratory Testing and Forensic Investigation", Davis and Berkeley, CA: University of California Pavement Research Center (RR-2009-02), 2009.

Kanitpong, K., Sonthong, S., Nam, K. Martono, W., Bahia, H., "Laboratory Study on Warm Mix Asphalt Additives", 86th Annual Meeting Compendium of Papers DVD, Washington, D.C., 2007.

Kavussi, A., Hashemian, L., "Properties of WMA-Foam Mixes based on Major Mechanical Tests", Journal of Civil Engineering and Management, 17(2), 207-216, 2011.

Kendall, M. and Gibbons, J., "Rank Correlation Methods", Fifth Edition, Oxford University Press, Oxford, England, 1996.

Kim, Y., Lee H., and Heitzman, M., "Validation of New Mix Design Procedure for Cold In-place Recycling with Foamed Asphalt for Iowa Department of Transportation", Transportation Research Board (TRB) Annual Meeting CD-ROM, 2006.

Kim, Y., Lee H., "Development of Mix Design Procedure for Cold In-Place Recycling with Foamed Asphalt", Journal of materials in civil engineering, 116-124, 2006.

Kim, H., Lee, S.J., Amirkhanian, S.N., "Rheology of warm mix asphalt binders with aged binders", Construction and Building Materials, 25, 183-189, 2011.

Kutay, M.E., Ozturk, H.I., "Investigation of Moisture Dissipation in Foam-based Warm Mix Asphalt Using Synchrotron-Based X-Ray Microtomography", ASCE Journal of Materials in Civil Engineering, Vol. 24, No 6, pp. 674-683, 2012.

Kutay, M.E., Arambula, E., Gibson, N.H. and Youtcheff, J., "Three-Dimensional Image Processing Methods to Identify and Characterize Aggregates in Compacted Asphalt Mixtures", International Journal of Pavement Engineering, Vol. 11, Issue 6, pp. 511-528. 2010.

Kutay, M.E., Ozturk, H., Abbas, A. and Hu, C., "Comparison of 2D and 3D Image-Based Aggregate Morphological Indices", International Journal of Pavement Engineering, Vol. 12, Issue 4, pp. 421-431. 2011.

Kristjánsdóttir, O., Muench, S.T., Michael, L. and Burke, G., "Assessing the potential for Warm Mix Technology Adoption", Transportation Research Record: Journal of the Transportation Research Board, No. 2040, Washington DC., 2007.

Kvasnak, A., West, R., Moore,J., Nelson,J., Turner,P. and Tran, N., "Case Study of Warm Mix Asphalt Moisture Susceptibility in Birmingham", Transportation Research Record: TRB 88th Annual Meeting Compendium of Papers DVD, 2009.

Lamb, H., "Hydrodynamics", Cambridge, England: Cambridge University Press, pp. 597. 1932.

Lange, C.R., Stroup-Gardiner, M.," Temperature-Dependent Chemical-Specific Emission Rates of Aromatics and Polyaromatic Hydrocarbons (PAHs) in Bitumen Fume", Journal of Occupational Environmental Hygiene, Cincinnati, Ohio, USA, 4(S1):72-6, 2007.

Larsen, O., Moen, Ø., Robertus, C., and Koenders, B., "WAM Foam Asphalt Production at Lower Operating Temperatures as an Environmental Friendly Alternative to HMA", In Proceedings of the 3rd Eurasphalt and Eurobitume Conference, Book 1, Foundation Eurasphalt, Breukelen, The Neterhlands, 641-650, 2004.

Lee, D.Y., "Treating Iowa's Marginal Aggregates by Foamix Process", Iowa Department of Transportation, Ames, HR-212, ISU-ERI-AMES-80221, 1980.

Lee D.Y., "Treating Marginal Aggregates and Soils with Foamed Asphalt", Association of Asphalt Paving Technologists, 50, 211-250, 1981.

Leek, C., Jameson G., "Review of Foamed Bitumen Stabilization Mix Design Methods", Austroads Technical Report, Austroads Publication No. AP–T178/11, 2011.

Lesueur, D., Clechc, H., Brosseaudc, A., Suchc, C., Cazacliuc, B., Koendersd, B., Cérinoe, P.J., Bonvalletf, J., "Foamability and Foam Stability", Road Materials and Pavement Design, 5(3), 2004.

Maccarone, S., Holleran, G., and Ky, A., "Cold Asphalt System as an Alternative to Hot Mix", 9th AAPA International Asphalt Conference, 1995.

MaineDOT, "Maine's Experience Utilizing Full Depth Reclamation with Foamed Asphalt", presentation at NESMEA 2004, Portsmouth, NH, 2004.

Mallick, R.B., Kandhal P.S., Bradbury R.L., "Using Warm-Mix Asphalt Technology to Incorporate High Percentage of Reclaimed Asphalt Pavement Material in Asphalt Mixtures", Transportation Research Record: Journal of the Transportation Research Board, V. 2051, 71-79, 2008.

Mallick, R. B., Bergendahl, J. and Pakula, M., "A Laboratory Study on CO_2 Emission Reductions through the Use of Warm Mix Asphalt", Transportation Research Board 88th Annual Meeting, Washington, D.C., 2009.

Marquis, B., Bradbury, R.L., Colson, S., Mallick, R.B., Nanagiri, Y.V., Jonathan S. Gould, J.S., Marshall, M., " Design, construction and early performance of foamed asphalt full depth reclaimed (FDR) pavement in Maine", Transportation Research Board 82th Annual Meeting, Washington, D.C., 2003.

MDOT, "Procedures for Aggregate Inspection", Michigan Department of Transportation, Construction and Technology Division, 2009.

Middleton, B., Forfylow, R.W., "Evaluation of warm-mix asphalt produced with the double barrel green process", Transportation Research Record: Journal of the Transportation Research Board, V.2126, 19-26, 2009.

Mohammad, L.N., Abu-Farsakh, M.Y., Wu, Z., Abadie, C., "Louisiana experience with foamed recycled asphalt pavement base materials." Transportation Research Record: Journal of the Transportation Research Board, V. 1832, 17-24, 2003.

Munch, B., Trtik, P., Marone, F., Stampanoni, M., "Stripe and ring artifact removal with combined wavelet-Fourier filtering", Optical Express, Vol. 17(10), 2009.

Muthen, K.M., "Foamed Asphalt Mixes: Mix Design Procedure", CSIR TRANSPORTEK Report No: CR-98/077, South Africa, 1998.

Nadeau, G., "Warm Mix and the 'Every Day Counts' Initiative", Asphalt Pavement, National Asphalt Pavement Association (NAPA), pp.16-21., 2012.

Namutebi, M., "Some Aspects of Foamed Bitumen Technology", Licentiate Thesis, Division of Highway and Railway Engineering, Department of Transport Science School of Architecture and the Built Environment, Royal Institute of Technology SE-100 44 Stockholm, 2011.

Namutebi,M., Birgisson, B., Bagampadde, U., "Foaming Effects on Binder Chemistry and Aggregate Coatability using Foamed Bitumen", Road Materials and Pavement Design, 12:4, 821-847, 2011.

Nataatmadja, A., "Some Characteristics of Foamed Bitumen Mixes", Transportation Research Record: Journal of the Transportation Research Board, Volume.1761, 120-125, 2001.

Nazzal, M.D., Qtaish, L.A., "The Use of Atomic Force Microscopy to Evaluate Warm Mix Asphalt", FHWA/OH-2012/19, 2013.

NCAT Asphalt E-news," Warm-Mix and RAP: A Winning Combination", National Center for Asphalt Technology NCAT at Auburn University, 24(1), 2012.

NCHRP Report 714, "Special Mixture Design Considerations and Methods for Warm Mix Asphalt: A supplement to NCHRP Report 673: A Manual for Design of Hot Mix Asphalt with Commentary", Transportation Research Board of the National Academies. Washington, DC, 2012.

NCHRP, Research Results Digest 374, 2012.

Neu, G.E., "Techniques of Foam Measurement", Journal of Society of Cosmetic Chemists, V.11, No.7, Pp. 390-414, 1960.

NIOSH Health Hazard Evaluation Report: Crumb –Rubber Modified Asphalt Paving: Occupational Exposures and Acute Health Effects (HETA #2001-0536-2864), 2001.

Powers, D., "Internal Report on 2008 Foamed Asphalt WMA Projects", Ohio Department of Transportation, 2008.

Prasad, R.J.C., Sreenivasu, T., Rao, M.V.G., "Polar Wavelet-Gaussian Filter for ring artifact suppression in CT image systems", International Journal of Computer Science & Communications Networks, Vol. 1(2), 186-195, 2011.

Prowell, B.D., "Warm Mix Asphalt: The international technology scanning program summary report", U.S. Department of Transportation, Federal Highway Administration American Association of State Highway and Transportation Officials, National Cooperative Highway Research Program, 2007.

Prowell, B., "Warm-Mix Asphalt: Best Practices", Presentation at 53rd NAPA Annual Meeting, 2008.

Prowell, B.D., Hurley, G. and Frank, B., "Warm Mix Asphalt: Best Practices", National Asphalt Pavement Association (NAPA) Quality Improvement Publication 125, 3rd Edition, 2012.

Raffaelli, D., "Foamed asphalt base stabilization", University of California Berkeley Institute of Transportation Studies, Technology Transfer Program, 2004.

Rand, D.A., "TxDOT Perspective of WMA and Where We are Headed", 2008 TxAPA Annual Meeting ,updated for 2009 Corpus Christi, TX.

Ramanujam, J.M. and Jones, J.D., "Characterization of Foamed-Bitumen Stabilization", International Journal of Pavement Engineering, 8(2), 111-122, 2007.

Rubio, M.C., Martinez, G., Baena, L., Moreno, F., "Warm Mix Asphalt: An Overview", Journal of Cleaner Production, 24, 76-84, 2012.

Ruckel, P.J., Acott, S.M., Bowering, R.H., "Foamed-Asphalt Paving Mixtures: Preparation of Design Mixes and Treatment of Test Specimens", Transportation Research Record: Journal of the Transportation Research Board, V. 911, USA, 88-95, 1983.

Ruhl, R., Lindemeier, B., "The German Bitumen Forum", Heinrich Lauck GmbH, 2006.

Sakr, H.A., Manke, P.G., "Innovations in Oklahoma foamix design procedures", Transportation Research Record: Journal of the Transportation Research Board, V. 1034, 26-34, 1985.

Saleh, M., "Characterization of Foam Bitumen Quality and the Mechanical Properties of Foam Stabilized Mixes", 10th International Conference on Asphalt Pavements (ICAP 2006), Quebec City, Canada, 2006.

Solaimanian, M., Milander, S., Boz, I., Stoffels, S.M., "Development of Guidelines for Usage of High Percent RAP in Warm-Mix Asphalt Pavements", Commonwealth of Pennsylvania Department of Transportation, Contact No. 510602, Project No. PSU 032, 2011.

Sunarjono, S., "Influence of foamed bitumen characteristics on cold mix asphalt properties", Thesis submitted to University of Nottingham for the degree of Doctor of Philosophy, 2008.

Schramm, L.L., Wassmuth, F., "In Foams: Fundamentals and Applications in the Petroleum Industry", Advances in Chemistry Series, 1994.

Schramm, L.L., "Emulsions, Foams, and Suspensions: Fundamentals and Applications", WILEY-VCH Verlag GmbH & Co. KGaA, Weinheim, 2005.

Sebba, F., "Foams and Biliquid Foams – Aphrons", Wiley: NewYork, 1987.

Shua, X., Huang, B., Shrum, E.D., Jia, X., "Laboratory evaluation of moisture susceptibility of foamed warm mix asphalt containing high percentages of RAP", Construction and Building Materials, Volume 35, 125–130, 2012.

Su, K., Maekawa, R., Hachiya, Y., "Laboratory Evolution of WMA Mixture for use in Airport Pavement Rehabilitation", Construction and Building Materials, 23(7), 2709-2714, 2009.

Xiao, F., Zhao, P.E.W., Amirkhanian, S.N., "Fatigue behavior of rubberized asphalt concrete mixtures containing warm asphalt additives",Construction and Building Materials, 23 (2009) 3144–3151 ,2009.

Xiao, F., Jordan, J., Amirkhanian,S.N., "Laboratory Investigation of Moisture Damage in Warm Mix Asphalt Containing Moist Aggregate", Transportation Research Record: Journal of the Transportation Research Board, 2126, 115-124, 2010.

Xiao, F., Punith, V.S., Putman, B.J., "Effect of Compaction Temperature on Rutting and Moisture Resistance of Foamed Warm Mix Asphalt Mixtures", Journal of Materials in Civil Engineering, 2012.

Wasiuddin, N.M., Selvamohan, S., Zaman, M.M, Guegan, M.L.T.A., "Comparative Laboratory Study of Sasobit and Aspha-Min Additives in Warm-Mix Asphalt", Transportation Research Record: Journal of the Transportation Research Board, 1998 , 82-88, 2007.

West, R., "Field Testing of Warm Mix Asphalt", Presentation at the Warm Mix Asphalt &Recycling Symposium, Sacramento, California, USA, 2009.

Wielinski, J., Hand, A., Rausch, D.M., "Laboratory and Field Evaluations of Foamed Warm-Mix Asphalt Projects", Transportation Research Record: Journal of the Transportation Research Board, 2126, 125-131, 2009.

Wirtgen GmbH, "Wirtgen Cold Recycling Manual", Windhagen, Germany, 2004.

You, Z., Goh, S.W., Dai, Q., "Laboratory Evaluation of Warm Mix Asphalt", Final Report, Michigan Technological University, 2011.

Yunus, C., Boles, M., "Thermodynamics:An Engineering Approach", 2nd Edition, New York: McGraw-Hill, Inc., 1994.

Zaumanis, M., "Warm Mix Asphalt Investigation", MS Thesis, Riga Technical University, Denmark, 2010.

Zeiada,W.A., Kaloush, K.E., Biligiri, K.P., Reed, J.X., Stempihar, J.J., "Significance of Confined Dynamic Modulus Laboratory Testing for Asphalt Concrete", Transportation Research Record: Journal of the Transportation Research Board, 2010, 9-19, 2011.

Zhao, S. Huang, B., Shu, X., Jia, X., Woods, M.," Laboratory Performance Evaluation of Warm Mix Asphalt containing High Percentages of RAP", 91st Annual Meeting of Transportation Research Board, Washington, D.C., 2012.